METROLOGY AND CHARACTERISATION OF DEFECTS IN THIN-FILM BARRIER LAYERS EMPLOYED IN FLEXIBLE PHOTOVOLTAIC MODULES

MOHAMED SALAH ELRAWEMI

A thesis submitted to the University of Huddersfield in partial fulfilment of the requirements for the degree of Doctor of Philosophy

The University of Huddersfield

School of Computing and Engineering

Mechanical Engineering Department

November 2015

Copyright Statement

i. The author of this thesis (including any appendices and/or schedules to this thesis) owns any copyright in it (the "Copyright") and s/he has given The University of Huddersfield the right to use such copyright for any administrative, promotional, educational and/or teaching purposes.

ii. Copies of this thesis, either in full or in extracts, may be made only in accordance with the regulations of the University Library. Details of these regulations may be obtained from the Librarian. This page must form part of any such copies made.

iii. The ownership of any patents, designs, trademarks and any and all other intellectual property rights except for the Copyright (the "Intellectual Property Rights") and any reproductions of copyright works, for example graphs and tables ("Reproductions"), which may be described in this thesis, may not be owned by the author and may be owned by third parties. Such Intellectual Property Rights and Reproductions cannot and must not be made available for use without the prior written permission of the owner(s) of the relevant Intellectual Property Rights and/or Reproductions.

Abstract

Flexible thin-film photovoltaic (PV) modules based on copper indium gallium selenide (CIGS) materials are one of the most recent developments in the renewable energy field, and the latest films have efficiencies at or beyond the level of Si-based rigid PV modules. Whilst these films offer significant advantages in terms of mass and the possibility of building-integrated photovoltaic (BIPV) applications, they are at present highly susceptible to long term environmental degradation as a result of water vapour transmission through the protective encapsulation layer to the active (absorber) layer. To maintain the PV module flexibility and to reduce or eliminate the water vapour permeability, the PV encapsulation includes a barrier layer of amorphous aluminium oxide (Al_2O_3) material of a few nanometres thickness deposited on a planarised polyethylene naphthalate (PEN) substrate. The highly conformal barrier layer of the Al_2O_3 is produced by atomic layer deposition (ALD) methods using roll-to-roll (R2R) technology. Nevertheless, water vapour permeation is still facilitated by the presence of micro and nano-scale defects generated during the deposition processes of the barrier material, which results in decreased cell efficiency and reduced unit longevity.

The state of the art surface metrology technologies including: optical microscopy, white light scanning interferometry (WLSI), atomic force microscopy (AFM) and scanning electron microscopy (SEM) were extensively deployed in this project as offline surface characterisation methods to characterise the water vapour barrier layer defects, which are postulated to be directly responsible for the water vapour ingress. Areal surface texture parameters analysis based on wolf pruning, area pruning and segmentation analysis methods as defined in ISO 25178-2; allow the efficient separation of small insignificant defects from significant defects. The presence of both large and small defects is then correlated with the barrier films functionality as measured on typical sets of Al_2O_3 ALD films using a standard MOCON® (quantitative gas permeation) test. The investigation results of the initial analysis finishes by drawing conclusions based on the analysis of the water vapour transmission rate (WVTR), defects size, density and distribution, where it is confirmed that small numbers of large defects have more influence on the deterioration of the barrier films functionality than large numbers of small defects. This result was then used to provide the basis for developing a roll-to-roll in process metrology device for quality control of flexible PV barrier films.

Furthermore, a theoretical model approach was developed in this thesis based on the water vapour diffusion theory to determine the cut- off level between large significant defects and small insignificant defects. The results of the model would seem to reveal that, in order to build up in process, non-contact optical defect detection system for R2R barrier films, the critical spatial resolution required for defect detection need not be less than 3 µm laterally and 3Sq nm (Sq= root mean square surface roughness deviation of non-defective sample area) per field of view (FOV) vertically. Any defect that has dimensions less than this appears to have a significantly lower effect on the PV barrier properties and functionality.

In this study, the surface topography analysis results and the theoretical model approach outcomes, both provide the basis for developing a R2R in process metrology device for PV barrier films defect detection. Eventually, the work in this thesis reports on the deployment of new (novel) in-line interferometric optical sensors based on wavelength scanning interferometry (WSI) designed to measure and catalogue the PV barrier films defects where they are present. The sensors have built-in environmental vibration compensation and are being deployed on a demonstrator system at a R2R production facility in the UK.

Declaration

No portion of the work presented in this thesis has been submitted in support of an application for another degree or qualification of this or any other university or other institute of learning.

Mohamed Elrawemi

Dedication

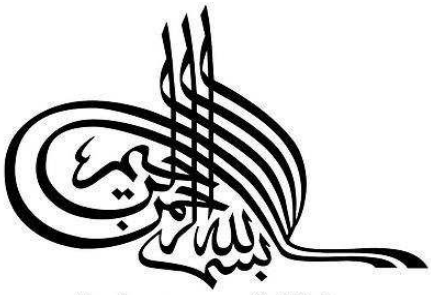

In the name of Allah,
the Most Beneficent,
the Most Merciful

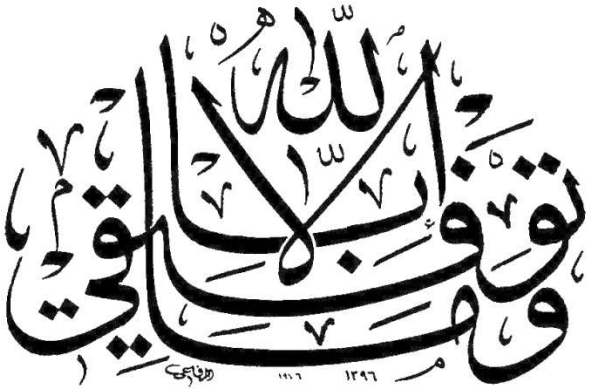

(The Holy Quran, 11:88)

To the soul of my father in his grave

To my family*, the near and far, for their endless love, support and encouragement.*

Acknowledgment

All praise and thanks are due to Almighty Allah who always guides me to the right path and has helped me to complete this thesis.

Foremost, I would like to express my sincere gratitude to my supervisor and my director of studies **Prof. Liam Blunt** for the continuous support, patience, motivation, enthusiasm, and immense knowledge, supervision, advice, and guidance that he has afforded me from the earliest stages of this research to the submission stage. His guidance helped me at all the times including in the research and writing of this thesis. I could not have imagined having a better supervisor and mentor for my Ph. D. study. Most vital of all, he provided me unflinching encouragement and support in various ways: giving me the chance to work in the EU funded "NanoMend" project, support to attend more than 12 conferences outside and inside the UK, and helping me to publish different papers in various journals. **I am really indebted to him more than he knows.**

Besides my supervisor, I would like to thank the rest of my thesis committee: **Dr. Leigh Fleming**, **Dr. Francis Sweeney** (University of Sheffield), **Dr. Graeme Greaves** (Electron Microscopy and Materials Analysis EMMA research group) and **Eng**. **Chris Dawson** for their encouragement, help, and insightful comments. Thank you so much for the arrangements and the time you spent to train me using surface metrology instruments.

My sincere thanks also goes to **Prof. Xiangqian**, **Dr. Hussam Muhamedsalih**, **Dr. Haydn Martin**, and **Dr. Feng Gao** for offering me the opportunities in their group and allowing me to work with them on diverse exciting optical instruments. I would like also to thank all my colleagues in the EPSRC Centre for Innovative and Manufacturing in Advanced Metrology. You all have contributed to creating a unique working environment. Special thanks also goes to the **Libyan government** represented by the **Libyan Cultural Attaché** in London for providing me with funding throughout all of the Ph. D. journey.

Parts of the thesis have been performed in an excellent collaboration with the **Centre for Process Innovation** (Durham, UK), the **National Physical Laboratory** (Teddington, UK), and **IBS Precision Engineering** (Eindhoven, The Netherlands). I would like to express my personal gratitude to **Dr. David Robbins** and **Dr. David Bird** for offering me the opportunity

to perform studies in their department site (CPI). I would like also to acknowledge the enormous help of **Phil Hollis** and **Steven Edge** for the useful information which they provided.

Last, but by no means least, my special, profound, and affectionate thanks, love, gratitude, and deep indebtedness are due to my **wife**, who has been struggling with me through this journey in order to secure and shape for ourselves a brighter future. Her understanding, support, commitment, and taking over full-time childcare responsibilities during my studies, have all made my success possible. At the same time, I would like to express my love and thanks to 'the beats of my heart', my children, **Lara** and **Lareen**, who are the only source of inspiration to me, and it is their love and innocent smiles that have made the hardship of this task bearable. My deep love and thanks are due to my **mother**, **brother** and **sisters**, and the entire family.

Sincerely

Mohamed Elrawemi

Table of Contents

List of Figures

List of Tables

List of Acronyms

PV	Photovoltaic	SiOx	Silicon Oxide
CIGS	Copper Indium Gallium Selenide	OLED	Organic Light-Emitting Diode
Si	Silicon	SLG	Soda-Lime Glass
BIPV	Building Integrated Photovoltaic	Ti	Titanium
AlOx	Aluminium Oxide	CTE	Coefficient of Thermal Expansion
IEC	International Electrotechnical Commission	PES	Polyethersulfone
R2R	Roll-to-Roll	UV	Ultraviolet
ALD	Atomic Layer Deposition	HfO_2	Hafnium Oxide
WVTR	Water Vapour Transmission Rate	HfSiO	Hafnium Silicate
WSI	Wavelength Scanning Interferometry	Ta_2O_5	Tantalum pentoxide
CdTe	Cadmium Telluride	TaN	Tantalum Nitride
Mo	Molybdenum	SiNx	Silicon Nitride
CdS	Cadmium Sulfide	HfN	Hafnium Nitride
ZnO	Zinc Oxide	Ru	Ruthenium
TCO	Transparent Conductive Oxide	Cu	Copper
ZnO: Al	Aluminium-doped Zinc Oxide	W	Tungsten
DH	Damp Heat	TML	Trimethyl Aluminum
PEN	Polyethylene Naphthalate	OH	Hydroxyl group
PET	Polyethylene Terephthalate	Al-O	Aluminium-oxygen
SEM	Scanning Electron Microscopy	STM	Scanning Tunnelling Microscope
AFM	Atomic Force Microscopy	LFM	Lateral Force Microscopy

WLI	White Light Interferometry	MFM	Magnetic Force Microscopy
NSOM	Near-field Scanning Optical Microscopy	CCI	Coherence Correlation Interferometer
FEG	Field Emission Gun	SPM	Scanning Probe Microscopy
CCD	Charge Coupled Device	RH	Relative Humidity
FOV	Field Of View	GPU	Graphics Processing Unit
AOTF	Acousto-optic Tunable Filter	SLED	Super-luminescent Diode
PZT	Piezo-electric Translator	NPL	National Physical Laboratory
VHX	Video Highway Xtreme	pm	Picometre
μA	Microampere	nA	Nanoampere
CPI	Centre for Process Innovation	IR	Infrared

List of Notations

l	Sample thickness.
S_{pd}	Peaks density.
D	Diffusivity / Diffusion coefficient.
C_{sat}	Concentration of water at saturation.
t	Elapsed time.
$\emptyset$	Concentration of diffusing substances.
P	Vapour/gas pressure.
S	Solubility coefficient.
P_r	Permeability coefficient.
ΔP	Partial pressure differential across a film.
q	Amount of permeant passing through a film.
Q	Amount of permeant passing through a film per unit of time.
R_0	Hole radius.
N	Number of defects (holes) in a sample area.
A	Total sample area.
$h(x, y)$	Height of the specific pixel.
$\Delta\varphi(x, y)$	Calculated phase shift over the scan range.
λ_{max}	The upper filtered wavelengths of the scan range.
λ_{min}	The lower filtered wavelengths of the scan range.

CHAPTER 1

1. Introduction

1.1 Overview

Conventional energy sources based on oil, coal, and natural gas have proven to be highly effective drivers of economic growth. However, they are simultaneously detrimental to the environment and human health (Akella, Saini, & Sharma, 2009), and hence there is a need to reduce fossil fuel usage to ease the subsequent problems of global warming, climate change and air pollution resulting from CO_2 emissions. Therefore finding access to alternative clean, efficient, reliable and renewable sources of energy with low or even no emissions that are environmental friendly, has attracted increasing research interest over time. One of the most promising attempts is the application of photovoltaic technology to utilise the huge amounts of energy that the earth receives every second from the sun.

The most common types of photovoltaic (PV) cells in today's industry are fabricated from either crystalline silicon or thin-film materials (P. F. Carcia, R. S. McLean, & S. Hegedus, 2010). The rigid construction of Si PV modules hampers their economic integration into residential and commercial buildings; however, thin film PV technologies may prove to be most appropriate with respect to cost, ease of manufacture and installation (Ahmad, 1995), and they are currently being considered for large scale power plants as well as building integrated photovoltaic (BIPV) applications (James, Goodrich, Woodhouse, Margolis, & Ong, 2011). These PV modules are based on the material copper indium gallium selenide $CuIn_{1-x}Ga_xSe_2$ (CIGS) as the absorber (p-type) layer and they are at present the most

efficient cells at or beyond the level of Si based rigid solar modules (Igalson & Urbaniak, 2005). These flexible devices are fabricated on polymer films (substrates) by the repeated deposition, and patterning of thin layer materials using roll-to-roll (R2R) technology (Yulia & Ronn, 2012), where the whole film is approximately 3 μm thick prior to final encapsulation (Bartholomeusz & Bartholomeusz, 2014).While this technology offers significant advantages in terms of mass and the possibility of BIPV applications (Bahaj, James, & Jentsch, 2007), they are at present highly susceptible to long term environmental degradation as a result of water vapour transmission through the barrier (protective) layers to the active (absorber) CIGS layer (N. Kim et al., 2012), thereby reducing cell efficiency, longevity and causing ultimately failure (Grover, Srivastava, Rana, Mehta, & Kamalasanan, 2011).

The basic methodology to prevent the water vapour permeability and to maintain the PV module flexibility, is to combine an oxide barrier layer (e.g. AlO_x) coating with suitable polymer substrates as a base material (Hirvikorpi, 2011). The highly conformal oxide layer (AlO_x) is produced by atomic layer deposition (ALD) methods (M. D. Groner, George, McLean, & Carcia, 2006), where the surface of the substrate film (usually polyethylene naphthalate) must be of very high quality (i.e. smooth). In order to achieve high quality, the substrate film is further planarised for smoothness and spike removal purposes prior to coating (Almanza-Workman et al., 2012). Nevertheless, it is hard to deposit the Al_2O_3 layer without any local defects. These are mainly caused by environmental particles formed during the deposition process (Bülow et al., 2014), consequently micro and nano-scale defects can be easily generated thus facilitating water vapour ingress and affecting the overall module efficiency and lifespan (Lee et al., 2013). These defects are believed to be inherently present in vacuum-deposited layers because of imperfections in the deposition process (intrinsic defects) or as a result of the presence of impurities in the vacuum chamber or on the coated

substrate (extrinsic defects) (Greener, Ng, Vaeth, & Smith, 2007). Thus, even if the substrate is coated with an inorganic barrier layer, the barrier performance of this multilayer structure is still expected to fall short for PV applications (Greener et al., 2007), due to the presence of defects.

In this project various approaches were applied to reduce the presence and the density of the defects on the barrier layers, by paying close attention to the substrates (raw material) cleanliness before the Al_2O_3 ALD coating process. These cleanliness approaches were seen to significantly lower the water vapour permeability, nevertheless it is still unlikely to meet the PV encapsulation requirements set by the international electrotechnical commission (IEC61646-2, 2008), which requires that the PV efficiency must not degrade below 100% after 1,000 hours in an environment of 85 °C and 85% relative humidity (RH). Therefore, to guarantee maximum quality, longer lifetime and enhanced product yield of the PV units, in-process high resolution and high speed surface inspection for the quality control of the manufacture of large area flexible PV barrier films is needed, and at present do not exist.

Using advanced in-line optical inspection techniques, the presence of the barrier films defects can be detected and the ALD coating process parameters enhanced. However, the current state-of-the-art surface metrology technology being employed by R2R PV manufactures, faces the challenge of speed versus resolution, and the requirements on positioning and stability are very demanding. It is therefore essential to go beyond the current state-of-the-art, which is the main aim of this study.

1.2 Aims

The quality requirements and line speed in the PV manufacturing industry predicate the use of off-line defect detection methods. Therefore to allow real-time defect detection it is

desirable to make use of non-contact optical-based in-line inspection systems, that can measure a wide area barrier films (up to 500 mm width) moving at speeds greater than 1 meters per minute. The current in process defect detection techniques cannot be employed to detect micro (<5 µm) and nano-scale defects such as pinholes, small particles and micro-cracks in the Al_2O_3 barrier layer and they face the challenge of speed versus resolution.

The overall aims of this study are to characterise, classify and determine the PV barrier films defects size-scale that have a negative effect the barrier film functional performance. This will enable the development of an in process (novel) metrology system based on high resolution interferometry capable of detecting surface defects such as pinholes, scratches, or particles down to a lateral size of 3 µm and a vertical resolution of 10 nm over a 500 mm barrier width. This would represent an improvements over the existing state-of-the-art laboratory and in process based metrology technology in terms of measurement speed, range and robustness against environmental disturbances in R2R PV production lines.

1.3 Objectives

The specific objectives of the research are given below in details they include:

- Measuring defect morphology, size-scale, density and distribution over the PV barrier films, using the state of the art laboratory based surface metrology techniques.
- Detailed scanning electron microscopy analysis into the nature of the barrier films defects.
- Detailed atomic force microscopy analysis for the barrier films defects.
- Provide a detailed knowledge of the nature of micro and nano-scale defects, which are responsible for the water vapor ingress into the PV final unit.

- Correlating the defects density and size with the PV barrier layer functional performance.
- Developing a comprehensive defects database which can be used to integrate in-line sensor design in a roll to roll production line.
- Developing a theoretical mathematical model to understand the mechanism of water vapor permeability through the PV barrier films defects.
- Enabling the implementation of an in process defect detection system.
- Implementation and verification of an optical system based on high resolution interferometer in a R2R PV barrier films production lines.
- Preliminary results from in process sensors and in situ performance study.

1.4 Contribution to Knowledge

This thesis seeks to introduce new research strategies for bridging the gap between academia and industry in the field of R2R PV barrier films with respect to the manufacturing processes and quality assurance. The major contribution to knowledge in this thesis can be summarised as the following:

Contribution 1- There has been no published research using quantitative surface metrology techniques, to investigate and catalogue flexible PV barrier film defects; this work addresses this knowledge gap.

Contribution 2- For the first time areal surface parameters have been used to assess barrier topography of ALD coatings for flexible PV substrates defects.

Contribution 3- There has been no published literature dealing with the correlation of defects density with the water vapor transmission rate (WVTR) using advanced surface topography analysis methods, this research seeks to present such a correlation using the latest surface metrology analysis methods.

Contribution 4- The defect quantification method based on the mathematical model is an original contribution and can be beneficial to the industry, providing quick and reliable means of assessing thin film quality for barrier applications.

Contribution 5- The ability to measure and effectively classify the features which are significantly affecting the PV barrier functionality provides novel information to enable automatic detection system to be implemented in situ.

Contribution 6- This thesis reports for the first time on the development and deployment of new (novel) in-line interferometric optical technique based on wavelength scanning interferometry (WSI), for detecting PV barriers defects.

Contribution 7- This thesis provides a new guidance and protocol for assessing large and multiple measurement data sets obtained from an in process optical measurement system.

1.5 Thesis Organisation

This thesis is laid out as follows:

Chapter 2- This chapter reviews the most common types of thin-film materials used to manufacture flexible PV modules, and describes the manufacturing process of thin-film flexible CIGS solar cells based on R2R technology (Flisom AG company, Switzerland). An explanation concerning the encapsulation processes to protect this technology from the general environment conditions, and the applications that can be useful while using this technology have been addressed in this chapter.

Chapter 3- This chapter gives an overview regarding the barrier films requirements of flexible PV modules according to the international electrotechnical commission (IEC) standard. The atomic layer deposition technique which has been used in this study for the barrier films coating purposes has been addressed. This chapter also gives an overview

regarding the measurements of the WVTR for testing the PV barrier films functionality and the other possible techniques to be used for the same purpose. Finally, this chapter ends with the previous conducted work related to defect characterisation of the barrier films and the knowledge gap in this specific area of research.

Chapter 4- This chapter gives an overview regarding the importance of surface metrology in PV industry and gives a deep explanation on the most available metrology techniques (offline and online), with emphasis more on the techniques that were employed extensively in the current study. A brief explanation of the most 3D surface feature parameters or descriptors that have been used to characterise surface defects were also demonstrated in this chapter.

Chapter 5- This chapter introduces the experimental work which has been carried out on the barrier films samples during the study. The developed protocol also covers the strategy of the samples measurements, and the possibility of correlating the defects density, morphology and size-scale with the WVTR using different surface topography analysis methods. Finally, a defect classification system was proposed to allow a unified classification system of defects to be implemented.

Chapter 6- This chapter investigates the pre-coating process effect (substrate cleanliness/ raw material) on the PV barrier film functionality. Also a new method for PV barriers defects characterisation was developed in this chapter, where the presence of the defects was calculated by means of feature segmentation analysis rather than the amplitude parameters. The results in this chapter concur with and confirm chapter 6 results.

Chapter 7- This chapter seeks to present a novel theoretical model approach that has been developed to model the quantity of water vapor permeating through the PV barrier film defects for two cases (single defect case & many defects case). The results of the model have

confirmed the experimental results based on surface topography analysis presented in chapter 5 and 6.

Chapter 8- This chapter reports on the deployment of a new in-line interferometric optical technique based on wavelength scanning interferometry (WSI) for detecting PV barriers defects in situ. In this chapter a comparison study between lab-based metrology techniques (described in chapter 4) and the WSI system was conducted and an in situ performance study was performed to verify the WSI system. Finally, data handling procedures to assess large and multiple measurement data sets obtained from an in process optical instrument is presented.

Chapter 9- This chapter will analyse the overall measurement results that were obtained by each of the techniques (off-line and in-line), followed by overall discussion which will determine the industrial scale up issues.

Chapter 10- The overall conclusion and the recommended future work based on the current study will be addressed in this chapter.

1.6 Publication and Awards

The work in this thesis has produced **6** peer reviewed international journal papers and **23** international conference papers (see appendix A).

CHAPTER 2

2. Flexible Thin Film Photovoltaics

2.1 Introduction.

Due to the limitations of the traditional rigid crystalline silicon photovoltaic (PV) cells, other thin absorber materials have been studied extensively over time. Flexible thin-film materials offer the best option in terms of producing solar cells, where the solar cells require less semiconductor material, therefore the material costs are substantially reduced (Rardin & Xu, 2011). The most acclaimed and most common thin film material for PV cells was consisting of copper indium diselenide, known as CIS (A. Goetzberger, Knobloch, & Voss, 1998). In the early 1978, high efficiencies without degradation were observed, which made this a very important material in the thin film solar industry. Recently, a similar but even more productive combination of copper, indium, gallium and selenium, known as CIGS, has been used (Inslee & Hendricks, 2009).

Thin film PV modules have several advantages over the traditional crystalline rigid silicon cells. The consumption of materials is less because the thicknesses of the active layers are only a few micrometres (Adolf Goetzberger & Hebling, 2000). Thin films PV cells can be deposited by a variety of vacuum and non-vacuum methods on inexpensive substrates such as glass. Also curved and/or flexible substrates such as polymeric sheets can be used, leading to lighter modules (Antony, 2004). The interest in flexible solar cells is steadily increasing, since high altitude platforms would benefit from rollable or foldable solar generators. Cars, aircraft, and various electric appliances could also cover part of their power demand from ambient illumination of their free-form cases (M. B. Schubert & Werner, 2006). Flexible PV thin-film technologies can also offer particular design options for building integrated

applications and have the potential to meet building-integrated PVs product requirements and regulatory requirements (Coonen, 2007).

2.2 Thin film Cells Materials

The high price of Si solar cell compared to thin-film solar cells is one of the main problems for the development of large-scale power-source application of photovoltaic systems. One of the solutions to achieve a reduction in this cost is the development of the thin film solar cell technology, which saves both materials and energy in the production of PV modules (Hamakawa, 2004). Thin film photovoltaics are currently based on three types of materials: amorphous silicon (a-Si), cadmium telluride (CdTe) and copper indium gallium selenide (CIGS). These types of materials have higher light absorptivity than crystalline materials (Hajimirza, 2013).

- **Amorphous Silicon (a-Si).**

Currently, amorphous silicon is the most common form of thin film photovoltaics. It consists of materials in which the atoms are not arranged in any particular order (atoms are disordered in structure). They do not form any crystalline structures, and they contain large numbers of structural and bonding defects. It absorbs solar radiation 40 times more efficiently than single-crystal silicon (Chagant, 2008). Despite the promising economic advantages, a-Si still has two major obstacles to overcome. One is the low cell energy conversion efficiency, ranging between 5-9%, and the other is the outdoor reliability problem in which the efficiency degrades within a few months of exposure to sunlight (Mah, 1998).

- **Cadmium Telluride (CdTe).**

This is a polycrystalline semiconductor compound made of cadmium (Cd) and tellurium (Te); it has a high light absorptivity level, where a micrometre thick compound can absorb 90% of the solar spectrum (Mah, 1998). CdTe thin films are currently receiving considerable

attention in PV technology since CdTe has the advantage of a direct band gap, which matches well with the solar spectrum (Sajeesh, 2013). CdTe solar cells have efficiency between 10% - 12% and hold the promise of low cost production (Bonnet & Meyers, 1998). However, the toxicity and availability of raw materials are the main drawbacks of this technology (Drygała & Dobrzański, 2003).

- **Copper Indium Gallium di-Selenide (CIGS).**

Cu (InGa) Se is a semiconductor material composed of copper, indium, gallium, and selenium. It has a chemical formula of $Cu\ In_x\ Ga_{(1-x)}\ Se_2$, where the value of x can vary from 1 (pure Copper Indium Selenide) to 0 (pure Copper Gallium Selenide) (A. Ruanthon, Thanachayanont, & Sarakonsri, 2013). It is a polycrystalline material which has the crystal structure, and because of the high absorption coefficient (10^5 cm^{-1}) a thin layer of 2 µm is sufficient to absorb the useful part of the spectrum (Harati et al., 2010). This material has yielded the highest conversion efficiency among all thin-film technologies, where an efficiency of 19.9% was obtained in a laboratory environment (Repins et al., 2008).

In the case of crystalline Si (indirect band semiconductor), the cell thickness required to absorb incident light is very large (100-200 µm), while in the case of thin-film solar cells (direct band semiconductor), a thickness of only 1-2 µm is required (Shirolikar, 2005) offering potential for significantly reduced material costs over conventional silicon solar cells. These materials help to make the mass production of solar cells more of a reality, and since CIGS can potentially have similar efficiencies to traditional cells, about 19.5% (Contreras, et al., 2005), this make it as one of the most promising new PV technologies. CIGS solar cells are prepared from a number of micrometer thin layers, each layer with specific thickness ranging from 0.15-1.8 µm (Movla, 2014), and every layer has its own function and features, where CIGS is just one of those layers. However, it is the most important one as it is the absorber layer (p-type material) (Saji, Choi, & Lee, 2011).

All the previously described thin-film technologies have their own advantages and disadvantages; table [2-1] compares the advantages and disadvantages of these technologies, where PV modules based on CIGS material have the highest demonstrated conversion efficiency. However, the manufacturing costs of CIGS cells have been traditionally high.

Table 2-1: Advantages and disadvantages of thin-film PV technologies (Tiwari et al., 2013).

Material	Maximum PV Efficiency in lab conditions	Advantages	Disadvantages	Cost/m^2
a-Si	14.6 %	▪ Mature manufacturing technology	▪ Low efficiency ▪ High equipment costs	High
CdTe	16.5 %	▪ Low-cost manufacturing	▪ Medium efficiency ▪ Rigid glass substrate	Low
CIGS	19.5 %	▪ High efficiency ▪ Glass or flexible substrates	▪ Film uniformity challenge on large substrates ▪ More costly than traditional processes	High

*Efficiencies are measured on small $1cm^2$ specimens under controlled conditions (real efficiencies are lower).

To sum up, although crystalline silicon materials have been the workhorse of the PV cells for the past two decades, recent progress in the thin-film technologies has led many industrial experts to believe that thin-films PV cells will eventually dominate the marketplace, and realise the goals of PV for a low price and reliable source of energy supply. CIGS thin-film solar cells have been considered to be the most promising alternatives to crystalline silicon solar cells because of their high solar to electricity conversion efficiency, reliability, stability and many application possibilities.

2.3 Structure of CIGS Solar Cells

The basic device structure of any solar cell consists of the following layers; substrate, window layer, active layer and the contacts to the external circuits (Antony, 2004). The basic structure of CIGS solar cells prior to the final encapsulation consists of five layers, and it can

be described based on Fig [2-1]. CIGS films are deposited onto substrates that have been metallised with Molybdenum (Mo) as a back contact to collect electric current. A thin buffer layer of Cadmium Sulfide (CdS) is deposited onto the absorber film, forming a junction between a p-type semiconductor (CIGS) and an n-type CdS layer. A transparent conductive window layer typically doped with zinc oxide (ZnO) forms the top contact of the device, resulting in a complete CIGS solar cell.

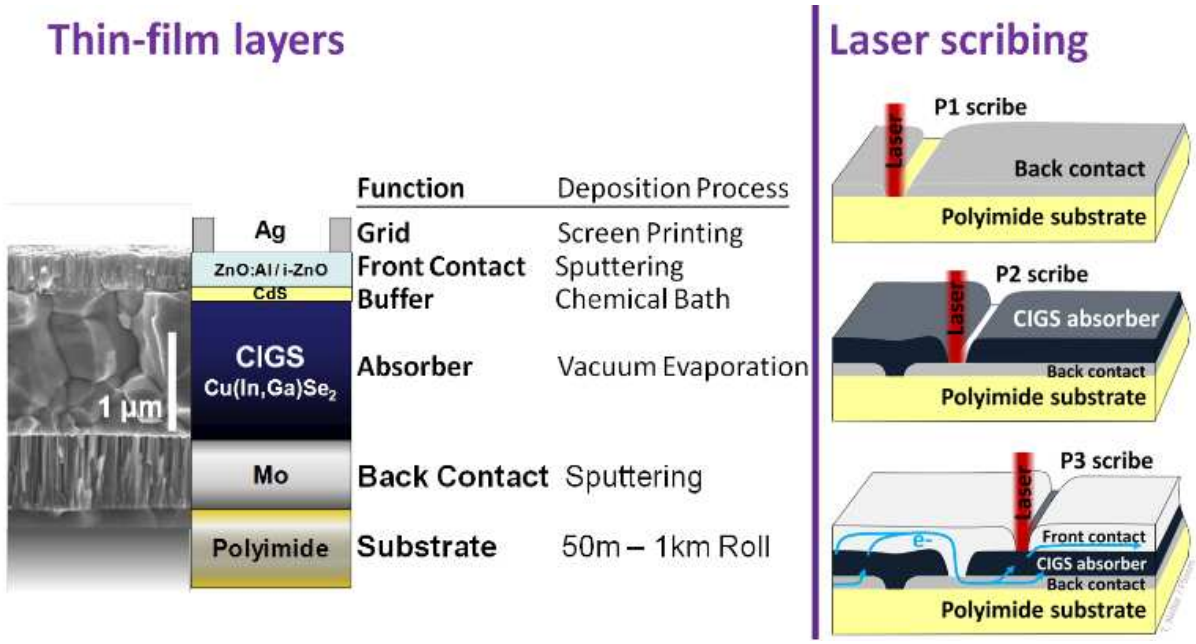

Figure 2-1: Structure of CIGS solar cells (Courtesy of Flisom, Switzerland).

As light passes through the ZnO and CdS layers, it is absorbed by the CIGS, creating electron-hole pairs. An electric field created at the CIGS/CdS junction draws negatively charged electrons to the ZnO layer, which generates a flow of positive charges in the opposite direction, producing an electric current. CIGS solar cells can be fabricated on both rigid and flexible substrates, adding to their desirability as the next generation photovoltaic material of choice. When properly sealed and laminated, CIGS modules can deliver stable performance while withstanding exposure to the elements, as well as direct solar radiation for over 20 years in the field (Brémaud, 2009).

CIGS PV modules technology offers significant advantages in terms of mass and the possibility of building integration (BIPV) applications (James et al., 2011), however, they are at present highly susceptible to long term environmental degradation as a result of water vapour permeation through the protective barrier layers to the CIGS PV cells, thus causing electrical shorts, efficiency drops and ultimately failure

2.4 Flexible Thin Film CIGS Solar Cells Manufacturing Process

Copper-indium-gallium-(di)-selenide (CIGS) semi-conductors comprise thin-film solar cells. Thanks to the high degree of light absorption, these solar cells are only two to ten micrometers thick prior to the final encapsulation. A roll-to-roll (R2R) process is used to apply the semi-conductors onto a polymer sheet. Fig [2-2] shows the R2R process to produce CIGS PV modules as applied by Flisom AG Company (Switzerland).

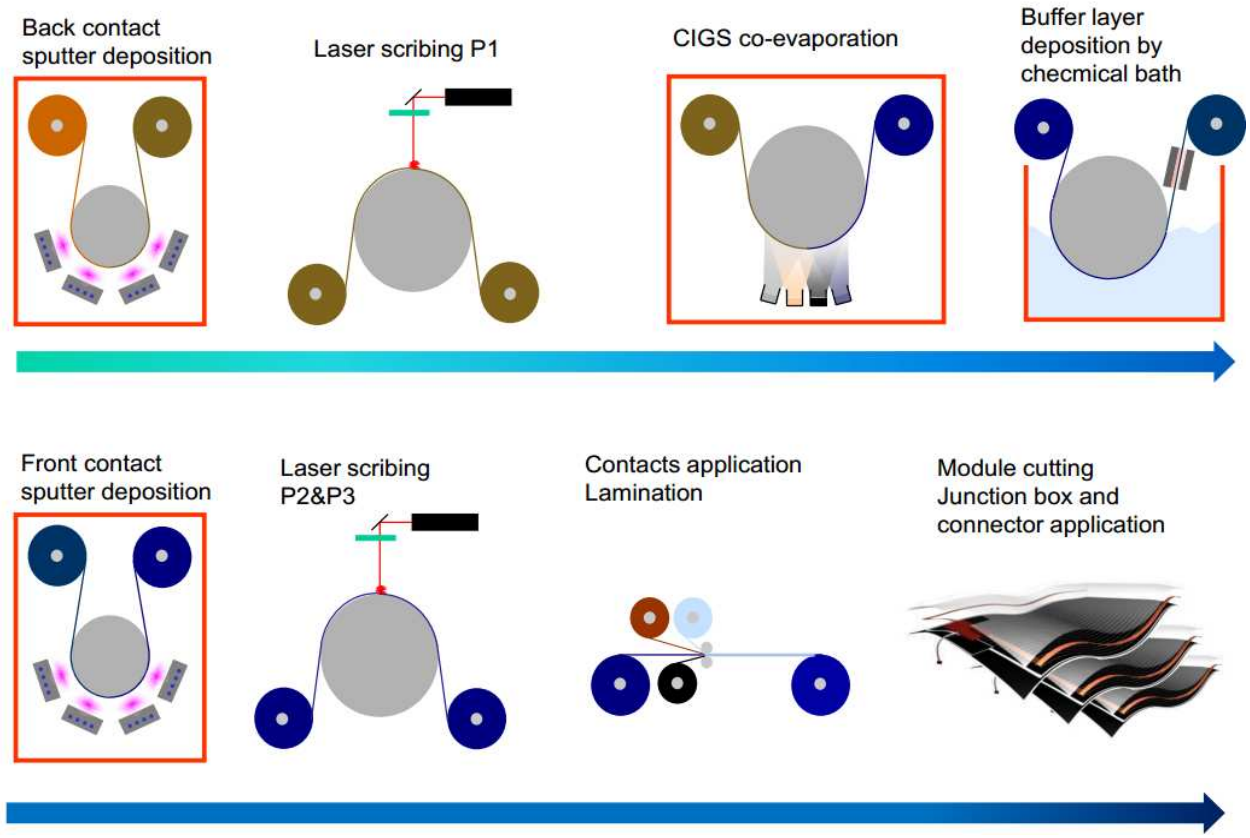

Figure 2-2: Roll-to-roll manufacturing process of CIGS solar modules (Courtesy of Flisom, Switzerland)

The roll-to-roll process comprises the following sequence of material deposition and laser scribing steps as shown in Fig [2-2]. Firstly, a very thin foil, or web of polyimide is progressively unrolled inside a vacuum chamber; then a metallic layer (Molybdenum) is sputter coated onto the web to create the back contact of the solar cell. The most common method used to deposit the Molybdenum is sputtering, especially in high volume manufacturing environments. After the coated web leaves the vacuum chamber, it passes over a laser that scribes lines (P1 scribe) into the metallic layer, which delineate the individual solar cell back-contacts. The laser is CNC controlled to give the desired cell size.

Secondly, the web enters a second vacuum chamber in which the four CIGS semi-conducting absorber layers—namely, copper (Cu), indium (In), gallium (Ga), and selenide (Se) are deposited. This layer can be manufactured by several different methods: The most common method is the vacuum-based process. The procedure in this technique is to co-evaporate or co-sputter copper, gallium, and indium onto a substrate at room temperature, then anneal the resulting film with a selenide vapour to form the final CIGS structure. Following these processes, a transparent buffer layer (CdS) is then deposited onto the CIGS layer using chemical-bath deposition (CBD) method in order to form a semi-conducting junction. The final web then passes over a further laser scribe line (P2 scribe), which delineates the individual solar cells' semiconductor components.

Thirdly, the web enters another vacuum chamber in which the front-contact layer is sputtered with a transparent conductive oxide (TCO). The web then passes over a laser scribe line (P3 scribe), which delineates the components on the front-contact layer, thereby creating the monolithically interconnected solar cells of a solar module. The final stage includes the application of the electrical front contact grids, electrical busbars, and protective lamination, before being rolled up for easy transportation and application of barrier layers.

2.5 Encapsulation

To ensure long-term performance and stability of the CIGS solar modules, encapsulation is required to prevent penetration of water vapour and oxygen into the device (G. Dennler et al., 2006). CIGS solar cells and their device components, including Mo and ZnO contact grid, have been shown to be damp heat (DH) sensitive or unstable (F. J. Pern & Noufi, 2011). The DH-induced degradation of Al-doped ZnO (Al: ZO) conductive window layer was reported to be a performance-limiting factor for CIGS mini-modules (F.-J. Pern & Noufi, 2012). Without any protection the solar module would degrade rapidly, mostly because of conductivity losses in front contacts and interconnections, since the electronic properties of ZnO: Al are sensitive to moisture and Mo, like any other metal contact can corrode and cause electrical shorts (Wennerberg, Kessler, & Stolt, 2003).

Flexible encapsulants consist of multi-layer combinations of polymer and inorganic dielectric layers such as SiOx or AlOx as shown in Fig [2-3]. Typically, used polymers are polyethylene naphthalate (PEN) or polyethylene terephthalate (PET).

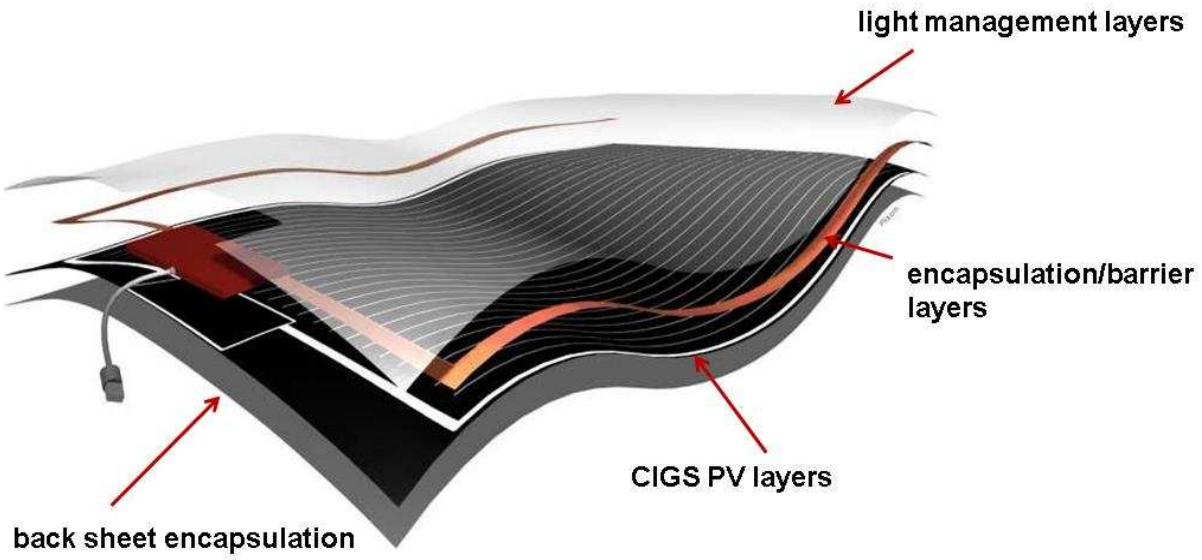

Figure 2-3: CIGS solar module encapsulation sheets (Source: Flisom).

A complete PV sheet consists of several layer groups as shown in Fig [2-3], i) back sheet encapsulation ii) the active CIGS layer iii) front transparent encapsulation iv) light management layer (optional). The overall thickness of the completed PV module after encapsulation is around 1.5 to 2 mm (Flisom AG, Switzerland).

At the present time no cost effective, flexible transparent encapsulation products can fulfil the flexible PV modules requirements. The water vapour transmission rate (WVTR) of present products is in the range of 10^{-1} g/m^2/day, while it should not be higher than 10^{-4} g/m^2/day to assure life-times of 20 years and more (M. D. Kempe, 2005; Müller, 2004). Several companies are currently working on this topic and have announced suitable products for availability soon, but they still have difficulties to adapt them to roll-to-roll process as shown in Fig [2-4].

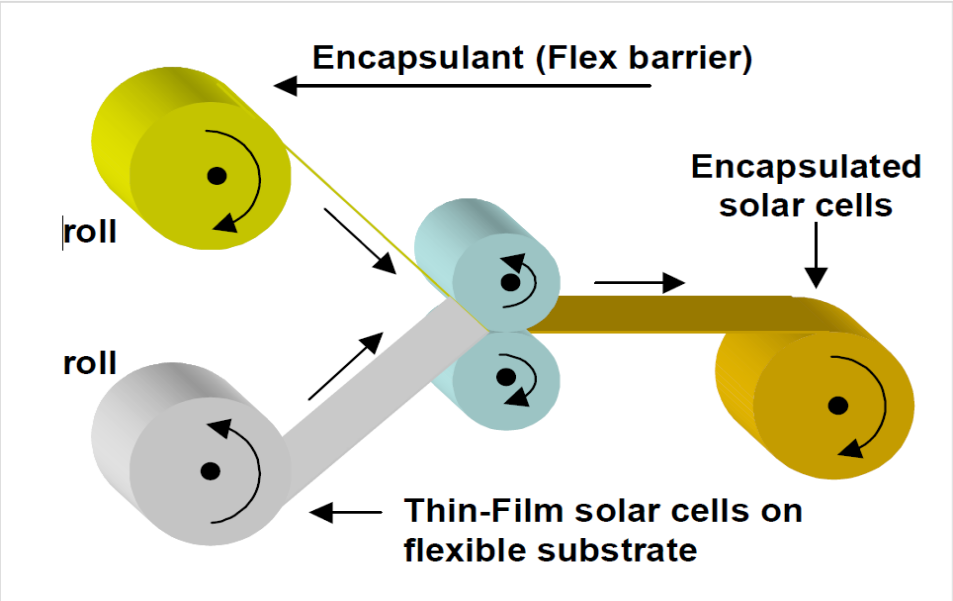

Figure 2-4: Roll-to-roll encapsulation process for flexible PV modules
(Source: http://www.flexonics.org/)

2.6 Applications

Cu (In, Ga) Se_2 (CIGS) solar cells on flexible substrates offer several advantages for their manufacturing as well as applications compared to solar cells on rigid glass substrates and/or Si-based solar cells. They are lightweight, can be applied on uneven surfaces and can be

rolled-up when not in use. From the industrial production point of view, manufacturing of flexible solar modules with a roll-to-roll deposition process offers considerable potential for cost effective solar modules. Not only will the mass production of flexible CIGS modules improve with inline roll-to-roll machines, but also other issues like shipments and installations will be easier, thanks to the light weight of the modules. However, roll-to-roll manufacturing equipment for CIGS deposition are neither well-developed nor easily available (Brémaud, 2009). A flexible solar module process enables the custom design of photovoltaic modules of various sizes and electrical characteristics for a large number of applications, this may include;

- Building-Integrated Photovoltaic (BIPV) on roofs and frontages.
- Mobile devices such as mobile phones, laptops and bags.
- Vehicles such as cars and ships.
- Easy to fit to curved or flexible surfaces.

Figure 2- 5: Flexible (CIGS) solar cell applications (Source: Flisom).

2.7 Summary

Roll-to-roll production and encapsulation processes of CIGS PV modules is less capital intensive, requires less energy, minimises material usage and is very efficient method

(Zweibel, 1999) . This way of production and encapsulation dramatically reduces the energy payback time of the photovoltaic system. However, long-term performance reliability of thin-film CIGS modules remains an important issue due to a considerably high failure rate, particularly during the strenuous damp heat (DH) exposure tests.

Undoubtedly, with the existence of flexible PV modules the future for solar PV electricity generation looks optimistic and very significant; it is also likely to be a growth market for the solar cell manufacturers as well as the equipment, instrumentation and quality assurance companies to support the PV modules production. Finally, the ability to provide a solution to the long term environmental degradation issue for this type of PV modules on a routine basis is the key to a reliable flexible PV solar cell products. More research is needed if this problem of degradation is to be overcome and this work constitutes the basis of this thesis.

CHAPTER 3

3. PV Barrier Layer Requirements

3.1. Introduction

For many years, one of the long-term goals of photovoltaic (PV) researchers has been to promote the development of cost-effective PV modules which have more than twenty years of usable, working life. Significant progress has been made (King, Quintana, Kratochvil, Ellibee, & Hansen, 2000; Ross Jr, 1984a, 1984b), but additional research is still required and manufacturers will have to establish rigorous quality control standards in order to achieve this long-term goal for scaled up manufacture. Lifetime improvement and prediction of the PV modules requires detailed information on the degradation mechanisms which are at play in the field and in accelerated aging tests (Carlsson, 2006).

The lifetime of CIGS solar cells has always been one of the most important issues because it is critically influenced by moisture permeating through small defects that appear in the coatings of the barrier films (K.-D. Kim, Shin, & Chang, 2012; J. S. Lewis & Weaver, 2004; Ramadas & Shanmugavel, 2012; Su et al., 2014). Therefore, the cells must be effectively encapsulated in order to satisfy the international standard (IEC61646-2, 2008) which requires that the efficiency does not degrade below 100% of starting efficiency after 1,000 hours in an environment of 85 °C and 85% relative humidity (P. F. Carcia et al., 2010). For applications in which PV modules are used in harsh environments, the barrier film is required to withstand high humidity and temperature or aqueous environments. A WVTR of ~10^{-1} g/m^2/day is sufficient for most packaging applications, but $\leq 10^{-6}$ g/m^2/day is ideally required for encapsulation of long-life flexible PV modules as shown in Fig [3-1]. To achieve a lifetime of

10,000 hours, the estimated WVTR should be around 10^{-6} g/m^2/day and the OTR should be around 10^{-3} cm^3/m^2/day at room temperature (IEC61646-2, 2008).

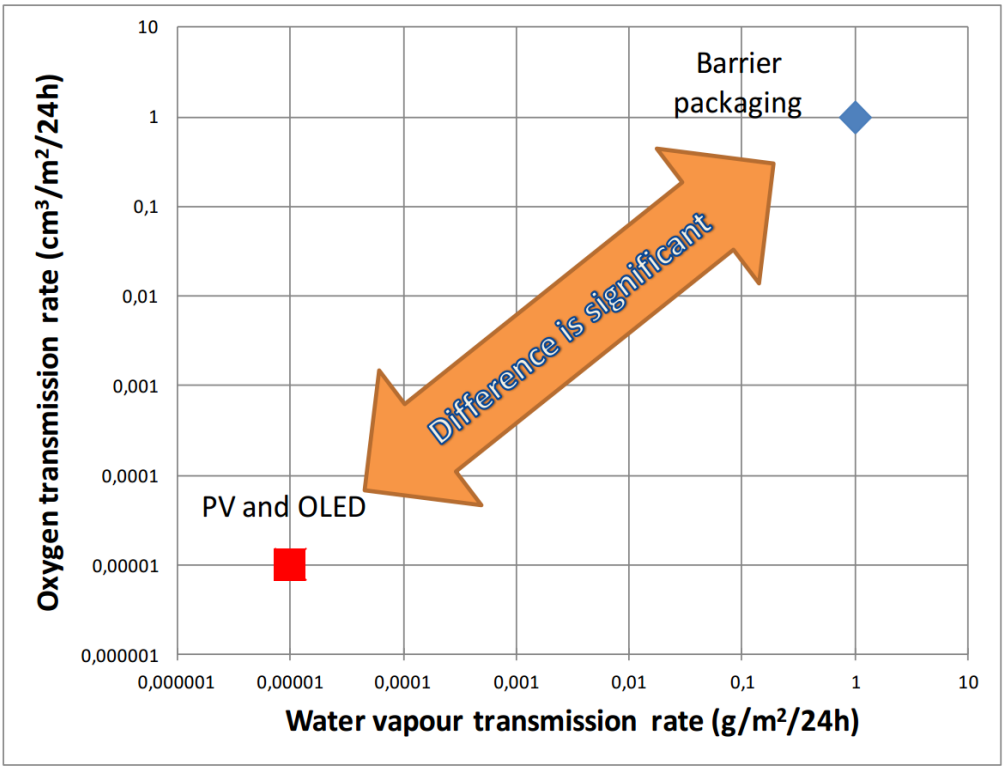

Figure 3-1: OTR versus WVTR requirements for different applications: Adapted from (G Dennler, Lungenschmied, Neugebauer, Sariciftci, & Labouret, 2005)

One solution to overcome the moisture problem and to satisfy the IEC61646-2 requirements is to encapsulate CIGS cells within defect free flexible barrier films, in order to achieve a lifetime of at least 20 years (P. F. Carcia et al., 2010).

3.2 Environmental Degradation of CIGS PV Modules

Cost-effective encapsulation which facilitates stable outdoor performance lasting more than twenty years is still a challenge. Some progress has been made for encapsulation (Brémaud, 2009; Czanderna & Pern, 1996; Peike, Hädrich, Weiß, & Dürr, 2013), but reliable and transparent encapsulation suitable for building applications still remains a challenge in terms of long term stability and cost effectiveness. The only cost-effective encapsulation possibility

for long-term stability currently available is the use of rigid glass. However, all benefits of flexibility and light weight disappear (Brémaud, 2009). Therefore, a robust, transparent, flexible encapsulation method for CIGS PV cells is needed. Meeting these requirements is a major concern for the manufacture of thin film CIGS cells. Different insulating materials as shown in table [3-1] can be used as a barrier films for the CIGS PV modules e.g. S_iO_x, T_iO_2 and Al_2O_3 (Kessler & Rudmann, 2004).

Table 3-1: Overview of common single layer permeation barrier techniques (Fahlteich, 2014)

Technology	**Widely used materials**	**WVTR range 38 °C/90% RH [g/(m^2.day)]**	**Typical layer thickness [nm]**	**Productivity (web speed or deposition rate) [m/min]**
Thermal or electron beam evaporation	AlO_x, S_iO_x	> 0.5 on PET	5…20	≈ 600
(Reactive)sputtering	Al_2O_3, SiO_2, Zn_2SnO_4	0.01on PET 0.001 on PEN	40…200	≈ 1
Plasma assisted chemical vapour deposition (PECVD)	S_iO_2, Si_3N_4, $S_iO_xN_y$	$< 10^{-3}$ 1	100…1000	≈ 1…0.1
Atomic layer deposition	Al_2O_3, TiO_2	$< 10^{-3}$	10…25	0.1 nm/cycle

The thermal silicon oxide (SiO_2) is a very good surface passivation material for flexible PV modules. However, the formation of thermal SiO_2 requires a high-temperature process (>1000 °C) which does not only increase the processing cost, but may also degrade the quality of the PV module (Kotipalli et al., 2013). Therefore, passivation materials that can be deposited at low temperatures are required. Al_2O_3 barrier material deposited by atomic layer deposition (ALD) technique with only few nanometers thickness are able to reduce the water vapour transmission rate to 10^{-3} g/m^2/day (M. D. Groner et al., 2006; Langereis, Creatore, Heil, Van de Sanden, & Kessels, 2006) or even lower (Carcia, McLean, Reilly, Groner, & George, 2006). The Al_2O_3 requires lower temperature than SiOx to be deposited on a polymer substrate (M. Groner, Fabreguette, Elam, & George, 2004).

Table [3-2] shows the properties of the insulating layers that can be used to prevent the water vapour ingress to the PV module. In order to not encounter delamination and adhesion problems, the substrate material should be chosen so that the coefficient of thermal expansion (CTE) lies in the range of the CTE of insulating layer, since the sample has to go through some changes in temperature during the ALD deposition process of the barrier layer.

Table 3-2: Properties of substrate and solar cells materials: Coefficient of thermal expansion (CTE) and density (Kessler & Rudmann, 2004)

Materials	**CTE [10^{-6} K^{-1}]**	**Density [g/cm^3]**
Substrates		
SLG	9	2.5
Steel	11-16	7.8
Ti	8.6	4.5
Al	23.1	2.7
Polyimide	12-24	1.5
Insulating layers		
S_iO_x	1-9	2.2-2.7
Al_2O_3	6-8	3.9
Solar cell layers		
Mo	4.8	10.2
CIGS	8-11	5.9
CdS	4.5	4.8
ZnO	4.75-2.9	5.6

More studies regarding the encapsulation technologies for CIGS cells have been carried out by (S.-H. K. Park et al., 2005). The authors reported a water vapor transmission rate of 0.03 g/m^2/day at 38 °C and 100% relative humidity for an ALD grown Al_2O_3 barrier that was 30 nm thick and deposited on both sides of a Polyethersulfone (PES) substrate. Conversely, Carcia et al. (2006) showed that 25 nm thick Al_2O_3 barrier films on poly (ethylene naphthalene) substrates can have a water vapor transmission rate of less than 1×10^{-5} g/m^2/day.

Furthermore, Carcia et al.(2010) compared the moisture sensitivity of CIGS cells protected by a 55 nm thick Al_2O_3 film deposited by the ALD technique, with equivalent CIGS cells protected with a glass layer, and one protected with an uncoated Polyethylene Terephthalate

(PET) film. This study of the three CIGS modules lasted for more than 1000 hours at 85 °C and 85 % RH with simulated solar illumination this in accordance to IEC61646-2 as shown in Fig [3-3].

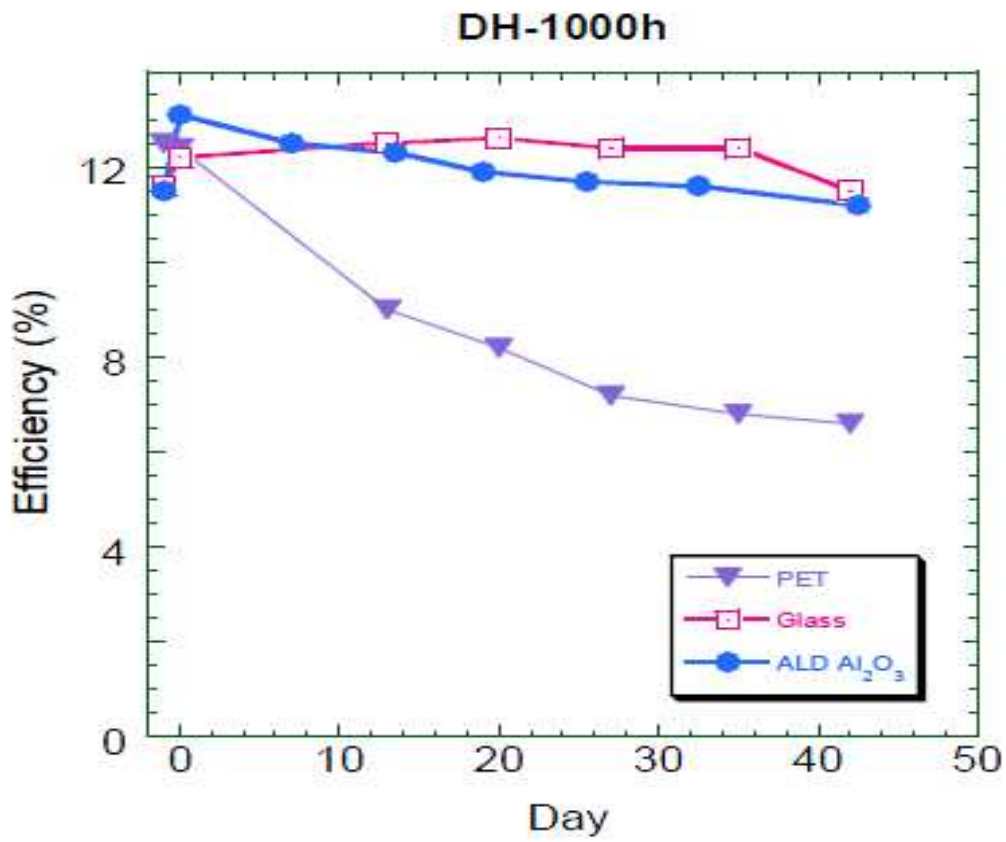

Figure 3-2: The relationship between CIGS efficiency and different barrier films (P. F. Carcia et al., 2010).

The results of the simulation test indicated that the CIGS cell when protected with the PET layer lost about half its efficiency (12.5 % → 6.6 %) after aging for 1020 h (42.5 days) at 85 °C and 85 % RH, whereas the CIGS cell protected with the 55 nm ALD Al_2O_3 barrier film and the cell with a glass layer showed only a small net change (< 3%) in efficiency as shown in Fig [3-2]. The loss in cell performance with a PET lid is very similar to the results reported by Schmidt et al. (2000) for non-encapsulated CIGS cells.

This remaining degradation in efficiency is considered to be mainly due to the presence of small defects (defect propagation) on the barrier film during ALD growth (A. Erlat et al., 1999). The ALD Al_2O_3 thin barrier film provided superior moisture protection for the CIGS cell compared to PET plastic film. In other words, no reduction in open circuit voltage or fill factor occurred in ALD Al_2O_3 thin film protected cells when compared to the PET protected cells (P. F. Carcia et al., 2010).

3.3 Selection of PV Barrier Film Materials

Aluminum oxide (Al_2O_3) films deposited through atomic layer deposition (ALD) are known to be effective permeation barriers due to their uniformity and assumed pinhole-free morphology. Studies regarding the selection of the encapsulation materials for PV modules have indicated that Al_2O_3 contains a very high density (up to 10^{13} cm^{-3}) of negative charges (n-type) which makes the material unique for CIGS (p-type) surface passivation (Hoex, Gielis, Van de Sanden, & Kessels, 2008; Kotipalli et al., 2013).

Moreover, several groups have recently reported excellent barrier properties for polymeric substrates coated with a thin layer of Al_2O_3 ALD. For example, Hegedus et al. (2010) studied two configurations; one where the Al_2O_3 was deposited directly on the substrate, and the other where it was deposited onto a flexible Ultraviolet Polyethylene Terephthalate (UV-PET) and laminated on to the substrate. The authors exposed samples with ALD barrier, and other barriers for comparison by accelerated degradation tests including 1000 hr. damp-heat, 1200 hour Ultra Violet (UV) and 10 freeze-thaw cycles. The authors proved that the ALD coating on Polyethylene naphthalate (PEN) (5 mm thick) polymer can reduce WVTR from ~1 g/m^2-day for the bare polymer to ~ $6x10^{-6}$ g/m^2-day at room temperature. Consequently, these ALD diffusion barrier films are very attractive as PV encapsulation layers to meet and satisfy the international standard (IEC 61646-2).

3.4. Barrier Film Properties

Polymer materials such as polyethylene naphthalate (PEN) or/ and polyethylene terephthalate (PET) consist of long straight-chain polymer molecules with weak chemical interaction between the chains (Hotchkiss, 1997). Therefore, small molecules such as water vapor and oxygen can diffuse around the polymer chains. The molecular building block for PEN and PET chains is shown in Fig [3-3].

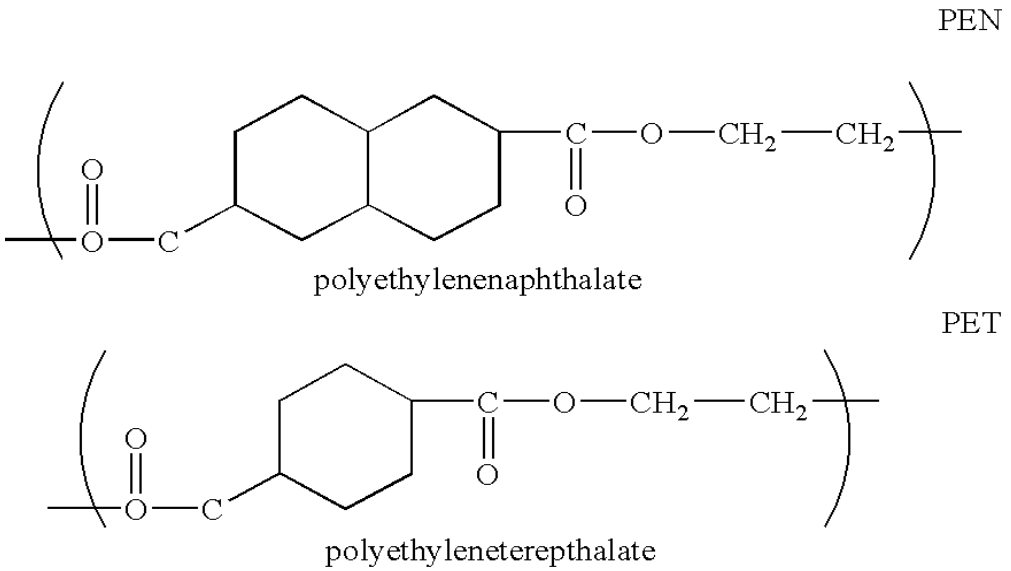

Figure 3-3: Structure of Polyethylene Naphthalate (PEN) and polyethylene terephthalate (PET) (Hansen, Myers, & Osakada, 1998)

Although polymers have strong covalent bonds (short range) along the chains, they have weaker (long range) bonding between chains (Ayache, Beaunier, Boumendil, Ehret, & Laub, 2010).The spaces between chains where there are no atoms make it easy for gas molecules to dissolve and diffuse in the PEN/PET layer. In addition, these spaces make the density of the polymer relatively low. In contrast 'ceramic' materials such as AlO_x and SiO_x are crystalline lattices with strong inter-atomic and inter-molecular bonds (Kailas, 2006), see Fig [3-4].

The bonding between atoms in ceramics is a combination of short range ionic and covalent bonding. Even for amorphous ceramics there is a high instance of short range ordering in three

dimensions, so there are few spaces between atoms for gas molecules to dissolve and diffuse. The tight packing makes for high density, depending of course on the atomic weights of the constituent atoms.

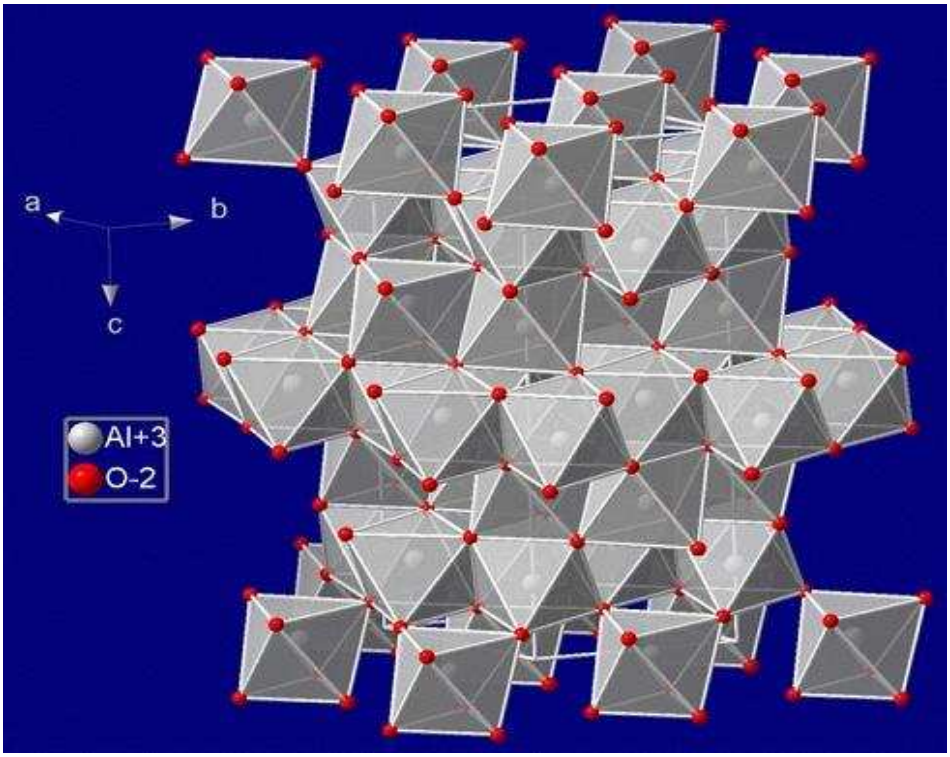

Figure 3-4: Structure of Al_2O_3 ("Blue Sapphire" Retrieved from webexhibits.com)

Although in an amorphous ceramic material such as Al_2O_3 the ordering of atoms over a long range is lower than for the crystalline material (a less regular lattice structure) (Carter & Norton, 2007), the ALD AlO_x is still an effective barrier material to protect CIGS PV modules from water vapor and oxygen ingress.

3.5 Cu (In, Ga) Se_2 Surface Coating

Nowadays, the following basic set of properties are basically required for CIGS solar cells coating materials to ensure PV devices durability: UV, oxygen and water barrier (Morlier, Cros, Garandet, & Alberola, 2013); thermal stability, transparency, anti-reflectance (Lu et al., 2011), anti-soiling, flexibility, durability, affordable cost, electrical isolation (Frach,

Bartzsch, Glöß, Fahland, & Händel, 2008). Some of these properties are competitive ones, for instance, high barrier properties may be achieved by increasing the number of coating layers (Logothetidis et al., 2010). However, a higher number of layers normally increases the cost and reduces the coating transparency and flexibility (Erler et al., 2003).

Moreover, Smith et al. (2014) indicate that the multi-layer approach only introduces a 'lag time' for equivalent thick barrier layers as shown in Fig [3-5]. With the requirements of 25 years for BIPV applications, the 'lag time' effect may not be sufficient; the preferred solution being an ultra-barrier single layer, ideally as thin as possible to allow flexibility without cracking and allowing higher line-speed production to be achieved. In order to maintain a high efficiency during their lifetime, solar cells require coating materials with several functions that are usually achieved with multilayer coatings (VaÅ, Noller, Mikula, Amberg-Schwab, & Weber, 2009), in which one or more layer have a specific functionality, such as gas and moisture barrier (Jorgensen et al., 2006; Langereis et al., 2006), liquid barrier and self-cleaning properties (Karunakaran, Lu, Zhang, & Yang, 2011).

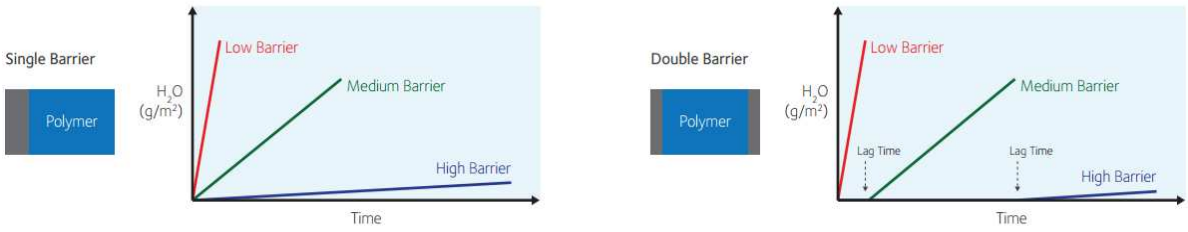

Figure 3-5: Schematic moisture permeation diagram (Smith et al., 2014)

A reduction of the number of layers would lower costs and also help to maintain a high transparency and flexibility. Carcia et al.(2010) argue that Al_2O_3 barrier coating of $\leq$ 50 nm thickness grown by ALD has a great potential for extending the lifetime of flexible CIGS solar cells by preventing degradation of the cells by moisture. The authors also proved that thin ALD Al_2O_3 coated on polymer substrates reduces moisture permeation by a factor of at

least 100,000×, corresponding to a water vapor transmission rate (WVTR) of 5×10^{-6} g-H_2O/m^2/day at room temperature, hence Al_2O_3 should protect CIGS cells sufficiently.

3.6 Atomic Layer Deposition (ALD)

Atomic Layer Deposition (ALD) is a controlled layer-by-layer deposition technique that enables the deposition of thin, smooth, and conformal films with atomic layer precision (S. M. George, 2009). This technology is able to meet the needs for atomic layer control and conformal deposition using sequential, self-limiting surface reactions. The resultant ALD films are highly conformal and their functional thickness can be as low as a few nanometers (Dingemans & Kessels, 2012). These outstanding properties can be employed to face processing challenges for various types of next-generation solar cells; hence, ALD for flexible PV modules has attracted great interest in academic and industrial research in recent years (Van Delft, Garcia-Alonso, & Kessels, 2012). As the barrier coating for the CIGS modules must be pinhole-free and defect-free, a barrier coating of Al_2O_3 grown by atomic layer deposition (ALD) is deemed to be crucial.

3.6.1 The Advantages of ALD

Due to the actual mechanism used to deposit films, ALD has several advantages over the other chemical and physical deposition techniques. The main advantages of the ALD are the extreme degree of conformality and uniformity which can be obtained regardless of the orientation or shape of the substrate; there are nearly no pinholes in the film (Johansson et al., 2010). ALD is also relatively effective at coating ultra-high aspect ratio substrates or substrates that would be difficult to coat with other thin film techniques. The following are the critical advantages of ALD technique according to Oxford Instrument report in 2011.

- Complete control over the deposition process is achieved at a nanometer scale.

- Conformal coating can be achieved even in high aspect ratio and complex structures.
- Pin-hole and particle free deposition is achieved.
- Excellent process control with wafer-to-wafer repeatability < ±1%.
- Up to 200 mm wafer with typical uniformity < ±2%.
- Effective step coverage even inside high aspect ratio structures.
- Low film impurities, particularly with plasma ALD.
- Growth at room temperature 25 ºC possible with plasma ALD.

3.6.2 Atomic Layer Deposition Approaches

The actual ALD coating consists of several reaction cycles. One reaction cycle is able to achieve about 0.1 nm layer thickness depending on the coating material and process parameters (Lahtinen et al., 2012). The thickness of a typical ALD coating is determined by the number of cycles and varies roughly from 1 to 100 nm. The temperature in the chamber can vary from room temperature to several hundreds of degrees Celsius. The role of temperature is to provide activation energy for the ALD process (thermal ALD). The reaction can also be activated using plasma (plasma-assisted ALD). Plasma-assisted ALD provides lower cycle periods and process temperatures for the system than thermal ALD (Johansson et al., 2010). ALD processing techniques can be divided into two types regarding substrate handling: batch and continuous processes (Putkonen, 2011).

3.6.2.1 Batch ALD Process

The batch process is a traditional technique in which the substrate to be coated remains stationary and the precursors are pulsed in turn onto the surface of the substrate. The actual coating process occurs in a modular chamber, which is filled with substrates. In a chamber, the substrates can be located close to each other because the precursor are able to penetrate into extremely small holes. Fig [3-6] shows a typical equipment used for batch ALD processing.

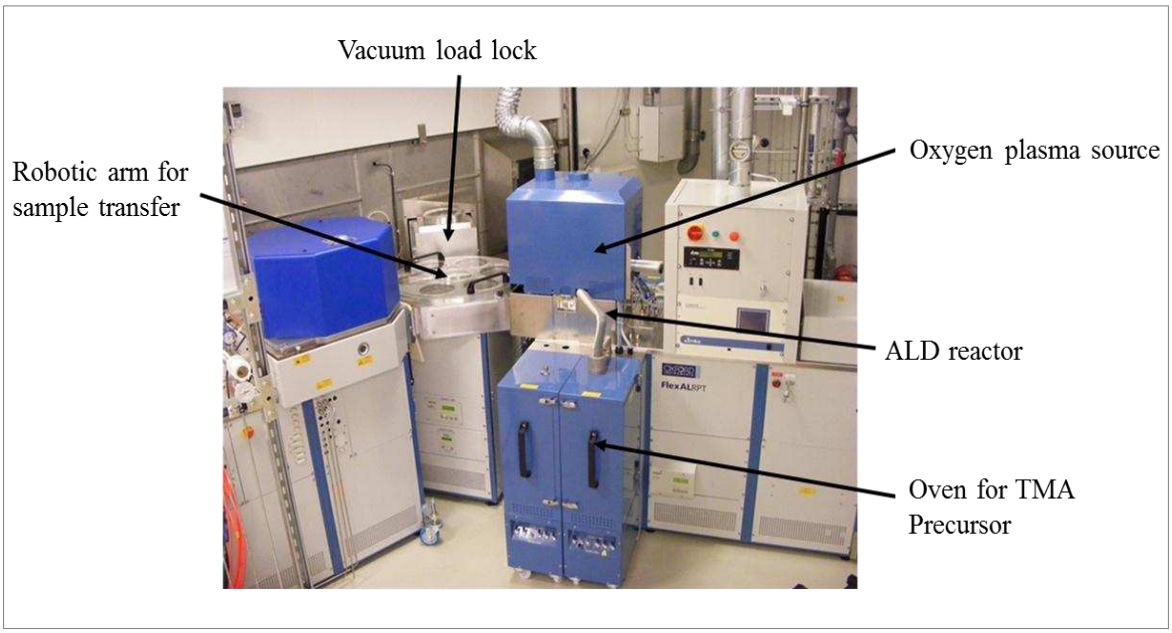

Figure 3-6: Vacuum Coating: Newcastle Oxford Instruments cluster tool for ALD/ sputter deposition

3.6.2.2 Continuous ALD Process

Since barrier layers are required to avoid the diffusion of the water vapor and/or oxygen through polymers for CIGS solar modules, and large-scale area need to be encapsulated, the ability to do roll-to-roll (R2R) coating instead of batch and continuous processes shown in Fig [3-7] would open huge possibilities for the technique to produce a huge amount of the barrier films in a short time with high quality.

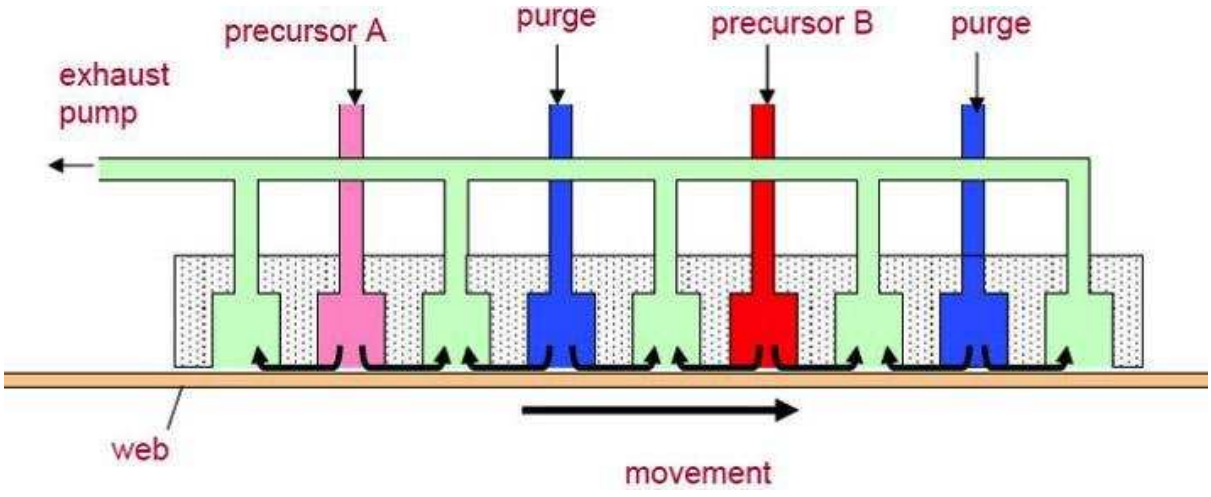

Figure 3-7: Schematic of continues ALD process (Johansson et al., 2010)

A schematic roll-to-roll ALD reactor being used in PV industry to produce large quantity of barrier material is shown in Fig [3-8]. This method demonstrated that a thin Al_2O_3 layer enhances the barrier performance as much as does the Al_2O_3 layer fabricated with the batch ALD process (Hirvikorpi et al., 2014).

Figure 3-8: Worlds first industrial scale R2R ALD machine WCS 500 (Soininen, 2013)

A typical ALD cycle conducted on a substrate functionalised with reactive surface consists of repeating the following characteristic four stages as shown in Fig [3-9]. The cycle starts by introducing the first precursor into the chamber which is flushed in the second stage (the chamber temperature can vary from room temperature to several hundreds of degrees Celsius). Then, another precursor is fed in and flushed, completing the four stages. After the complete reaction cycle, one atomic layer of desired coating is chemically bonded to the substrate surface. Each reaction cycle adds amounts of material to the substrate surface and the result is a surface saturated with up to a monolayer of the desired compound. Sequential

repetition of the ALD cycle results in layer-by-layer growth with precise control of the deposition thickness. Thus, to grow a material layer, cycles are repeated as many times as required for the desired thickness.

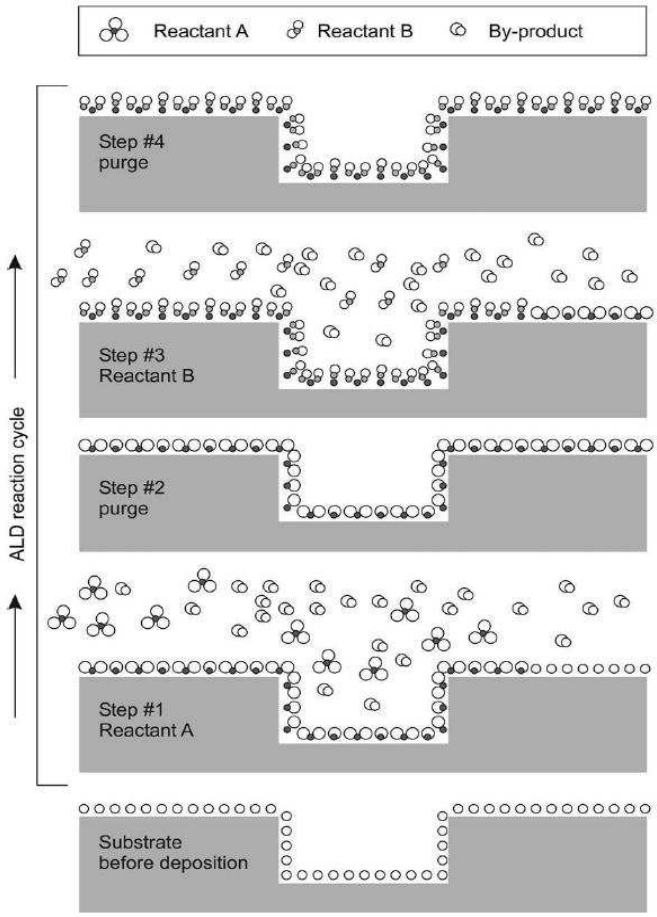

Figure 3-9: principle of ALD reaction cycle (Puurunen, 2005)

According to Johnson et al. (2014), ALD can deposit a very wide range of materials which include:

- **Oxides**, including HfO_2, HfSiO, **Al_2O_3**, Ta_2O_5, TiO_2, La_2O_3, SiO_2, ZnO
- **Nitrides**, including TiN, TaN, AlN, SiNx, HfN
- **Metals**, including Ru, Cu, W, Mo

However, the current study will focus on the Al_2O_3 as it will be used as a barrier coating for CIGS PV modules.

3.6.3 ALD Cycle for Al_2O_3 Deposition on PEN Substrate

This review will concentrate on the deposition process of the Al_2O_3 deposited by ALD for polyethylene naphthalate (PEN) substrate surface, using Trimethyl Aluminum (TML) and H_2O. In air H_2O vapor is adsorbed on most surfaces forming a hydroxyl group, so with the PEN substrate this will form PEN-OH. After placing the PEN in the reactor, TML is pulsed into the reaction chamber.

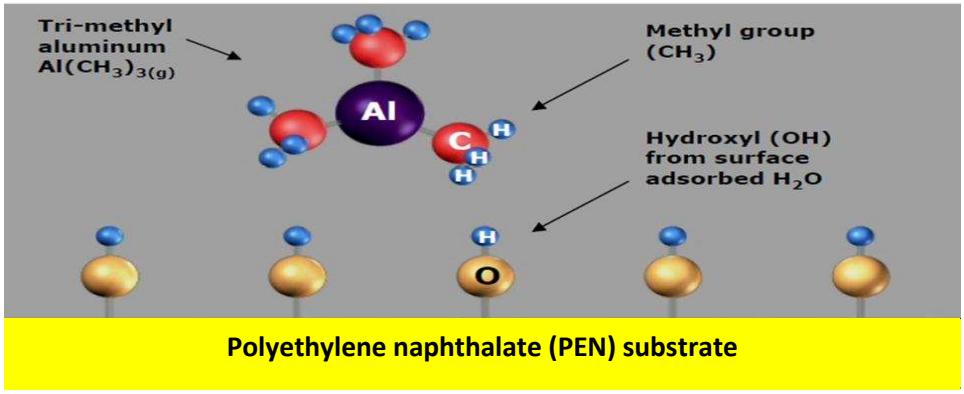

Figure 3-10: Hydroxyl group (Douwe Monsma & Becker, 2006)

In the next step, Trimethyl Aluminum (TMA) reacts with the adsorbed hydroxyl groups, producing methane as the reaction product.

$$Al(CH_3)_3 + PEN\text{-}OH \longrightarrow PEN\text{-}O\text{-}Al(CH_3)_2 + CH4 \quad \ldots\ldots\ldots\ldots\ldots\ldots (1)$$

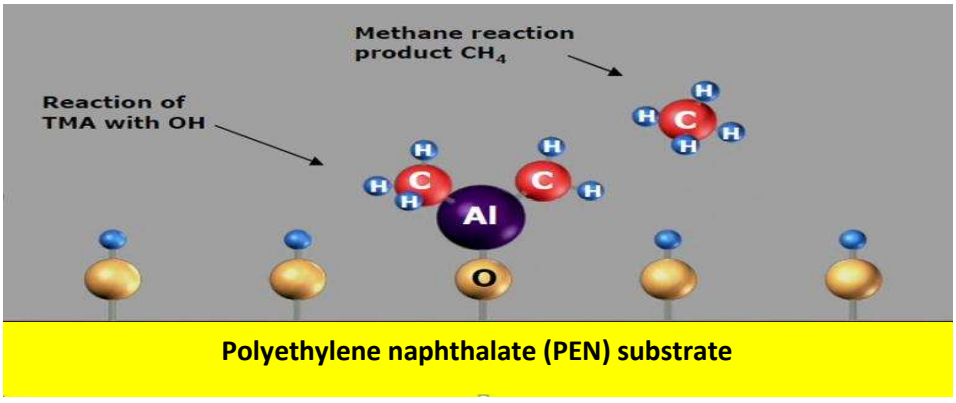

Figure 3-11: Reaction product (Methane) (Douwe Monsma & Becker, 2006)

After the TMA and methane reaction product is pumped away, water vapor (H_2O) is pulsed into the reaction chamber. H_2O reacts with the dangling methyl groups on the new surface forming aluminum-oxygen (Al-O) bridges and hydroxyl surface groups, waiting for a new TMA pulse.

$$_2H_2O + PEN\text{-}O\text{-}Al\ (CH_3)_2 \longrightarrow PEN\text{-}O\text{-}Al\ (OH)_2 + 2CH_4 \quad \ldots\ldots\ldots\ldots\ldots\ldots\ (2)$$

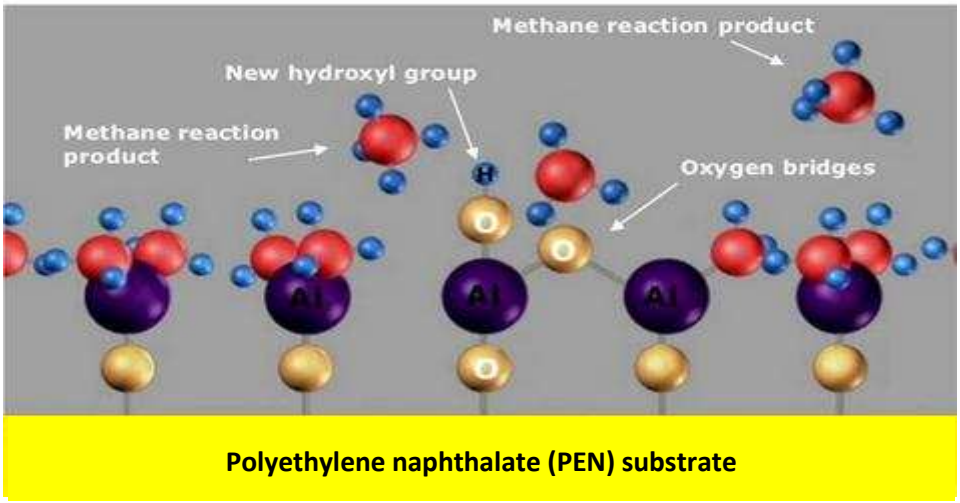

Figure 3-12: Aluminum-oxygen (Al-O) (Douwe Monsma & Becker, 2006)

Lastly, the reaction product (methane) is pumped away. Excess H_2O vapor does not react with the hydroxyl surface groups, again causing perfect passivation to one atomic layer. The OH is now available for further reactions.

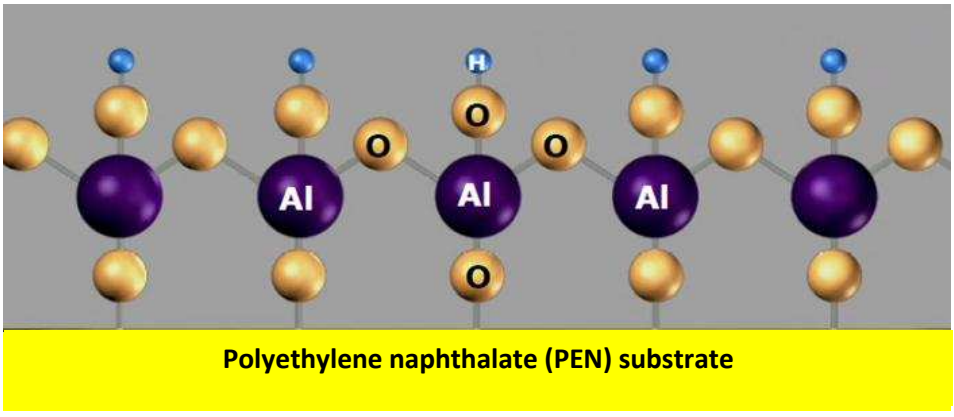

Figure 3-13: One atomic layer of Al_2O_3 (Douwe Monsma & Becker, 2006)

The above process represents only one cycle, and then these processes are repeated to give the required ALD layer thickness.

3.6.4 Water Vapour Transmission Rate Measurement Techniques

Thin-film solar cells made from CIGS material have several advantages over traditional crystalline silicon solar cells. However, flexible CIGS thin-films also have one big drawback; they are liable to failure under long-term exposure to environmental conditions such as rain water and humidity. The major difficulty of introducing thin film solar cells into the commercial market is their limited lifespan when exposed to water vapour and oxygen.

There are several techniques that can be used to measure the PV barrier films functionality, ranging from gravimetric (Cup) technique that measures the gain or loss of moisture by mass, to highly sophisticated instrumental techniques, which use sensors that in some designs can measure extremely low transmission rates. The original standard for testing water vapour transmission of high barrier materials is referred to in the industry as "the cup method" (Troedel, 1999). This method involves placing a small sample of the test materials over the top of a pre-made metal cup. The cup may contain water, in which case the water vapor would pass through the test material and the cup would lose weight over time. This method has always had several major shortcomings. It is a very tedious method, the results are very operator dependent, and it will take a very long time to measure high performance barrier material as they will take a long time to come to equilibrium; furthermore, the results obtained on high performance barrier materials may not be very accurate (Troedel, 1999).

This was followed in the early 1970's by “Gravimetric Test” method to measure WVTR of flexible barrier materials using an infrared detection technique. This method also involved clamping the test material into a test chamber with moist sponges on the outer chambers and an infrared photocell beam to detect the moisture in the central chamber. This method did

provide measurements in far less time and with better precision than the traditional cup method. However, it has a WVTR limit of 1×10^{-1} g/m^2/day (S. Schubert, Klumbies, Müller-Meskamp, & Leo, 2011). In the mid-1980's, an improved isotactic method (MOCON®) was developed using a modulated infrared sensor. One of the great advantages of this method was its use of five samples in a "conditioning" position to help reduce time to steady state equilibrium. This method involves the test specimen to be held such that it separates two sides of a test chamber as shown in Fig [3-14].

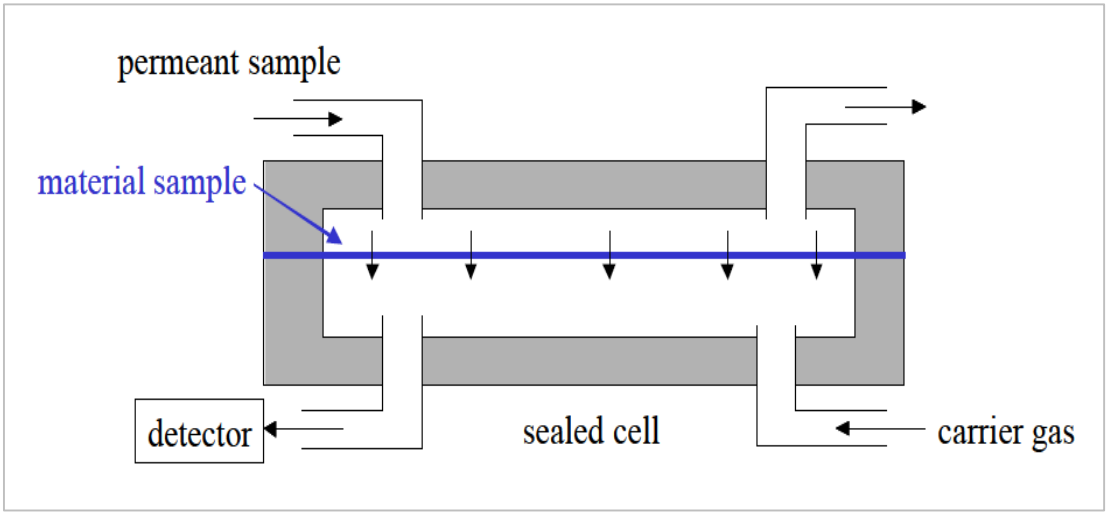

Figure 3-14: WVTR Test using an infrared detection technique (Duncan, Urquhart, & Roberts, 2005)

One side of the sample, the “wet side”, is exposed to the gas or vapor to be studied; this can be done statically or with a continuous stream of permeate gas to maintain a constant pressure concentration (Duncan et al., 2005). On the detector side, the "dry side", the sample is subjected to a zero relative humidity, the permeating gas or water vapor is swept away with a carrier gas (usually nitrogen) and fed into a sensor (infrared). The detector is often specific to the permeating types. Lastly, the permeability of the film is determined from the amount or rate of permeation and experimental parameters such as time, sample area, sample thickness, pressure difference, concentrations, etc. the permeability of the film can be calculated.

This method known as “MOCON®” provides measurements in far less time and with better precision than the traditional cup method. However, the condition under which the measurement is made has a considerable influence on the result. Both the temperature and humidity across the sample need to be measured, controlled and recorded with the results. In fact, no two results should be compared unless the conditions are the same (Duncan et al., 2005).

Another relatively effective method for testing such low permeation rates under certain ambient conditions is the calcium resistivity method (Reese, Dameron, & Kempe, 2011), also known as the Ca Button Test, this method is based on the corrosion (oxidation) of thin calcium films. It involves observation of the optical changes as Ca converts to a transparent Ca salt as water vapour permeates through the barrier material. Because a visual change is observed, the Ca test can distinguish between bulk permeation and defect-based permeation, however it has the disadvantages that, it does not differentiate between oxygen and water vapour permeation and it is notoriously difficult to get quantative measurements using this method (Stevens, Tuomela, & Mayer, 2005). The great advantage of the method is that it gives an insight into the permeation mechanism. By looking at the sample with an optical microscope it is possible to spot local defects as well.

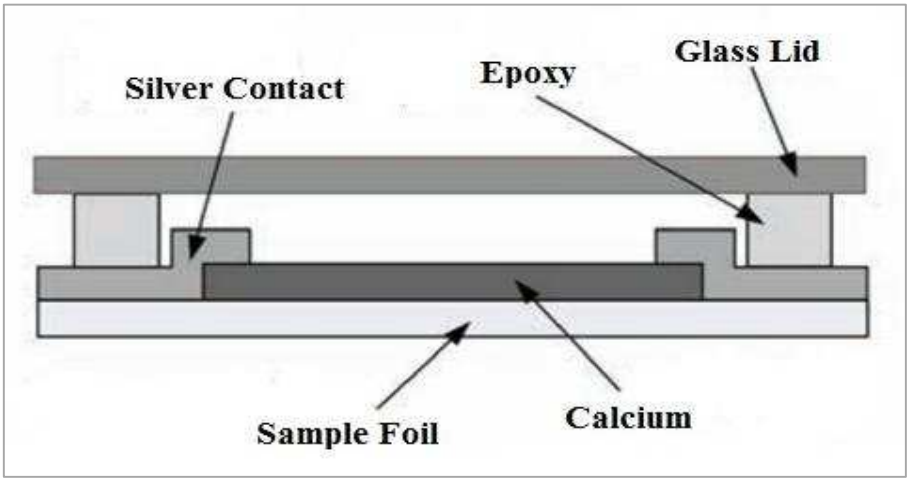

Figure 3-15: Cross section view of Ca corrosion test (Bertrandad & George, 2011)

3.7 Summary

Roll-to-roll ALD of thin films is the ultimate goal for coating flexible PV barrier materials. This development is significant since R2R processing would allow ALD to address many applications in a cost-effective manner. Although this method demonstrated that a thin Al_2O_3 layer enhances the barrier performance as much as does the Al_2O_3 layer fabricated with the batch ALD process, defects which may appear on the film surfaces during the Al_2O_3 growth can be highly significant in deterioration of the PV module performance and lifespan. Therefore, understanding the functional significance of these defects is a very important aspect for the development of both the product and the manufacturing process itself, where in situ surface inspection system can be developed and implemented.

A limiting factor for implementation of flexible PV is that the cost/m^2 of the barrier is the most expensive of the presented layer processes. Multi-layer solutions are expensive and as a consequence single layer defect free R2R produced barrier are viewed as the way forward where cost could be < €10/m^2 (Source: NanoMend User Need report).

CHAPTER 4

4. Surface Metrology

4.1 Introduction

In the world of PV industry, surface metrology plays a crucial role in product development, process enhancement, and quality assurance. The PV industry is currently experiencing greater than 20% annual growth, that is expected to continue and possibly accelerate in the coming years (Schleicher-Tappeser, 2012). To minimise the cost-per-watt of PV modules, conversion efficiency must be maximised as designs move from the research lab to full-scale production, and quality must be maintained throughout the manufacturing cycles.

Accurate measurements of the defects of transparent barrier thin films are important in all thin film photovoltaic technologies, for example surface roughness measurements of the PV barrier films are important to interpret the performance of photovoltaic devices (Maniscalco, Kaminski, & Walls, 2012). With the added information provided by surface metrology techniques, PV manufacturers are able to increase yield and lower the overall production cost of the PV modules through quantification, qualification or monitoring of various process steps (Novak, 2010). A range of surface metrology techniques is commonly available for characterising the physical attributes of the PV barrier films defects. These can range from quick, subjective inspection by a person, to an automated quantitative inspection by an instrument. Surface metrology measurements can be performed off-line (lab-based techniques), where the part (barrier film) is removed from the manufacturing process and brought to the inspection station (Brown, 2010), and/or on-line (in process), where the barrier film is inspected during the manufacturing process. This chapter describes the instruments

capability and set ups utilised for various measurements towards the characterization of the PV barrier films defects.

4.2 Surface Characterisation Methods

PV barrier defects can be characterised and measured by using large numbers of surface metrology methods, and each particular method has its own advantages and disadvantages. The types of surface topography measuring equipments can be divided into two classes, those used on-or in-line such as Pneumatic, Light Scatter, and those used in the laboratory such as Atomic Force Microscopy (AFM), Scanning Electron Microscopy (SEM) and White Light Interferometry (WLSI). The following figure shows the classification of these methods.

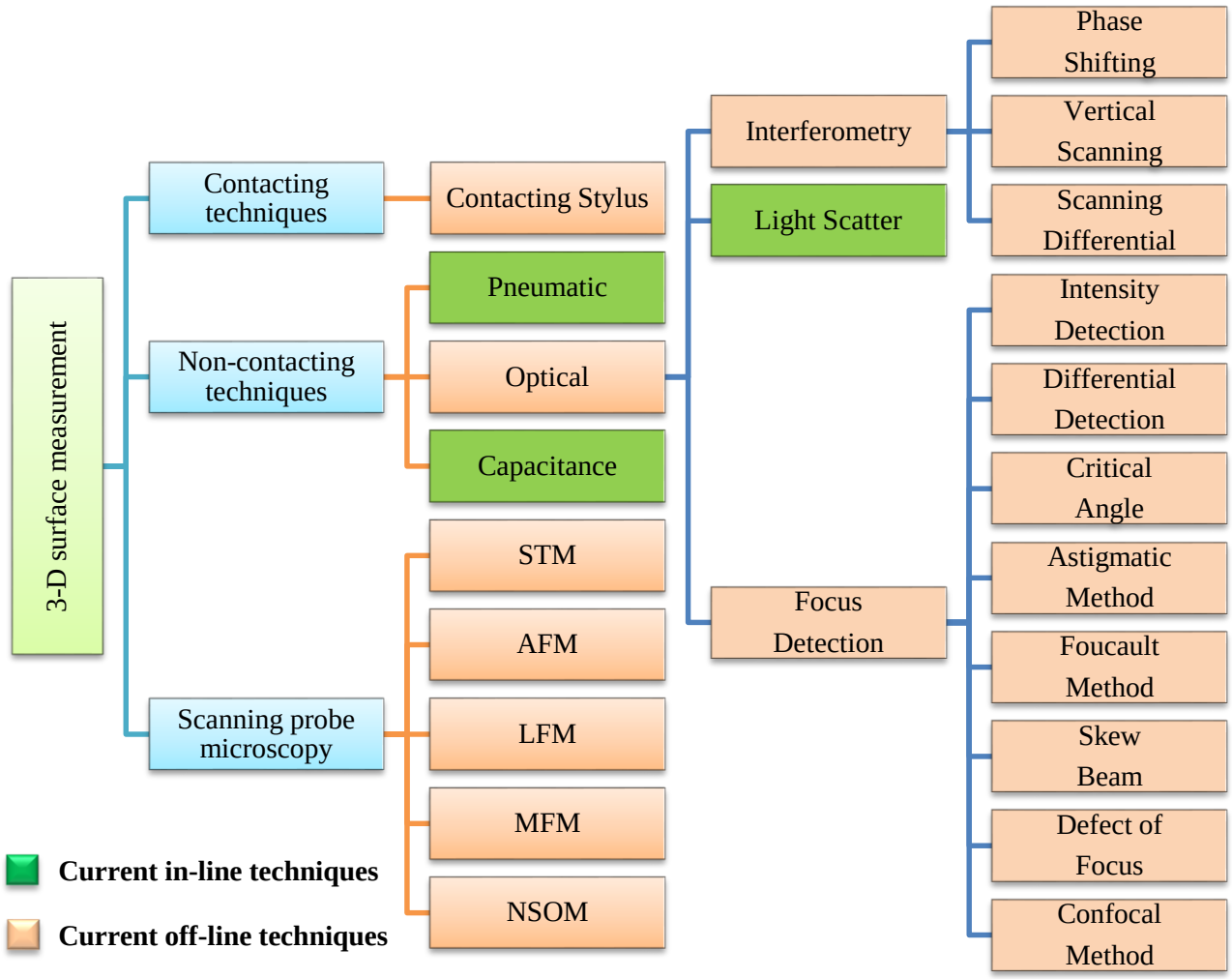

Figure 4-1: Classification of surface metrology methods (Waterworth, 2006)

In this study lab-based (offline) surface metrology techniques reviewed in this chapter and the use of feature parameters according to ISO 25178-2 will be comprehensively involved in characterising exemplar barrier coatings of PV modules. A further aim of the study using offline metrology is to define the minimum size of defect that has a significant effect on barrier function and use this defect size to target inline inspection.

4.3. Off-line Defect Detection Techniques

Non-contact lab-based metrology techniques such as, Coherence Correlation Interferometry (CCI), Scanning Electron Microscopy (SEM) and Atomic Force Microscopy (AFM) can provide the ability to measure surface features of the PV barriers on a nanometer scale, and it can also play a very significant role in the development and production of all designs of CIGS PV modules. In this study the following metrology methods were used as offline techniques for PV barriers defects characterisation;

- A white light interferometry.
- Scanning electron microscopy.
- Atomic force microscopy.

4.3.1 White Light Scanning Interferometry Method

A schematic of a scanning interferometer is shown in Fig [4-2]. The upper beam splitter directs light from the light source towards the objective lens. The lower beam splitter in the objective lens splits the light into two separate beams. One beam is directed towards the sample and the other beam is directed towards an internal reference mirror. The two beams recombine and the recombined light is sent to the detector. Due to the low coherence of the white light source, the optical path length to the sample and the reference must be almost identical, for interference to be observed (Leach et al., 2008). The detector measures the

intensity of the light as the interferometric objective is actuated in the vertical direction (z-axis) and finds the interference maximum.

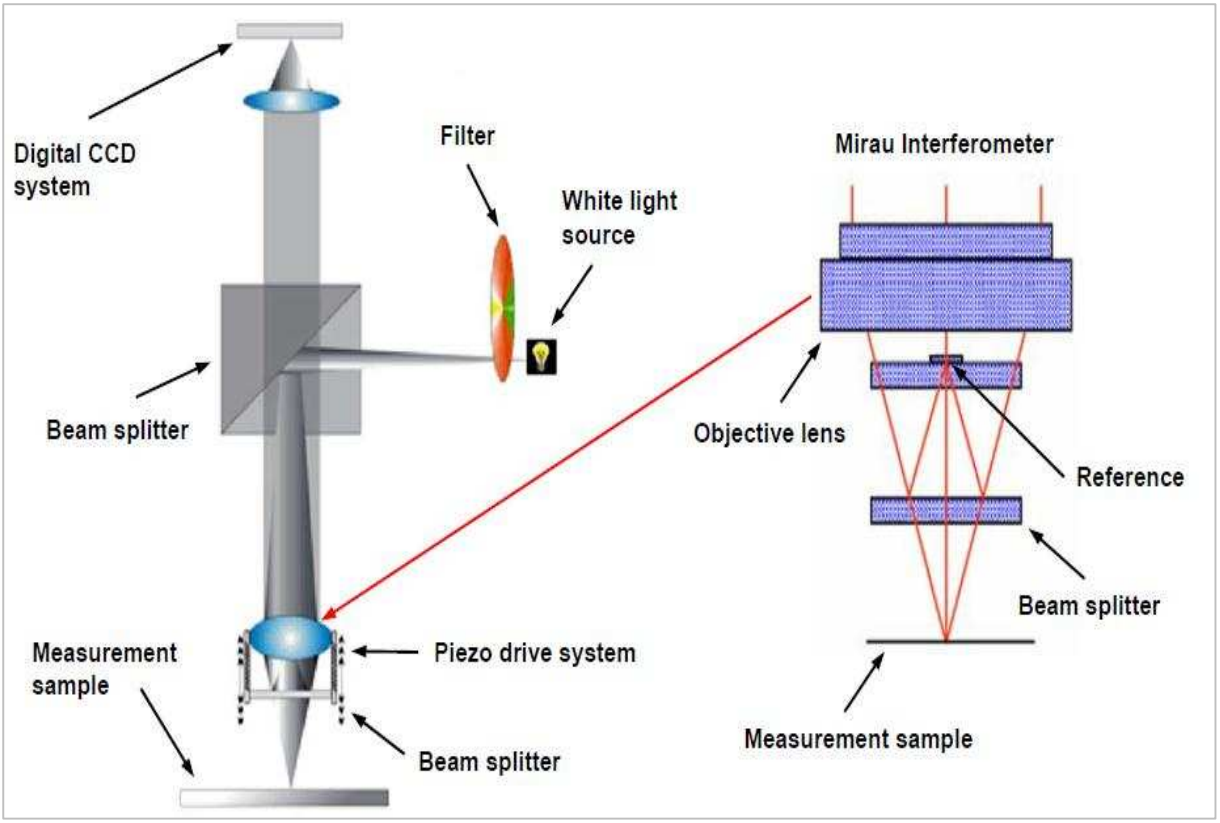

Figure 4-2: Principle of the coherence correlation interferometry (Leach et al., 2008)

Each pixel of the sensor measures the intensity of the light and the fringe envelope obtained can be used to calculate the position of the surface. As the objective lens is moved a change of intensity due to interference will be observed for each pixel when the distance from the sample to the beam splitter is slightly the same as the distance from the reference mirror to the beam splitter. If the objective is moved downwards, the highest points on the surface will cause interference first. This information can be used to build up a three dimensional map of the surface. Fig [4-3] shows how the interference is built up at each pixel in the camera array. The accuracy and the repeatability of this method depends on many parameters including the control and linearity of the vertical actuator, the performance of the camera, the design of the

metrology frame, the stability of the sample and the environment. However, the vertical resolution is sub nanometer.

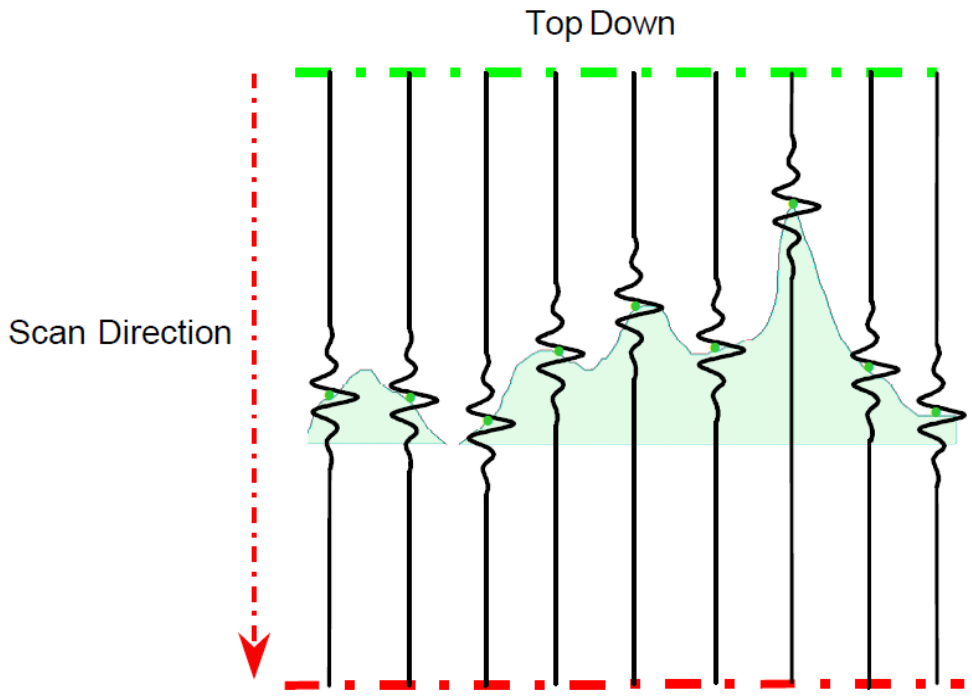

Figure 4- 3: interference at each pixel in the camera array (Leach et al., 2008)

4.3.1.1 Talysurf CCI 3000 Instrument

Talysurf CCI (Coherence Correlation Interferometer-3000) (Taylor Hobson Ltd., Leicester, UK) has been used in the present study as a white light scanning interferometry technique. The general configuration of the instrument is shown in Fig [4-4]. The CCI combines a coherence correlation algorithm with a high-resolution digital camera array to generate a three dimensional representation of a structure by scanning the fringes through the surface and then processing the information to transform the data into a quantitative three dimensional image with sub nanometre vertical resolution. The data can then be used to generate accurate quantitative parameters such as Sa mean surface roughness (ISO25178-2, 2012).

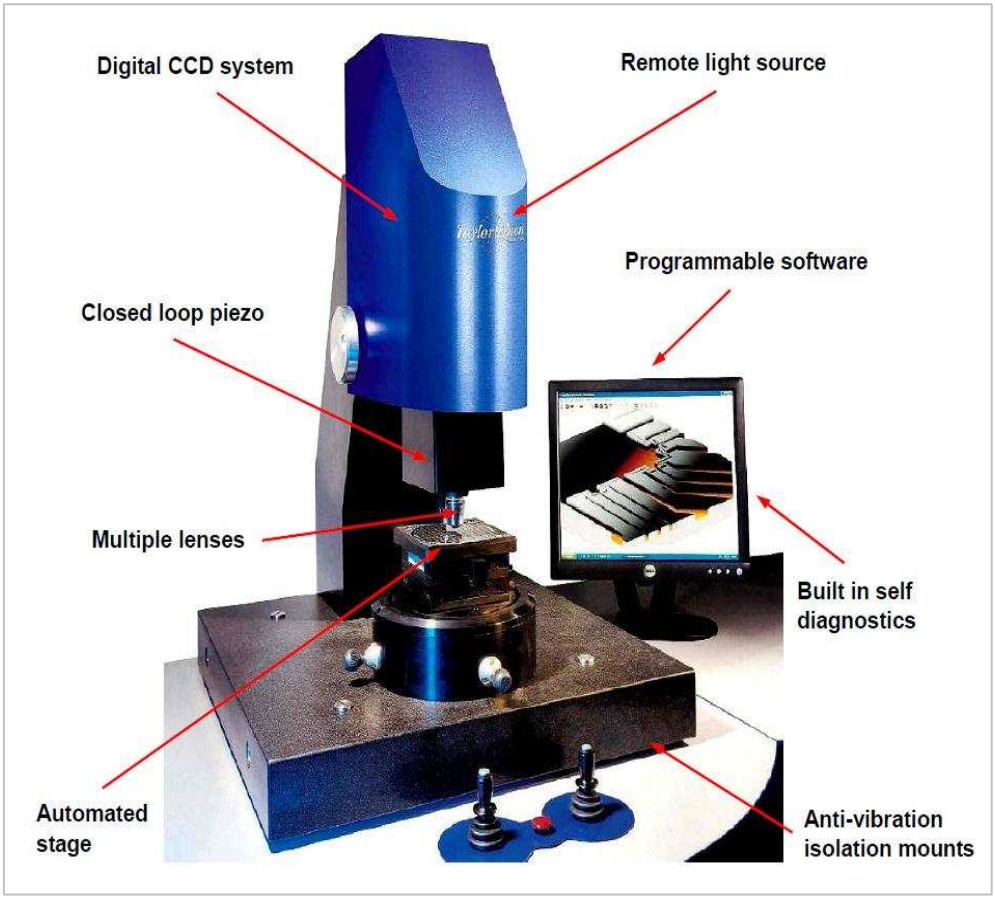

Figure 4-4: Talysurf CCI 3000

Talysurf CCI 3000 brings an unparalleled level of performance to the non-contact 3D optical measurement with high resolution and excellent sensitivity to the reflective light. Almost all material types including glass, metal, and polymer with a reflectivity between 0.3% and 100% can be measured. Its typical specifications are summarised in table [4-1].

Table 4-1: Talysurf CCI 3000 technical specification (Source: Taylor Hobson Ltd.)

Talysurf CCI 3000	**Specifications**
Vertical resolution	0.01nm
Maximum lateral resolution	0.88 µm
Vertical range	100 µm
Field of view (lens dependant)	0.9 x0.9 mm^2
Data points 1024x1024 pixel array	1024x1024 pixel array
Root mean square repeatability (noise)	0.003 nm
Working distance	4.7 mm
Typical measurement time	10–20 seconds

4.3.1.2 Talysurf CCI 3000 Instrument Calibration

Calibration of the Coherence Correlation Interferometry (CCI) is an important factor in producing reliable and repeatable measurements. Therefore, it is important to calibrate the instrument whenever a major adjustment has been made to the instrument or to the environment in which it is housed. The frequency of calibration is dependent upon a number of factors such as environment of use, instrument stability and any regulatory requirements particular to the application. Different types of calibration need to be performed these include;

i. **Lateral or spatial calibration:** Lateral or spatial calibration of a CCI determines the characteristics of the x and y measurement capability and allows for a correction to be applied. This can be achieved by measuring a calibrated pattern, for example a series of concentric circles.
ii. **Vertical calibration:** Vertical calibration allows for the correction of any unwanted motion effects in the vertical (z) measuring axis. This calibration is generally achieved through the use of a step height of calibrated dimension.
iii. **Form correction:** Form correction serves to correct errors associated with the reference optics or in the objective lens assembly. Form correction is generally achieved through single or multiple measurements taken of a reference flat surface.

4.3.2 Atomic Force Microscope Method

The Atomic Force Microscope (AFM) method is classified as one of a wide variety of scanning probe microscopes and accompanying techniques, which were developed in the early 1980's (A. Lewis et al., 2003). The AFM is a device capable of investigating several physical characteristics of a material with sub-nanometer resolution, using the interaction force between a cantilever tip and a sample surface (C. Kim, Jung, Youm, & Park, 2011).

The AFM is operated in either of two modes contact mode or tapping mode. In the contact mode, the tip adheres to the sample surface with a finite force as it is dragged across the surface. The finite adhesion forces deform the tip and the sample so that contact occurs over a finite area. This area is greatly influenced by the tip sharpness and is increased by any additional spring force (Hutter & Bechhoefer, 1993). In fact, this basic technique of the AFM is not adopted to examine such surfaces due to problems of friction and adhesion. Therefore, the tapping mode of operation was developed to overcome drawbacks of contact mode (Binnig, Quate, & Gerber, 1986). However, the higher resolution and the faster scan can be achieved by the contact mode (Casuso, Kodera, Le Grimellec, Ando, & Scheuring, 2009; Rohrer & Binnig, 2006).

5.5.2.1 Principle of AFM in Contact Mode

The principle behind the operation of an AFM lies in the contact mode. The AFM tip is first manually brought close to the sample surface. Then the scanner makes a final adjustment in tip–sample distance based on a set point determined by the user.

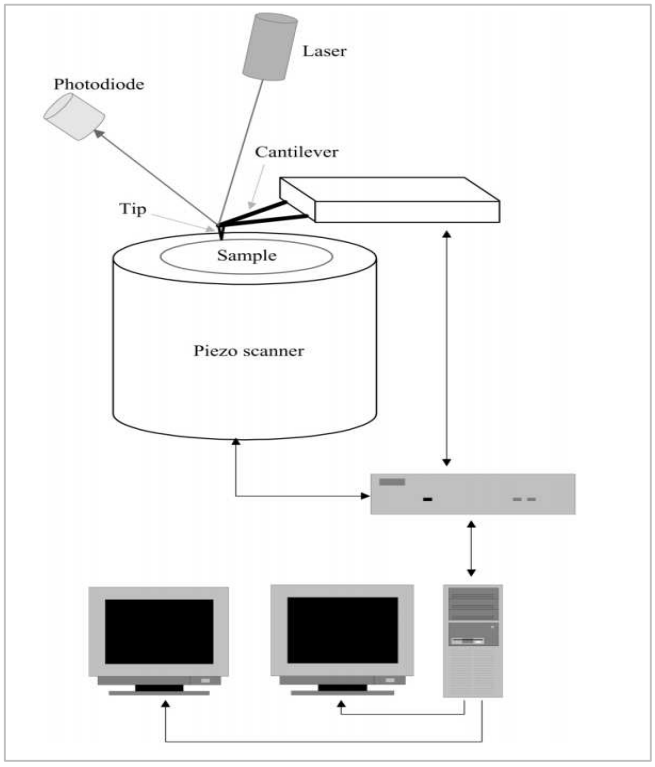

Figure 4-5: Components of AFM (Santos & Castanho, 2004)

The tip, now in contact with the sample surface through any adsorbed gas layer, is then scanned across the sample using a piezoelectric actuator—either by moving the sample or the tip, relative to each other. A laser beam aimed at the back of the cantilever–tip assembly reflects off the cantilever surface to a split photodiode, which detects the small cantilever deflections. A feedback loop maintains constant tip–sample separation by moving the scanner in the z direction to maintain the set point deflection. The sample surface roughness is directly related to the vertical movement of the piezo scanner.

5.5.2.2 Principle of AFM in Tapping Mode

This mode uses oscillation of the cantilever tip to impact the target sample for a minimal amount of time. This intermittent contact reduces the damage done to the soft surface and to the tip, compared to the amount done in contact mode. Therefore, the tapping mode is the method of choice for imaging functionalised soft surfaces. In this mode; the AFM scans the sample surface with a very tiny and sharp tip mounted at the end of a flexible cantilever as shown in Fig [4-6].

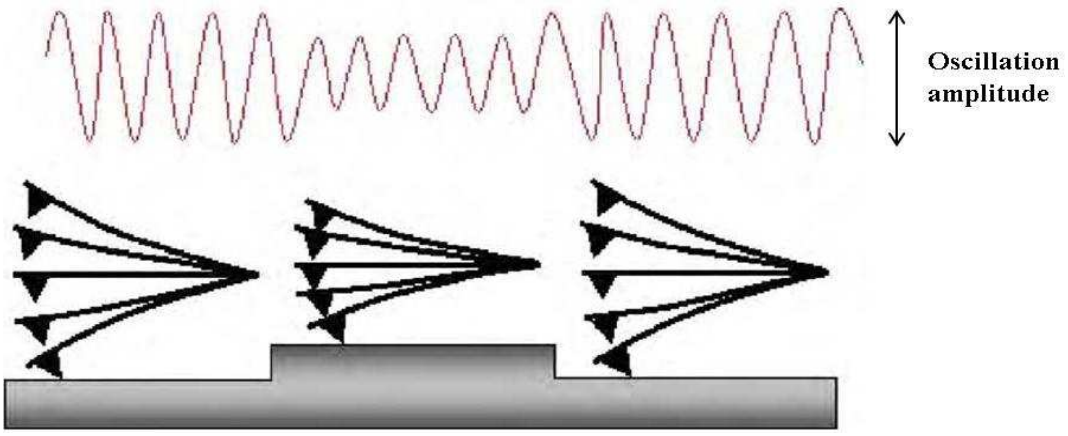

Figure 4-6: AFM tips operating in the tapping mode (Alessandrini & Facci, 2005)

The tip is oscillated and moved towards the sample (Binnig et al., 1986). Only intermittently touching or “tapping” occurs on the sample. Hence the dragging forces during scanning are

significantly reduced (Tamayo & Garcia, 1996). Moreover, during oscillation, the tip goes through both the attractive and repulsive regions of the tip-sample force field.

The cantilever is oscillating close to its resonance frequency. An electronic feedback loop ensures that the oscillation amplitude remains constant, such that a constant tip-sample interaction is maintained during scanning. Forces that act between the sample and the tip will not only cause a change in the oscillation amplitude, but also change in the resonant frequency and phase of the cantilever (Alessandrini & Facci, 2005).

The amplitude is used for the feedback and the vertical adjustments of the piezoscanner are recorded as a height image across the x-y scan range. Simultaneously, the phase changes are presented in the phase image (topography). The advantages of this mode are the elimination of a large part of permanent shearing forces and the causing of less damage to the sample surface, even with stiffer probes (Rohrer & Binnig, 2006).

- **Advantages:**

- High lateral resolution (1 nm to 5 nm).

- Lower forces and less damage to soft samples in air.

- Lateral forces are virtually eliminated so there is no scraping.

- **Disadvantage:**

- Slower scan speed than in contact mode.

Bruker's Dimension Icon® Atomic Force Microscope (Bruker Ltd., Coventry, UK) as shown in Fig [4-7] has been employed in the current study. The instrument was used in contact mode to achieve higher resolution and faster scan speed than tapping mode, where there is no damage was noticed on the samples using this mode. The instrument typical specifications are summarised in table [4-2].

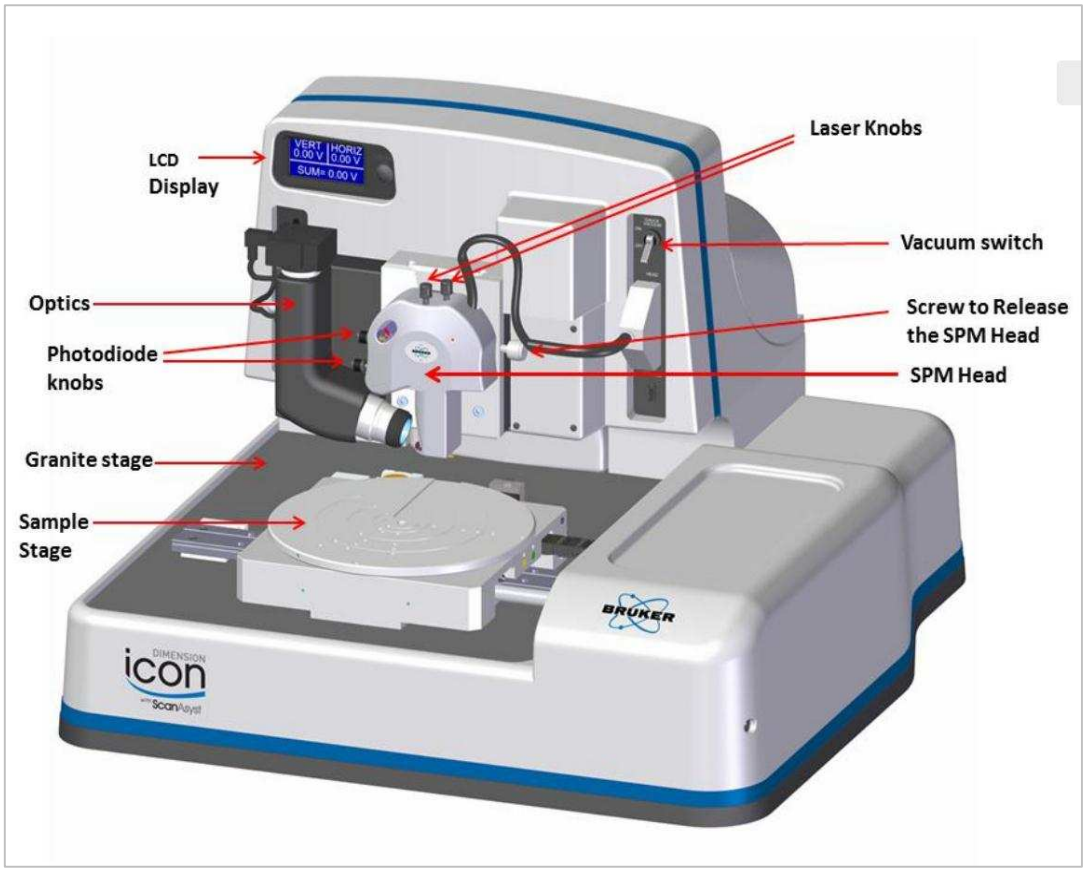

Figure 4-7: Bruker's Dimension Icon® Atomic Force Microscope

Table 4-2: Bruker's Dimension Icon® AFM technical specification

Parameter	Icon® AFM
X-Y scan range	90 µm x 90 µm typical, 85 µm minimum
Lateral resolution	< 2 nm (tip radius dependant)
Vertical resolution	< 0.3 Angstrom
Z range	10 µm typical in imaging and force curve modes, 9.5 µm minimum
Vertical noise floor	< 30 pm RMS in appropriate environment
Sample size/holder	≤ 210 mm diameter, ≤ 15 mm thick

4.3.3 Scanning Electron Microscopy Technique

Scanning microscopy generally includes SEM, scanning probe microscope (SPM), and scanning tunnelling microscope (STM). As the SEM is the one that is frequently employed in this research study, an introduction to SEM is herein provided. It is much like an optical microscope in that one of its main purposes is to "see" with a high depth of field the detail in

samples. The first SEM instrument was designed by Stinzing and Knoll in Germany in the early 1930s. The design of the SEM is based mainly on the development work by Oatley and Nixon in Cambridge and the first commercial version of a SEM was designed by Stewart and Snelling in 1965 (Novotna, 2014).

The more recent computer development has also strongly increased the performance of SEMs and imaging analysis. However, since SEM uses electrons as the source of illumination rather than light, far superior resolutions are obtainable. SEM is a type of electron microscope that scans the sample surface with a high-energy focused beam of electrons to record surface information. The instrument is made up of two main components, the electronic console and the electron column as shown in Fig [4-8].

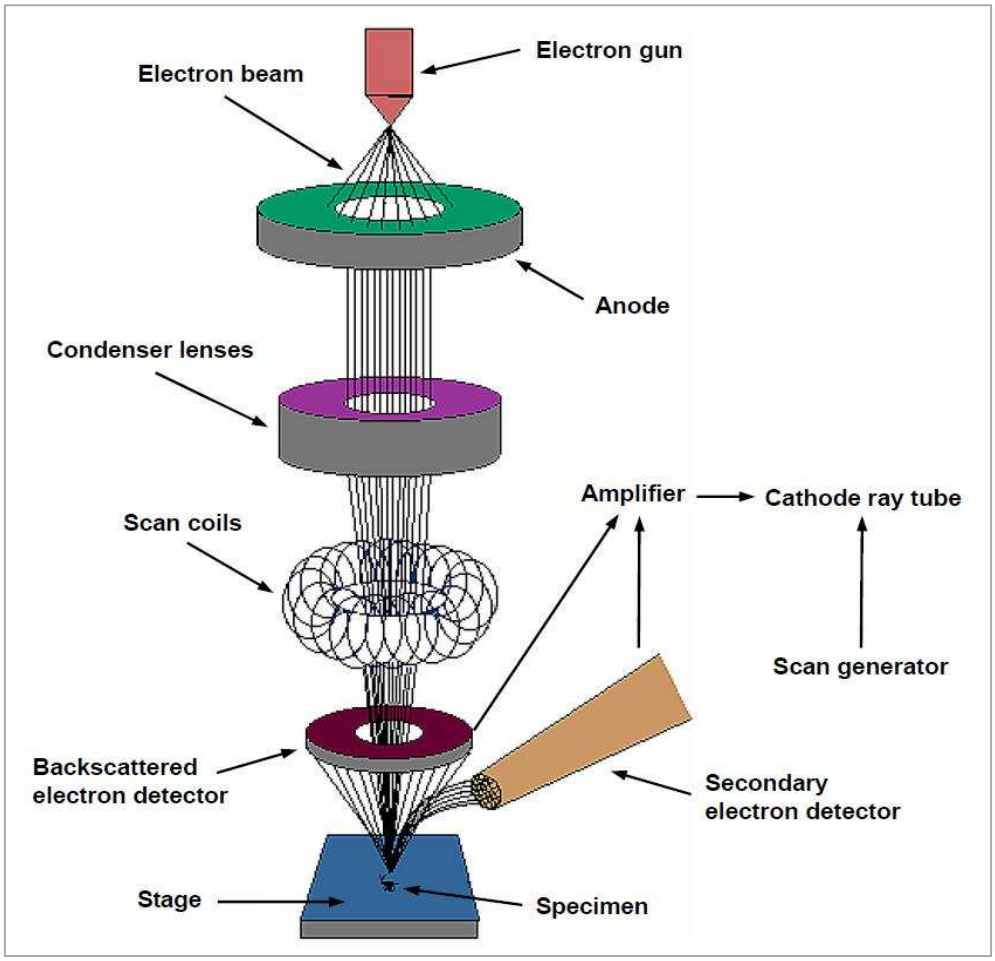

Figure 4-8: Scanning Electron Microscopy

The electron console provides controls and switches that allow for instrument adjustment such as filament current, accelerating voltage, focus, magnification, brightness and contrast. The electron column is where the electron beam is generated under vacuum, focused to a small diameter, and scanned across the surface of a specimen by electromagnetic deflection coils. The lower portion of the column is called the specimen chamber. The electron column comprises the following components.

- Electron gun, to generate free electrons.
- Condenser lenses, to cause the beam to converge and pass through a focal point.
- Scanning system, to form the image.
- Specimen chamber.

5.5.3.1 SEM working principle

The SEM is an instrument that produces a greatly magnified image by using electrons instead of light to form an image (Nisha, 2013). A beam of electrons is produced at the top of the microscope by an electron gun. The electron beam follows a vertical path through the microscope, which is held within a vacuum.

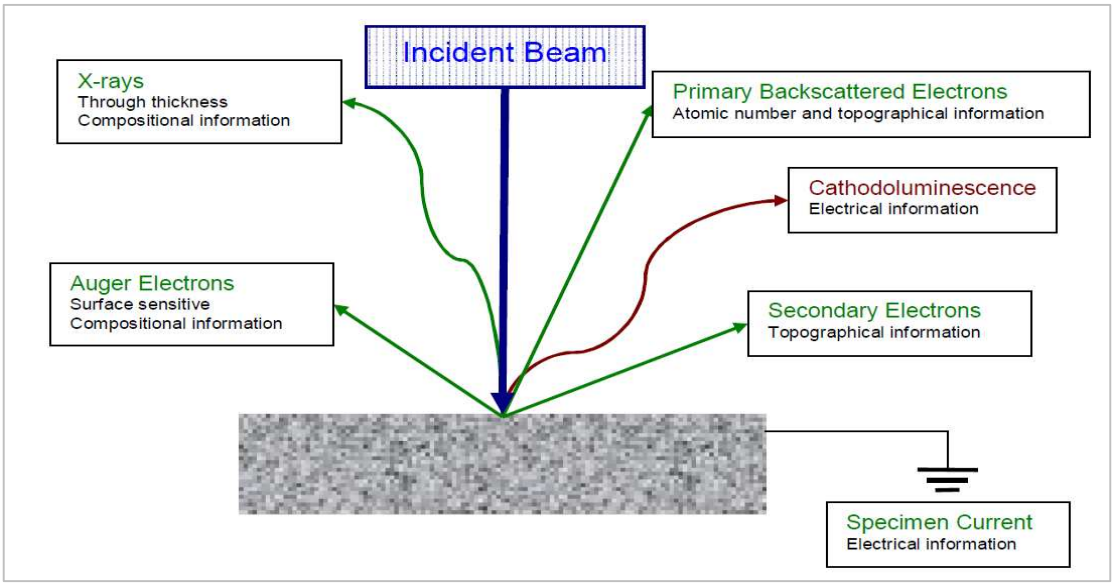

Figure 4-9: SEM working principle (Waterworth, 2006)

The beam travels through electromagnetic fields and lenses, which focus the beam down toward the sample. Once the beam hits the sample, electrons and X-rays are ejected from the sample. Detectors collect these X-rays, backscattered electrons, and secondary electrons. In the present study emitted secondary electrons imaging is primarily used. The detectors convert them into a signal that is sent to a screen similar to a television screen, and that produces the final image (Stefanaki, 2008).

JEOL JSM–6060 (Oxford Instruments, UK) as well as Quanta 250 FEG ESEM (The Wilton Centre, UK) shown in Fig [4-10] and Fig [4-11] respectively were employed in this present research. The intuitive computer interface and standard automated features, such as auto-focus, auto-gun alignment, and automatic contrast and brightness, allow the instruments to be very easily operated. In addition, the specimen chamber can accommodate a sample of up to 32 mm in diameter. The instruments typical specifications are summarised in table [5-3].

Figure 4-10: The scanning electron microscope—JEOL JSM–6060

Figure 4-11: The scanning electron microscope — Quanta 250 FEG

Table 4-3: The typical specifications of JEOL JSM–6060 and Quanta 250 FEG ESEM

JEOL JSM–6060	**Specifications**	**Quanta 250 FEG ESEM**	**Specifications**
Resolution	3.5nm guaranteed	Resolution	0.8 nm at 30 KeV
Magnification	8x to 300,000x	Magnification	14x to1000000 x
Probe current	1pA to 0.3μA	Probe current	≤ 200 nA
Accelerating voltage	0.5 to 30kV	Accelerating voltage	200 V to 30 kV

4.4 Criteria for Instruments Selection

There are many instruments that can be used for 3-D surface measurements, but selecting the right instrument can be difficult task for operators. Morris (2001) argues that the starting point in choosing the most suitable instrument of a particular quantity in a factory or other systems is the specification of the instrument's required features: resolution, sensitivity and dynamic performance. However, Stedman (1987) argues that the performances of metrology instruments are limited mainly by the specifications of a number of critical components, such

as probe geometry, transducer, sensitivity, accuracies of the ways, scan length and scale resolution.

It is clear that the previously described instruments have specific vertical and horizontal measurement ranges for which they are best suited. Additionally, certain aspects of their physical attributes (probe size and geometry, transducer sensitivity, movement error scan length, datum, scale resolution etc.) also define their most suitable performance window. The capabilities of surface texture instrumentation can be understood by using plots in the amplitude-wavelength plane as developed by Stedman in 1987. The method is based around the limiting response of the instrument to sinusoidal surface perturbations. The limiting factors considered are the vertical range and resolution, and the horizontal range and resolution, which usually relate to the horizontal datum and probe size/geometry. An amplitude–wavelength plot for the instruments is presented in Fig [4-12].

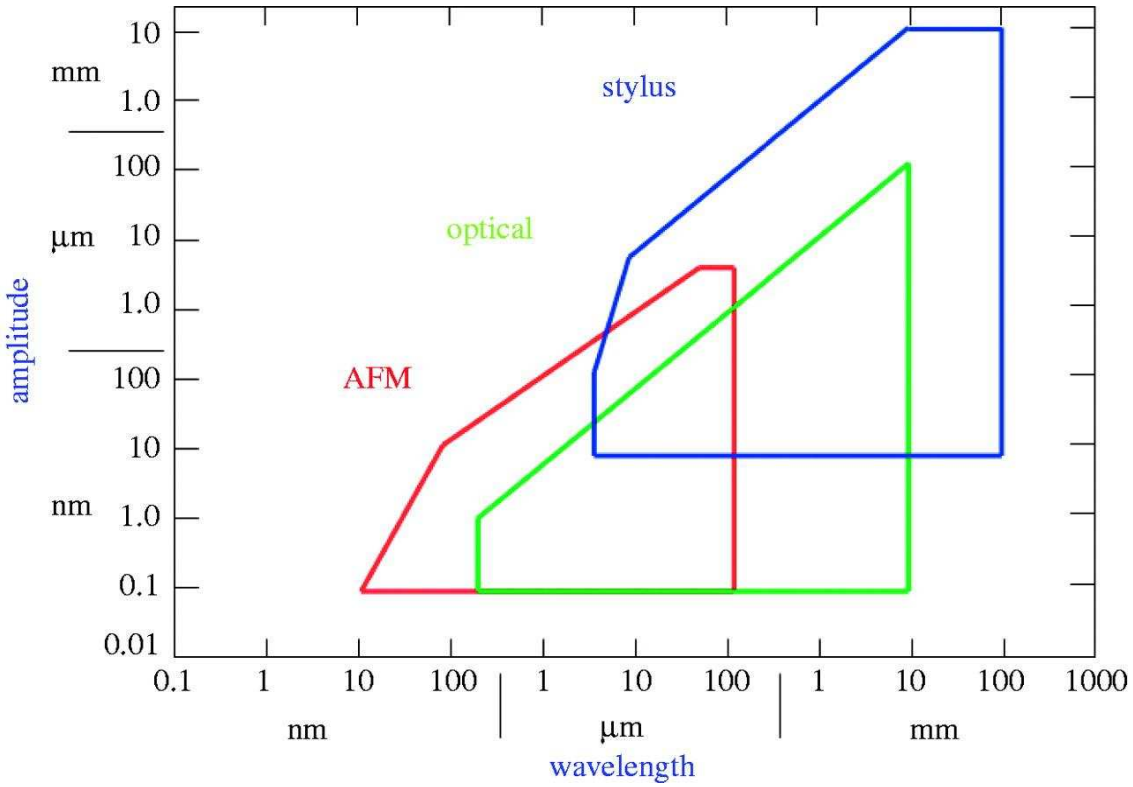

Figure 4-12: Amplitude-wavelength plots (X. iang et al., 2007)

The axes represent vertical (i.e. feature amplitude) and lateral (feature wavelength) dimensions. Each polygon in the figure (Stedman diagram) indicates the working area of an instrument. Any instrument will have minimum sized features it can resolve often the amplitude detectable depending on the wavelength, which can be represented by a particular position of points on the plane. Similarly the size of the instrument (if nothing else) dictates the largest feature it can handle (range), also plotted as a locus; Thus a closed polygon can be constructed for any instrument inside which lie all the combinations of features that the instrument can measure properly. The lengths of lines drawn parallel to the axes from any point, P, in the polygon gives an indication of the ratio of range to resolution, the longer the length, the bigger the ratio (Mainsah, Greenwood, & Chetwynd, 2001).

The amplitude-wavelength map clearly shows that the specific working areas of the different instruments and defines the instruments' suitability for making a given measurement. The large working area of the stylus instruments illustrates its wide applicability. However, in such application (barrier films defect detection), the stylus will not be used as it is expected to cause a scratch or crack kind of defects over the PV barrier film. It should be noted that the SPM/AFM systems both are non-contacting techniques, and have the highest resolution but limited range. Interferometric systems have a high resolution and a greater range than the scanning microscopes which will be extensively employed in this study. However, they have a more limited lateral resolution.

To sum up, it should be stated that, all the previous described techniques in this chapter are lab based, and cannot be easily used for process control. Therefore; detecting defects off-line is difficult, time consuming and expensive. This procedure can often result in large quantities of PV barrier films being manufactured before defects are detected and corrective action taken. In addition the quality requirements and line speed have been increasing (>1 meters

per minute) and off-line methods are not efficient under these conditions. Hence, it is desirable to make use of a camera-based or other optical based in-line inspection systems after each important production segment so that it is assured that, only completely inspected parts that have been found to be good enough remain for the next processing step. However, CCD camera based techniques have limited lateral detection limits and cannot describe the morphology of defects.

4.5. CCD Camera Defect Detection Systems

Charge Coupled Device (CCD) technology is commonly used at present for the purpose of detecting defects in PV barrier films production lines "in process" as shown in Fig [4-13].

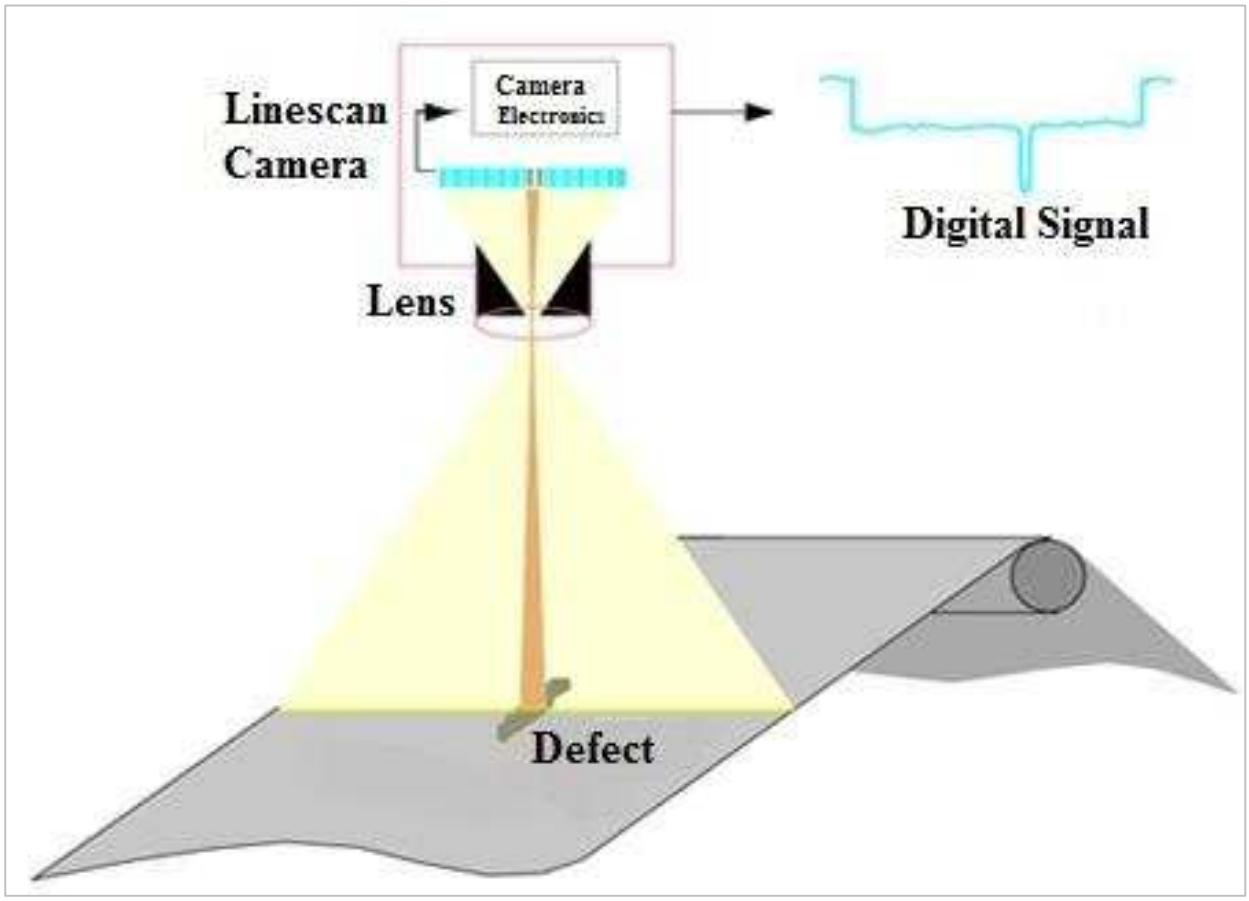

Figure 4-13: CCD linescan camera: fundamentals of operation (Keith Masters, Paul Steinbacher, & O'Connell, 2010)

The CCD functions by converting light energy to an electrical charge that can be measured and processed by a computer. Visual detection systems applied to moving PV barrier sheets use a one dimensional array of detection elements known as a line scan camera(Keith Masters et al., 2010) . By using a line scan camera, the entire sheet or web can be continuously scanned and the video signal converted to an electrical signal as shown in Fig [4-13].

This system (CCD) ensures that only non-defective areas continue down the production line. Immediately after the basic substrate is coated, the camera will reliably detect any substrate defects, specific-edge defects or structural defects. This process prevents defective material from proceeding to the subsequent costly coating processes, which will contribute significantly to the cost optimisation of the thin-film barrier films production. However, the CCD system cannot identify the type of defect exist, they are limited to 10 µm lateral resolution and require complex illumination systems (ISRA VISION AG, University of Huddersfield summer school, 2015).

4.6 Areal Field Parameters

Data collected from the PV barrier samples can be used to establish parameters or visual 3D and 2D images describing the desired features of the surface. The vast majority of surface texture parameters are defined as field parameters. The term field refers to the use of every collected data point measured in the evaluation area, as opposed to feature parameters that only take into account specific points, lines or areas.

Field parameters allow the characterisation of surface heights, slopes, complexity, wavelength content, etc. They are defined in the specification standard ISO 25178 part 2 (ISO25178-2, 2012). ISO areal field parameters are presented along with guidance on their use in appendix (B).

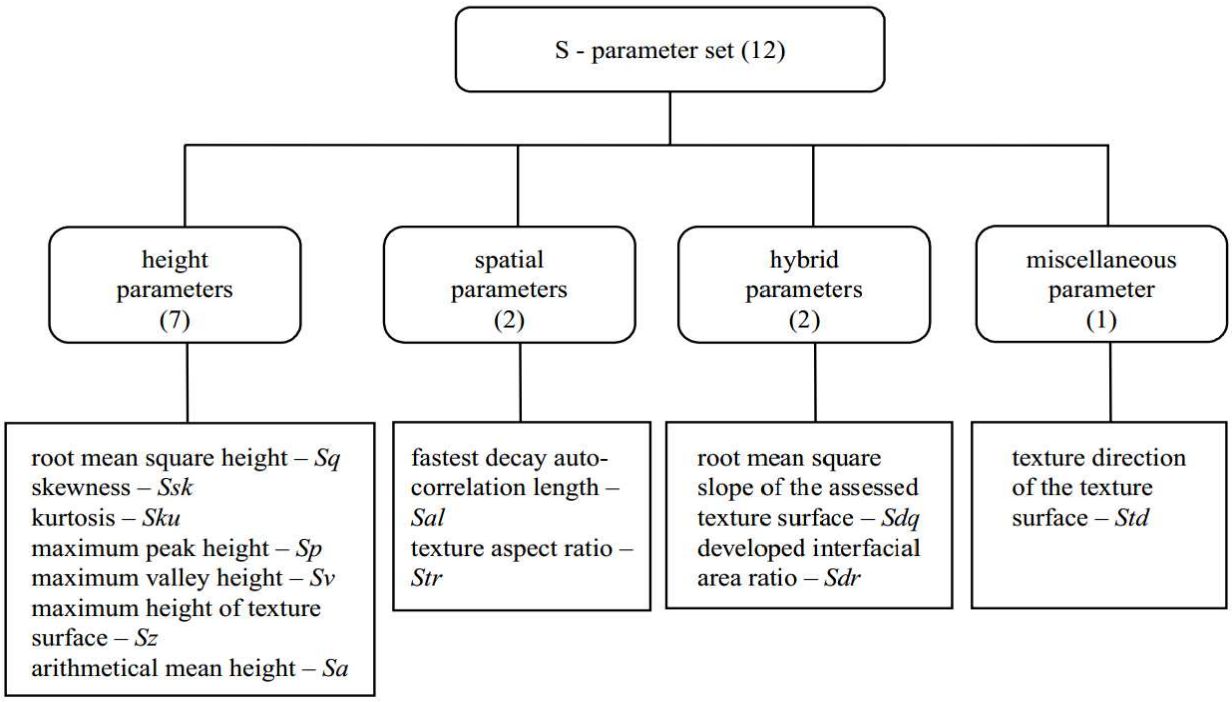

Figure 4-14: Areal Field Parameters (X. Jiang et al., 2007)

4.7 Areal Feature Parameters

Unlike field parameters, where every point on the surface is taken into account in the calculation, the category of feature parameters takes into account only identified features on the surface. Features are considered because they play a significant role in a particular function. Significant features are identified by segmentation of the surface and selected by a discrimination method known as "pruning". Parameters are then calculated to quantify the characteristics of the selected features (Blateyron, 2013). Feature characterization does not in general have specific feature parameters defined but has instead a toolbox of pattern recognition techniques that can be used to characterize specified features on a scale-limited surface (X. Jiang et al., 2007b), e.g. to calculate the peaks density Spd (number of peaks per unit area).

Spd= FC; Wolfprune: X%; All; Count; Density, where X= the prune height.

Fig [5-16] shows the feature parameters set as given in ISO 25178-2, and in appendix (B) these parameters are presented along with guidance on their use.

Note: other parameters can be formulated providing their "toolbox" designation is given.

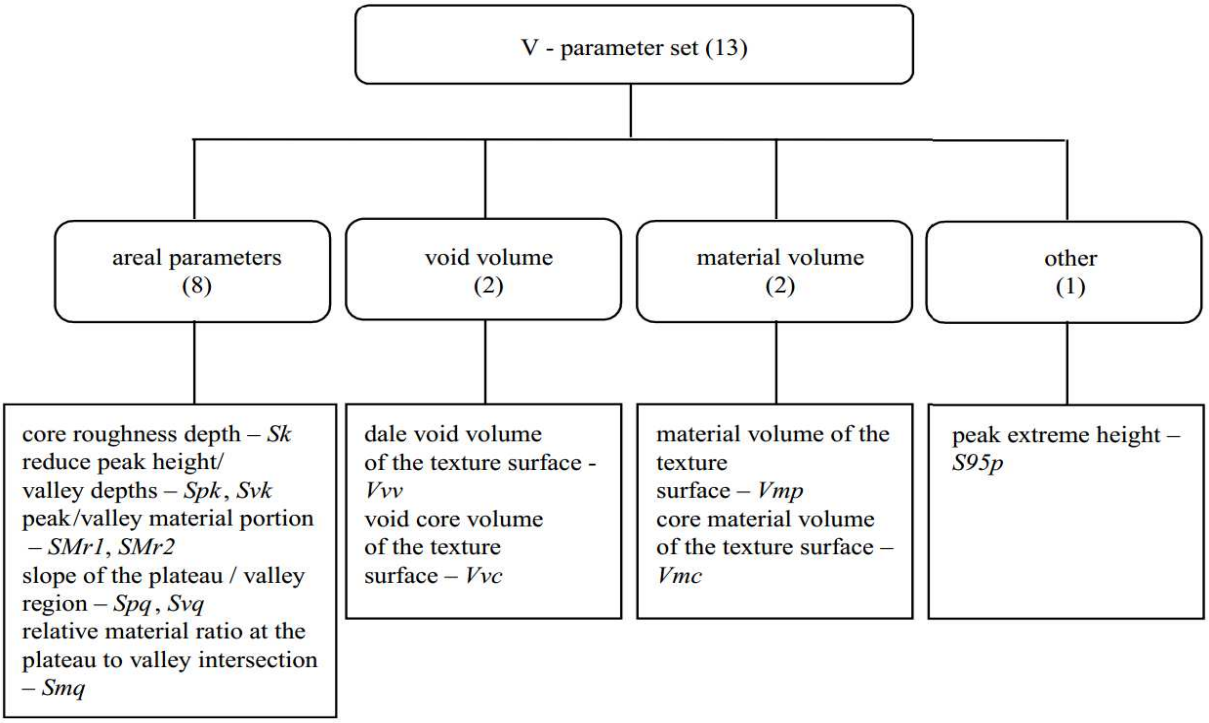

Note: each parameter has a specific toolbox specification

Figure 4-15: A feature parameter set as given in ISO 25178-2 (X. Jiang et al., 2007)

4.8 Defects Characterisation of PV Barrier Films

One of the major challenges in the development of flexible PV modules is the protection of the PV materials from damage by ambient moisture and oxygen. Modelling of moisture degradation of flexible CIGS cells indicates that a flexible encapsulation with a water vapour permeation or transmission rate (WVTR) of between 10^{-4} g-H_2O/m^2-day and 10^{-6} g-H_2O/m^2-day is needed for a lifetime >20 years (P. F. Carcia et al., 2010). A defect-free thin ALD

Al_2O_3 coating on polymer substrates has been shown to reduce moisture permeation to a WVTR of ~$5x10^{-6}$ g-H_2O/m^2-day at room temperature (M. D. Groner et al., 2006).

Zhang et al., (2009) stated that the quality of the barrier film is determined by defects in the film, such as pinholes or cracks that allow leakage of reactive species. The author provided limited information about the morphology of individual defects, indicating that defects are likely to result from particle contamination on the polyethylene terephthalate (PEN) substrate. The particles are believed to mask the polymer substrate and prevent Al_2O_3 ALD coating. The particles then move or are dislodged after the Al_2O_3 ALD coating process and leave an uncoated region of the polymer substrate so water vapour can penetrate through these uncoated regions, degrading the PV functional performance. Therefore, the need to characterise defects in the barrier film has become increasingly important to improve the barrier film's performance and to understand the morphology of defects to identify the origin of defects and to improve the barrier film quality.

Bottomley (2012) studied defects in Al_2O_3 ALD using atomic force microscopy (AFM) plus the application of the calcium test. The results demonstrated that the major cause of device failure was point defects in the barrier films caused by airborne dust which adheres to the film surface before application of the barrier. Moreover, the author developed a theoretical model to give an improved understanding of the defect problems in flexible display devices. The author found that the resistance of the barrier films to gas transmission is controlled mainly by nano-scale defects created during the fabrication of the oxide barrier layer.

Erlat et al., (2001) stated that large defects may dominate the permeation properties of the barrier film. The size and density of these defects are believed to be strongly dependent on the intrinsic properties of the oxide layer. Oxygen transmission rates as low as 1 cm^3/m^2-day-atm and water vapour transmission rates below 0.2 g/m^2-day have been achieved, and these

values are explained by the relatively low density of defects in the barrier layers. However, the authors did not determine the size of significant large defects.

Lee (2013) measured the root-mean-square (RMS) roughness of the sputtered ALD films to determine their surface coverage characteristics on PET substrates. After the ALD film covered the PET substrate, the surface roughness was seen to be significantly reduced. The result specifies that the surface smoothness of the ALD film can possibly restrict the development of defects originating from the substrate and make the subsequently sputtered film more conformal and denser, resulting in a reduced WVTR. Moreover, (Garcia-Ayuso, Vázquez, & Martínez-Duart, 1996) studied the relationship between the surface morphology and water vapour diffusivity of barrier coatings on polymeric (PET) films using the atomic force microscopy (AFM) technique. The authors observed that no correlation exists when the surface roughness is measured over large scanned areas owing to the inhomogeneous coating morphology. However, for scan sizes restricted to representative zones of 0.5 μm wide, free from bumps and pinholes, it is found that those films smoother than the PET substrate show a low water vapour permeability.

This thesis will go beyond the work carried out by the authors mentioned earlier in this section and seeks to introduce such a correlation between the defects size, density, morphology and WVTR using quantitative metrology techniques and the latest areal feature parameters analysis as stated in ISO25178-2. The work also seeks to provide important information regarding the target of the defect size which has a detrimental effect on the functional performance of the barrier film by allowing water vapour ingress to the PV unit.

4.9 Summary

PVs Manufacturers today face a number of technological challenges in PV production lines; micro-scale defects can appear at any stage of the PV barrier films coating process, allowing

water vapour ingress to the final PV unit, and resulting in reduced yield, efficiency, as well as reduced product longevity and performance. These defects are unlikely to be detected as the offline (lab-based) metrology techniques are impractical and time consuming and the existing online techniques face the challenge of speed versus resolution. Therefore, this thesis contribution will go beyond the current state-of-the-art in-line detection system, where an optical system based on high resolution interferometers will be verified and implemented in order to measure defects down to 3 µm later size in approximately 1 s (Muhamedsalih, 2013). However, before the use of the inspection system, defects classification in terms of significance, type and morphology need to be investigated firstly and correlated with the PV barrier films functionality using lab-based (offline) metrology techniques. This will aid to create a comprehensive database for the development of the required defect sensors.

CHAPTER 5

5. Measurements and Experimental Procedures

5.1. Introduction

Transparent barrier films such as Al_2O_3 used for prevention of oxygen and/or water vapour permeation are the subject of increasing research interest when used for the encapsulation of flexible PV modules. Despite the excellent barrier properties provided by this material, all published literature (P. F. Carcia et al., 2010; M. D. Groner et al., 2006; Johansson et al., 2010; C. Y. Park, An, Jang, Lee, & Choi, 2014) have shown that, there is some remaining permeation, even when the barrier coating is reasonably thick (≥ 50 nm). This outstanding transmission is assumed to be attributed to the presence of small (micro and/or nano-scale) defects on the barrier film coating (Bottomley, 2012; Koo, Choi, Baik, Lee, & Lee, 2005; J. S. Lewis & Weaver, 2004). This chapter seeks to give an overview and catalogue Al_2O_3 barrier film surface defects (shape, size-scale, density, and morphology) which have a detrimental effect on the PV module performance and lifespan. In order to understand in more details the factors that affecting the efficiency and the lifespan of the PV modules a correlation needs to be established between the barrier film defects and the barrier film functionality. As discussed previously this will ultimately help to provide the basis for developing R2R in-process metrology devices for quality control assurance of PV modules and organic electronics.

5.2. Experimental Details

Surface measurements conducted to characterise uncoated and barrier Al_2O_3 ALD coated polymer films will be reported in this section. The surface topography of the barrier films is assessed using surface metrology instruments mentioned in chapter (4), and analysed using

the latest feature parameters set (ISO25178-2, 2012). The presence and the distribution of the defects is then correlated with the water vapor transmission rates (WVTRs) as measured on representative sets of barrier films using Isostatic standard test (MOCON®) discussed previously in chapter (3), section (3.6.4). The aim was to establish a possible correlation between the defects density and distribution with the WVTR.

5.2.1 Test Specimen Fabrication (Test 1)

In this study, a set of four 80 mm diameter samples coated with 40 nm of Al_2O_3 using the ALD method (see chapter 3, section 3.6.3) were assessed, along with a non-coated substrate. Special care taken during the transportation as well as during measurements of the samples to avoid any possible damage. The substrate material used in the present study was Polyethylene naphthalate (PEN), and the thickness of this material is specified to be 123 µm as shown in Fig [5-1]. The specimens were produced by the Centre for Process Innovation (CPI) as part of the NanoMend project (NanoMend FP7- 280581).

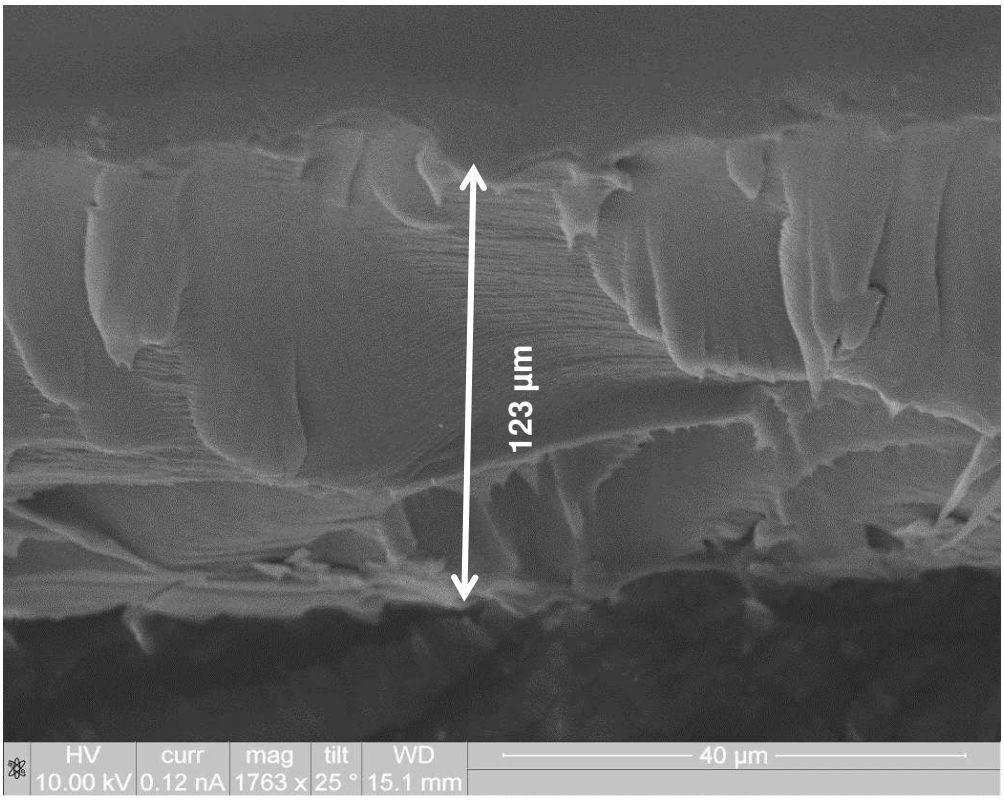

Figure 5-1: Cut cross-section of the polyethylene naphthalate base material

This material (PEN) has a good transparency and relatively low cost but it has a high density of "pits" and "peaks" from fillers and other defects such as dust and surface scratching (Almanza-Workman et al., 2012) and as shown in Fig [5-2] from present measurements.

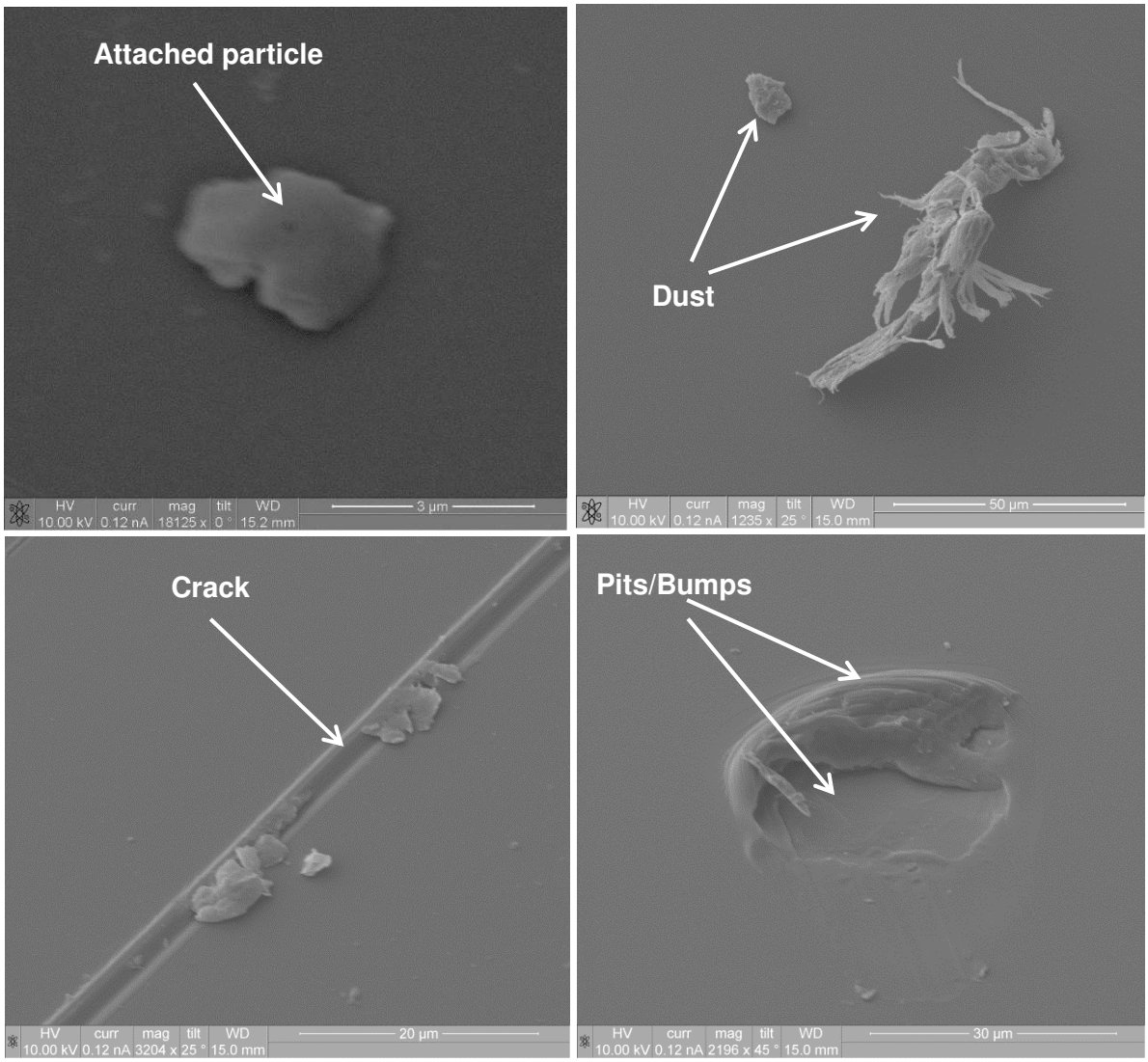

Figure 5-2: Defects in the polyethylene naphthalate film substrate

The base film (PEN) inherent roughness can have a highly detrimental effect on the barrier performance. Therefore, when this base material (PEN) is coated with a barrier layer such as Al_2O_3, the barrier performance of this multilayer structure can also fall short of the stringent water vapour transmission rate requirements for PV applications ($<5x10^{-5}g/m^2/day$). One solution, the subject of this investigation, is the addition of a planarised hard coat to the film surface (Almanza-Workman et al., 2012). This coating is deposited using spin coating

method as a wet coat to the polymer during manufacture and acts to increase the smoothness of the surface by capturing existing debris and counteracting the effect of scratches which may be present on the raw base film after production as shown in Fig [5-3].

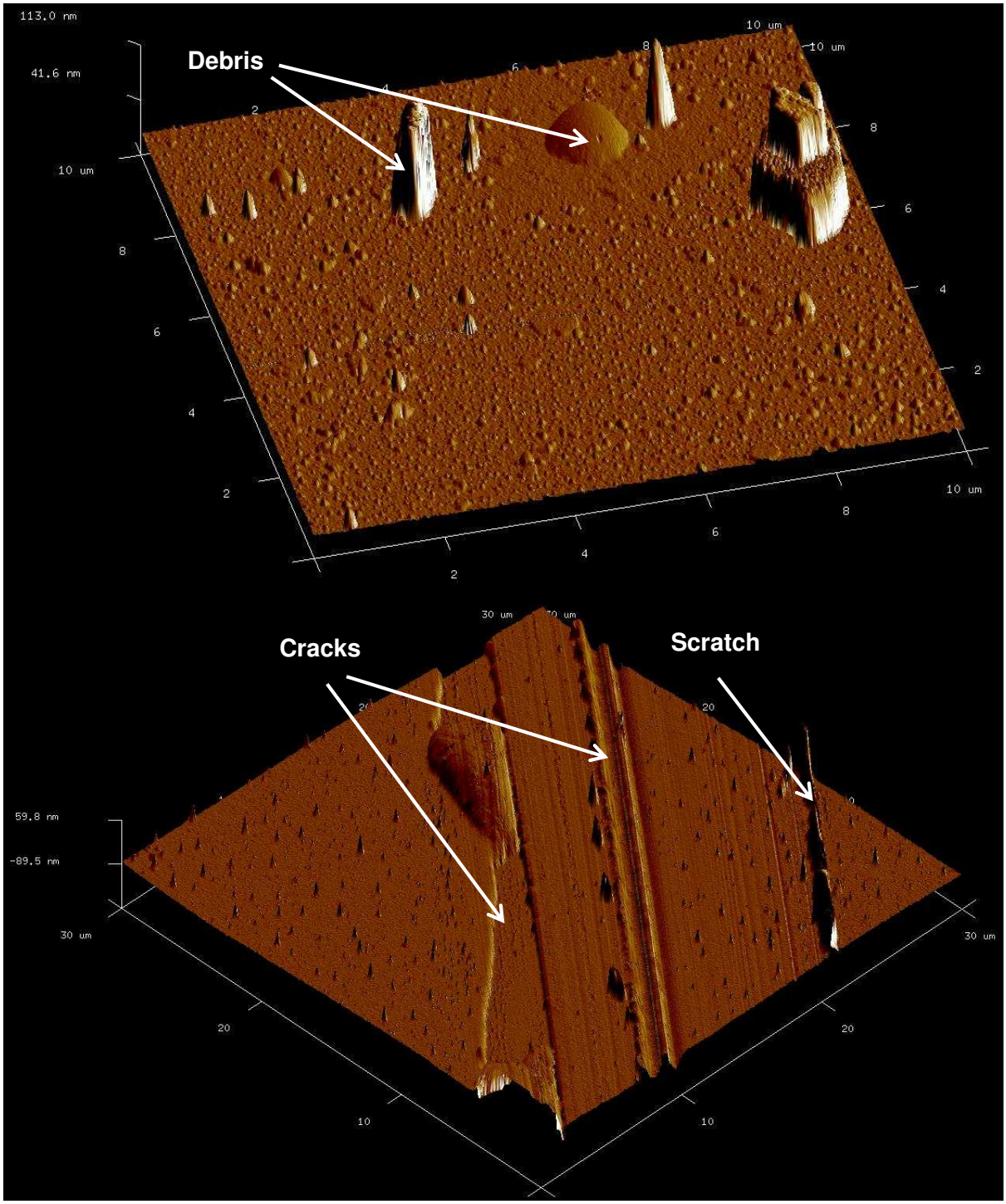

Figure 5-3: AFM 10×10µm and 30×30µm showing defects present on the raw base film after production

In the present study another PEN thin-layer of approximately 2-3 microns thick was applied on top of the PEN substrate to planarise the pits and spikes features as shown in Fig [5-4] and as shown in Fig [5-5] from present measurements.

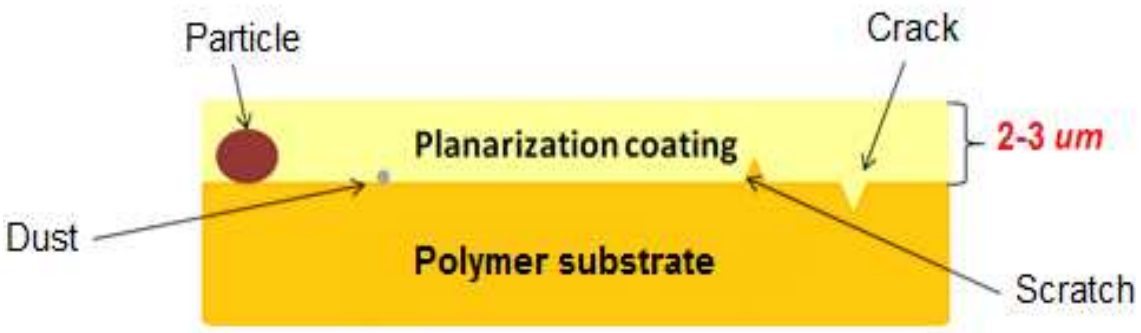

Figure 5-4: A schematic diagram of polymer planarisation coating

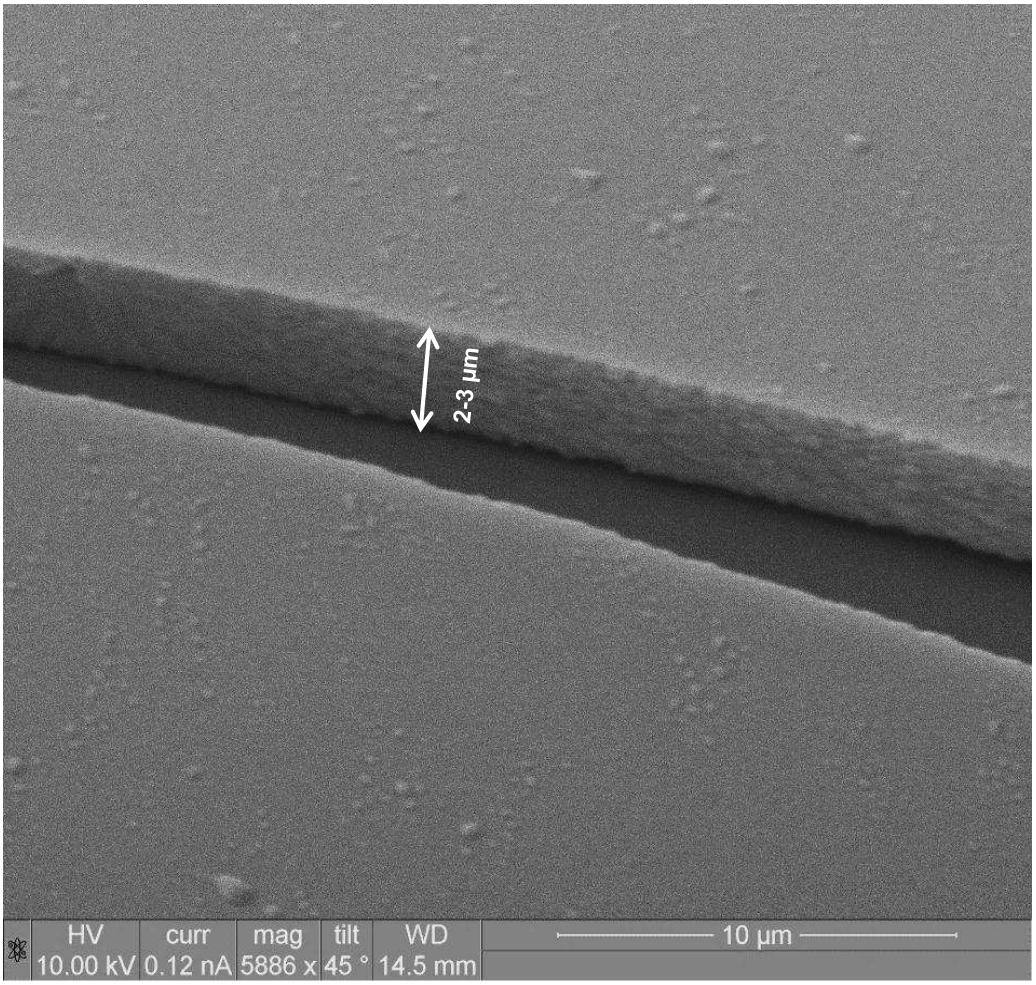

Figure 5-5: Cross-section of the PEN planarised layer

Following the planarisation process a barrier film of Al_2O_3 was deposited by thermal and plasma-assisted ALD employing Tri-methyl aluminium Al $(CH_3)_3$ precursor dosing together with a H_2O oxidant source as explained in chapter 3 (section 3.6.3). The ALD depositions were made using Oxford Instruments FlexAL tool (see section 3.6.2), and Trimethyl Aluminium (TMA) was used as the metal precursor. The reactor temperature used to deposit the aluminium oxide was 120°C and the pressure was very low (<0.1mBar), 312 reaction cycles were made to produce 40nm Al_2O_3 layers on the PEN substrate. The 40 nm thick Al_2O_3 ALD is incorporated on top of the planarised layer as shown in Fig [5-6].

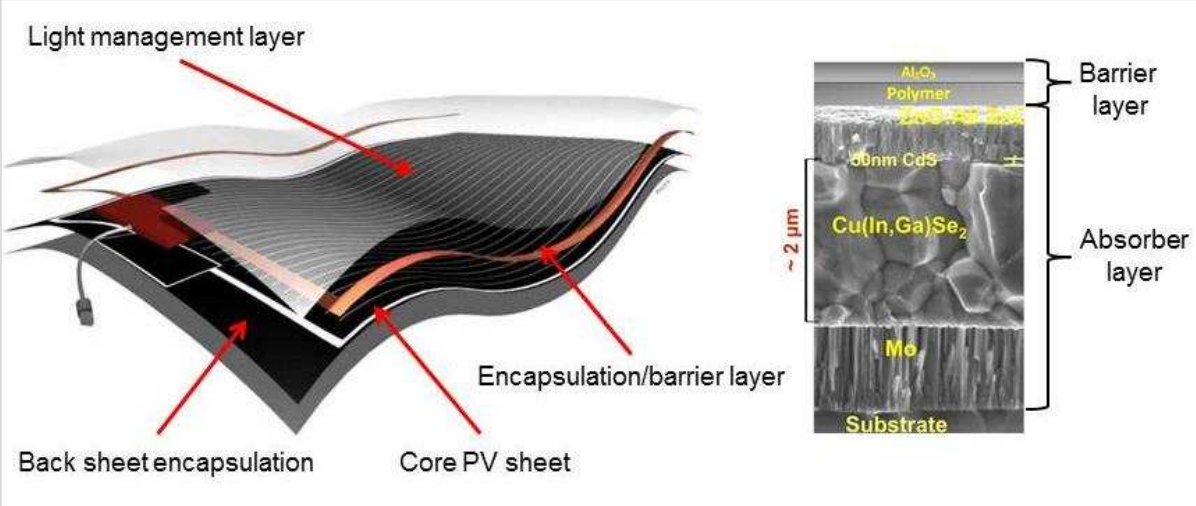

Figure 5-6: Schematic cross-section of CIGS PV cell (Courtesy of Flisom, Switzerland)

5.2.2 Environmental Degradation Test

All the coated samples are measured for the WVTR using Isostatic standard test (MOCON®) instrumentation prior to the surface measurements. Fig [5-7] shows the MOCON® instrument parts. This method (MOCON®) involves the test specimen being held such that it separates two sides of a test chamber as shown in Fig [5-8] and explained in chapter 3 (section 3.6.4). One side of the sample, the "wet side", is exposed to a water vapor at 38 °C and 90% relative humidity (RH). On the detector side, the "dry side", the sample is subjected to a zero relative

humidity; the permeating vapor is swept away with a carrier gas (nitrogen) and fed into a sensor/detector which is usually infrared.

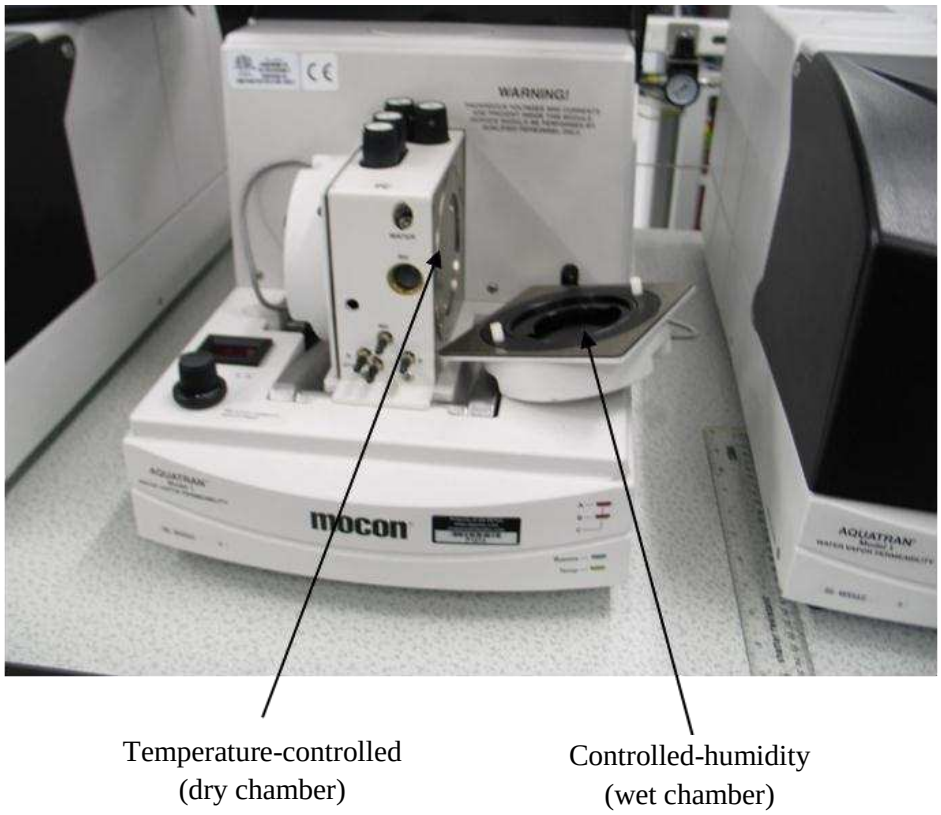

Figure 5-7: WVTR test (MOCON®) components

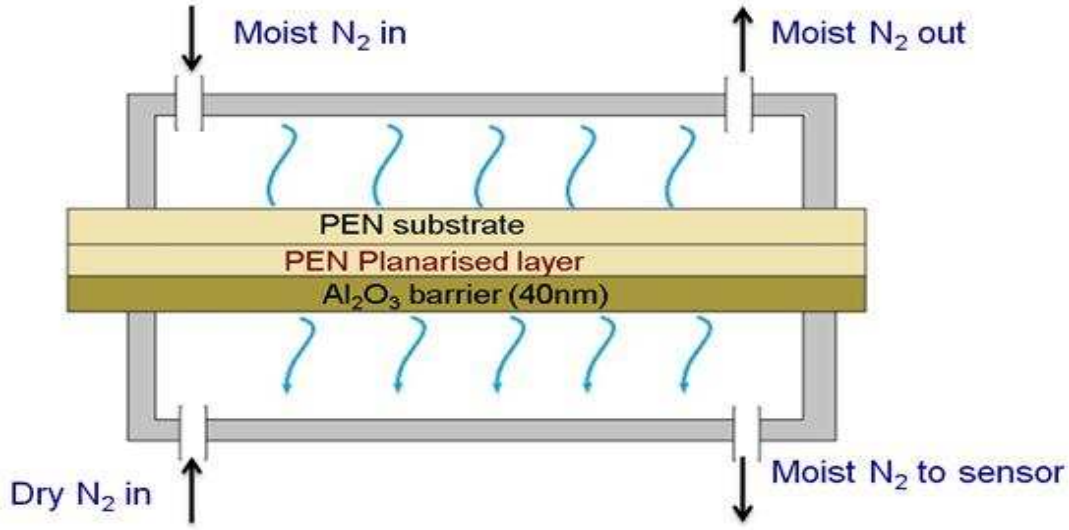

Figure 5-8: WVTR Test using an infrared detection technique

5.2.3 Water Vapor Permeation Theory

The permeability of the film is determined from the amount or rate of water vapor permeation and experimental parameters such as time, sample area, sample thickness, pressure differences, concentrations, temperature and relative humidity (RH). Assuming Fickian diffusivity (i.e., diffusivity is independent of concentration), the transient WVTR can be described by the following equation (Michael D Kempe, 2006).

$$WVTR = \frac{DC_{sat}}{l}\left[1 + 2\sum_{n=1}^{\infty}(-1)^{n} \quad e^{\frac{-Dn^2\pi^2 t}{l^2}}\right] \tag{5-1}$$

Where, D is the diffusivity (cm^2/s) and it is determined by the time required to reach steady state, after which the water saturation concentration was determined by steady-state WVTR; l is the sample thickness; t is elapsed time (hrs.), and C_{sat} (g/cm^3) is the concentration of water at saturation. The WVTR values of the samples are shown in table [5-1], the samples were independently randomly numbered so there was no influence on the analysis of the samples.

Table 5-1: Water vapor transmission rate at specified conditions 38˚C and 90% RH (Test 1)

Sample code.	Water vapour transmission rate (g/m^2/24 hrs.)	Stabilisation time (days)
2701	1.1×10^{-3}	11 days
2702	1.3×10^{-3}	11 days
2705	4.1×10^{-3}	5 days
2706	2.0×10^{-3}	5 days

The results show that sample (2705) had the highest WVTR. This study's hypothesis is that the presence of micro/nano-scale defects, (size and distribution) might play a critical role in determining the WVTR. An investigation was conducted into which type and size of the micro and nano-scale defects have a negative effect on the PV barrier performance and lifespan. This investigation was performed with no prior knowledge of the WVTR values.

5.3. Defect Detection Methodology

Since defects in the barrier film of the PV module are expected to seriously reduce their conversion efficiency and usable lifespan, the inspection and understanding of the functional significance of these defects is a very important aspect for the development of both the product and the manufacturing process. In this chapter, surface metrology techniques particularly optical microscopy, coherence correlation interferometry (CCI 3000), atomic force microscopy (AFM) and environmental scanning electron microscopy (ESEM) were used to measure the previously tested samples.

5.3.1 Optical Microscopy Analysis

Initially an optical microscope (Keyence VHX-600 digital high dimension charge-coupled device (CCD)), equipped with 20–200× objective lenses was utilised in a clean room environment (class 10000) for initial characterization of the samples. This technique was employed to give an initial indication of the types of surface features existing on the samples' surfaces before carrying out any further measurements.

Figure 5-9: Keyence optical microscope

The investigation shows that, different types of features were noted on each sample; these features are different in terms of their type, width, distribution and morphology. A typical examples of these features is shown in Fig [5-10] and Fig [5-11]. The figures show pit type features in the Al_2O_3 layer. Where it is observed that in Fig [5-10] a pit type feature has allowed the water vapor to permeate through the barrier causing delamination of the Al_2O_3 layer from the planarised PEN layer around the pit boundary.

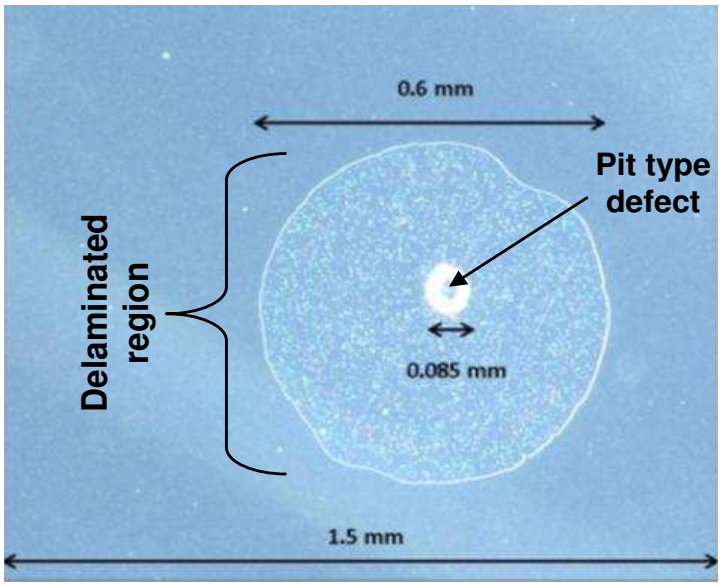

Figure 5-10: Form and scale of (a) large defect feature

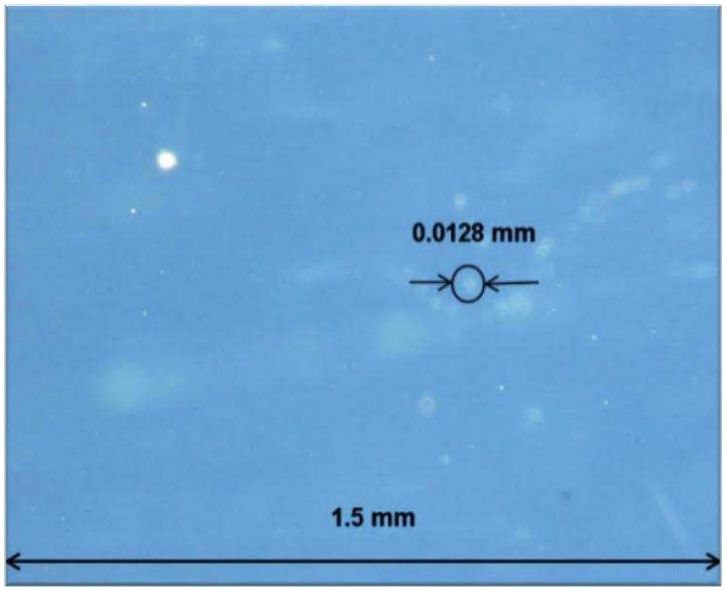

Figure 5-11: Form and scale of small defect feature

5.3.2 White Light Scanning Interferometry Analysis (Test 1)

The recording of the size-scale of the features observed from the previous survey using the optical microscope was completed using white light scanning interferometry (WLSI). This method was used to carry out 3D surface analysis, and provides a number of important parameters; including surface roughness, feature height, width and density. These parameters could possibly have a large influence upon the barrier layer functionality (Conroy, 2012). However, further work still needed to determine the size, density of the surface features and the other parameters which could have a negative influence on the barrier film lifespan and functionality. The WLSI instrument used in this study was the Ametek Taylor Hobson CCI 3000 (Coherence Correlation Interferometer). The instrument has been calibrated according to its manufacture specifications mentioned in chapter (4) section 4.3.1.2, and was used in a clean room environment (class 10000) to avoid any possible damage and contamination of the samples.

A 20× objective lens was used; this lens gave a measurement area (field of view) of roughly 1 mm^2 and a potential vertical resolution of about 0.1 nm with lateral resolution of approximately 0.88 µm. In the study which follows, it was considered important to identify the surface topography features in the Al_2O_3 layer as these were thought to be directly contributed to the WVTR value. Cataloguing and determining the significance of these features, and measuring their size, distribution, area and volume as well as the ability to classify these features and determine correlation with WVTR, is considered as a basis for developing a suitable in-line defect detection system. All the Al_2O_3 ALD samples including the uncoated substrate were measured using the WLSI technique. 700 measurements, equating to 14% of the total surface area of all the specimens was measured.

The measurements showed the Al_2O_3 barrier layer has many features; these features varied

from one sample to another. Fig [5-12] and Fig [5-13] show typical examples of these defects as characterised by CCI instrument. Other types of defects observed during this investigation are included in appendix (C).

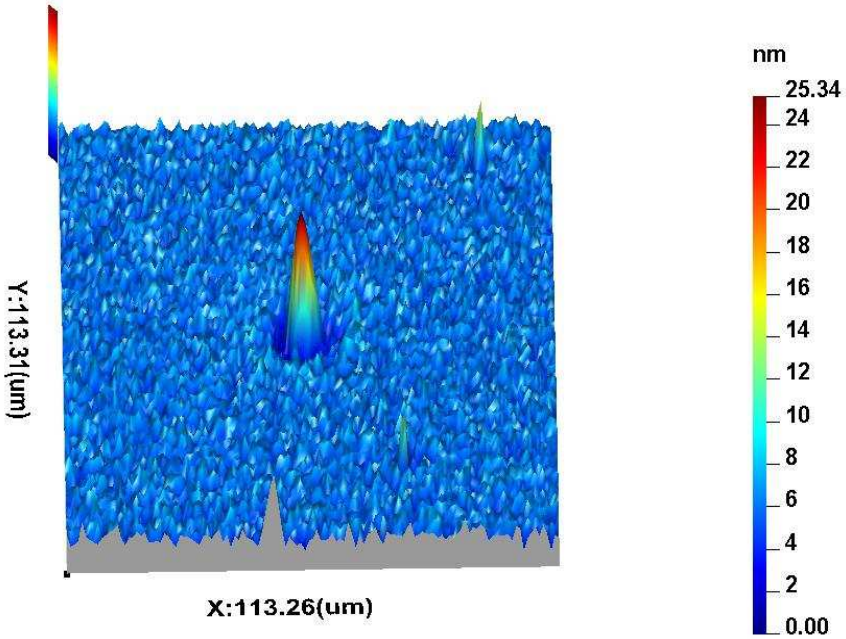

Figure 5-12: Peak type defect

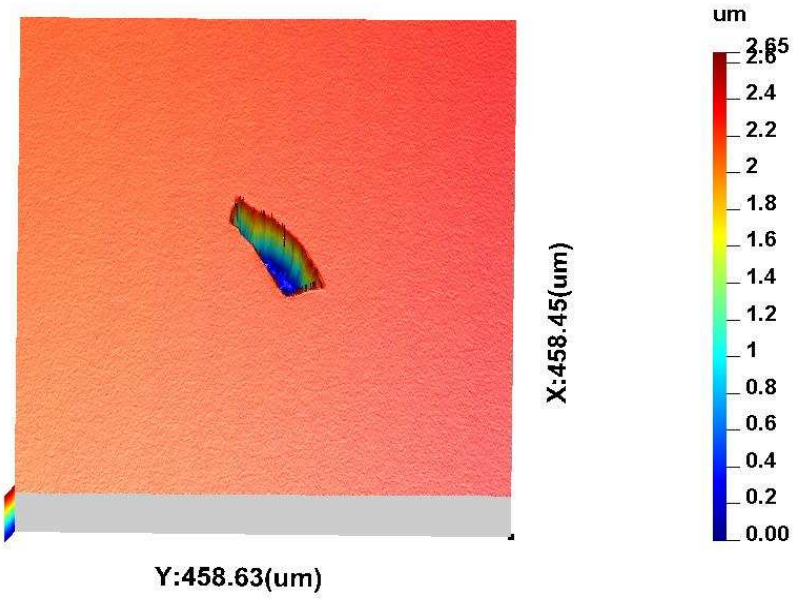

Figure 5-13: Hole type defect.

The data collected from the CCI has been filtered, and the purpose of employing a filter is to remove aspects of the surface topography which are not required for further analysis, and to

select elements of a surface which are required for further examination and evaluation. The measured topography data in this study contains three major features of information (roughness, waviness and form). Hence, to examine surface roughness, the waviness and form components must be removed from the data-set before analysis. (K. Stout, Sullivan, Dong, Mainsah, & Luo, 1993) recommended the use of the robust Gaussian filter, saying, 'The Gaussian filter is ideally suited for smoothing surfaces with rich features' (p.173). Surface roughness and waviness can be separated with no phase distortion for both separated components in a single filtering procedure.

This method of filtering is strongly based on the assumption that the micro-geography of the surface is constructed of similar sinusoidal waveforms with various wavelengths. In this study, all of the measurement data files have been levelled and filtered using 'Surfstand' software package in order to;

- Extract the surface features of interest from the measured data for further analysis.
- Remove unwanted small-scale features and measurement errors (noise and spikes).

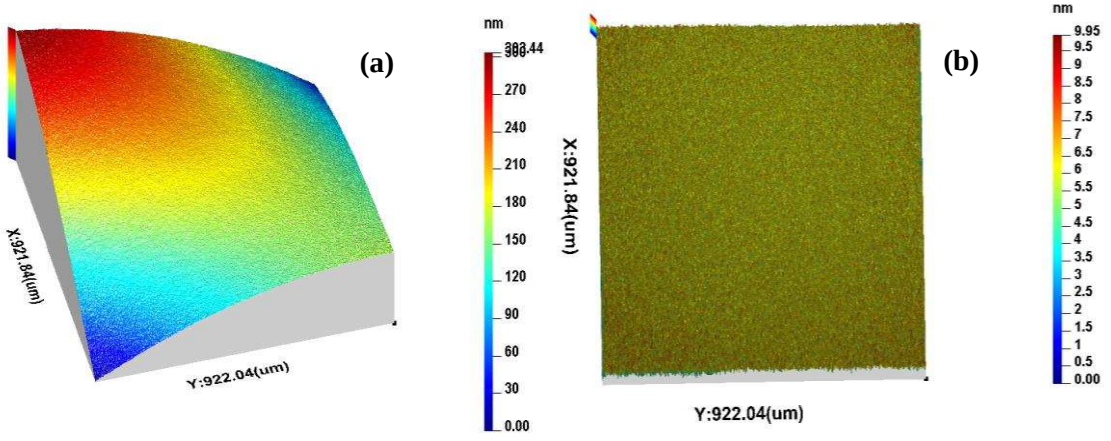

Figure 5-14: Filtration process (a) before filtration (b) after filtration

Standard analysis approaches based on areal field parameters and in particular the surface roughness, standard deviation and skewness parameters were applied for the overall data using

"Surfstand" toolbox in attempt to differentiate between the most defective and non-defective samples. The parameter Sa (roughness mean height) has been applied to the surfaces data, table [5-2] shows the mean value of the roughness average of 700 independent measurements for each sample.

Table 5-2: S_a parameters mean value

Sample No.	S_a parameters mean value (nm)
Sample 2701	0.88
Sample 2702	0.80
Sample 2705	0.78
Sample 2706	0.87
Uncoated /Sample	1.0

The parameter S_q (RMS Roughness) results shown in Fig [5-15] indicated that, sample (2705) has more large defects than the other characterised samples as it has the highest minimum and maximum Sq values (7.4 nm < S_q < 96 nm) due to the existence of large defects on the samples surface presented in Fig [5-13].

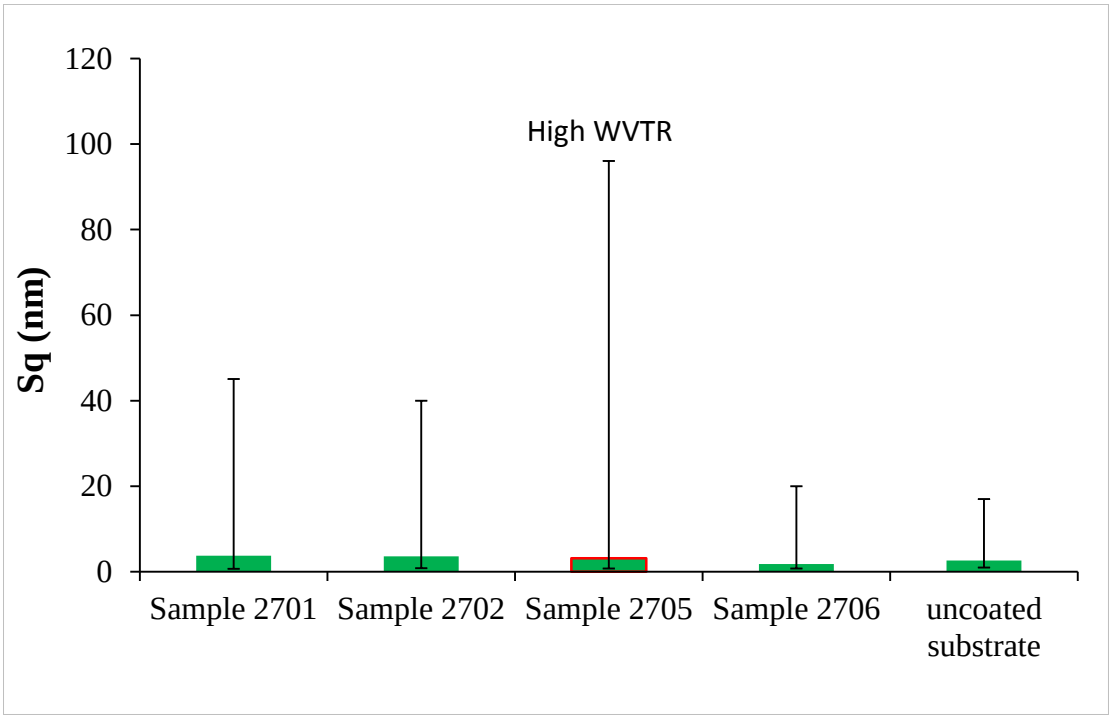

Figure 5-15: Standard deviation averages of the samples (The error bars represent the maximum and the minimum Sq values obtained)

The parameter skewness (S_{sk}) has also been applied to the surface data for the purpose of investigating the distribution of the defects. This parameter has indicated that there are two types of features presence on the samples' surfaces, which are peaks and dales as shown in Fig [5-16]. Where,

S_{sk}	> +1	peak dominated surface
S_{sk}	< -1	valley dominated surface
S_{sk}	-1 < 0 > 1	peaks + valley present in the topography

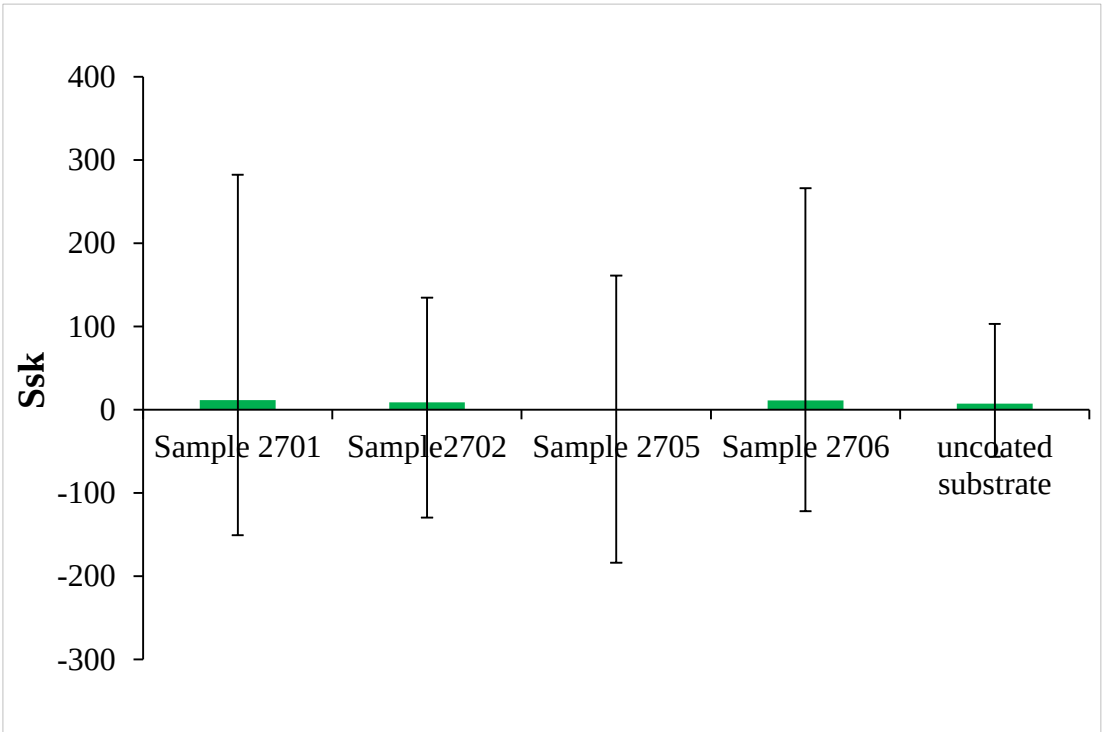

Figure 5-16: S_{sk} value variations of the samples

The overall results of using the areal field parameters indicated that there are possibly significant pits (dales) and peaks on the surfaces for each sample. However, this method of analysis proved insufficient to isolate outliers nor distinguish the significance of defects or any possible topographical differences in sample 2705. Therefore, a method of 'Wolf pruning' (ISO25178-2, 2012) was utilised to carry out topography segmentation analysis. This method (Wolf pruning) provides a reliable approach for extracting features of functional interest and by accurately excluding insignificant geometrical features that are induced such as

measurement noise, small topographical features and measurement errors. The procedure used here consists of finding the peak or pit (dale) with the small height difference below a defined threshold and combining it with the adjacent topographical saddle point as shown in Fig [5-17].

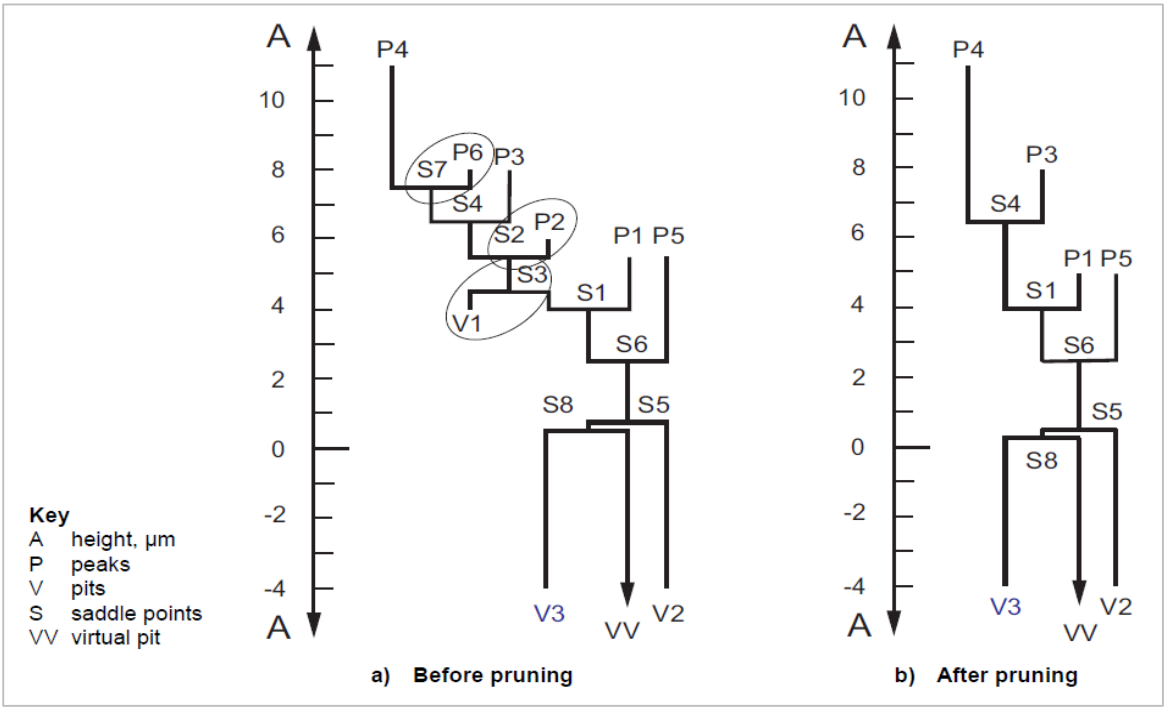

Figure 5-17: Wolf pruning method (ISO25178-2, 2012)

The aim of this method is to leave only those peaks and dales that are deemed to be significant in the resultant three dimensional output data. The density of the peaks of one data file sample was found to be 4.89 pts/mm^2 at 1% Wolfprune. The density reduced to 2.47 pts/mm^2 at 20% Wolfprune. This "toolbox" method was adapted using Surfstand software package to automatically detect the density of significant peaks (S_{pd}) and the density of significant dales (pits) features (S_{dd}), where the threshold selected to give pruning of only those peaks and dale features that are greater than 20% of the maximum peak to valley magnitude (Sz) of non-defective sample. Appendix (D) shows the density of peaks and density of dales detected by this method. In this procedure a parameter S_{fd} (S_{fd} = the number of significant peaks + significant dales) was adopted in the toolbox and used to define the significance of any

peak/pit greater than 20% of the total peak to valley roughness (S_z) of a non-defective sample, see Fig [5-18]. Using this default, the results showed no clear correlation between defect density and WVTR. It can be seen that sample 2705 had the highest WVTR as shown in table [5-1] but the lowest defect density as shown in Fig [5-19].

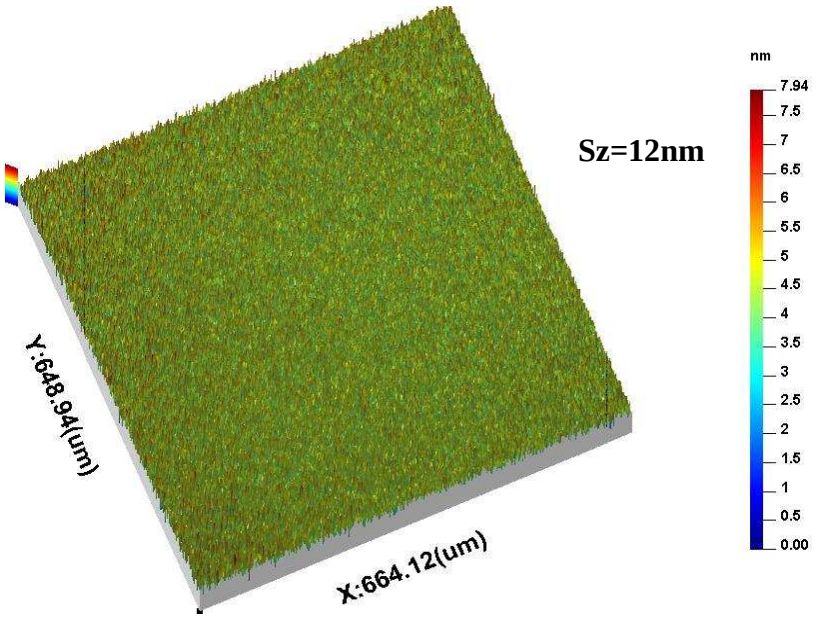

Figure 5-18: Peak to valley roughness (S_z) of non-defective sample

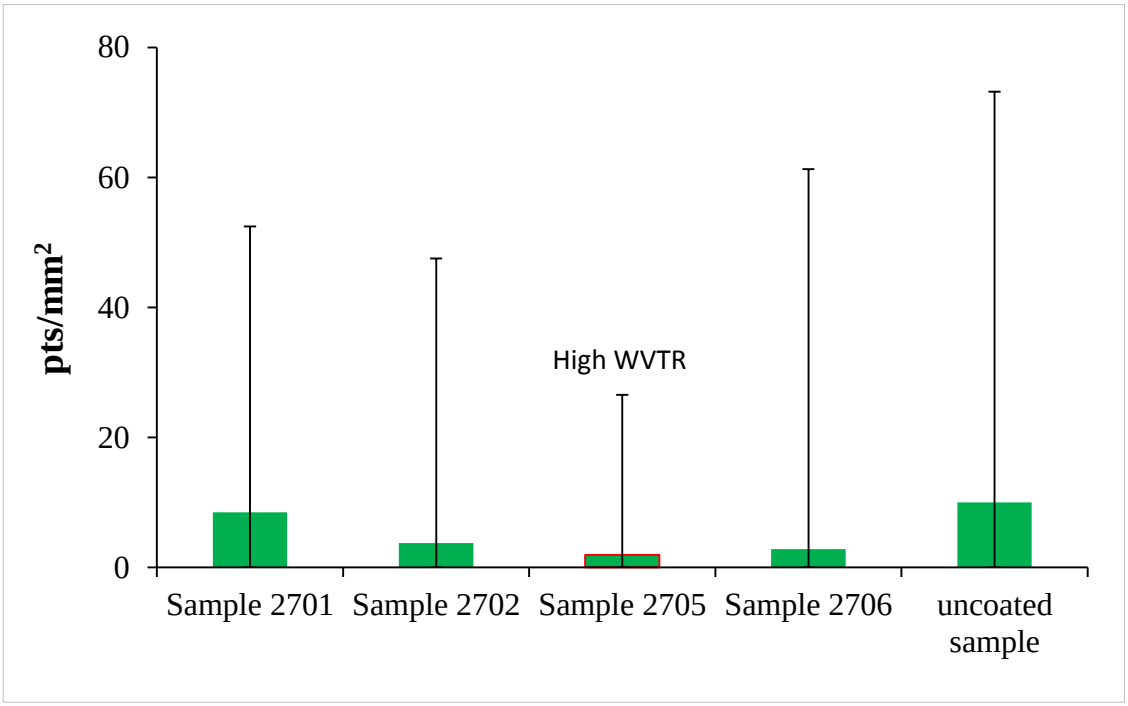

Figure 5-19: Defects density (all data files)

A further analysis conducted with additional prune conditions on two samples that have the same WVTR test stabilisation time, which are sample 2705 (highest WVTR value) and sample 2706 (lower WVTR value); In this case additional lateral dimension criteria were introduced in order to isolate only the largest defects (in the xy plane). The criteria of being assigned as a large defects was (±3xSq vertical) based on the normal Gaussian distribution of the data as shown in Fig [5-20] and (15µm lateral) based on the visual assessment of the samples, where Sq is the standard deviation of non-defective sample, see Fig [5-21].

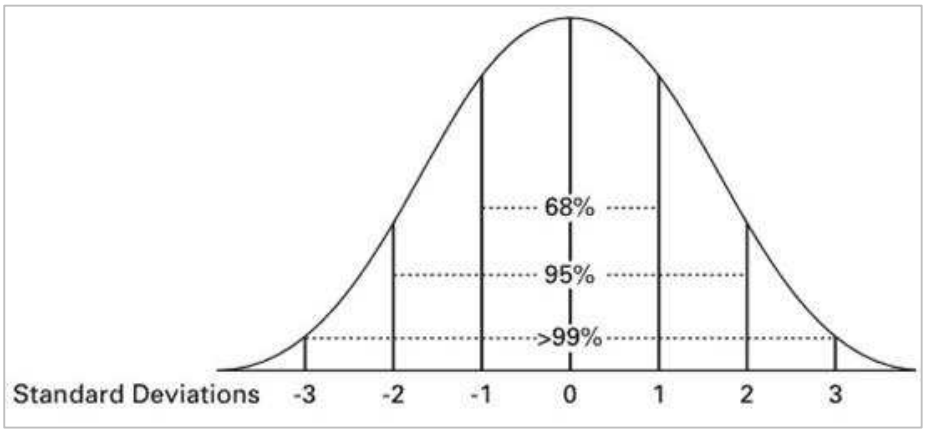

Figure 5-20: The standard normal distribution

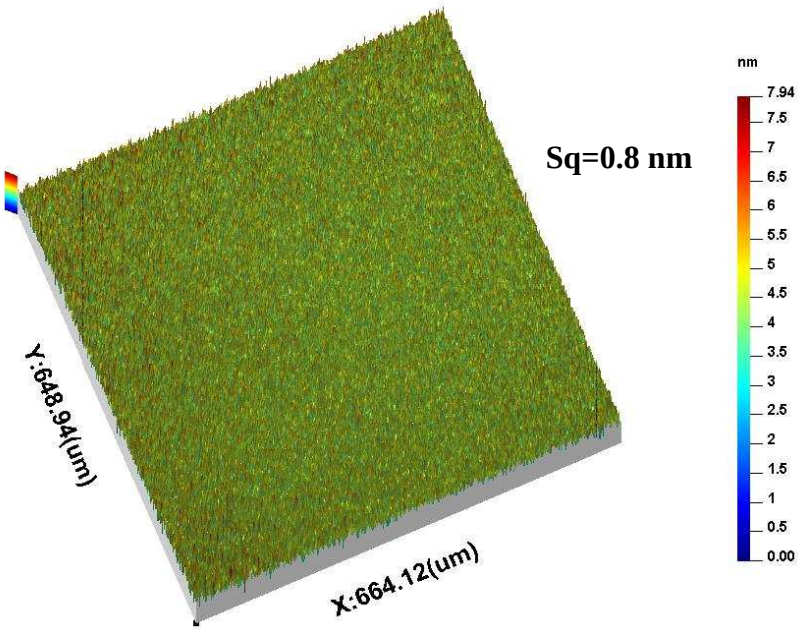

Figure 5-21: Standard deviation of non-defective sample

The defects were measured and recorded for effective discrimination between significant and non-significant defects as shown in Fig [5-22], and findings would appear to suggest that small numbers of large defects (as detected by the optimal prune criteria) are the dominant factor in determining WVTR.

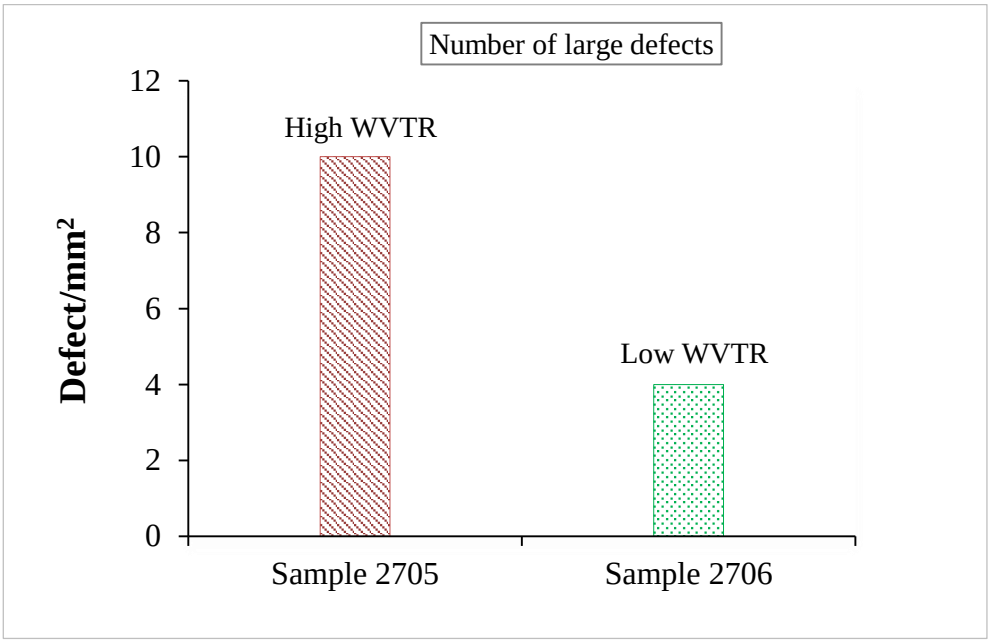

Figure 5-22: Significant defects count for two similar samples.

Based on the criteria mentioned above, the size (height, depth and width) for all the observed defects are summarized in table [5-3].This table catalogues all the observed features and their size scale, and appendix (C) shows 3D images for theses defects.

Table 5-3: Types of defects and their size scale

Type of defect	**Feature Size**	
	Height/depth	**Width**
Spikes	≥ ±3x Sq height	≤ 3 µm (~3sample spacings)
Cracks	≥ ±3x Sq depth	≥ 300 µm length (1/3 field of view)
Scratches	≥ ±3x Sq height	≥ 300 µm length (1/3 field of view)
Ghost defects (unmeasurable feature)	not measurable	≥3 µm width
Pinholes	≥ ±3x Sq depth	≤ 3 µm lateral dimension
Peaks	≥ ±3 x Sq height	≥3 µm width
Holes	≥ ±3x Sq depth	≥ 3 µm lateral dimension

5.3.3 Environmental Scanning Electron Microscopy (ESEM) Analysis

The high lateral spatial resolution of ESEM imaging can provide information about defects in the Al_2O_3 barrier layer that are beyond the resolution of optical interferometry or standard microscopy techniques. Imaging of the Al_2O_3 barrier layers was performed using a FEI Quanta 250 field emission gun environmental scanning electron microscope (FEG-ESEM). The instrument has a higher resolution, higher magnification (up to2 million times) and greater depth of field compared to the optical microscopy. The instrument allowed for the visualisation of the structures of the Al_2O_3 layer that would not normally be resolvable by optical microscopy. The spatial resolution of the instrument in environmental mode is approximately 1.4 nm at 30 keV when performing secondary electron imaging (FEI, 2009).

To image the Al_2O_3/polymer structure low vacuum mode was employed using water vapor at pressures between 120-400 Pa. An off axis large field detector was used to collect the amplified secondary electron signal emitted from the specimen; this detector has the advantage of providing images with a relatively large field-of-view. At these pressures the charging effects of the samples are mitigated, thus allowing high contrast imaging of these electrically insulating samples to be undertaken without the need for a conductive surface coating. Elimination of the surface coating means the Al_2O_3 surface can be directly imaged, and no modification to the surface by the deposition of a conductive coating can be assured, which would be necessary using standard high vacuum mode SEM imaging.

An investigation of typical defects previously detected and catalogued by WLSI and optical microscopy was further extended by using the ESEM. To better image the surface of the Al_2O_3 layer a sample tilt of 40° and electron beam energy of 30 keV was employed. Applying these conditions, a cross-sectional electron micrograph was collected near the edge of the Al_2O_3/polymer structure; see Fig [5-23]. The instrument also allowed for the visualisation of small features that would not normally be visible by the optical microscopy, Fig [5-24] shows

a 40 nm Al_2O_3 barrier layer which exhibits pit like defects between 100 nm to 500 nm in diameter on the surface.

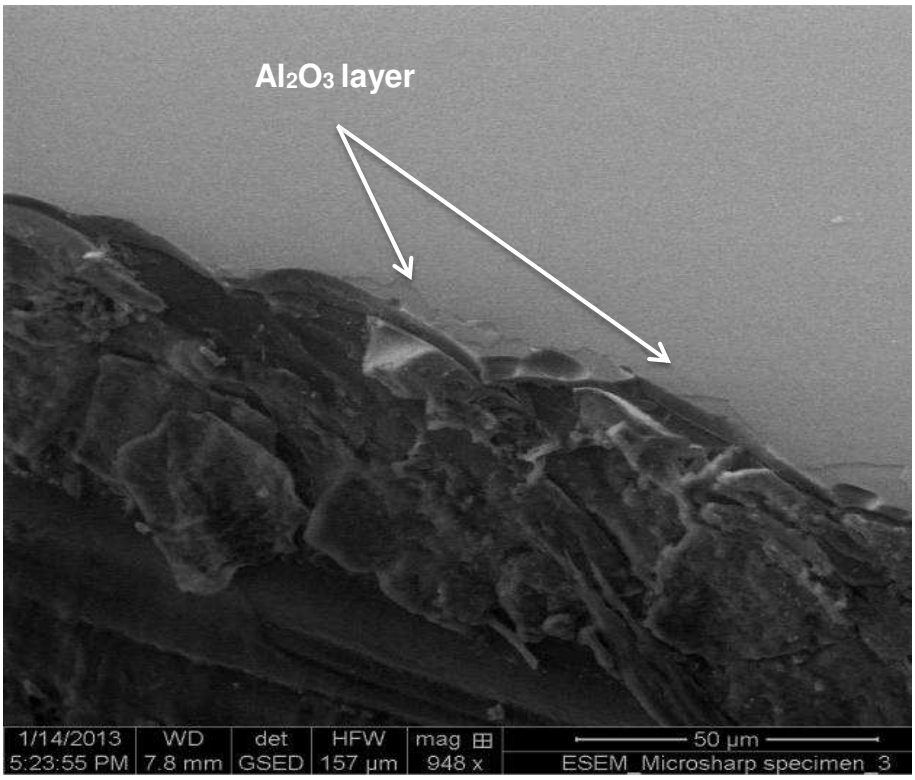

Figure 5-23: Al_2O_3/polymer cross-section (partially delaminated)

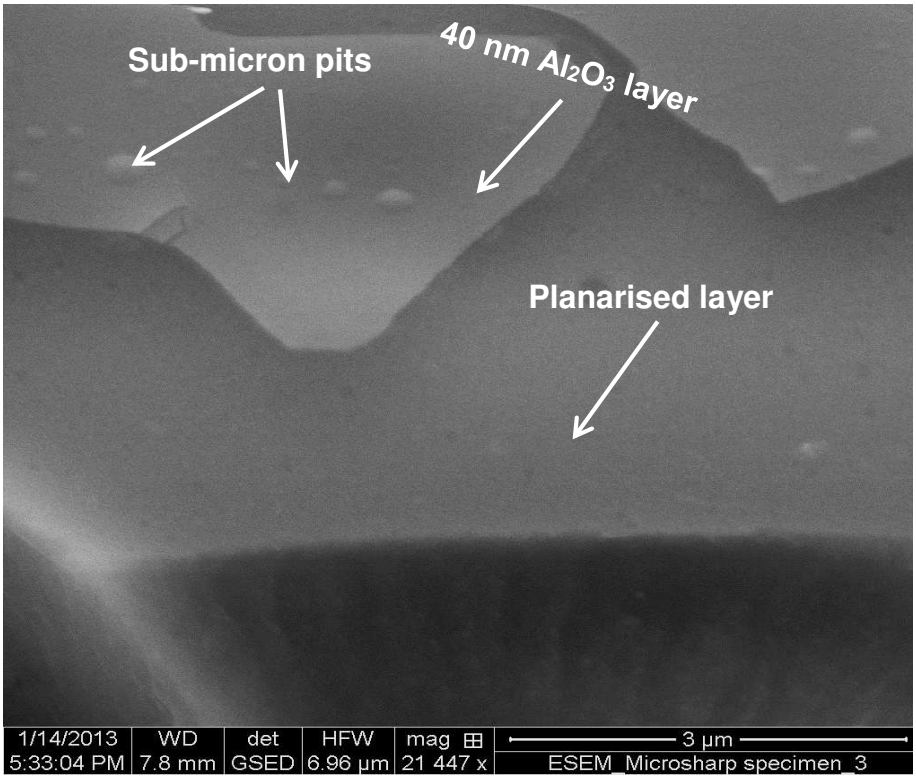

Figure 5-24: Typical pits type defects (partially delaminated)

Moreover, Fig [5-25] shows an image of a typical hole defect of approximately 4 µm in diameter in the Al_2O_3 layer, and a region of differing contrast is observed surrounding this hole; this is attributed to the delamination of the Al_2O_3 layer from the underlying polymer structure due to water vapor penetration.

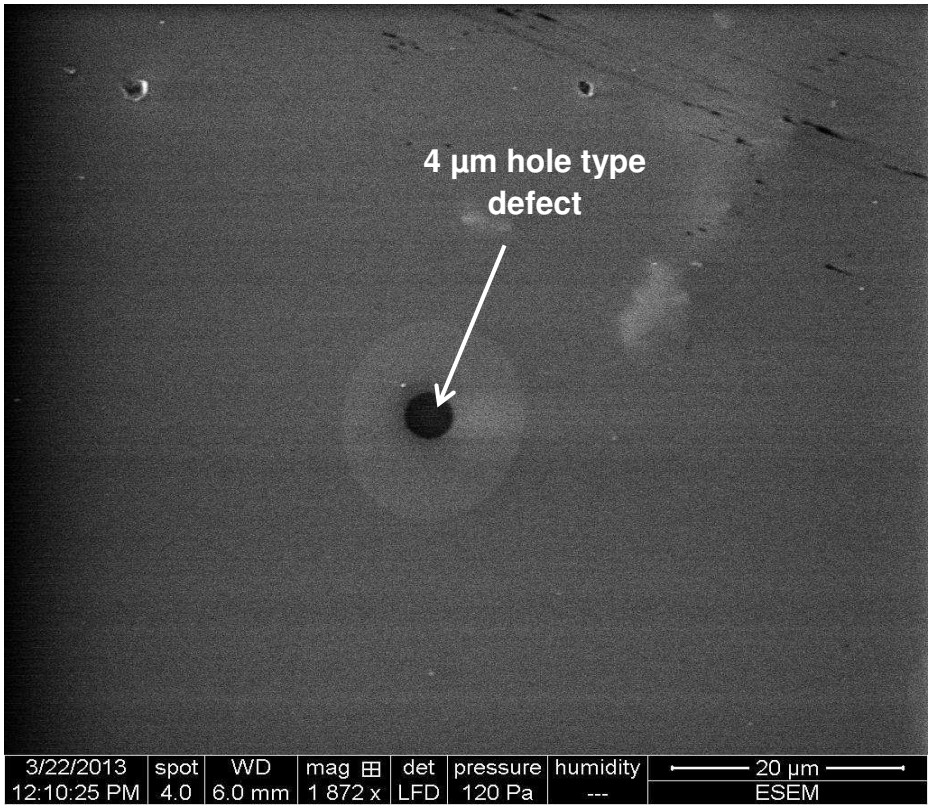

Figure 5-25: Typical hole type defect

The focused ion beam (FIB) image of the Al_2O_3 ALD coating is shown in Fig [5-26]. It shows the thickness of the Al_2O_3 ALD barrier coating. This cross-sectional image obtained using the FIB confirm the conformal ALD-Al_2O_3 layer with high aspect ratio. The image is in low quality due to the charging effects of the Al_2O_3 material, the surface of the sample has accumulated charge because the electrons are not allowed to escape from the surface via a conductive path. Thus, the image performed by the SEM were very poor. Insulating and semiconducting materials such as the Al_2O_3 should be coated with a conductive material to prevent surface charging so the charging effects of the samples can be mitigated. The

following image shows the best image that has been obtained after optimising the instrument conditions while using standard high vacuum mode.

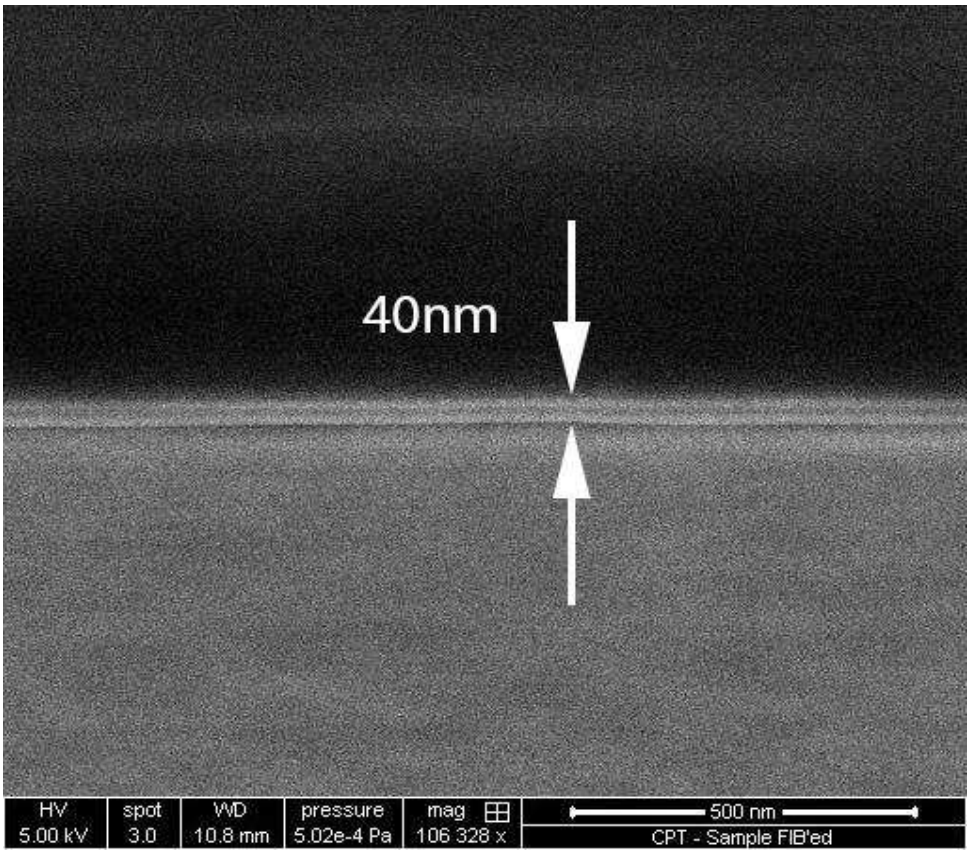

Figure 5-26: The FIB image of Al_2O_3 encapsulated PEN film

5.3.4 Atomic Force Microscopy Analysis

Although the object targeting and the image acquisition can be more rapid using the ESEM, aluminum oxide is difficult to examine as it has a tendency to rapidly charge, resulting in beam divergence and image degradation. In contrast, AFM can analyse the samples with minimal sample preparation, thus preserving surface textures and allowing repeat analyses without the risk of charging (Bottomley, 2012). The AFM can produce an equal or higher data resolution image of an equivalent area, but with the addition of absolute x, y and z values for any features observed. In this study, a Bruker's Dimension icon® Atomic Force Microscope (AFM) was used to characterise the Al_2O_3 ALD barrier films. The technique

allowed much smaller defect sizes to be examined than would be possible by the ESEM and WLSI. It has been also used to determine the size of the peaks (particles) over the films which were not detectable by the ESEM or the conventional optical microscopy technique. Fig [5-27] shows different peaks type defect captured by this technique.

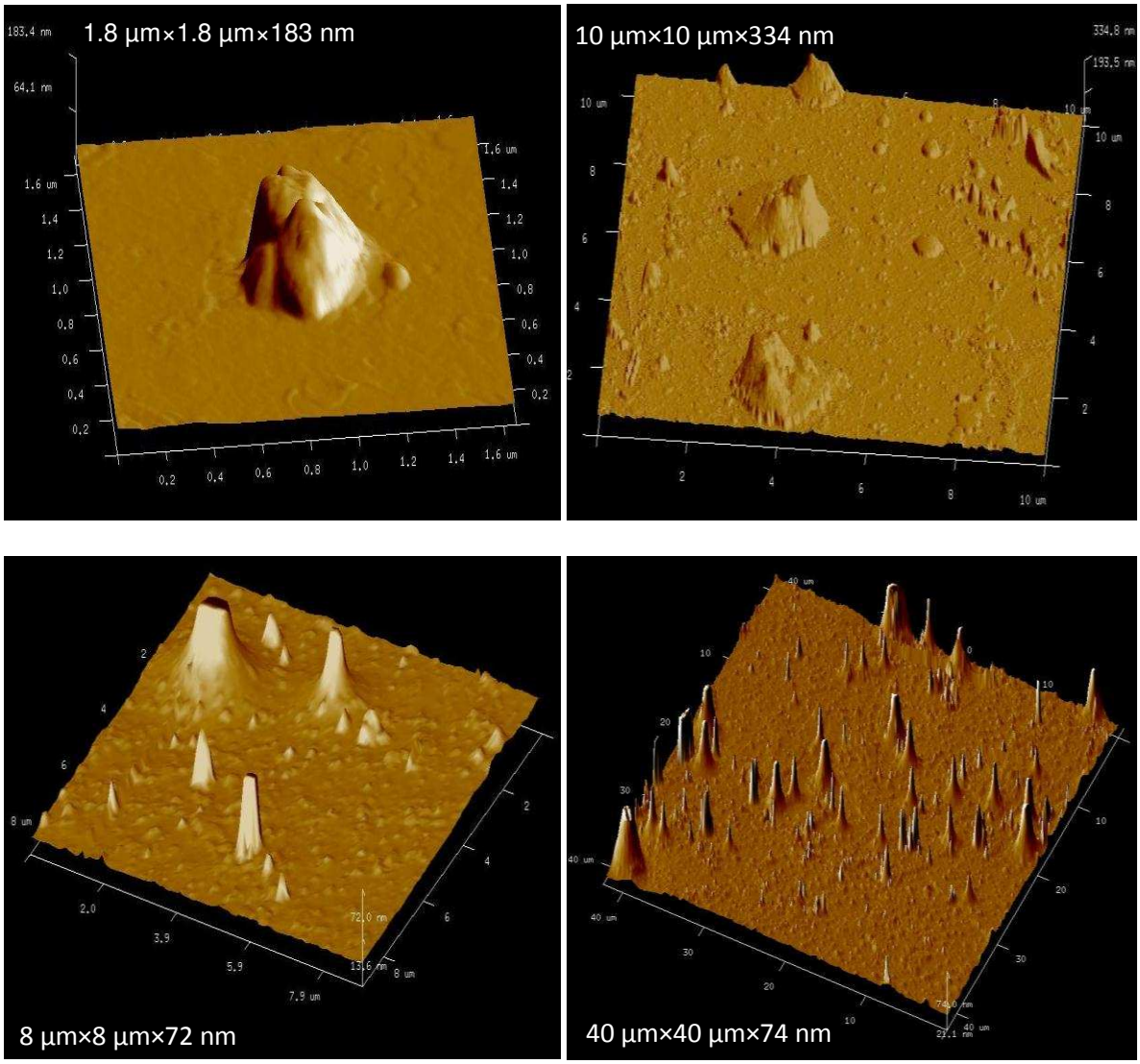

Figure 5-27: AFM images-peaks type defect

5.4 Defects Classification System

A defect classification system was developed as shown in Fig [5-28], in order to enhance the interpretation of defect data within this project and across the large area substrate sector in

general. At present no such system exists, however very recently a system for defect classification in the die polishing industry has been proposed (Rebeggiani, Rosén, & Sandberg, 2011). This system has now been adopted and modified for the current project and allows a unified classification of defect to be implemented. This classification system lists the most detrimental defects correlating with high WVTR. The proposed system is based on breaking the defect types down into four main groupings and symbols;

(i). Inwardly directed defects- holes, scratches, cracks.

(ii). outwardly directed defects - particulate debris.

(iii). Differing appearance to surroundings - delamination, stripes.

(iv). Surface relief – high roughness, waviness.

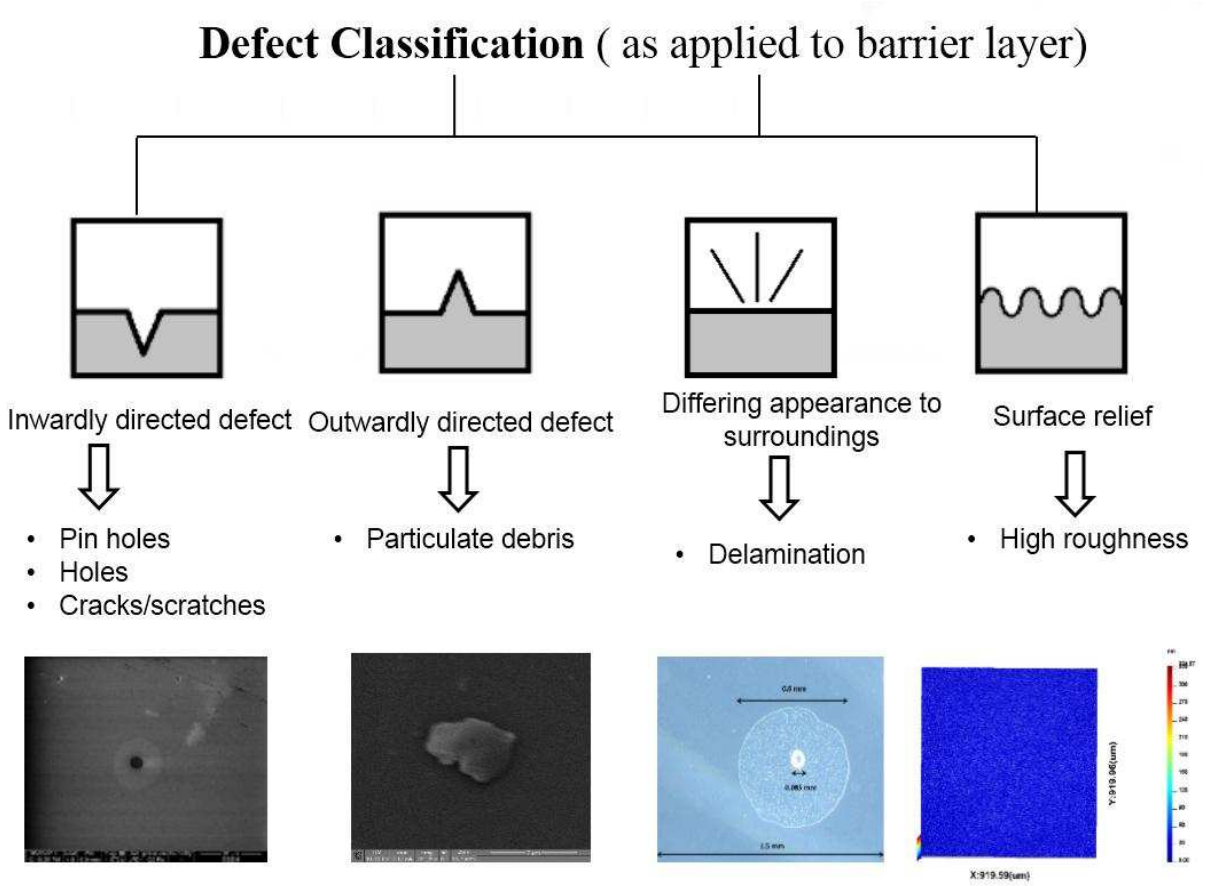

Figure 5-28: Classification of defects on PV barrier substrate

5.5 Summary

The Al_2O_3 barrier film is known to improve the PV lifespan due to the reduction in WVTR. This improvement can be seriously affected and potentially reduced when defects in this barrier film are present. Surface metrology techniques have provided the ability to measure and effectively characterise these types of defects. Information has also been provided on what type of defects will impede the PV performance and lifespan. Feature segmentation analysis has provided a clear evidence for the correlation of surface defects size, defect density, and the transmission of water vapor through the barrier coating layers. The investigation in this chapter concludes that the total permeation rate corresponding to small numbers of larger defects is much greater compared to the total permeation rate corresponding to large numbers of small pinhole-type defects over the same area of substrate as evidenced by Fig [5-19] and Fig [5-22]. This result provides important information which will be in valuable in the future development of an automatic in-line defect detection system, and suggests that in-line inspection systems should concentrate on measuring the presence of "large" defects rather than expending processing effort on trying to characterise large numbers of "small" defects.

CHAPTER 6

6. PV Substrates Cleanliness Effect (Test 2)

6.1. Introduction

Defects in the PV barrier films are inherently present because of imperfections in the deposition process (intrinsic defects) or as a result of the presence of impurities on the film substrate (extrinsic defects) (Greener et al., 2007).Therefore, even if the substrate is coated with an inorganic barrier layer (Al_2O_3), the barrier performance is still expected to fall short for flexible PV applications. Surface cleanliness of the substrate materials from the 'external' or damage contaminants such as air-borne debris, particulates, scratches, etc. is an important factor to improve the coating quality of the PV barriers and to reduce the presence and the density of the defects. In this chapter, general approaches to reduce the density of the defects on the substrate layers before the ALD deposition processes including various cleaning methods were taken into consideration. These improvements to the substrate materials may significantly contribute in lowering the water vapor permeability. The investigation was carried out on a second set of samples produced in exactly the same way as test 1 (chapter 5); however the pre coating procedures were varied as shown in table [6-1] in order to investigate the effect of cleanliness on the WVTR results.

Table 6-1: Al_2O_3 samples pre coating conditions (Test 2)

Sample No	Practice No	Conditions
12k1001	Practice 1	Polymer surface unprotected before loading for ALD coater
12k1002		
12k0902	Practice 2	Polymer surface protected to the last moment before loading into ALD coater. However, some visible scratches were reported on sample 12k0902
12k0901		
12k0803	Practice 3	Contact cleaning of the polymer before ALD coating
12k0804		

These samples have an 80 mm diameter area that has been ALD coated with 40 nm Al_2O_3, where each pair of samples was prepared in a clean room under different conditions.

6.2. WVTR Test Results

Following the coating process, the samples were measured for water vapor transmission rate (WVTR) using Isostatic standard test (MOCON®- AQUATRACE2) instrumentation at specified conditions of (38 °C and 90% RH, respectively) prior to the surface measurements. The instrument technical specifications are stated in table [6-2], and the water vapor transmission rate results are shown in table [6-3].

Table 6-2: MOCON®- AQUATRACE2 technical specifications

WVTR Range	5 x 10 $^{-4}$ gm./(m^2 - day) – 5 gm/(m^2 - day)
Sensor	AQUATRACE2
Test Temperature Range	(5 - 50 ° C)
Relative Humidity (RH)	Films - 100% RH
Test Sample Sizes	Films - 50 cm^2

Table 6-3: Water vapor transmission rate at specified conditions 38 °C and 90% RH (Test 2)

Sample No	**Water vapor transmission rate (g/m^2/24 hrs.)**
12k1001	$5x10^{-4}$ (equal to detectable level)
12k1002	$<5x10^{-4}$ (below detectable level)
12k0902	$1x10^{-3}$ (above detectable level)
12k0901	$<5x\ 10^{-4}$ (below detectable level)
12k0803	$6x10^{-4}$ (above detectable level)
12k0804	$<5x10^{-4}$ (below detectable level)

6.3. 3D Surface Measurement Procedures

A coherence Correlation Interferometer (CCI-3000) was used again in this study to conduct areal surface analysis over a relatively large field of view without contacting or otherwise damaging the samples. The data taken from the CCI can provide a number of important areal surface texture parameters, with a nanometer-level accuracy and repeatability, making them ideal to predict the functional performance of the samples. The investigation in this study was performed on the previously described samples (table 6-1); where in this case approximately

100% of the overall area was measured on each sample (≥ 2000 measurements) using X20 objective lens, and this lens allows this instrument to measure a sample area of approximately 1 mm^2 (imaged onto a CCD array of 1024×1024 pixels). A new method has been developed based on "feature segmentation" to analyse the overall measurements data collected in this study.

6.3.1 Visual Inspection Analysis

The presence of defects is postulated to be directly responsible for higher WVTR levels. As a result, simple counting of the data files with defects present (significant or non-significant) as shown in Fig [6-1] based on the visual assessment if the CCI data was undertaken. In this initial phase no specific criteria is applied as a means of identifying which defects are responsible for the high WVTR value. No correlation was obvious as to which defects were responsible for the high WVTR. Thus to evaluate functionally significant attributes, such as defects density, size and distribution, feature parameters (X. Jiang et al., 2007) were used to effectively discriminate between the most significant and non-significant defects.

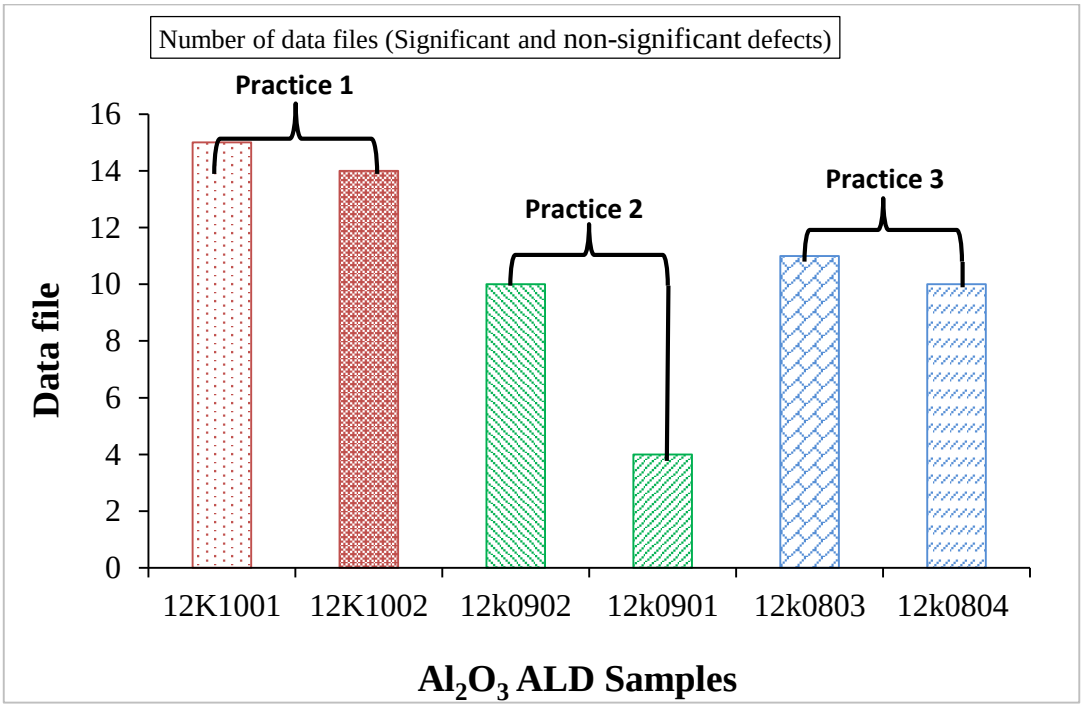

Figure 6-1: Data files containing defects for Al_2O_3 ALD samples

6.3.2 Areal Parameters Analysis

Choosing a set of areal parameters which are functionally correlated in such applications is a particularly difficult topic. Noise and measurement errors can also create artificial “small” insignificant features which need to be accounted for. It is therefore essential to distinguish between those features that are functionality significant from those which are non-functionally significant. The solution to this problem in most cases is usually based on analysing large amounts of experimental data (De Chiffre et al., 2000).

To facilitate the examination of the relevant surface texture (roughness) , the waviness and form components were removed using a suitable robust Gaussian filter at 0.025 cut-off length (K. Stout et al., 1993). Numerous numerical parameters have been proposed previously (ISO25178-2, 2012; K. J. Stout & Blunt, 2000) and in the present study initially only simple amplitude parameters were investigated.

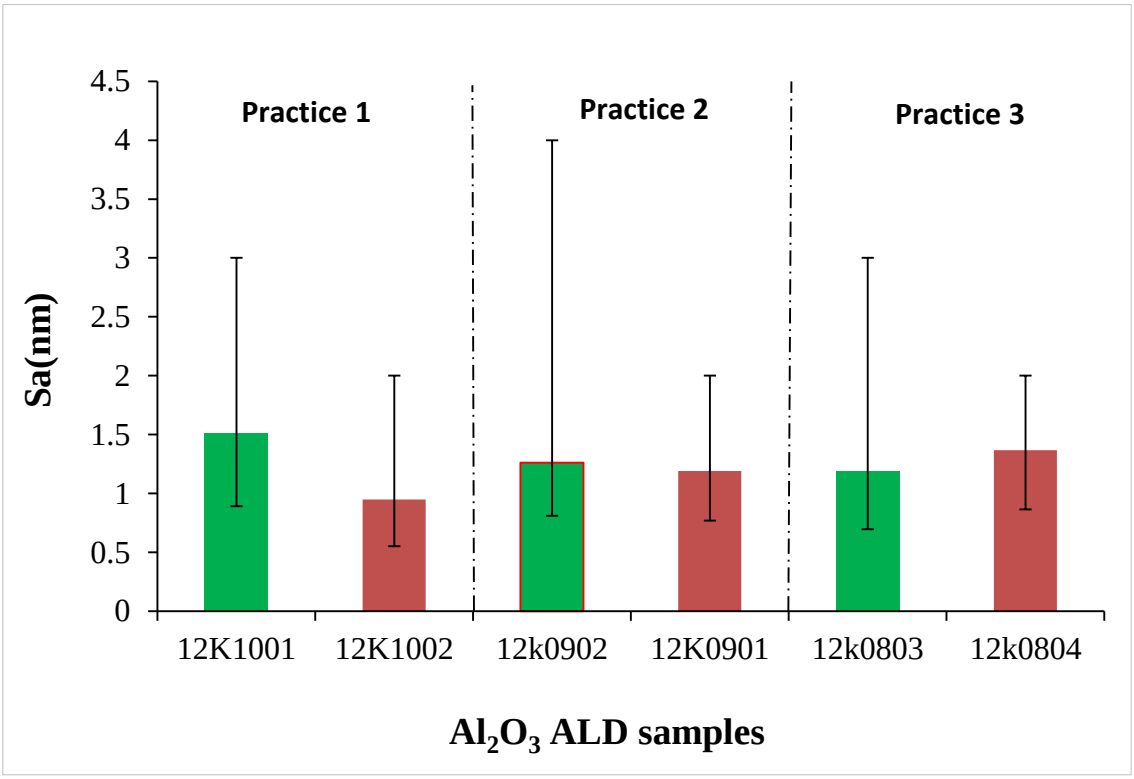

Figure 6-2: Variations in roughness average

The average roughness parameter Sa results shown in Fig [6-2] does not clearly differentiate between the most defective and non-defective samples. However, this parameter has shown that samples coded (12k001, 12k0902 and 12k0803) have a higher average roughness variations than the other samples, and this was attributed to the existence of larger defect sizes on these samples than others. This conventional analysis method (which use all the data at all scales) has shown to be deficient if functionally significant topographic features need to be characterised. Using this parameter, the results showed no clear correlation with the WVTR results.

6.3.3 Feature Segmentation Analysis

The present study is based upon the supposition that defects above a certain scale determine the water vapor transmission through the barrier coatings. To this end feature segmentation analysis (ISO25178-2, 2012) was implemented using Surfstand software package in order to separate the significant from non-significant surface topography features. Feature parameters are not specifically defined by an equation, as are field parameters but are a toolbox (Surfstand) of pattern recognition techniques (see appendix B).

The characterisation consisted of five steps; (1) selection of type of texture feature, (2) segmentation, (3) determine the significant features, (4) selection of feature attributes, and (5) quantification of feature attributes statistics. Therefore, a method of area pruning was performed by trying out various segmentation criteria. The segmentation was applied by means of an "iterative" process. The protocol used for characterising the barrier films was as shown in Fig [6-3] and explained in this section.

Firstly, the surface was filtered to eliminate data noise, where the box filtering (Gaussian filtering) uses a cut-off of 2^n points; where n is the smooth level (from 1 to 5), and n was specified to be 5. After smoothing edge processing was performed on the data using a Sobel

type operator (Blunt & Xiao, 2011).The edge data is then "pruned" by means of Wolf pruning where all data elements below 10 % (default) of the Sz value (of the edge filtered surface) are combined (Blunt & Xiao, 2011), and those elements higher than 10% Sz (default) were retained as significant. Following Wolf pruning an area prune was applied where if an area was found to be less than 5 µm lateral diameters (this area being defined by optical and SEM analysis) it was deemed insignificant and combined with its neighbouring region.

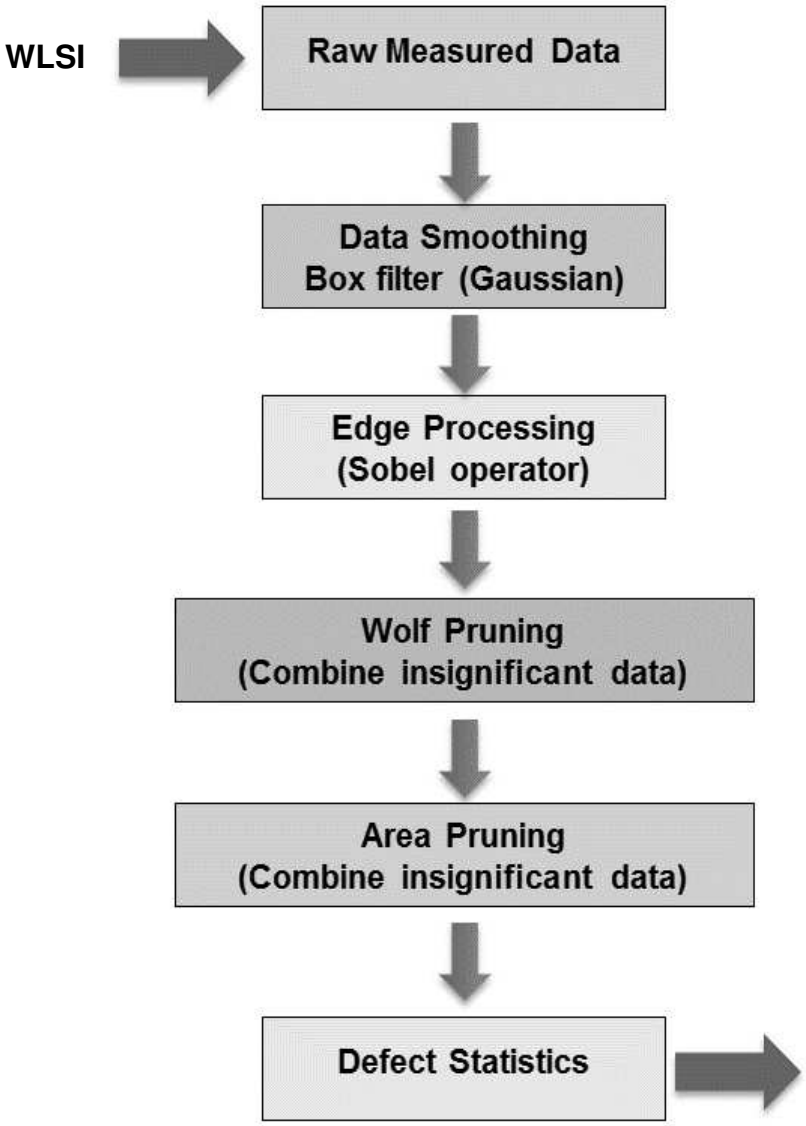

Figure 6-3: Feature segmentation analysis process

Fig 6-4 (a-b) show defects following the segmentation process for three different samples. The figure shows the power of the procedure for extracting defects from the surface data. Following the extraction the defect density for significant defects can be simply calculated.

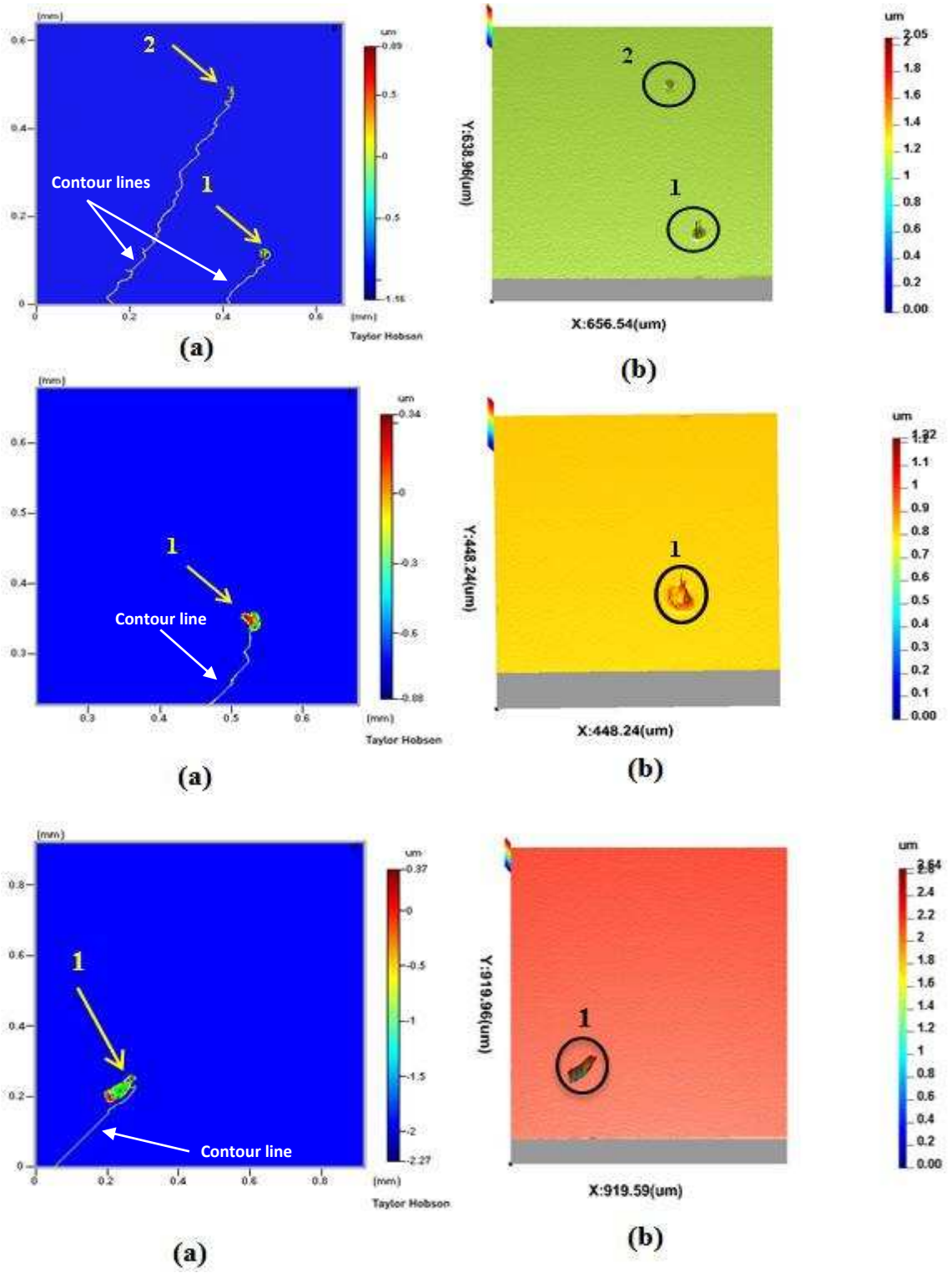

Figure 6-4: (a). Defects count after segmentation, (b). Defects before segmentation

6.4 Correlation between Defects Size-scale and WVTR.

As a result of the lack of correlation between the defects size-scale and the WVTR values using the conventional surface analysis method (S_a-parameter) as mentioned in section (6.3.2), segmentation analysis (Blunt & Xiao, 2011; ISO25178-2, 2012; Wang et al., 2011) was carried out using the criteria outlined in section (6.3.3) on the data measured by the CCI (WLSI) instrument. The results in Fig (6-5) indicate that for each pair of samples corresponding to a differing pre-processing of the polymer prior to the ALD coating that, the sample with the highest WVTR value (12k0902) corresponds to the sample with the highest defect density of ≥ 5 µm in lateral dimension. The sample with the lowest WVTR value (12k0901) shows the lowest defects density of ≥ 5 µm in lateral dimensions. This sample (12k0901) had the least contaminating processing prior to coating. Additionally, contact roller cleaning has little or even marginally worse effects on the defect count as compared to un-cleaned/exposed substrates. Finally, it is interesting to note that where visible large scratches were reported (sample 12k0902) the highest defect density and WVTR occurred.

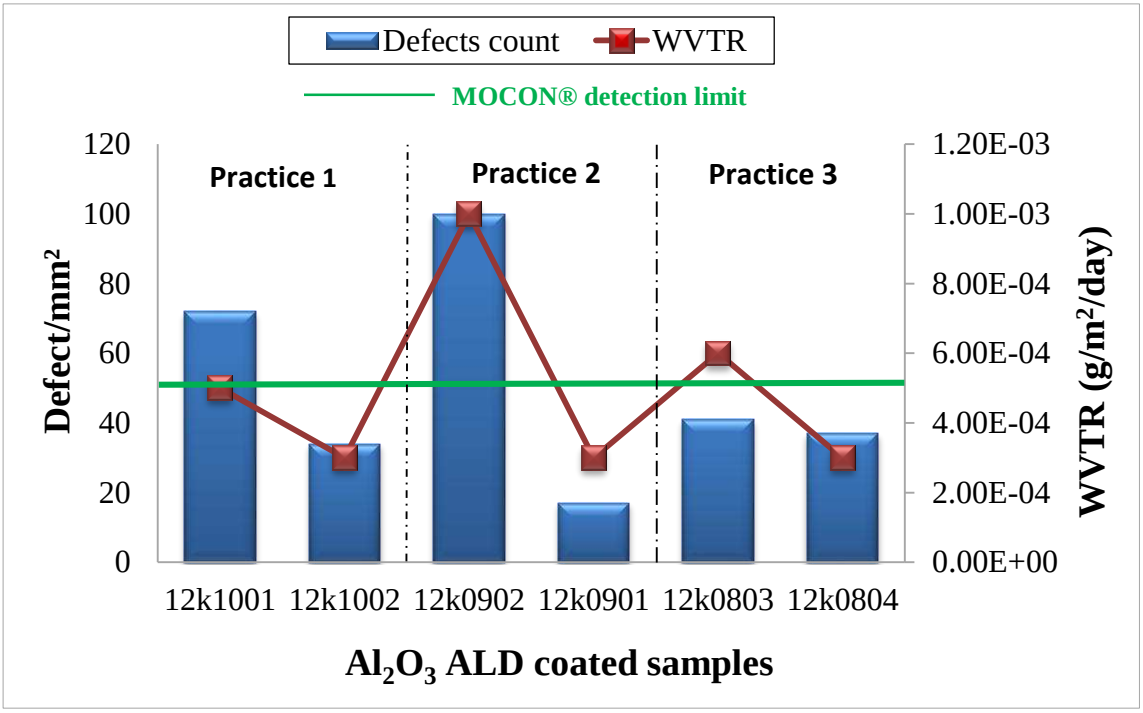

Figure 6-5: Defects density versus WVTR values

6.5 Pre-coating Process Effect (effect of cleanliness on WVTR)

The study in this chapter presented in Fig (6-5) has demonstrated those samples (12k1001 and 12k1002) which were deliberately left exposed in a clean room environment over night show high numbers of defects, but the MOCON® tests show a low WVTR indicating that the films have collected particles, but the particles are not a significant impact on the WVTR. Sample 12k0901 has fewer large defects recorded than the other samples. This is believed to be attributed to the nature of sample handling conditions. The procedure for sample handling and purging/cleaning of the ALD coating equipment was optimised for this sample. This ensured few or even no particles were present on the surface prior to the ALD process. Therefore, the WVTR value was very low. In contrast to this, sample 12k0902 prepared with the same conditions as sample 12k0901 demonstrated a higher large defect count than the other samples, and had the highest WVTR value ≈ 1×10^{-3}g/m^2/day. This sample has larger defects than the other investigated samples (visible scratches/cracks) as shown in Fig [6-6] which may have had a negative effect on the barrier properties thus giving an increase in the WVTR.

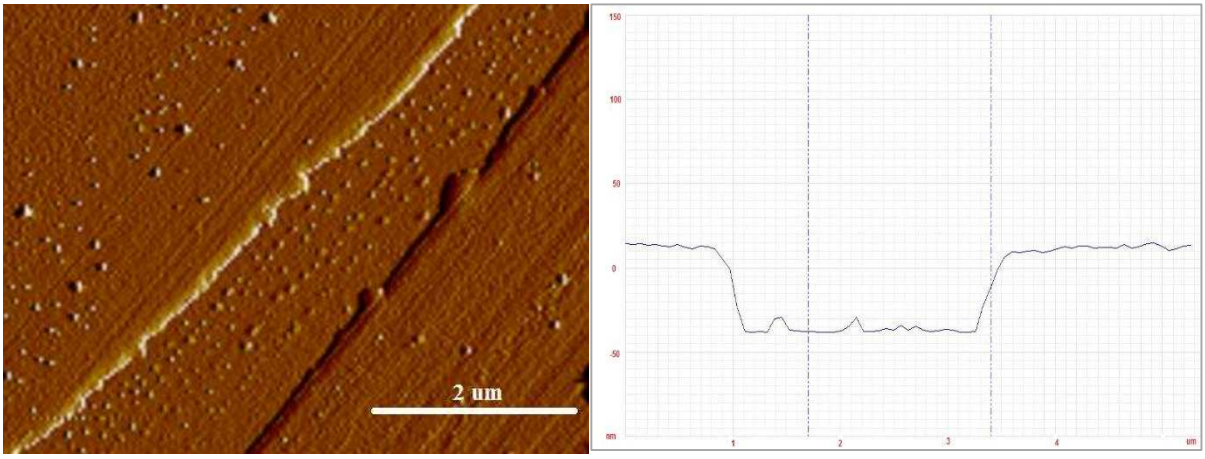

Figure 6-6: Crack in the ALD coating

Lastly, sample (12k0803 and 12k0804) show evidence of more particles and scratches when compared to sample 12k0901 (optimised handling process), indicating that the web-roller

used to clean the substrates before the ALD process, may increase the WVTR by causing scratch type defects or alternatively only remove particles leaving pinholes.

The investigation in this chapter seems to concur with previous published literature (Zhang, Zhang, et al., 2009), individual defects or pinholes are generally caused by particulate contamination or the surface roughness of the substrate. Individual film defects are believed to be the critical features limiting the performance of barriers. These defects must be controlled to assure high barrier quality and efficient barrier manufacturing. The authors also note that these defects could be observed by (FE-SEM). However, the location and density likely result from particle contamination on the PEN substrate. The particles are believed to mask the polymer substrate and prevent effective Al_2O_3 ALD coating. The particles then move or are dislodged with Al_2O_3 coating after the coating process, thus leaving an uncoated region of the polymer substrate as shown in Fig. [6-7] and Fig [6-8] resulting in high water vapour ingress. Other examples of such defects are included in appendix (E).

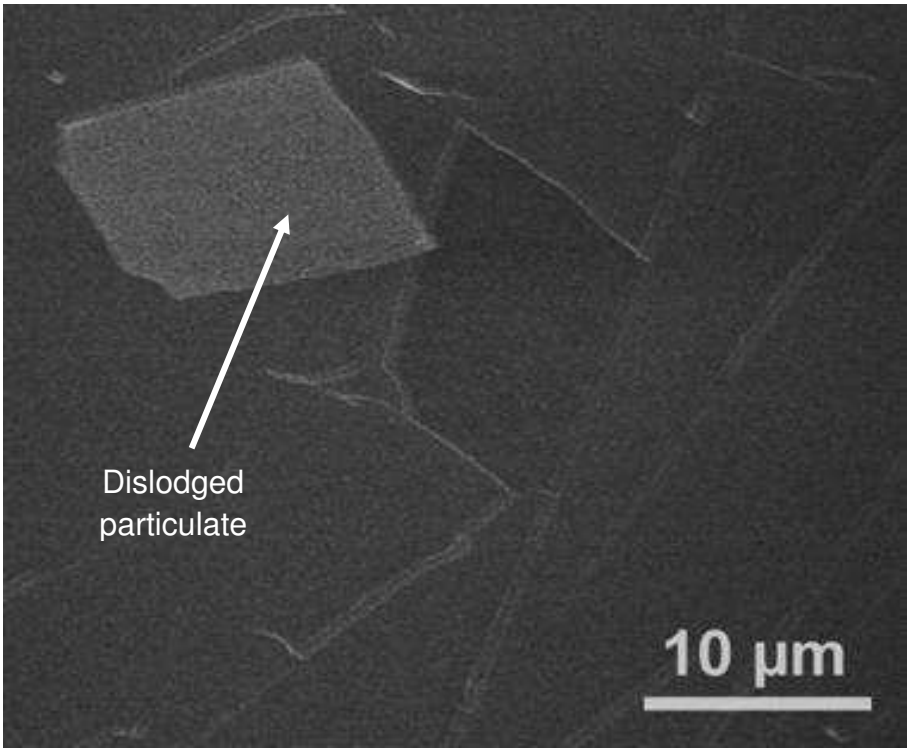

Figure 6-7: Particle dislodged after the coating process

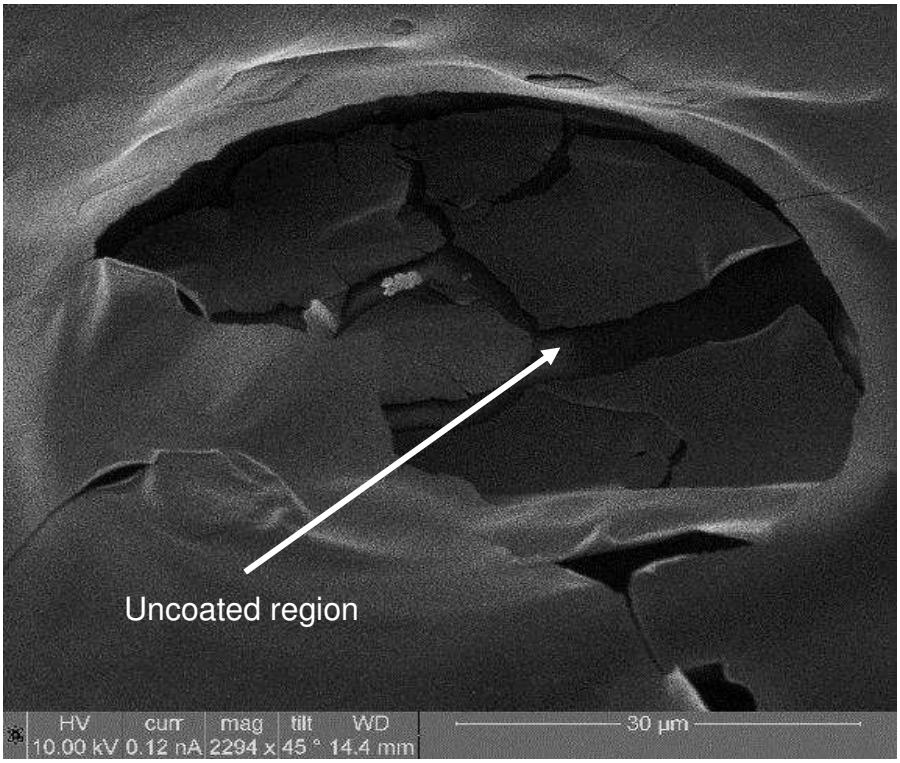

Figure 6-8: Uncoated region of the polymer substrate

Based on the study conducted in this chapter, to optimise the coating process and achieve low WVTR value, longer lifespan and best efficiency, the following criteria are recommended to be followed when preparing the polymer layer (substrate) for ALD coating.

- Contamination must be avoided as much as possible (practice 1 is probably less effective).
- Cleaning has limited effect. However, damage caused by the cleaning tool was seen to be detrimental to WVTR, so it must be avoided.
- Limiting atmospheric exposure ensures best WVTR results (Practice 2 is likely to be more effective).

6.6 Summary

To summarise, the study in this chapter gave a good insight into the best practice to be used when preparing the samples for Al_2O_3 ALD coating process, and the type of defects which

have detrimental effects on the WVTR value. Areal surface texture parameters have been shown to be a potentially effective tool to predict the PV barriers performance and develop a process quality assessment protocol. The type, size and density of the defects which have a negative effect on the WVTR value were determined. Surface segmentation through area pruning method with optimised threshold conditions was shown to have the ability to extract information pertaining to significant defects. The approach has indicated that there is a clear evidence of correlation between defects size-scale and the transmission of water vapor through the barrier coating layer. The total permeation rate appears to be determined by the presence of small numbers of larger defects. These results in this chapter provide further novel information to enable the development of automatic detection measurement system based on in the line measurement.

CHAPTER 7

7. Theoretical Model

7.1 Introduction

Thin layers of aluminium-oxide (Al_2O_3) of the order of a few tens of nanometres deposited via the atomic layer deposition (ALD) method have been introduced in this study to allow the PV modules transparency and flexibility and to provide an effective barrier layer. These barrier films ideally have WVTR of less than 10^{-4} g/m^2/day (Dameron et al., 2008). The term 'barrier' here refers to the ability of Al_2O_3 to resist the diffusion of water vapour into and through itself. Nevertheless, the barrier properties are often influenced by a wide range of variables, making conclusions regarding film properties sometimes difficult. It is known that barrier film permeability can be affected by the chemical and physical structures of the barrier, concentration of the permeant, temperature and humidity (Chainey, 1989; Hotchkiss, 1997) as well as surface defects on the barrier coating that may be induced during the deposition processes (Zhang, Bertrand, Yang, George, & Lee, 2009; Zhang, Zhang, et al., 2009).

Da Silva Sobrinho et al. (2000) stated that the source of defect-driven permeation has been primarily attributed to pinhole defects (Chatham, 1996; Hanika, Langowski, Moosheimer, & Peukert, 2003) more recent studies have shown that in the absence of pinhole defects permeation rates are still reduced by three orders of magnitude over the substrate material (A. Erlat et al., 1999). Any remaining permeation is shown to be the result of defects in the sub-micrometre and material discontinuities such as dislocations, are produced by the surface microstructure (Garcia-Ayuso et al., 1996) and/or low density of the films (A. Erlat et al., 1999; A. G. Erlat et al., 2004; Garcia-Ayuso et al., 1996). More detailed reviews of

permeation mechanisms and the performance of various permeation barriers have been given elsewhere (Chatham, 1996; J. S. Lewis & Weaver, 2004).

To date the research reported has used experimental data to argue that correlations exist between larger defects and WVTR. A question that arises is did the author simply change the segmentation criteria until a correlation was found or was the reported correlation realistic. In this chapter a theoretical model is developed to allow modelling the amount of water vapour that permeates through PV barrier film defects. The results of the model are then compared to experimental results presented in chapter (5) and (6), where defects measured using surface metrology techniques are correlated with WVTR.

7.2 Theoretical Background of Water Vapour Permeation

The first study of gas permeation through a polymer layer was conducted by Thomas Graham in 1829 (Suloff, 2002). Graham observed a loss in volume of a wet pig bladder inflated with CO_2. In 1866, Graham formulated the solution diffusion process, where he postulated that the permeation process involved the dissolution of penetrant, followed by transmission of the dissolved species through the membrane. Fick (1855) by analogy to Fourier's law of heat conduction, proposed the law of mass diffusion, which is stated as "the mathematical theory of diffusion in isotropic substances is based on the hypothesis that the rate of transfer of diffusing substances through unit area of a section is proportional to the concentration gradient measured normal to the section" (Feng, 2001). Fick's first law of diffusion is mathematically expressed as:

$$J \text{ or } F \text{ or } q = -\mathrm{D}\frac{\partial \phi}{\partial \mathrm{x}} \tag{7-1}$$

Where J, F, or q is the rate of transfer per unit area of section, ∅ is the concentration of diffusing substances (g/cm^3), and x is the space co-ordinate measured normal to the section.

If q and ∅ are both expressed in terms of the same unit of quantity, D is then independent of the unit and has dimensions length^2 time^{-1}.

In the late 1870s, Stefan and Exner demonstrated that gas permeation through a soap membrane was proportional to the product of solubility coefficient (S) and Fick's diffusion coefficient (D) (Allafi, 2008). Based on these findings, von Wroblewski constructed a quantitative solution to Graham's solution-diffusion model (v. Wroblewski, 1879). The dissolution of gas was based on Henry's law of solubility (Henry, 1803), where the concentration of the gas in the membrane was directly proportional to the applied gas pressure:

$$P = \frac{\phi}{S} \tag{7-2}$$

Where P, is the vapour/gas pressure and S, is the solubility coefficient.

Henry's law of solubility in equation (8-2), states that a linear relationship exists between the external vapour pressure (P) and the corresponding concentration of the water vapour (∅) within the surface of a barrier (S. C. George & Thomas, 2001).

7.3 Theoretical Model

Ashley (1985) developed an equation to calculate the permeability coefficient of the water vapour through a polymer barrier film. The equation was based on Henry's law of solubility (Henry, 1803), Fick's laws of diffusion (Fick, 1855), Stefan and Exner's findings (Su-Huai, Zhang, & Zunger, 1998) and Von Wroblewski hypothesis (v. Wroblewski, 1879). (Ashley, 1985) indicated that the permeability coefficient (P_r) depends on the solubility coefficient (S) as well as the diffusion coefficient (D). Eq. (7-3) expresses the permeability in terms of solubility and diffusivity.

$$P_r = D \times S\left(\frac{cm^3 cm}{cm^2.s.p_a}\right) \quad (7\text{-}3)$$

Solubility coefficient (S) = volume of vapour per unit volume of polymer per unit pressure (Lee et al., 2013). Unit of $S = \frac{cm^3(273.15k;1.013\times10^5 P_a}{cm^3 \times P_a}$

Diffusion coefficient (D) is the process by which a substance is transported from one part of a system to another as a result of random molecular motions and has a unit of $\frac{cm^2}{s}$ (Cozmuta, Blanco, & Goddard, 2007). So the unit of permeability coefficient (P_r) can be expressed as $\left(\frac{cm^3 cm}{cm^2.s.P_a}\right)$, and it can be defined as the volume of vapour passing through a unit area of the barrier layer per unit time, with a unit pressure difference across the sample (Ashley, 1985).

$$P_r = \frac{(\text{quantity of permeant})\times(\text{film thickness})}{(\text{area})\times(\text{time})\times(\text{pressure drop across the film})}$$

$$P_r = \frac{q \times L}{A \times t \times \Delta p}\left(\frac{cm^3 cm}{cm^2.s.p_a}\right) \quad (7\text{-}4)$$

Where q is the amount of permeant passing through a film of thickness L and over area A during time t driven by a partial pressure differential Δp across the film (Debeaufort, Voilley, & Meares, 1994). In a typical water vapour permeation measurement, for example, a "MOCON" test, ΔP in Eq. (7-4) corresponds to the partial pressure difference between nitrogen containing water at 90% RH on one side, and ultra-pure nitrogen on the other side. In this type of permeation test there is no pressure gradient across the sample $\left(\frac{\partial p}{\partial t}\right)$=0 as shown in Fig [7-1] (Metz, 2003)**.** Therefore, it is then reasonable to use the absolute value of the permeant's partial pressure p, instead of ΔP (A. Da Silva Sobrinho, Czeremuszkin, Latreche, & Wertheimer, 2000) thus, Eq. (7-4) can be presented as the following;

$$P_r = D \times S = \frac{q \times L}{A \times t \times P} \left(\frac{cm^3 cm}{cm^2 . s . p_a} \right) \quad (7\text{-}5)$$

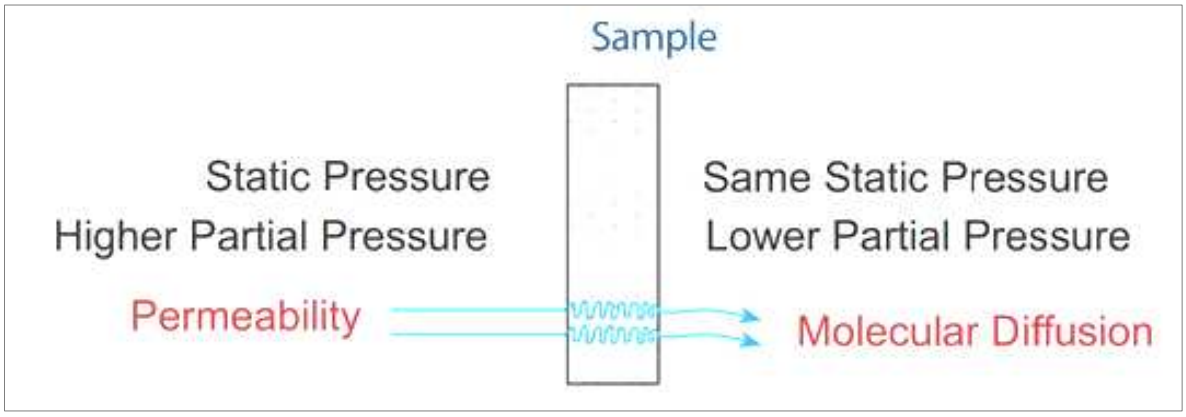

Figure 7-1: Pressure gradient across a barrier film ("MOCON®," 1997).

Da Silva Sobrinho et al. (2000) developed an equation to determine the amount of permeant per unit of time (Q) through the polymer; this equation was based on Henry's law of solubility (Henry, 1803).This equation is mathematically expressed as;

$$Q = \frac{q}{t} = \frac{A \times D \times S \times P}{L} = \frac{A \times D \times \phi}{L} \quad (7\text{-}6)$$

Where; the validity of Henry's law is assumed, and Ø represents the water vapour concentration in the film surface and it has been estimated to be 1 g/cm^3 (A. Da Silva Sobrinho et al., 2000). For the case of water vapour which has a little (Oyama & Stagg-Williams, 2011) or even no interaction with the barrier film (Bertrand, Higgs, Young, & George, 2013; A. Da Silva Sobrinho et al., 2000), the water vapour transmission is completely governed by defects geometries and densities (A. Da Silva Sobrinho et al., 2000).

In the present chapter a model of water vapour permeation through the barrier film defects is presented to study the effect of the defects on water vapour permeation.

7.3.1 Single Defect Case

The defect-dominated diffusion modelling framework for describing moisture and gas transport through inorganic barrier layers was first proposed by Prins and Hermans (M. George, 2014). Simply stated, this approach assumes that water or gas molecules can traverse within an inorganic layer only through existing defects or pinholes (Greener et al., 2007). The basic assumption of the model presented in this chapter is that the combined film of thickness L is made up of a transparent flexible barrier coating of (Al_2O_3) with a single circular hole (defect) of radius (R_0), and that it is exposed to permeant water vapour from the lower side as shown in Fig [7-2]. This orientation is consistent with that used in a MOCON® test. Considering only steady-state permeation, where temperature and partial pressure of the water vapour are constant, and the total pressure is the same on both sides of the barrier layer. The next step is to determine the amount of the water vapour q_H, leaving the barrier film, see Fig [7-2].

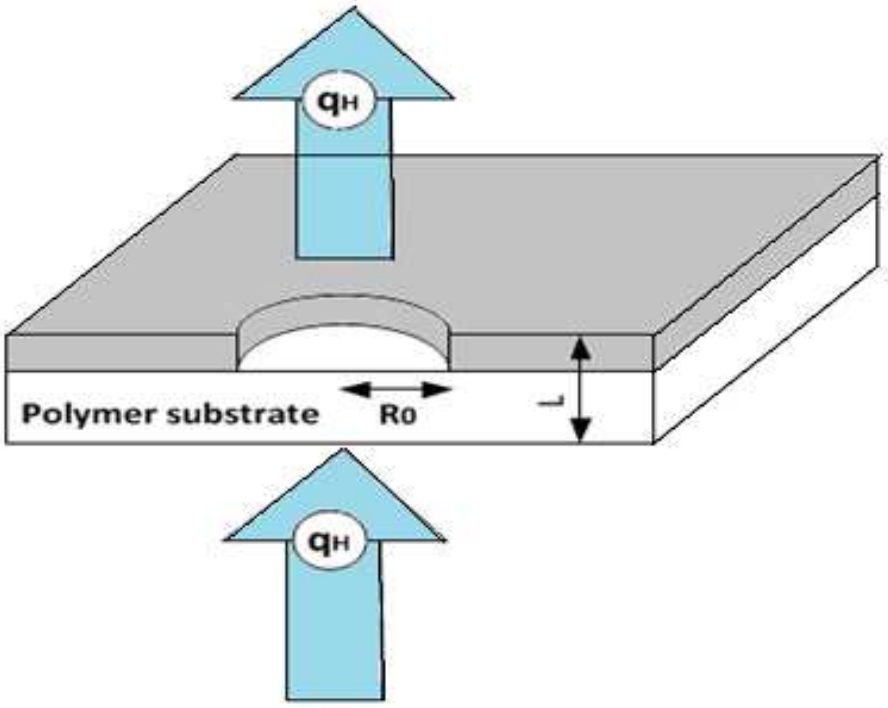

Figure 7-2: A schematic representation of a hole type defect in a coated barrier film.

In steady state, this amount is clearly determined by the water passing through the defect in the barrier. However, in the case of the hole in the barrier film as shown in Fig. [7-2], the amount of permeant traversing the polymer and through the hole per unit time can be provided by modifying Eq. (7-6) and introducing the barrier film as having a circular "hole" area $\left(\pi R_0^2\right)$.

$$Q = \frac{q_H}{t} = \frac{\pi R_0^2 D\phi}{L} \tag{7-7}$$

Where R_0 is the hole radius, D is the diffusion coefficient of the barrier film (cm^2/s), ∅ is the water vapour concentration (g/cm^3) and L is the combined film thickness. However, to determine the rate of the water vapour that penetrates hole over the substrate area ($g/m^2/day$), Eq. (7-7) can be expressed as the following (Debeaufort et al., 1994);

$$WVTR = \frac{Q}{A}\ (g/m^2/day) \tag{7-8}$$

Where; Q is the amount of the water vapour passing through a film of thickness L and area A during time t driven by a partial pressure differential P across the film (Debeaufort et al., 1994).

7.3.2 Case of Many Defects

Independent holes, assumes that the presence of one does not affect water vapour permeation through the other, so that their respective quantities of water vapour permeation are additive (A. S. Da Silva Sobrinho, Latreche, Czeremuszkin, Klemberg-Sapieha, & Wertheimer, 1998). So far, a theoretical model to determine the amount of the water vapour per unit of time, traversing a single hole in a barrier coating has been assumed and in order to discuss water vapour permeation through a barrier coating containing numerous defects (holes), Eq. (7-8) can be modified for (N) holes as follows:

$$WVTR = \sum_0^N \left(\frac{Q}{A}\right) N \tag{7-9}$$

N, is the number of defects (holes) in the sample area.

7.4 Experimental Details

The experimental study (test 1) was based on a set of two 80 mm diameter Al_2O_3 ALD samples presented in chapter 5 (section 5.2.3). These two samples were coded as 2705 and 2706, and the reasons for choosing these two samples are, they both have the same stabilisation time, both have higher WVTR values than the other two samples and they were both manufactured at the same conditions. The Al_2O_3 transparent ceramic material has an effective WVTR of less than 5×10^{-6} g/m^2/day (P. F. Carcia et al., 2010). The base film substrate used in this study was PEN material; where the thickness of this substrate is specified to be 125 µm. According to the manufacturer's data, this material has a water vapour diffusion coefficient of 4×10^{-12} cm²/s at 38 ºC, and WVTR of 4 g/m^2/day at 38 ºC and 90% RH. Prior to the surface measurements, the Al_2O_3 ALD samples were measured for WVTR using Isostatic standard test (Aquatran1-MOCON®) instrumentation at 38 ºC and 90% RH as mentioned previously in chapter (5). The lower detection limit of the instrument is 4×10^{-4} g/m^2/day, and the uncertainty of the measurements is 2×10^{-4} g/m^2/day for the calibration offset and 2×10^{-4} g/m^2/day for the actual measurement, giving a total of $4x10^{-4}$ g/m^2/day. The water vapour permeation test results (MOCON®) show that sample coded 2705 had a WVTR of 4.1×10^{-3} g/m^2/day and sample 2706 had a WVTR of 2.0×10^{-3} g/m^2/day (the WVTR for sample 2705 is twice as high as the WVTR for sample 2706). The WVTR results were obtained after a stabilisation time of 5 days.

7.5 Surface Topography Analysis

In this study, quantitative surface measurement was carried out using optical interferometry (WLSI) and the topography was characterized using areal parameters (ISO25178-2, 2012). The proportion of the surface area characterised was 14% of the total area of each sample equating to 703 mm^2, this comprised approximately 700 measurements per sample. Initially,

standard statistical field parameters (Blunt & Jiang, 2003; K. J. Stout & Blunt, 2000) in particular the root mean square surface roughness deviation (Sq) (K. J. Stout & Blunt, 2000), were calculated for the overall 3D surface data (defective and non-defective) in an attempt to investigate any correlations between the surface topography measurement and the WVTR results.

Applying this method to the recorded 3D surface data, the results in Fig [7-3] which represents the mean value of the surface roughness for the samples showed no real differences or correlations between the studied samples other than a greater spread of root mean square roughness values for sample 2705 (high WVTR) as represented by error bars. This result seems to strongly agree with previous published work (Garcia-Ayuso et al., 1996), where the authors observed that no correlation exists when the surface roughness is measured over large scanned areas owing to the inhomogeneous coating morphology (Garcia-Ayuso et al., 1996).

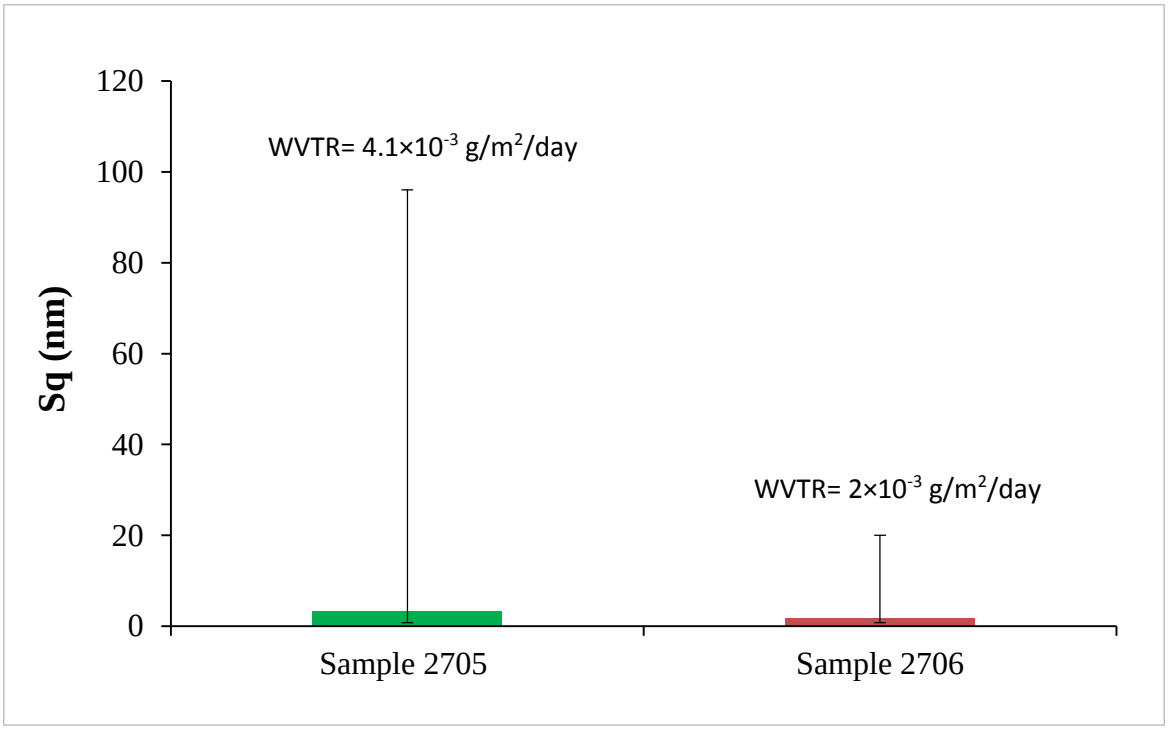

Figure 7-3: The calculated mean surface roughness (S_q) over 700 measurements (The error bars represent the maximum and the minimum S_q values obtained).

The results in Fig [7-3] show no clear correlation between the mean Sq value taken over the measured area of the samples and the WVTR. It can be seen that the mean Sq values are similar for both sample, while the WVTR is substantially different. Following this initial analysis only data files with defects (peaks and holes) were selected for further investigation in attempt to investigate such correlation between defects size, density, distribution and morphology. Fig [7-4] shows the number of data files with defects present on the surfaces, where each data file represent 1 mm^2 of the total measured area of 703 mm^2. The results in Fig [7-4] indicate that sample 2706 has higher defects density than sample 2705. However, the question remains here why does sample 2706 still show lower WVTR although it has a higher defect density?

At this point, segmentation analysis (ISO25178-2, 2012) was carried out on the surface topography data (areas with defects present) of the samples data files shown in Fig. [7-4], to extract and quantify only the significant defects present on the substrate.

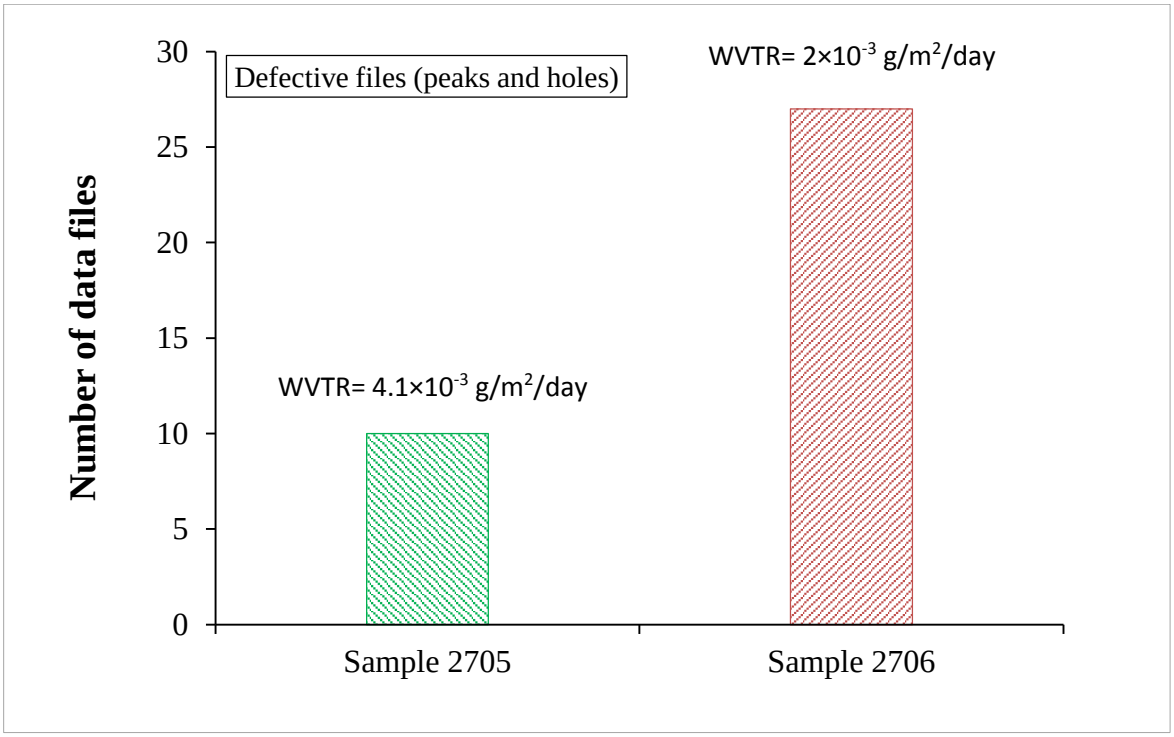

Figure 7-4: Number of data files with defective regions (defects defined as holes or peaks)

This method of analysis (segmentation) allows the extraction of information pertaining to specific "significant" topographical features from topography data using a series of mathematical and thresholding techniques (Blunt & Jiang, 2003; ISO25178-2, 2012). In the present case a significance value of ± 3Sq vertical height [where, Sq for non-defective sample area = 0.8 nm, see Fig. (7-5a)] and 15 µm (based on SEM analysis) lateral size was applied to compare the presence of significant defects on both samples.

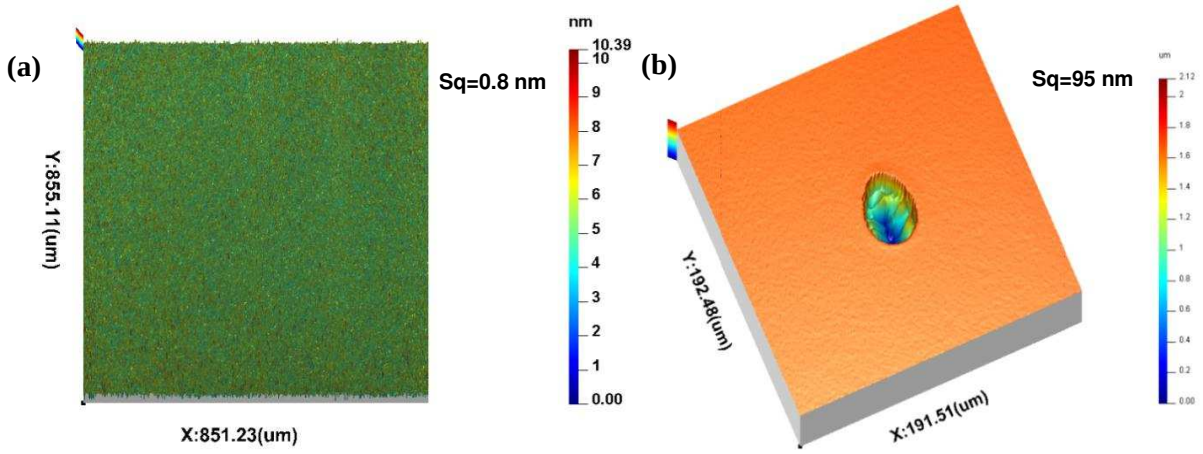

Figure 7-5: Surface topography for (a) non-defective area (b) defective area of a sample. (Note difference in Sq value).

Wolf pruning and area pruning (ISO25178-2, 2012; X. Jiang et al., 2007) are implemented for extracting the features of functional interest by accurately excluding insignificant geometrical features, such as measurement noise and error and small topographical features. As a starting point, this method was applied to count only defects where the scale is greater than the background surface roughness variation over the total measured area as shown in Fig [7-6]. In the present case defects are assumed to manifest themselves as both negative topographical features (holes) and positive features (particulates), where the particulates are also considered as a defect. Zhang et al. (2009) stated that particulates may be dislodged post coating or provide shadowing thus resulting in areas of uncoated substrate. Using the criteria outlined above (± 3Sq vertical and 15 µm lateral) it was possible to segment the surface data and record the defect density/count across the surface data sets collected from the Al_2O_3 ALD

coated barrier layers. Fig [7-7] shows significant defects count at +/- 3Sq vertical and 15 µm lateral pruning conditions. The analysis of the results in Fig [7-7] showed that there was evidence of correlation between the number of large defects and the WVTR value. The high WVTR specimen (2705) had a larger density of significant defects as compared to the better performing substrate (2706).

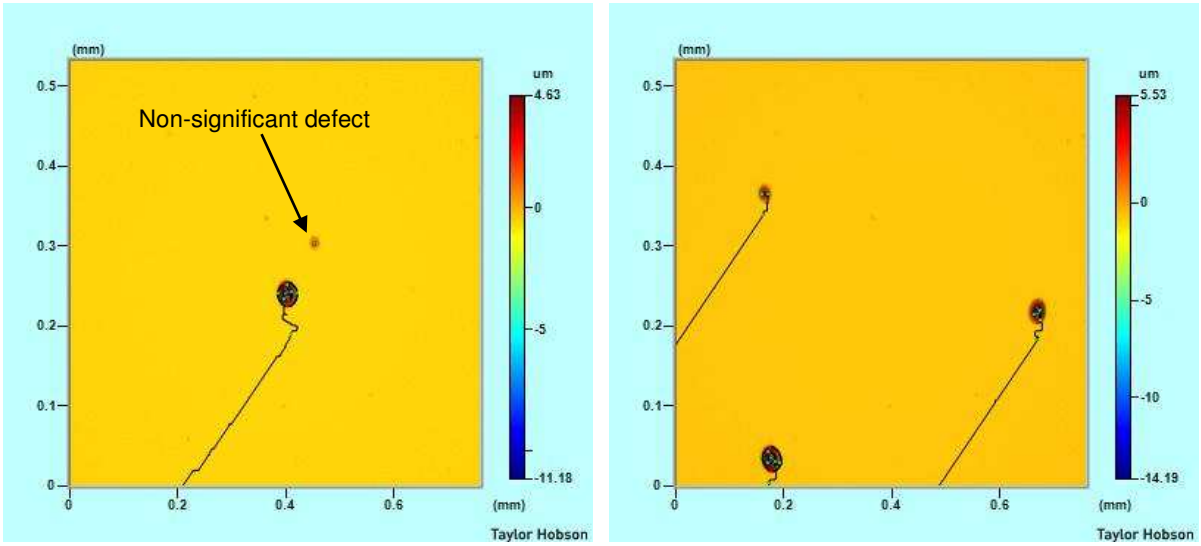

Figure 7-6: Segmentation analysis for multiple defects

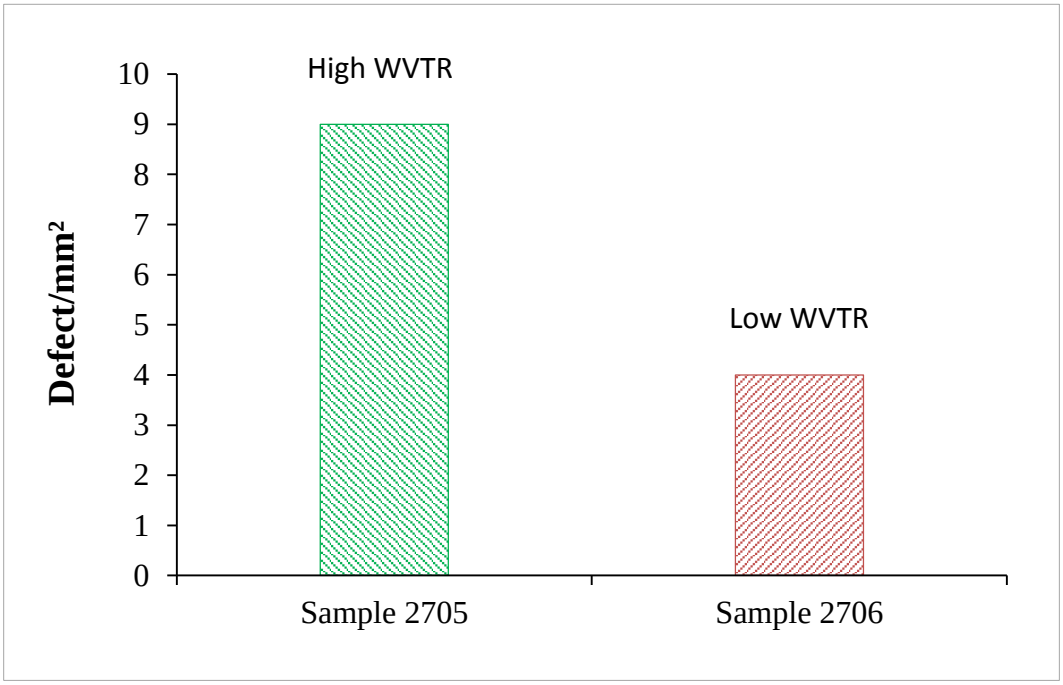

Figure 7-7: Defects density at (± 3Sq vertical and 15µm Lateral) pruning conditions

This result in Fig [7-7] seems to agree with previous published work (A. Erlat et al., 2001), which stated that large defects may dominate the permeation properties of the barrier film. However, even for sample (2706) there are still circa four significant defects affecting the barrier performance by allowing water vapour ingress. The question that remains is, are larger defects more significant in terms of WVTR and what is the cut off level between large significant defects and small insignificant defects in the present case?

Hence to investigate the lower limit of the defect size that is potentially significant, different area pruning conditions were applied on the data whilst the height prune condition of ±3Sq remained the same. Using these criteria (different width pruning and ± 3Sq height), the defect density count appeared to converge at around 2.5 µm (lateral dimension) as shown in Fig [7-8]. When larger pruning values are used to define significance, the defect density level was consistently higher for the sample with the higher WVTR (2705) and from approximately 5 µm down to 1 µm; the defect density count remained stable.

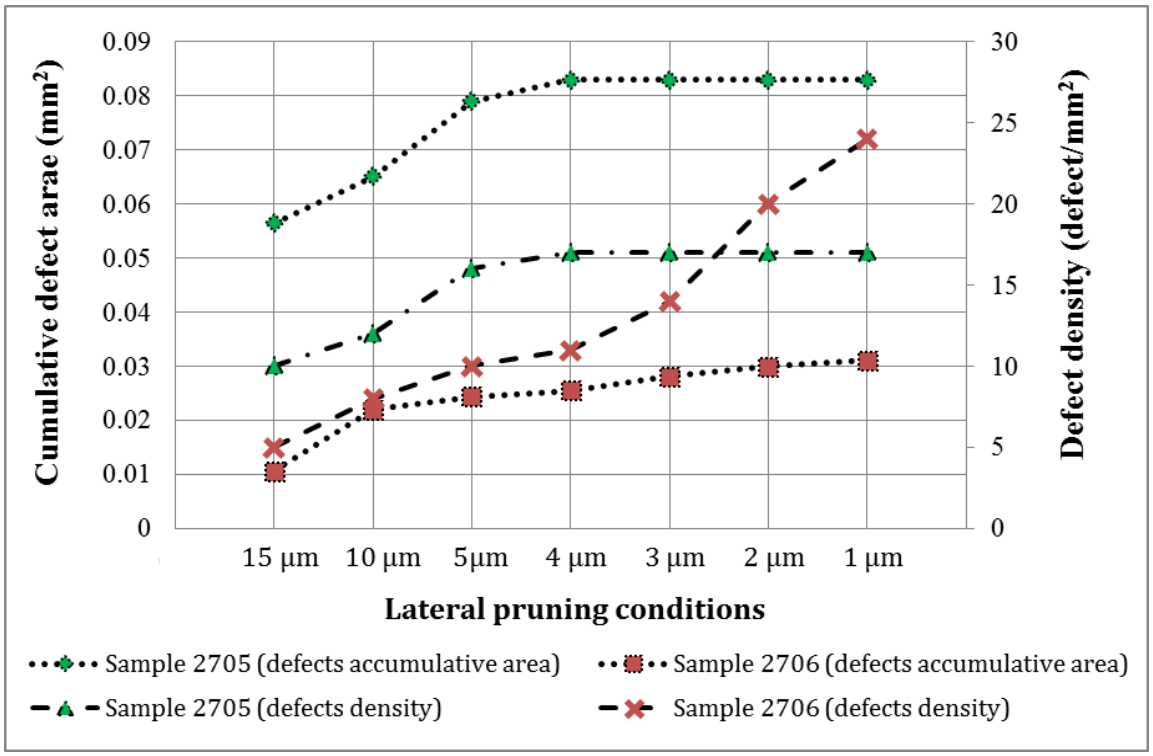

Figure 7-8: Defects count and accumulative area at different lateral pruning conditions for the measured area (703 mm^2) of two similar samples.

Interpretation of the data suggests that, for defects less than 1 µm and up to approximately 2.5 µm size, sample 2706 shows a higher defects density at ~24/mm^2 while the defect density for sample 2705 remains stable at 17/mm^2. Above 2.5 µm, the decreased defects density for sample 2706 throughout is highly significant. This result indicates that the sample with higher density of defects > 3µm exhibits inferior barrier properties. Moreover, the figure also shows a plot of the accumulated surface area of the defects measured on the two samples. The results show that when all defects with lateral widths down to 1 µm (resolution of WLSI) are used in the analysis, sample 2705 (high WVTR) consistently has a higher cumulative surface area value, but accompanied by a lower defect density. Consequently the results would indicate that when developing a metrology technology for defect characterization on these types of barrier coatings only significant defects, which have a very detrimental effect on barrier functionality need to be quantified. Based on the results in Fig [7-8], it is possible now to classify the defects in terms of their size in relation to their significance.

Table 7-1: Type and size of significant/non-significant defects in the Al_2O_3 barrier film

Type of defect	**Feature Size**	
	Vertical (Sq)	**Lateral**
Significant (holes and particulates)	≥ (±3Sq) nm / field of view	≥ 3 µm lateral dimension
Non –significant (holes and particulates)	≤ (± 3Sq) nm / field of view	≤ 3 µm lateral dimension

7.6 WVTR Analysis and Results Discussion

The cumulative defect area (over a total measured area of 703 mm^2) for samples 2705 and 2706 were found to be 0.083 mm^2 and 0.03 mm^2 respectively as shown in Fig [7-8]. If a homogenous distribution of the defects is assumed across the whole of the sample area (5024 mm^2), then the cumulative defect areas may be scaled up linearly and are found to be 0.012%

and 0.004% of the total sample area as shown in Fig [7-9]. This should result in WVTRs of 4.86×10^{-4} g/m^2/day and 1.65×10^{-4} g/m^2/day respectively, based on the ideal values of the WVTR for the Al_2O_3 material (see section 7.4).

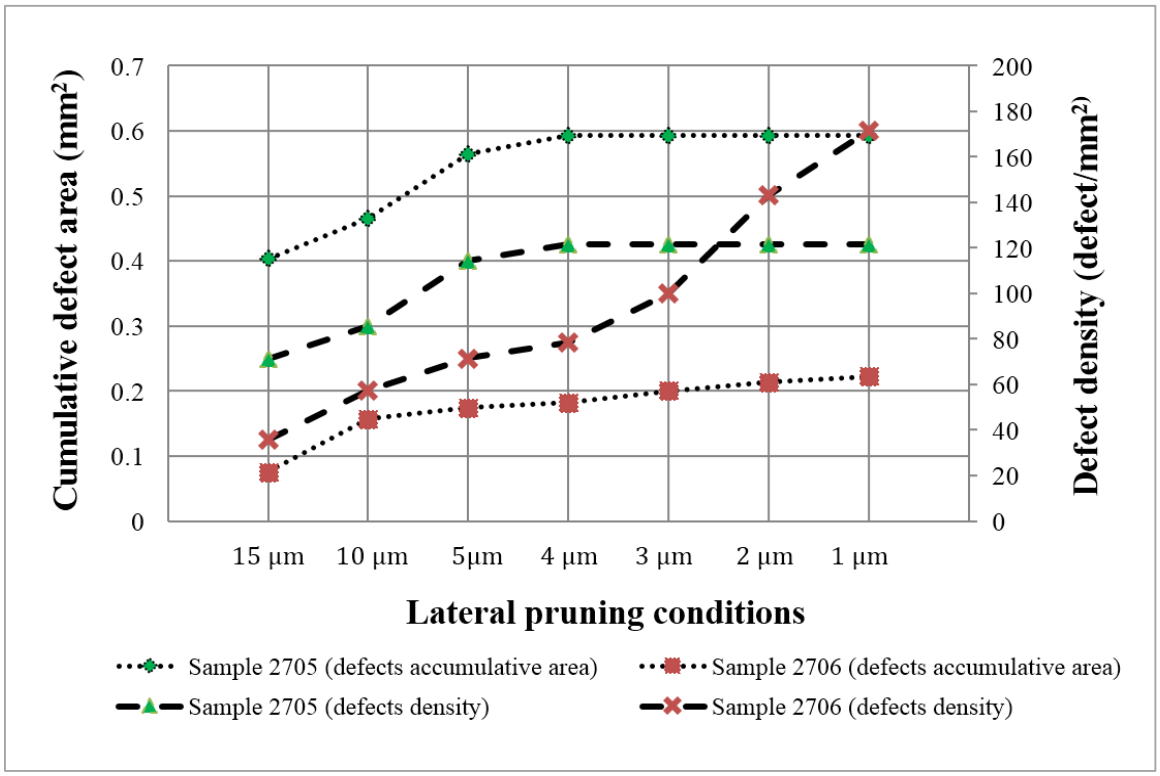

Figure 7-9: Defects count and accumulative area at different lateral pruning conditions for the whole sample area (5024 mm^2)

The experimental WVTR of the samples, taken after a stabilisation time of 5 days, were found to be 4.1×10^{-3} g/m^2/day (sample 2705) and 2×10^{-3} g/m^2/day (sample 2706). Consequently using this method (the ratio of the defective area to non-defective area) does not give reliable results for quantifying the water vapour permeation through the samples, see Fig [7-10]. However, when referring back to the theoretical model presented earlier in section (7.3) and using Eq. (7-8) and Eq. (7-9) for the given sets of parameters and variables for each sample, as shown in appendix (F), and substituting all the known data (sample area, sample thickness, number of defects, diffusion coefficient, water vapour concentration and the accumulative area of the defects) into Eq. (7-9), the theoretical model based on the approach

of Da Silva Sobrinho et al. (2000) led to results which are similar to those obtained by surface topography analysis (Liam Blunt, Mohamed Elrawemi, Leigh Fleming, & Francis Sweeney, 2013; M Elrawemi, Blunt, Fleming, & Sweeney, 2013) discussed earlier in and experimental WVTR test results. Calculations are shown in appendix (F).

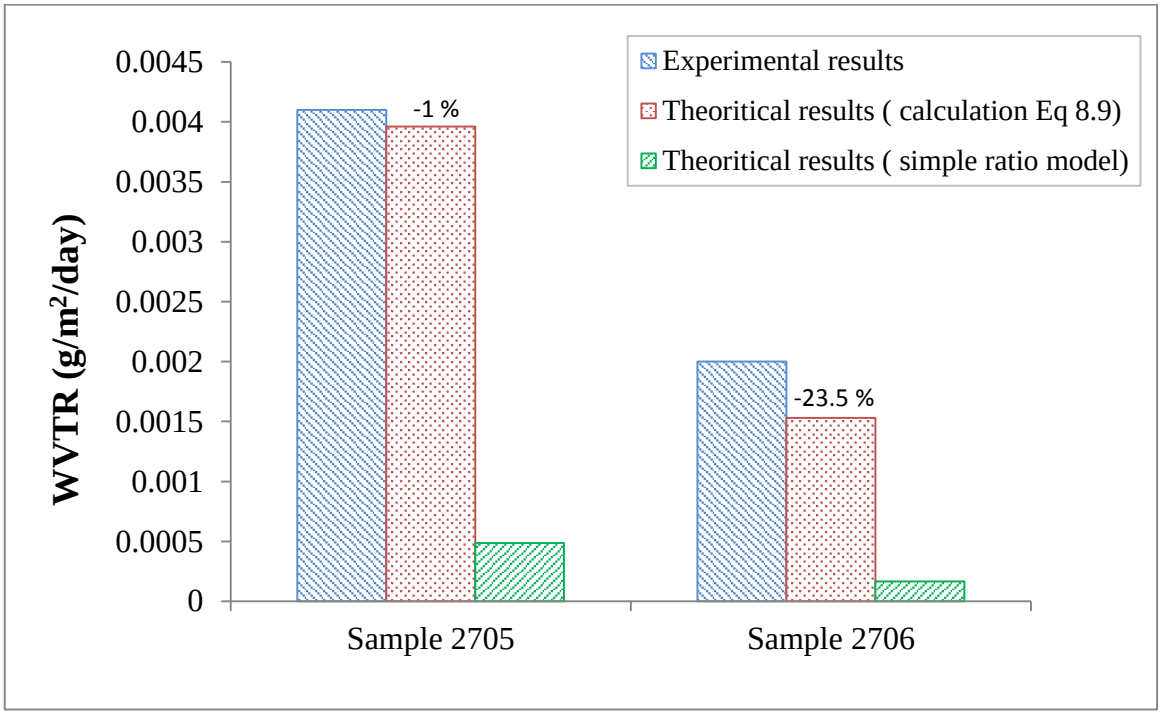

Figure 7-10: Comparison between the theoretical and experimental results

The results in Fig [7-10] indicate that sample 2705 has a higher WVTR value than sample 2706 using both the simple ratio model and the theoretical (calculation) model. This result is similar to that obtained experimentally using water vapour permeation test in section (7.4). This would seem to indicate that the theoretical model presented in this chapter after Da Silva Sobrinho et al. (2000) has the potential to be used for understanding the mechanism of water vapour permeation through flexible PV barrier films defects, where defects with 2.5 µm diameter are taken into consideration.

7.7 Summary

To summarise, the investigation for the conditions studied in this chapter has shown that, the

total permeation rate through small numbers of larger defects is much greater than the total permeation rate through large numbers of small pinhole-type defects over the same area of substrate, and that using the measured data in a theoretical model yields similar results for WVTR. The segmentation analysis results and the theoretical model approach in this chapter, both appear to indicate that the major contributing factor for determining the WVTR is the total number of larger defects, where the sample with higher density of defects > 3 µm exhibit inferior barrier properties.

The model presented in this chapter could therefore also be used for the understanding of the overall PV module efficiency, performance and lifespan. In addition to this, the results would seem to indicate that, for such substrates produced under the stated conditions, the critical spatial resolution required for defect detection need to be capable to capture 3 µm lateral size defects, as any defect that has less than this lateral size seems to have a much lower effect on the barrier properties. This model has been further evaluated by CPI using a calcium test and found to give good correlation with defects (Private communication with CPI- David Bird)

CHAPTER 8

8. Implementation of Online Defect Detection System

8.1 Introduction

The relationship between surface morphology, defects density and water vapor permeability through 40 nm Al_2O_3 barrier coatings produced by ALD (S. M. George, 2009) on 125 µm polyethylene naphthalate (PEN) substrates, has to date only been studied in the laboratory (Blunt et al., 2013; Elrawemi et al., 2013), and presented previously in this thesis. However; detecting defects off-line is difficult and time consuming. New methods of manufacturing ALD barrier films by R2R methods are emerging Fig [8-1], however using only off-line defect detection can result in large quantities of barrier films being manufactured and integrated into the PV unit before defects are detected and process parameters optimised.

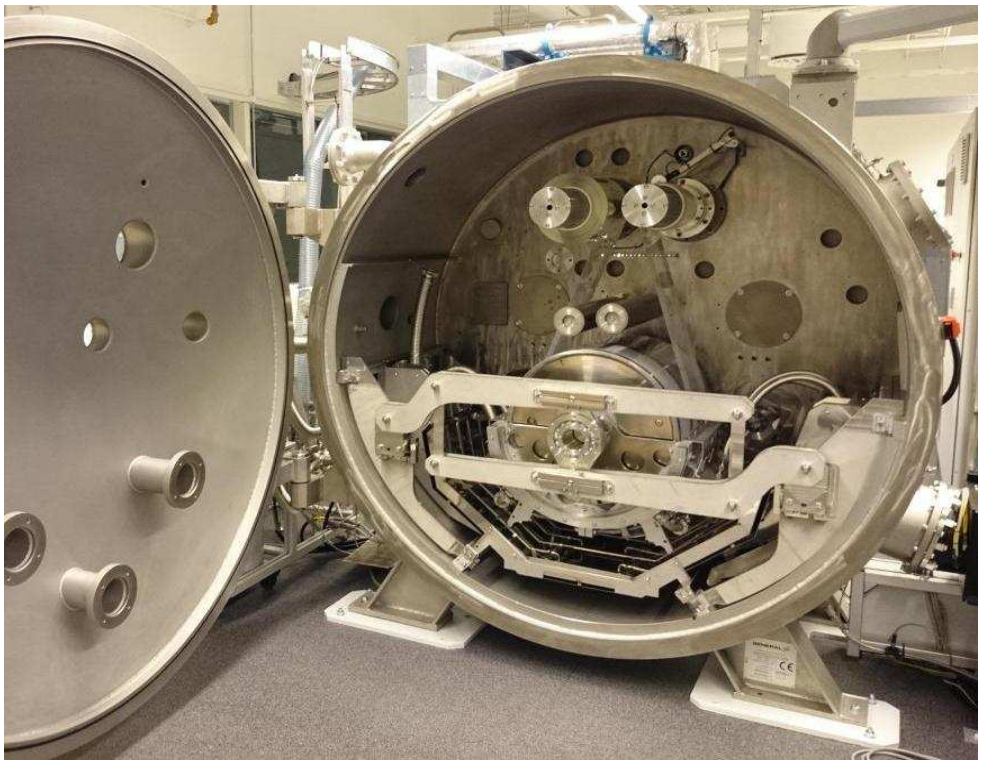

Figure 8-1: Beneq WCS 500 roll-to-roll ALD reactor (Courtesy of CPI, UK)

8.2. In process Defect Detection Techniques

Several researchers have presented methods for non- destructive "in process" defect detection for PV modules. Rueland et al. (2005) proposed a technique to detect crack type defects by transmitting a high intensity flashlight through the PV films, capturing the image with a CCD camera which is placed after an optical filter. The light intensity is then directly correlated with the thickness of film material. Hence, by identifying bright areas in the images, defects down to approximately 5 µm width in the film can be analysed. However, Belyaev et al. (2006) proposed an experimental methodology using a resonance ultrasonic vibrations (RUV) system to detect cracks in PV substrates. This technique enabled fast data acquisition and matching solution for throughput analysis of solar cell production lines and capable of non-destructively detecting millimeter length cracks.

Hilmersson et al. (2008) detected cracks in PV films using a vibration method in the form of an impact test as a non-destructive way. This technique can detect cracks with lengths of ≥ 100 µm, however the major drawbacks are that the time required to test the wafer and the sample preparation process. Moreover, Connor et al.(1998) proposed scanning acoustic microscopy (SAM) technique to be used as a method of determining the presence of µ-cracks, though this method is not feasible during the mass production of PV cells. This method showed its limitation since the time required to scan a 100 mm by 100 mm wafer was between 10- 15 minutes. The SAM method, however, did allow for cracks ≥ 5 µm in length to be detected.

Rakotoniaina et al.(2004) employed an Ultrasound Lock-in Thermography (ULT) method to detect cracks in PV modules. This method can detect cracks with lengths ≥100 µm and it takes around 5-10 seconds to inspect a 100 mm by 100 mm film. While more than a couple of seconds are accepted for quality control, this long acquisition time makes ULT unsuitable for in-line detection.

Ancuta et al. (2011) detected and analysed accumulated particles, cracks and local imperfections in the production process over different PV surfaces using infrared (IR) thermography method. Defects invisible to the naked eye are determined and analysed using the temperature factor for PV modules. The results indicated that the IR method can be effectively utilised for detection of defects as small as a few millimeters in a very short time of about 1 second. The IR was seen a fitting way to detect invisible defects in their first stages of development, localise the problem in a very short time and taking measures to avoid further damage.

Krysinski et al. (2014) introduced a prototype industrial camera based defect detection system for R2R applications. The prototype method was based on dark-field (DF) imaging principle, where the sensors of the system are associated with the presence of the defects and the intensity of the scattered radiation travelling from the sample which, if defect-free, should transmit specularly incident light. The shortcomings of the designed prototype are that it is unable to detect defects smaller than 10 µm in lateral dimension, and cannot identify the type of defect.

A variety of groups and corporations are pursuing various in-line measurements for the flexible display industry, including bright-field inspection systems and scanning interferometers for 3D measurements (M. George, 2014; Wegner, 2014). A single shot interferometry system "FlexCam" developed by 4D Technology being used currently to detect defects for PV barrier films manufactured by R2R technology as shown in Fig [8-2]. This interferometric method relies on laser interferometry to acquire 3D surface data, and it acquires all the phase-shifting information in 10 microseconds (Kimbrough, 2015), and the acquisition time depends only on the camera exposure time (i.e. frame rate). The goal for the FlexCam is to provide about a 2 µm lateral resolution and a 2 nm vertical resolution over a

field of view (FOV) of roughly 4 mm ×0.2 mm. This technology can provide areal measurements in milliseconds however; it has a limited vertical range, which is a problem to identify and classify large vertical defects and mitigate the ability to position the tool at optimal height to allow measurement (M. George, 2014).

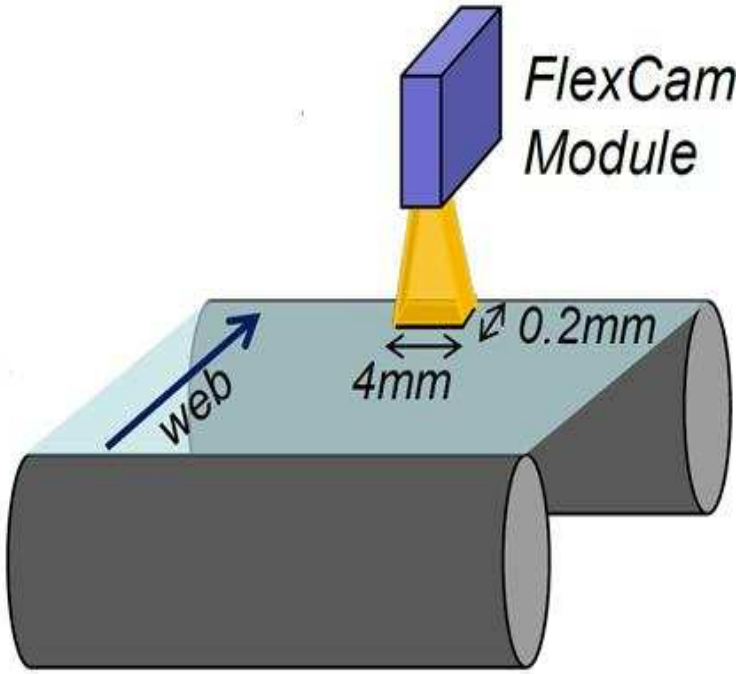

Figure 8-2: In-line defect detection system (M. George, 2014)

The literature review in this chapter confirmed that all the previous described surface metrology techniques cannot be employed to detect and identify micro-scale (<5 µm lateral size) defects such as pinholes, small particles and micro-cracks in the Al_2O_3 barrier layers, which are responsible for the water vapor ingress, and they also face the challenge of speed versus resolution. However, to facilitate in process measurement for R2R produced substrates two challenges need to be addressed; i) the measurement must be fast and non-contact ii) the measurement must be carried out in a "noisy" working environment.

One of the only feasible measurement solutions is optical interferometry, however interferometric measurement techniques are extremely sensitive to environmental noise such

as mechanical vibration, air turbulence and temperature drift. Thus, controlling the impact of noise on measurement quality is essential if the interferometric approach is to be implemented for in process measurements.

This chapter reports on the validation, deployment and optimisation of new (novel) in-line interferometric optical technique based on wavelength scanning interferometry (WSI), for detecting PV barrier defects (≥ 3 µm lateral size) with a vertical range of 100 µm as shown in Fig [8-3].

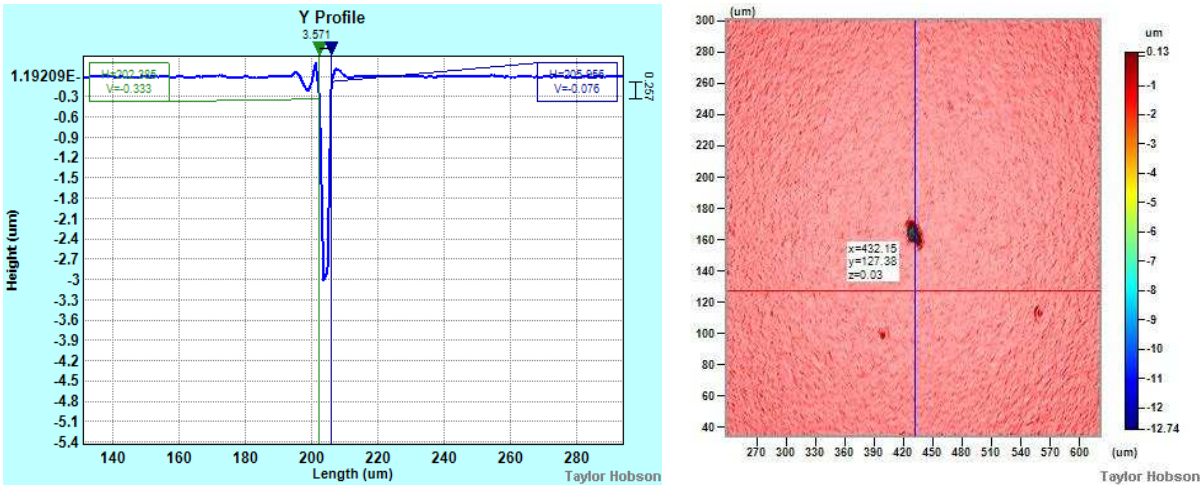

Figure 8-3: Defect measured using WSI (3µm lateral size)

The basic system design was developed by Jiang et al,. (2010). The instrument has a built in environmental vibration compensation capability, providing areal measurements at a high speed of less than 1 s per field of view (FOV). The technique is currently being deployed using a demonstration system at a R2R production facility. The results show the capability of the WSI to be used as a quality assurance tool in R2R production lines, where the results compare favourably with results obtained through off-line optical techniques (i.e., the Coherence Correlation Interferometer (CCI) 3000 of Taylor-Hobson, Ltd).

8.3 Wavelength Scanning Interferometry (WSI)

Current industry standard interferometry systems generally work by mechanically shifting the phase of the fringes by scanning the position of an objective lens relative to the substrate/surface being measured. Such a technique is too slow to perform large numbers of measurements required to enable in process defect detection analysis for large area thin film barriers. The Wavelength Scanning Interferometer (WSI) shown in Fig [8-4] can take areal measurements without mechanical movement by simply changing the wavelength of a broadband light source in an interferometer setup using an acousto-optical tuning technique (Xiangqian Jiang et al., 2010). This wavelength scanning process can ensure a phase shifting operation faster than the conventional mechanical scanning methods. Also, defects can be measured effectively in a factory environment because the WSI has an active close-loop vibration compensation system (Muhamedsalih, Jiang, & Gao, 2013).

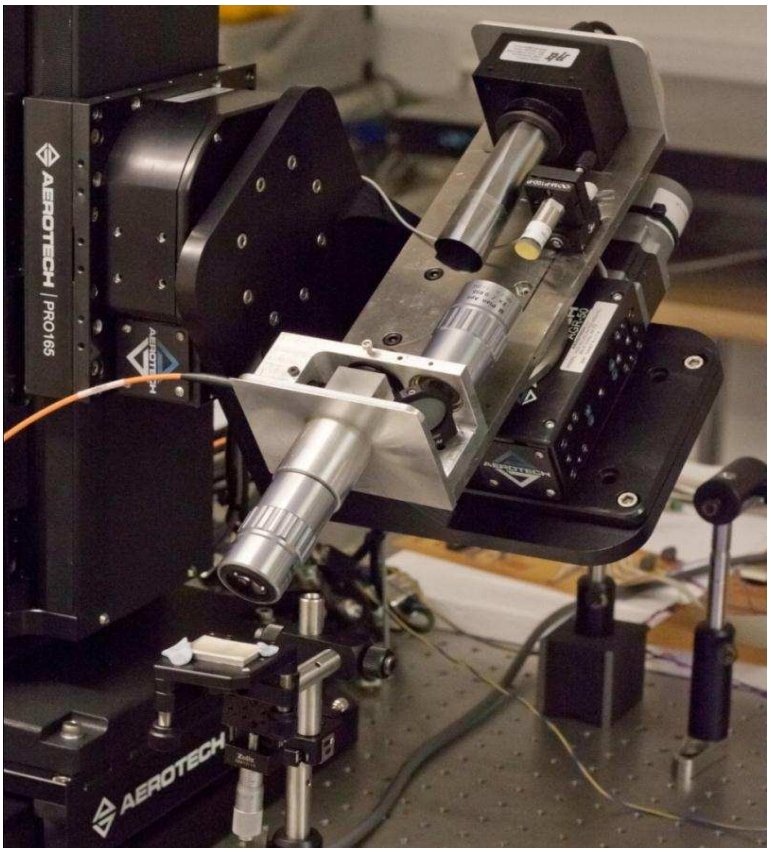

Figure 8-4: WSI test setup

The current time for data acquisition of the WSI is approximately 2 seconds, where a 3D areal measurement analysis is achieved by using a graphics processing unit (GPU) to accelerate the computing process to less than a second per FOV.

8.3.1 WSI Measurement Principle

The measurement principle of the WSI is based on determining the phase shift of a constructed interference fringe while the wavelength of the illuminating light is scanned (Muhamedsalih et al., 2013). The wavelengths of the white light, obtained from a halogen lamp, is scanned through a visible range, from 683.42 nm to 590.98 nm, by filtering a narrow spectral band using an acousto-optic tunable filter (AOTF). The system comprises two interferometers that share a common optical path, see Fig [8-5].

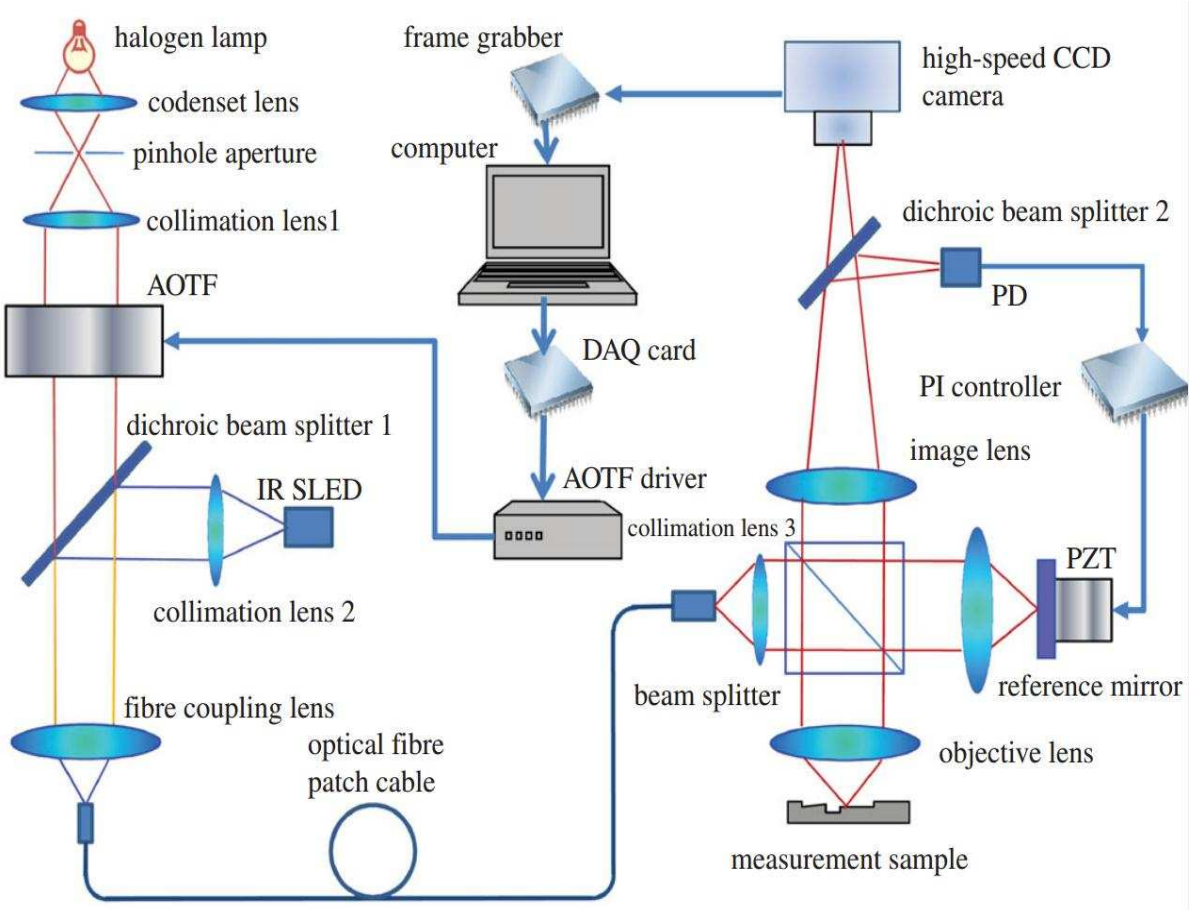

Figure 8-5: Schematic representation of WSI system (Xiangqian Jiang et al., 2010)

The interferometer uses a filtered white light source for measuring surface topography. Another interferometer using a super-luminescent diode (SLED) is used to monitor the unwanted optical path change, due to barrier surface movement or temperature drift, and acts as a feedback sensor for an active servo control to the reference mirror to cancel out the change in the optical path (Muhamedsalih, 2013).

The noise cancellation is achieved by moving the reference arm mirror using a piezo-electric translator (PZT) which acts according to the manipulated feedback signal. The noise cancellation can ensure the fringe stabilisation before the wavelength scanning measurement process is carried out (Xiangqian Jiang et al., 2010). As such, any alteration in the optical path (vertical) will be considered as a noise source and can be compensated by the control active loop if the noise range is within the stabilization bandwidth. The stabilization bandwidth is typically dependent on the translation range of the PZT and frequency response of the system. In this application, PZT type P-840, from PI Ceramic, has a travel range up to 15 µm and the control frequency response is up to 3 kHz.

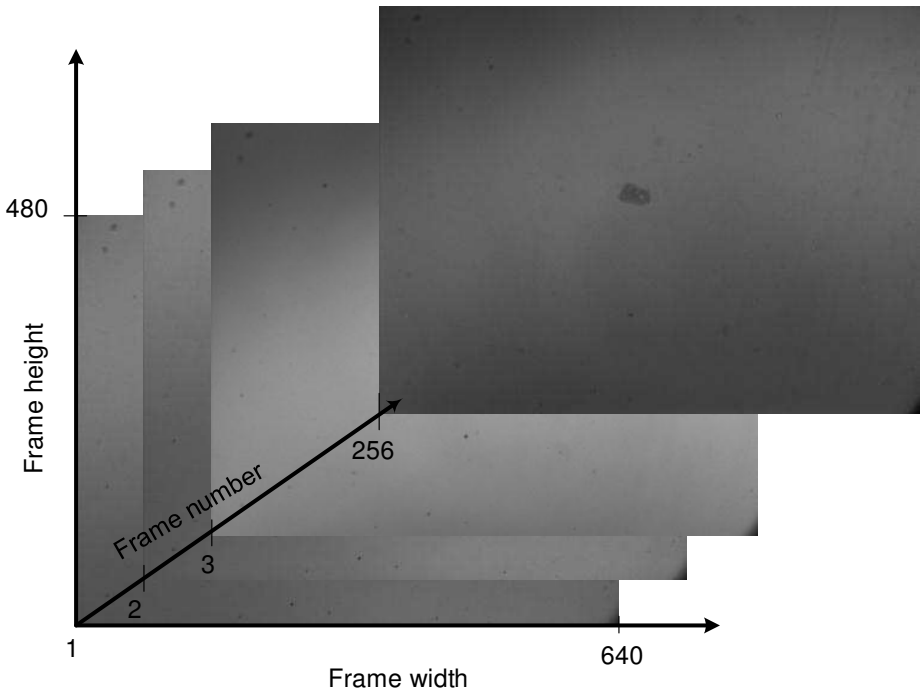

Figure 8-6: Interferograms collected from a single pixel

Typically 256 interferograms can be captured by the current CCD camera; each pixel in the obtained interferogram represents a specific point on the sample surface as shown in Fig [8-6]. The number of interferograms taken depends on specific requirements for precision and range of the measurement. By isolating a single pixel (which corresponds to a specific point on the sample) from the interferogram set, a sinusoidal change of intensity with respect to the wave number (reciprocal of wavelength) is apparent, Fig [8-7].

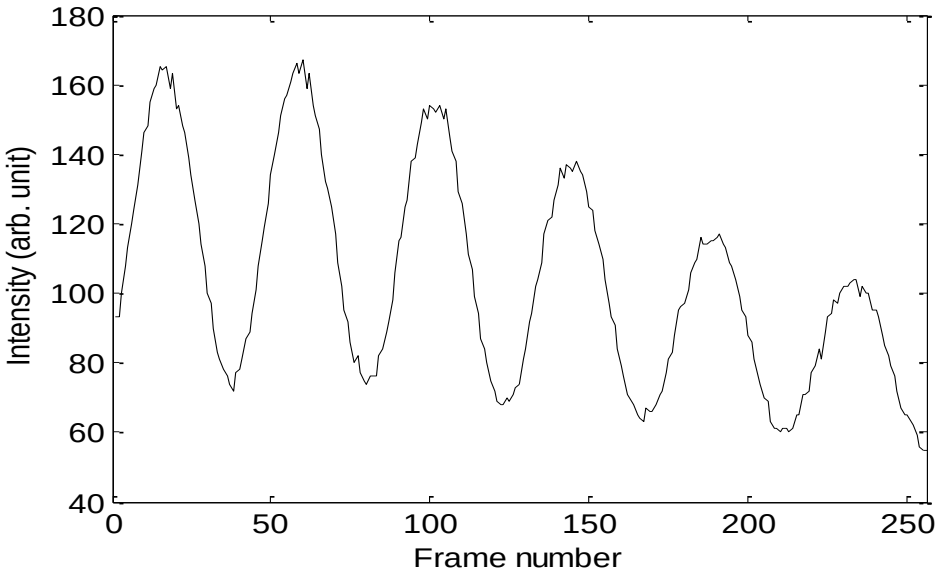

Figure 8-7: Change of intensity across a single pixel

The overall phase shift across the wavelength scan range can be obtained from the intensity signal using Fourier transforms. The height of the point represented by the pixel can then be calculated by:

$$h(x,y) = \frac{\Delta\varphi(x,y)}{4\pi\left[\frac{1}{\lambda_{max}} - \frac{1}{\lambda_{min}}\right]} \quad (8\text{-}1)$$

Where, $h(x,y)$ is the height of the specific pixel, λ_{max} , and λ_{min} are the upper and lower filtered wavelengths of the scan range respectively and $\Delta\varphi(x,y)$ is the calculated phase shift over the scan range (Muhamedsalih et al., 2013). As a result, the height value can be calculated after extracting the overall phase change produced by scanning the wavelength

through a spectrum bandwidth of approximately 100 nm in the visibly region. However, in order to guarantee the sufficient phase change and avoid zero optical path difference, an offset distance with magnitude of 5 µm has been introduced into the interferometer between the beam splitter and the reference objective lens (i.e. produced unbalanced arms for the interferometer) (Muhamedsalih, 2013).

8.3.2 Preliminary Results of in Process System (WSI)

The WSI system, being employed within this study is a critical tool for the evaluation of surface topography where measurement speed is a critical factor and the system must be embedded within the context of the manufacturing environment. As part of this research project, the WSI system was implemented as a demonstrator sensor in a R2R demonstrator for the detection of defects in the Al_2O_3 ALD barrier films as shown in Fig [8-8]. The initial implementation of the system acquires a series of static images and thus allows significant areas but not the entire substrate surface to be measured.

Figure 8-8: WSI system implemented as a demonstrator for R2R barrier films inspection

8.4 Comparative Study between CCI and WSI

Exemplar samples of Al_2O_3 ALD barrier film were first measured using off-line metrology technique (CCI) in order to detect and measure the defects and compare them later with the WSI measurement results. Table [8-1] shows the technical specifications of each technique.

Table 8-1: WSI and CCI technical specification (Kaplonek & Lukianowicz, 2012; Muhamedsalih, 2013)

Specifications	Method	
	CCI	**WSI**
Area (objective dependent)	0.3-7.2mm^2	0.5-1.8mm^2
Vertical resolution	0.001 nm	15 nm
Vertical range	100 um	100um
Lateral resolution	0.36 um	2.98 um
Repeatability of surface (noise)	0.003 nm	7 nm
Typical measurement time	10-20 seconds	<1 second

Typically, the lateral range and resolution are varied for different objective lenses and imaging sensor sizes. The WSI has the potential to increase the current lateral range and resolution by simply changing the CCD sensor size and lens objectives.

Table [8-1] also shows that the vertical range for both instruments is equal, but this value mainly depends on the focus depth of the objective for the WSI. However, in this study, the defects vertical depth does not exceed several micrometres which are within the limit of focus depth of high magnification objectives.

8.4.1 WSI System Verification

In this study, both systems (CCI and WSI) are calibrated and should yield closely comparable results. A 5X objective lens giving sample spacing of 1.19 µm was used in the WSI, and for the CCI a 20X objective lens giving sample spacing of 0.9 µm was used. The initial measurement procedure was as follows; more than 100 typical defects were measured by

each of the techniques (CCI-3000 and WSI). These defects were found to have lateral dimension ranges of 20-60 µm; see Fig [8-9] as an example.

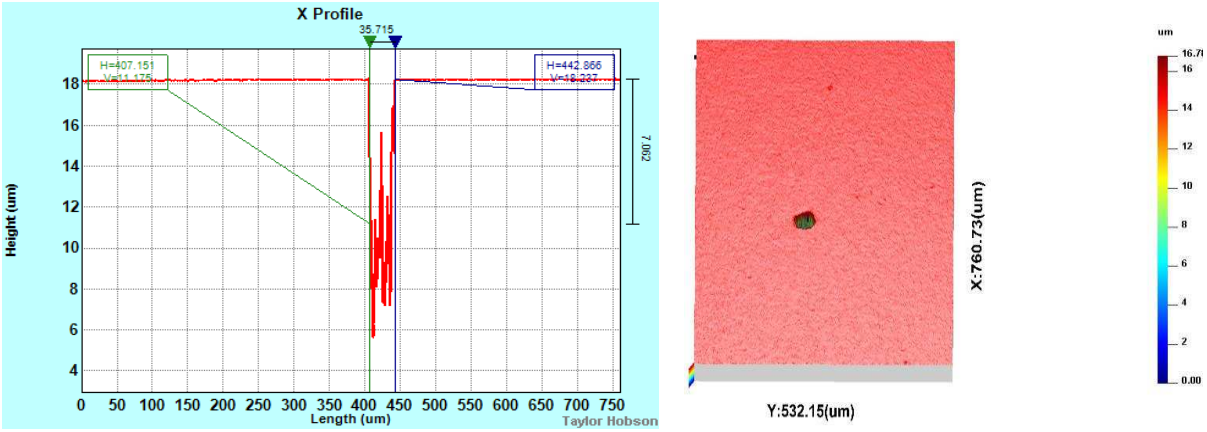

Figure 8-9: Defect measured using WSI system

The measurements results also reveals that, the surface roughness parameter value for defect free sample measured by the WSI is higher when compared to the CCI-3000 method. The high roughness value of the WSI data was due to the high noise floor level generated during the operation process of the WSI technique. This noise is most likely generated from accumulative effects of environmental noise, WSI resolution and measurement uncertainty. However, this tolerance in the magnitude of surface roughness does not affect the defect detection ability nor characterisation since the coating thickness of the Al_2O_3 layer is approximately 40 nm and the noise limit is below the significance level defined for the critical vertical scale of significant defects.

Moreover, Fig [8-10] and Fig [8-11] show the same defect which has been measured by both techniques CCI-3000 and WSI. Both instruments give similar values for the average vertical defect height which is approximately 1 µm.

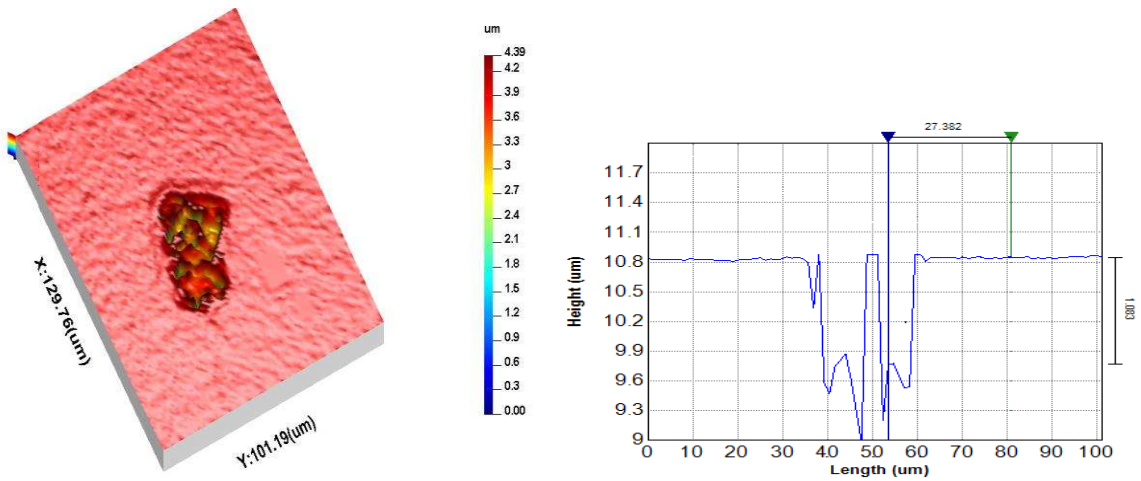

Figure 8-10: Defect measurement using WSI

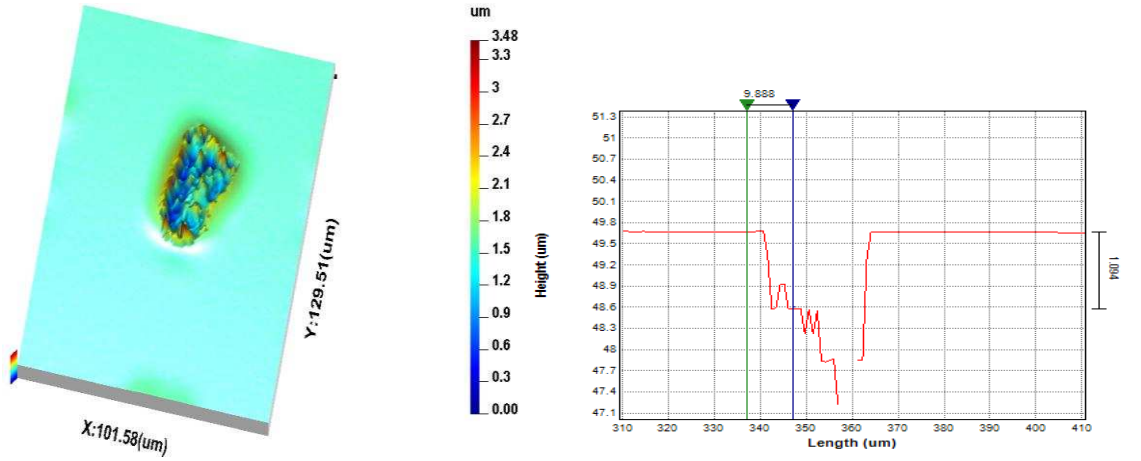

Figure 8-11: Defect measurement using CCI

As an initial assessment for the WSI measurements, it was found that the results are very comparable to the off-line technique (CCI-3000). For such thin barrier layers the lateral dimensions are of critical functional importance.

Examples of the defect size/scale captured by the techniques are shown in Fig [8-12]. The result reveals that, the WSI system has accurately and reliably captured defects that have been previously detected by the CCI instrument. Therefore, the WSI technique can be an efficient and optimal system to be used for in process thin film barrier defect inspection.

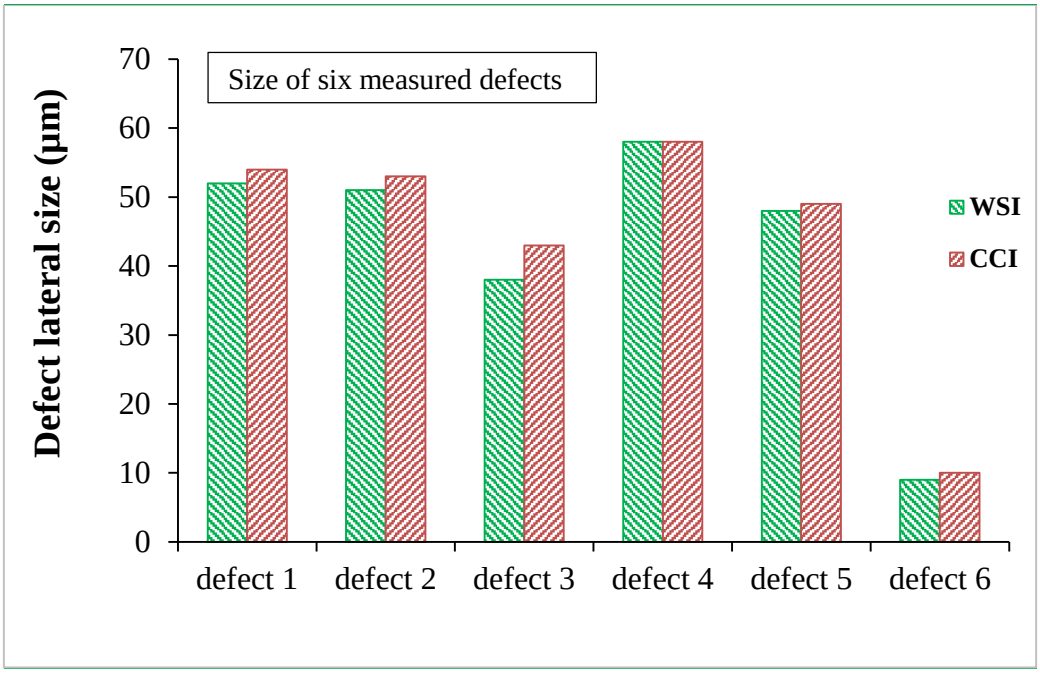

Figure 8-12: Defects lateral size measured offline and online process

8.4.2 WSI Performance Study

Further analysis was conducted on two other Al_2O_3 ALD coated samples to assess the capability of the WSI to distinguish between PV substrates that have a high water vapor rate, and those which have a low water vapor rate. In this case the correlation being based on the detected defect density. The samples having 72.75 cm² areas were initially measured for water vapour transmission rate (WVTR) using a traceable in house developed instrument at the National Physical Laboratory (NPL) as shown in Fig [8-13]. The instrument has a higher WVTR sensitivity limit of 3×10^{-5} g/m^2/day than the commercial MOCON® test which has a WVTR sensitivity of 3×10^{-4} g/m^2/day, the instrument can also measure the performance of larger sample areas than the MOCON® instrument (73 cm^2 instead of 50 cm^2); Fig [8-14] shows the WVTR test results for the two samples. Following the WVTR test, the samples were measured by CCI-3000 instrument using 20X lens objectives and WSI using 5X lens objective, covering about 13% of the total sample area in a clean room (class 10000). The protocol used in this study is to measure all the visible defects over the substrates.

Figure 8-13: Traceable in house WVTR measurement instrument

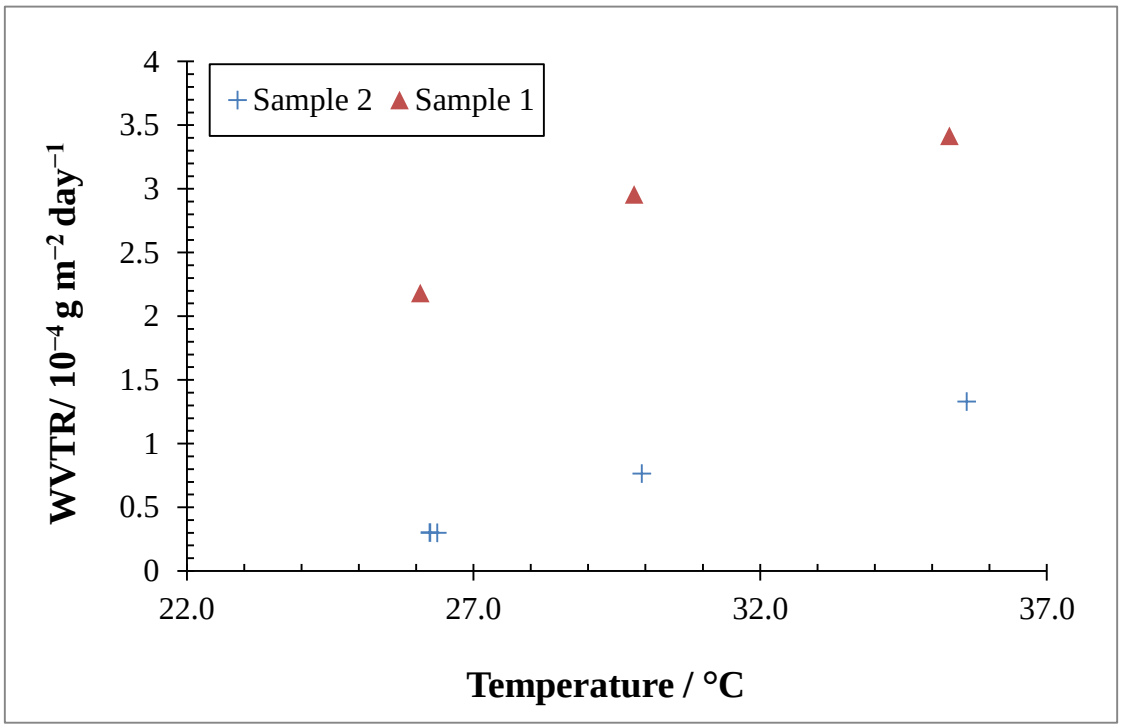

Figure 8-14: WVTR test results

The collected data from both instruments (CCI and WSI) were analysed by means of "segmentation analysis" (ISO25178-2, 2012) using the "Surfstand" software package, and the

criteria used to segment and count only significant defects were ((3×Sq vertical ≈ 20% Sz) and 3 µm lateral) this is in accordance with previous studies conducted by the authors (Mohamed Elrawemi et al., 2014).

The result of the analysis in Fig [8-15] revealed a clear correlation between the defects size, density and the measured WVTR, and also shows the capability of the WSI to capture such defects. The analysis also appears to specify that the sample with higher density of defects which satisfy the criteria of > 3µm lateral spacing and 3*Sq vertical exhibits inferior barrier properties, and a clear difference in density values for two samples can be distinguished.

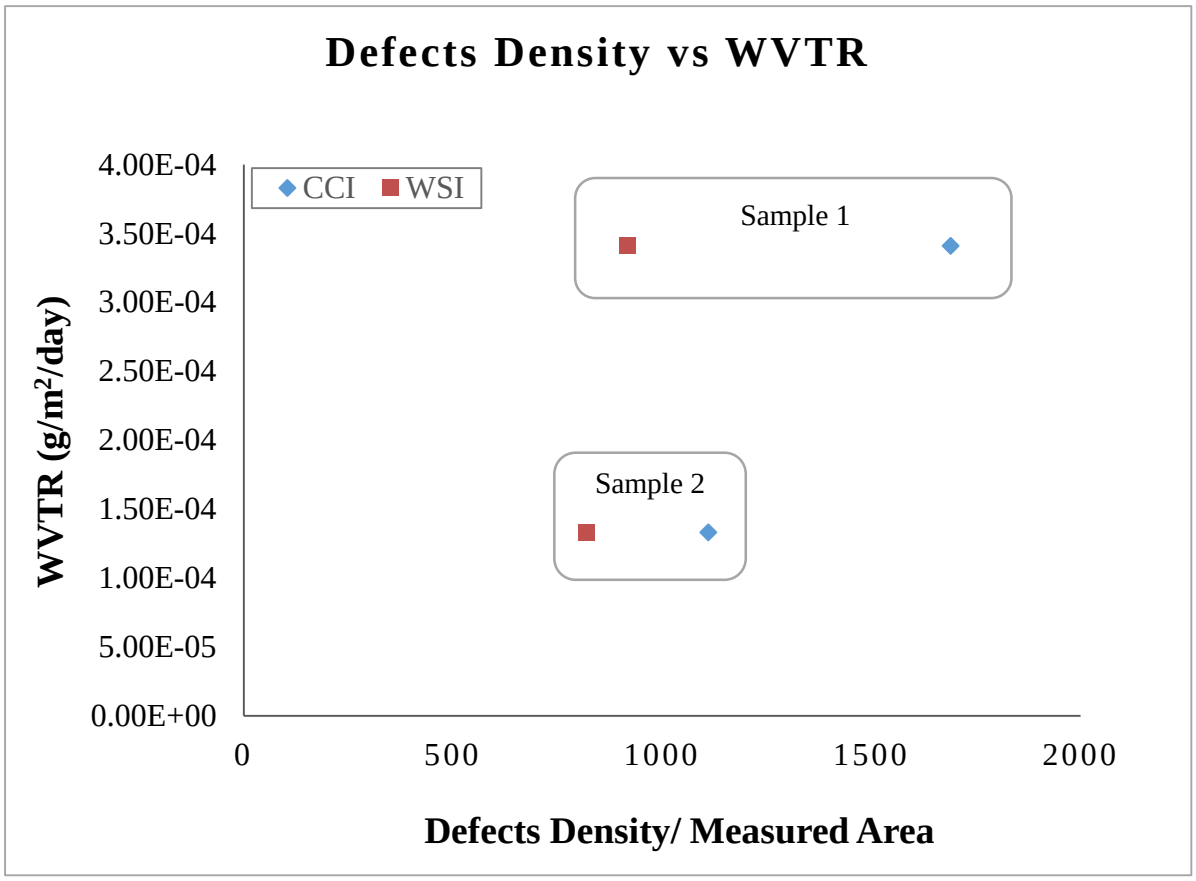

Figure 8-15: Defects density versus WVTR for two samples

This result indicates that, the WSI system has accurately and reliably captured the morphology of defects that have been detected by the offline CCI technique. The WSI

technique is consequently considered to be an efficient and optimal system to be used for in process thin film barrier defects inspection.

8.5 WSI Integration in R2R Demonstrator

To show the capabilities of this high precision system (WSI), a demonstrator system has been constructed in situ as a proof of concept at the Center for Process Innovation (CPI) in the UK. The whole demonstrator is contained in a Class 1000 clean room. The Al_2O_3 ALD barrier film translation in y-direction is facilitated by a barrier film re-winder, as shown in Fig [8-16]. The re-winder set up allows a large working area, where the high precision system (WSI) can be implemented.

Figure 8-16: Photo of DOEL demonstrator / re-winder

The instrument was integrated with an auto-focus linear stage mounted on a transverse stage as shown in Fig [8-17] so that the full width (500 mm) of the foil can be covered. In addition,

to deploy the WSI system consideration of the movement of the substrate film has been a further challenge. In this case an air bearing guidance system based on a New Way Air Bearing Ltd. has been employed as shown in Fig [8-17], in collaboration with IBS Precision Engineering (Netherlands) (IBS, 2013).

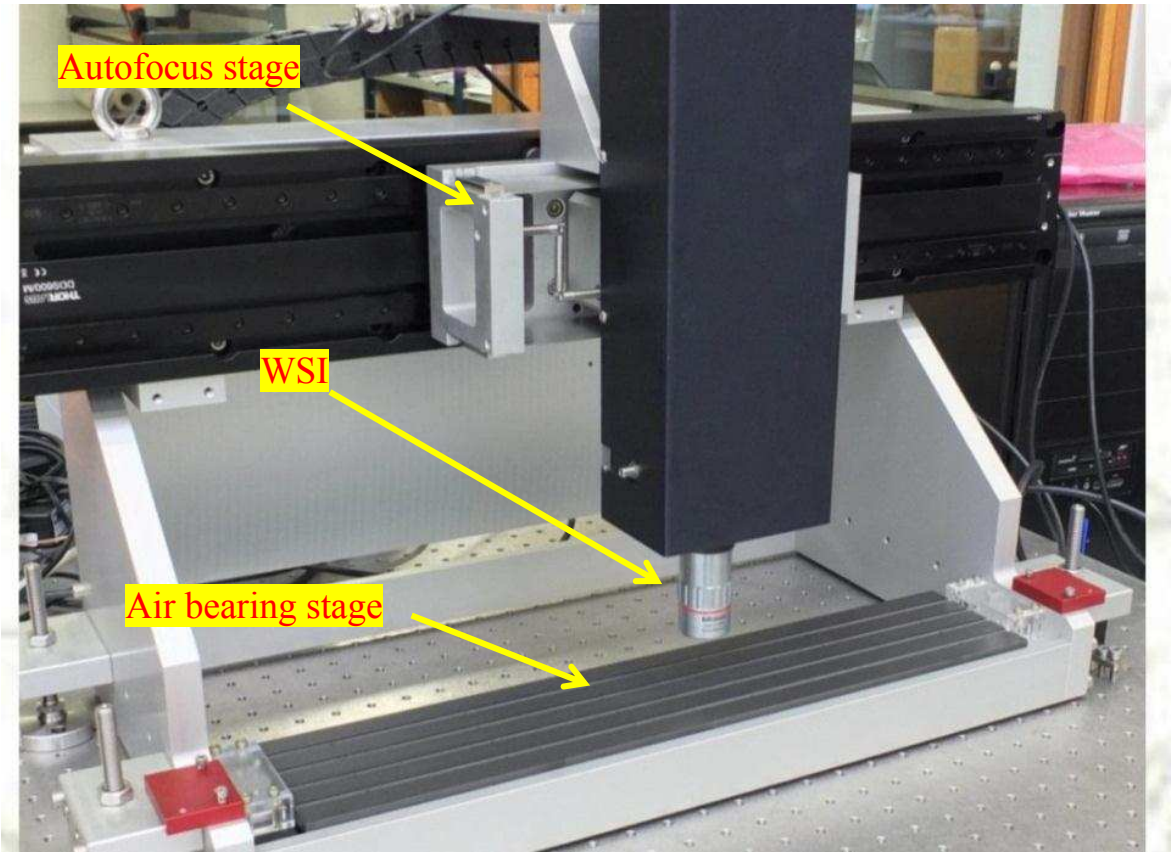

Figure 8-17: WSI integration in situ

The Air Bearing performance was investigated by IBS Precision Engineering using an optical sensor which scanned across a barrier film. Under optimal conditions the substrate height deviation can be kept within < 5µm, Fig [8-18] shows the surface height changes across a 50.5mm substrate when it is stabilised in the measurement zone. One of the inspection challenges is to perform a high fidelity surface measurement despite of the possible vibrations introduced by the air bearing stage. This challenge can be overcome by using the built-in active control loop in WSI to compensate for the environmental disturbances.

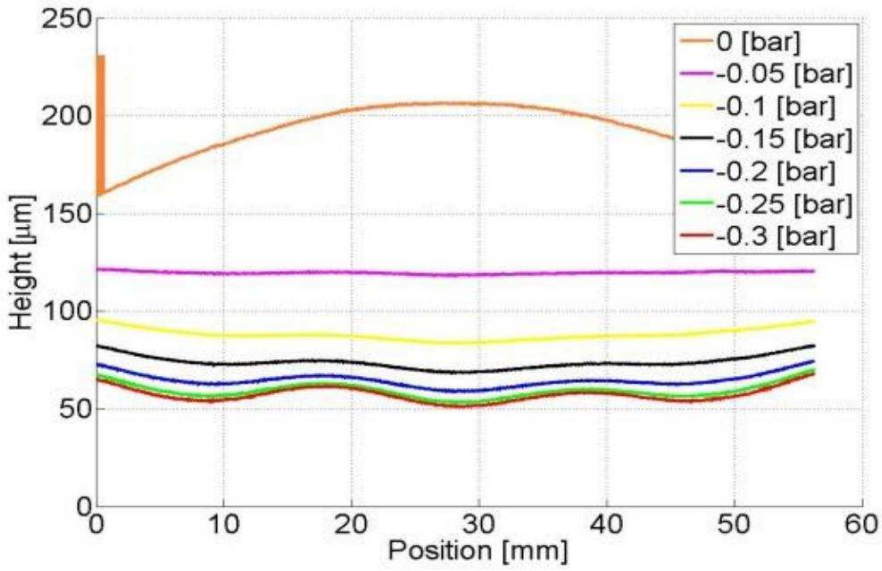

Figure 8-18: Height variation across substrate using air bearing (Courtesy of IBS Precision Engineering, Netherlands)

The system setup of the proof of concept system and WSI head is shown in Fig [8-19]. The WSI is combined with a traverse stage to provide full coverage of the barrier film in spite of the limited FOV of the instrument. In the operation process the sheet product is scanned laterally by shifting the WSI one FOV (including 10% overlap) of each measurement step.

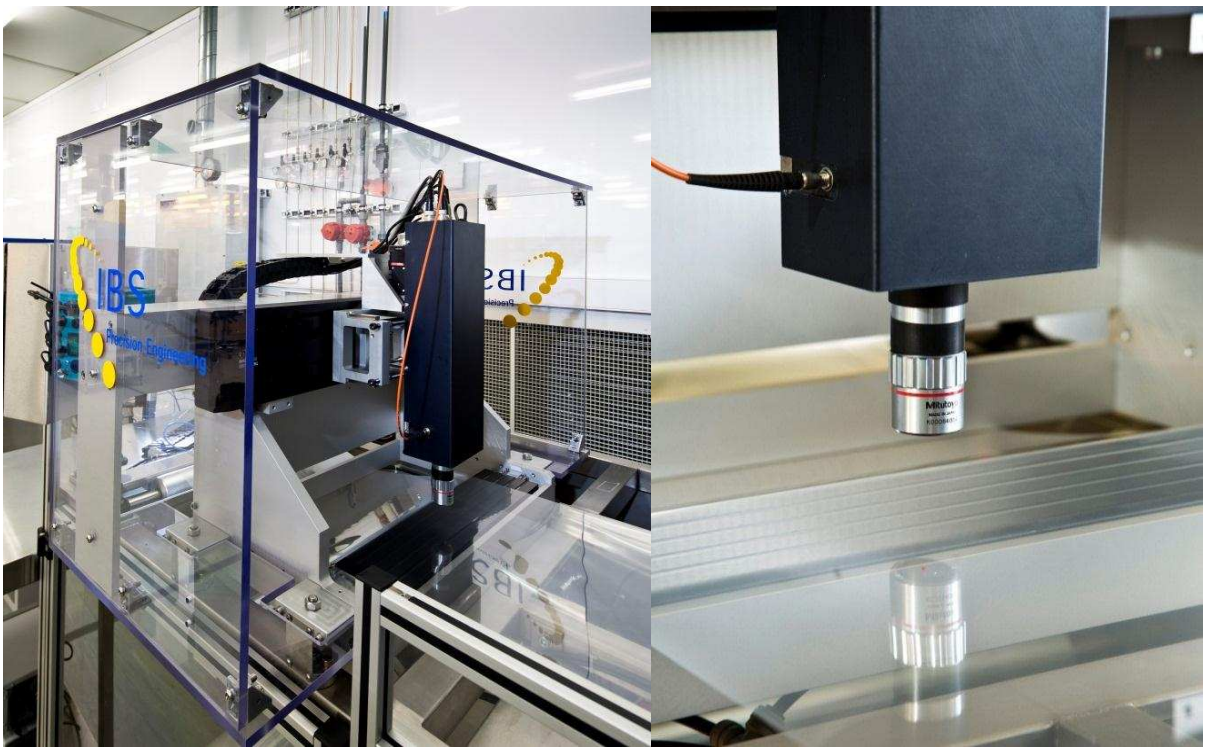

Figure 8-19: A schematic view of the proof of concept system and WSI head

8.6 In situ Performance Study

The initial implementation of the system was to acquire a series of static images and thus allow significant area but not the entire substrate surface to be measured. The WSI system has been implemented in a R2R demonstrator as shown in Fig [8-19], and calibrated by measuring 1.2 µm standard step height sample (Bento Box) supplied by the NPL. The results of the calibration artefact show that the measurement precision is better than 20 nm, see Fig [8-20].

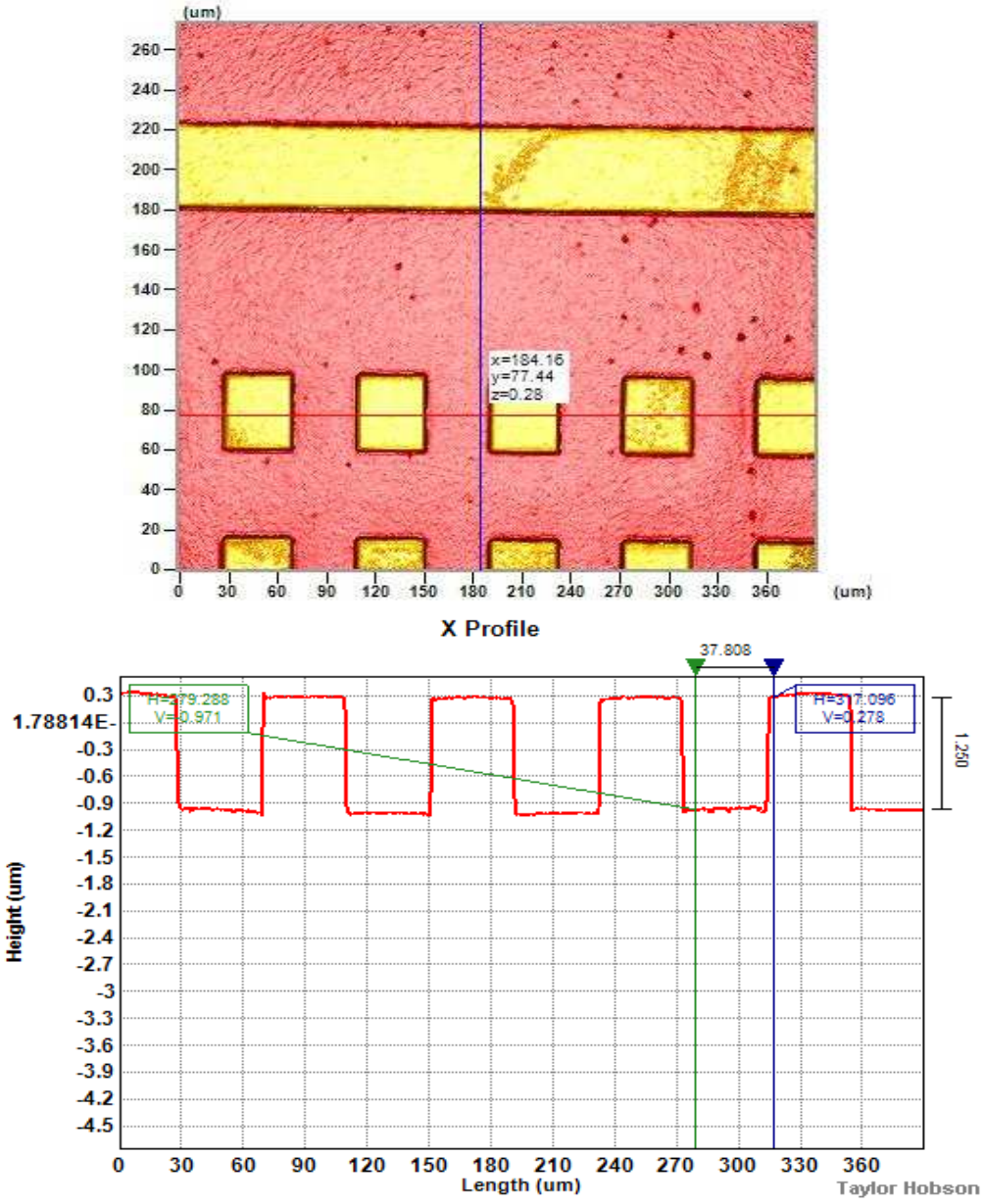

Figure 8-20: Measured results for standard step height sample using WSI

Gold coated PET film has been measured to obtain preliminary results in situ, where three defects are detected as shown in Fig [8-21]. Following that the system was run to capture a series of static images (areal measurements) over the Al_2O_3 ALD foil, having 216 measurements in 1 hour, and thus allow significant but not the entire substrate surface to be measured.

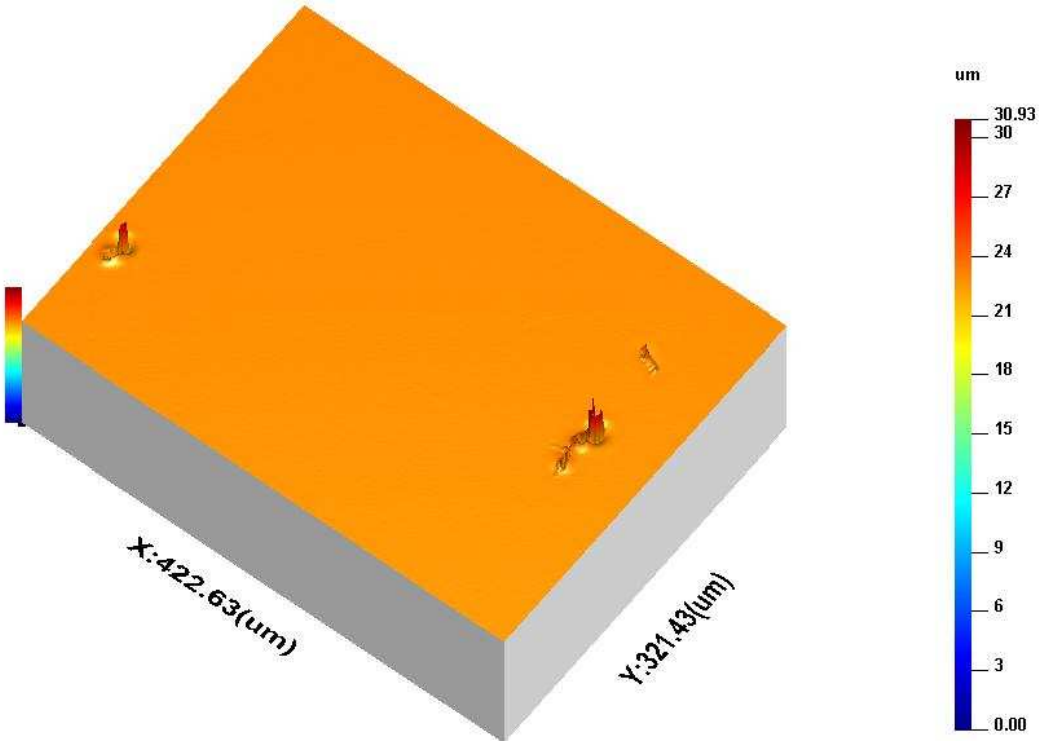

Figure 8-21: In situ coated film measurement

8.7 Industrial Scale up Issues and Data Handling Procedure

One of the main challenges for the application of such metrology is how to assess large and multiple measurement data sets obtained from an in process optical instrument. When measuring the surface topography over large area substrates (approximately 500 mm film foil width) with a limited field-of-view (FOV) of the optical instrument (WSI) will produce hundreds/thousands of measurement files. Assessing each file individually to find and analyse defects manually is time consuming and impractical. Therefore, a computerised

solution to assess these files by monitoring surface topography parameters (Sq and S_{dd}) was created based on the algorithms shown in figure [8-22].

Comparing parameter values to an experimentally determined threshold value, obtained from extensive lab-based measurement for ALD coating which have been explained in chapter (5, 6, 7 and 8), can indicate the existence of the defects for certain FOV's, this process can be repeated automatically for chosen parameters and the existence of defects can be indicated for the entire set of measurement files spontaneously without interaction from the inspector. A running defect log and associated defect statistics associated with the captured set of data files can be generated. This section outlines the implementation of the auto-defect logging using advanced areal parameters and its application in a proof of concept system at the Centre for Process Innovation (CPI).

8.7.1 Optimisation of Surfstand for Efficient Extraction of Defect Statistics

The Surfstand software is a commercial surface topography characterisation software tool developed as a result of the Surfstand project leading to a new software package known by the same name. This software allows multiple data formats to be viewed, filtered and numerically characterised (Blunt & Jiang, 2003). The principal aim was to form the base for a new set of international standards by developing mathematical analytical techniques for characterising the topography (texture and roughness) of engineering surfaces. The software is used mainly with stylus-based or optical profilometers, optical microscopes and scanning-probe microscopes. Its working principle is similar to other commercial surface metrology software such as TalyMap and MountainsMap and SPIP, where the surface features, roughness and other calculations can be conducted using different functions in the software toolbox. In addition, a series of graphics, such as the surface topography, 2D analysis of defects, mesh map, top view map and contour map of the surface, can be easily generated

using this toolbox. The toolbox was extensively used throughout this project to analyse the data captured by the CCI and the WSI.

The average roughness of Al_2O_3 ALD coating without defect, using WSI, is found to be Sq ≈ 7 nm. Previous study demonstrates that the significant defects will increase the roughness Sq (with defect) larger than ±3*Sq (no defect) i.e. Sq (with defect > ±21nm). Moreover, the segmentation analysis results and the theoretical model approach in chapter (7), both appear to indicate that the major contributing factor for determining the WVTR is the total number of larger defects, where the sample with higher density of defects > 3 µm exhibit inferior barrier properties. These criteria are considered to be the basis for developing the "Surfstand" toolbox as shown in Fig [8-22] in order to capture and count the number of defects that are seriously affecting the Al_2O_3 ALD barrier performance.

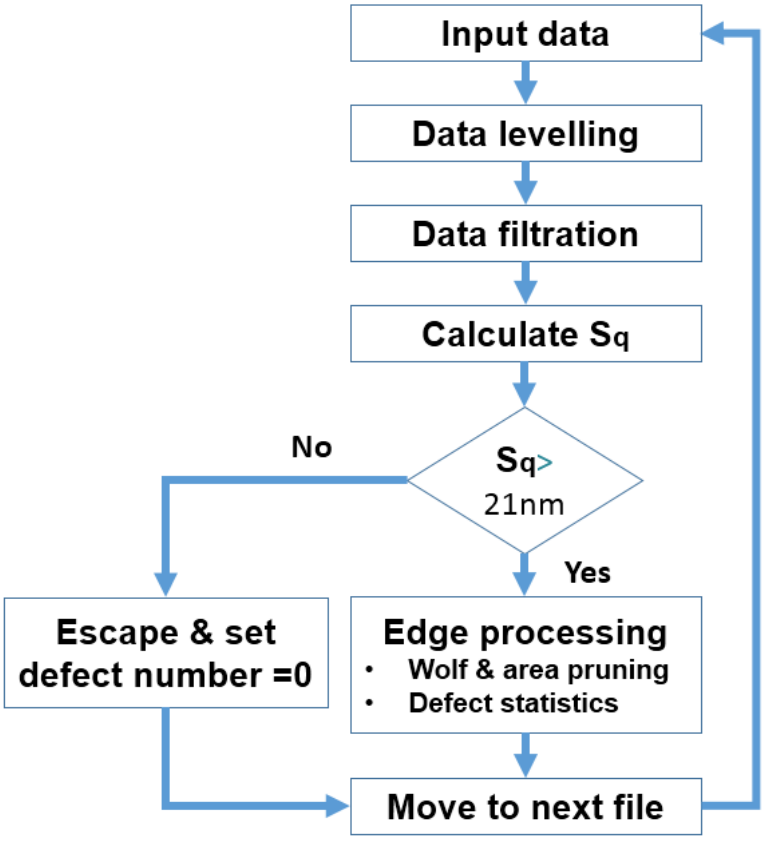

Figure 8-22: Extraction of Al_2O_3 ALD defect statistics procedure using WSI

The following figure [8-23] shows the Surfstand (toolbox) interface, where if the Sq of the measured surface is greater than the threshold limit (21 nm), the surface will be subject to data segmentation procedure to extract the significant defects as shown in the figure. Otherwise, the measurement will be treated as defect free surface. For data segmentation, the edge processing using Wolf and area-pruning methods are employed to identify and characterise the defects.

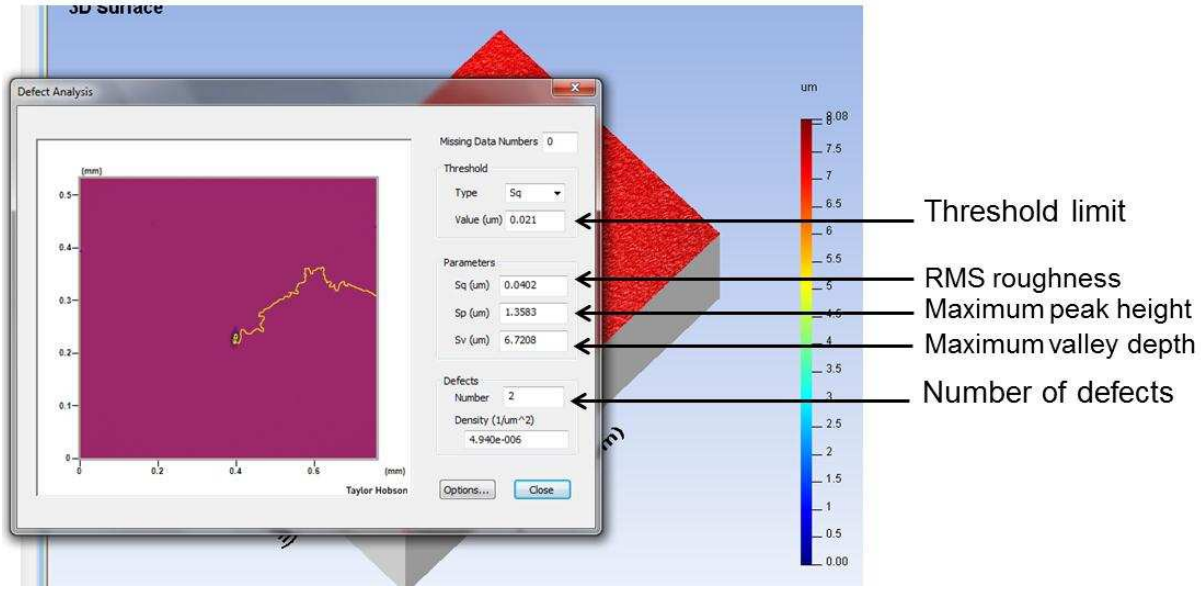

Figure 8-23: Surfstand (toolbox) interface

DefectsOutput - Notepad

File Edit Format View Help

File Name	Missing Data	Sq Value(um)	Sp Value(um)	Sv Value(um)	Defects Number	Defects Density(1/um^2)
p1	0	0.013512	0.167268	1.211728	0	0.0000000
p10	0	0.008776	0.178558	0.376893	0	0.0000000
p100	0	0.054110	1.428052	8.203407	1	2.305e-006
p101	0	0.066044	8.092217	6.069404	9	2.075e-005
p102	0	0.036756	1.428892	4.900036	2	4.610e-006
p103	0	0.155251	4.074205	18.013100	2	4.610e-006
p104	0	0.092417	4.716363	9.277656	8	1.844e-005
p105	0	0.160350	3.587061	16.407406	4	9.221e-006
p106	0	0.103912	2.741945	13.174541	22	5.071e-005
p107	0	0.109479	5.027643	10.032352	5	1.153e-005
p108	0	0.122309	3.211112	15.662971	1	2.305e-006
p109	0	0.127985	3.537587	15.200192	2	4.610e-006
p11	0	0.048769	1.113212	10.223041	2	4.940e-006
p110	0	0.073023	1.900081	10.368506	1	2.305e-006
p111	0	0.112940	2.949974	12.328129	2	4.610e-006
p112	0	0.095846	3.194979	11.642429	1	2.305e-006
p113	0	0.048052	7.984729	6.021550	11	2.536e-005
p114	0	0.097775	2.405353	12.302823	1	2.305e-006
p115	0	0.062832	1.495073	8.417302	9	2.075e-005
p116	0	0.041706	0.858395	5.494088	3	6.916e-006

Figure 8-24: Defects output

The procedure in Fig [8-23] can be repeated to analyse the entire measured files to extract and count defects and determine a chosen surface parameters such as deviation of the surface,

the highest peak of the surface and the lowest valley of the surface (Sq, Sp and Sv) and determine the position of the defective area as given in the output text file shown in Fig [8-24]. This model can be used for on-line inspection system for roll-to-roll manufacturing process without the need for interaction from the inspector.

8.8 Summary

It is well established that the performance of flexible PV modules is compromised by the presence of defects in the barrier layers. Laboratory established measurements indicated that defects that have a lateral size of $\geq 3\mu m$ have very detrimental effect on the barrier film functionality. Metrology methodologies based on optical interferometery and segmentation analysis method have proved to be a powerful tool in the Al_2O_3 ALD barrier surface characterisation. In order to implement in process metrology during the production of R2R barrier coating optical Interferometery must be applied. To overcome the environmental noise a novel compensated wavelength scanning interferometry system have been implemented, this system has shown the ability to overcome environmental vibration and additionally to perform high speed measurement in situ providing areal measurements in less than a second per FOV.

The work in this chapter concludes that, wavelength scanning interferometer has been shown as a solution to R2R barrier films defects measurement challenges, the system has been demonstrated and the output results compare favorably with commercial lab optical based instrumentation and functional assessment. Consequently, the WSI is considered to be a strong candidate for integration into quality assurance systems for developing the field of R2R manufacture

CHAPTER 9

9. Overall Discussion

In the PV industry when manufacturing high volume large area barrier films, the manufacturing process involves the deposition of nano-scale layers on large area substrates. Economical, effective and functional barriers can be achieved by a reduction in the thickness of the barrier material from micro to nano-scale, however the probability of creating critical defects during manufacture in the film increases as the thickness decreases. The density and size of defects and particles on the barrier film surface was found to be a critical factor in the reliability of barrier films as substrate for flexible solar cells.

Thin transparent layers of Al_2O_3 on polymer films used in this study were found to be significantly enhance the permeation barrier properties of polymer films. The work carried out in this thesis has shown that defects that are responsible for the water vapour ingress are in the range of few micrometres to tens of micrometres in lateral size, and a few manometers to tens of micrometres in vertical size. However, not only do the barrier layers need to have a low defect density, but also the existing substrate particles and defects need to be covered and planarised before ALD coatings.

Surface passivation schemes based on ALD may be a natural choice for future developments regarding thin-film solar cells and other next-generation concepts that require ultra-thin conformal films. The nature of defects in the Al_2O_3 ALD films was studied and found to be caused by surface irregularities on the substrate (e.g. scratches and surface spikes or holes), and by incorrect process conditions or caused by particle contamination on the original substrate. The particles may act as a mask to prevent the deposition of the ALD film. The particles may then be displaced to yield the pinhole defect, thus allowing water vapour

ingress. If the ALD film can nucleate easily on the underlying substrate, the ALD film is not expected to reveal defects in the absence of surface roughness or particle contamination. It is hoped that the information provided on coating technology in this thesis will contribute significantly to improve the lifespan, conversion efficiency and the functional performance of industrial solar cells, and further reducing the price of solar electricity in the long term.

Effective inspection is the key for further processes such as optimising the coating processes and/or applying local repair/cleaning techniques to remove the defects from the film surface before final use. In order to ensure effective and high barrier film yield, the key challenge is to inspect the substrate surface at production speed with sufficient resolution to detect i) the presence of problem defects on the starting foil surface, and ii) defects as they appear during the coating and patterning processes. Due to the nature of these processes, the inspection methods have to have no contact with the film surfaces.

The literature review in this thesis has shown that, there are no effective inspection methods that can be applied in such a case. This thesis introduced a novel non-contact metrology technique that is currently employed for Al_2O_3 ALD surface inspections. The technique has the potential to be applied to real-time on-line measurement of high precision surfaces such as those resulting from roll-to-roll film processing. The proposed system is potentially key for mass production of high quality, high efficiency photovoltaics and other roll-to-roll film productions. The success of this product will help mankind to convert solar power to electricity more efficiently and more cost effectively.

CHAPTER 10

10. Conclusion

The overall aims of this study was to characterise, catalogue and provide a better understanding of the PV barrier films defects, and to enable the development of an in process (novel) metrology system based on high resolution interferometry to detect the presence of the PV barrier films defects. The following objectives were set out in order to achieve this goal:

- Measuring defects size-scale, density and distribution over the PV barrier films.
- Provide a detailed knowledge of the nature of micro and nano-scale defects, which are responsible for the water vapor ingress.
- Correlating the defects density with the PV barrier layer functional performance.
- Developing a defect database (catalogue) used to integrate in-line sensor design.
- Developing a theoretical mathematical model to understand the mechanism of water vapor permeability through the PV barrier films defects.
- Enabling the implementation of an in process defect detection system.

In order to fulfill the aims and the objectives, a number of experimental studies associated with theoretical analysis were performed. The following conclusions can be drawn from the work accomplished in this research project:

- The relationship between the surface morphology and water vapour diffusivity of barrier coatings on PEN substrates is studied and explained.
- Surface metrology techniques have provided the ability to measure and effectively characterise the Al_2O_3 ALD film defects.
- Information has also been provided on what type of defects will impede PV performance and lifespan.

- Sq (RMS) in the absence of functional parameters can give an indication of increased barrier film roughness. However, the limitation of the parameter is that does not indicate the defect source (i.e. what is the source).
- The pruning process attempts to "un-pick" the RMS indication and assigns connection and functional significance of the defects. However, for data analysis both values need to be monitored at all times.
- This first application of feature segmentation analysis has provided a clear evidence for the correlation of surface defects size, defect density, and the transmission of water vapour through the barrier coating layers.The existence of pinholes has been reported as being directly related to the final coating quality.
- The investigation in chapter (5, 6, 7 and 8) reveals that the total permeation rate corresponding to small numbers of larger defects is much greater compared to the total permeation rate corresponding to large numbers of small pinhole-type defects over the same area of substrate.
- The study confirmed that small numbers of large defects are largely responsible for the observed water vapour permeability.
- The overall results of the study would seem to indicate that, the critical spatial resolution required for defect detection need not be less than 3 µm, as any defect that has less than this lateral size seems to have a much lower effect on the barrier properties.
- Non-contact measurement is the only obvious option to be used for the purpose of defect detection in such ultra-smooth surfaces.
- The wavelength scanning interferometer has been introduced as a solution to the measurement challenges, the system has been demonstrated as an in process technique and the output results compare favourably with laboratory based instrumentation.
- In process metrology for large area substrates is seen to be a strong technology driver.

10.1 Potential Future Work

The main focus of any future work would be to eliminate defects from the barrier films during the production process. It has been demonstrated in this study that failures which exist on flexible PV modules are a result of defects in the protective barrier layers. These defects are sometimes present on the surface of the substrate before the application of the protective layer or/and may be generated during the coating process, these defects have been shown to be capable of perforating the barrier film. As the morphology and size of the defects are now known, work to eliminate these defects from the production process can now be employed with the goal of removing them completely and allowing the PV barriers to be produced with long lifetimes. To implement the fundamental knowledge on defects in this thesis into a R2R manufacturing environment, a number of issues need to be addressed before full implementation of wavelength scanning measurement. These may include;

1- Although cleaning methods of the PV barrier films have been explained in this thesis, further investigation is required before the best practice can be recommended.
2- Data overlap between captured measured maps needs further studies.
3- Developing an effective stitching method to analyse the captured maps.
4- Studying the effect of limiting the vibration environment in R2R deployment of WSI.
5- Applying multiple sensors to cover much more measured area of the produced foils.
6- Proposed future work would include development of a method to detect and evaluate defects while the rolls are rotating and the film is in motion.
7- Consideration need to be taken into account for data storage.

11. References List

[1]. A. Ruanthon, Thanachayanont, C., & Sarakonsri, T. (2013). Preparation of CIGS p-type semiconductor used as thermoelectric material by sol-gel. Journal of Material Science and Applied Energy, 3(2), 10-13.

[2]. Ahmad, E. (1995). Growth and characterisation of Cu (In, Ga) Se_2 thin films for solar cell applications. (Doctoral dissertation), University of Salford, UK.

[3]. Akella, A., Saini, R., & Sharma, M. (2009). Social, economical and environmental impacts of renewable energy systems. Renewable Energy, 34(2), 390-396.

[4]. Alessandrini, A., & Facci, P. (2005). AFM: a versatile tool in biophysics. Measurement science and technology, 16(6), R65.

[5]. Allafi, A. R. (2008). Effect of Different Percent Loadings of Nanoparticles and Food Processing Conditions on the Properties of Nylon 6 Films. (Doctoral dissertation), The Ohio State University, Columbus, USA.

[6]. Almanza-Workman, A. M., Jeans, A., Braymen, S., Elder, R. E., Garcia, R. A., de la Fuente Vornbrock, A.,Jam, M. (2012). Planarization coating for polyimide substrates used in roll-to-roll fabrication of active matrix backplanes for flexible displays. Paper presented at the SPIE Advanced Lithography, San Jose, California, USA.

[7]. Ancuta, F., & Cepisca, C. (2011). Failure analysis capabilities for PV systems Recent Res. Energy, Environ. Entrep. Innov (pp. 109-115). Romania: University Politehnica of Bucharest.

[8]. Antony, A. (2004). Preparation and characterisation of certain II-VI, I-III-VI2 semiconductor thin films and transparent conducting oxides. (Doctoral dissertation), Cochin University of Science and Technology, Kerala, India.

[9]. Ashley, R. (1985). Permeability and plastics packaging Polymer permeability (pp. 269-308): Springer.

[10]. Bahaj, A., James, P. A., & Jentsch, M. F. (2007). Photovoltaics: added value of architectural integration. Proceedings of the ICE-Energy, 160(2), 59-69.

[11]. Bartholomeusz, B. J., & Bartholomeusz, M. (2014). Enhancement of semiconducting photovoltaic absorbers by the addition of alkali salts through solution coating techniques: Google Patents.

[12]. Belyaev, A., Polupan, O., Dallas, W., Ostapenko, S., Hess, D., & Wohlgemuth, J. (2006). Crack detection and analyses using resonance ultrasonic vibrations in full-size crystalline silicon wafers. Applied Physics Letters, 88(11), 111907.

[13]. Bertrand, J. A., Higgs, D. J., Young, M. J., & George, S. M. (2013). H_2O Vapor Transmission Rate through Polyethylene Naphthalate Polymer Using the Electrical Ca Test. The Journal of Physical Chemistry A, 117(46), 12026-12034.

[14]. Bertrandad, J. A., & George, S. M. (2011). Atomic Layer Deposition on Polymers for Ultralow Water Vapor Transmission Rates: The Ca Test. Paper presented at the 54th Annual Technical Conference Proceedings of the Society of Vacuum Coaters, Chicago.

[15]. Binnig, G., Quate, C. F., & Gerber, C. (1986). Atomic force microscope. Physical review letters, 56(9), 930.

[16]. Blateyron, F. (2013). The areal feature parameters Characterisation of Areal Surface Texture (pp. 45-65): Springer.

[17]. Blunt, L., Elrawemi, M., Fleming, L., & Sweeney, F. (2013). Correlation of micro and nano–scale defects with WVTR for aluminium oxide barrier coatings for flexible photovoltaic modules. International Journal of Precision Technology, 3(3), 290-302.

[18]. Blunt, L., Elrawemi, M., Fleming, L., & Sweeney, F. (2013). Correlation of micro and nano–scale defects with WVTR for aluminium oxide barrier coatings for flexible photovoltaic modules. IJPTECH, 3(3), 290-302. doi: 10.1504/ijptech.2013.057055

[19]. Blunt, L., & Jiang, X. (2003). Advanced techniques for assessment surface topography: Development of a Basis for 3D Surface Texture Standards" Surfstand": Elsevier.

[20]. Blunt, L., & Xiao, S. (2011). The use of surface segmentation methods to characterise laser zone surface structure on hard disc drives. Wear, 271(3), 604-609.

[21]. Bonnet, D., & Meyers, P. (1998). Cadmium-telluride—Material for thin film solar cells. Journal of Materials Research, 13(10), 2740-2753.

[22]. Bottomley, J. A. (2012). Novel application of atomic force microscopy to the analysis of barrier film defects. (Doctoral dissertation), University of Birmingham, Birmingham, UK.

[23]. Brémaud, D. J. L. (2009). Investigation and development of CIGS solar cells on flexible substrates and with alternative electrical back contacts. (Doctoral dissertation), ETH Zurich, Zurich.

[24]. Brown, A. (2010). Surface Characterisation in the Semiconductor Industry. Retrieved 9 October, 2014, from:

http://www.ceram.com/uploads/resources/whitepapers/Semicondutor_Industry_White_Paper.pdf

[25]. Bülow, T., Gargouri, H., Siebert, M., Rudolph, R., Johannes, H.-H., & Kowalsky, W. (2014). Moisture barrier properties of thin organic-inorganic multilayers prepared by plasma-enhanced ALD and CVD in one reactor. Nanoscale Research Letters, 9 (1), 223.

[26]. Carcia, P., McLean, R., & Hegedus, S. (2010). Encapsulation of Cu (InGa) Se_2 solar cell with Al2O3 thin-film moisture barrier grown by atomic layer deposition. Solar energy materials and Solar cells, 94(12), 2375-2378.

[27]. Carcia, P., McLean, R., Reilly, M., Groner, M., & George, S. (2006). Ca test of Al_2O_3 gas diffusion barriers grown by atomic layer deposition on polymers. Applied physics letters, 89(3), 031915-031915-031913.

[28]. Carcia, P. F., McLean, R. S., & Hegedus, S. (2010). (Invited) ALD Moisture Barrier for Cu (InGa) Se_2 Solar Cells. ECS Transactions, 33(2), 237-243.

[29]. Carlsson, T. (2006). Stability diagnostics for thin-film photovoltaic modules. (Doctoral Dissertation), Helsinki University of Technology, Espoo (37)

[30]. Carter, C. B., & Norton, M. G. (2007). Ceramic materials: Springer.

[31]. Casuso, I., Kodera, N., Le Grimellec, C., Ando, T., & Scheuring, S. (2009). Contact-mode high-resolution high-speed atomic force microscopy movies of the purple membrane. Biophysical journal, 97(5), 1354-1361.

[32]. Chagant, V. R. (2008). Study of structural and spectroscopic properties of small ZnS clusters by DFT. (Doctoral dissertation), University of Texas, El Paso. (AAI1461143)

[33]. Chainey, M. (1989). Transport phenomena in polymer films (Vol. 4). New York Marcel Dekker, Inc.

[34]. Chatham, H. (1996). Oxygen diffusion barrier properties of transparent oxide coatings on polymeric substrates. Surface and Coatings Technology, 78(1–3), 1-9. doi: http://dx.doi.org/10.1016/0257-8972(95)02420-4

[35]. Connor, Z. M., Fine, M. E., Achenbach, J. D., & Seniw, M. E. (1998). Using scanning acoustic microscopy to study subsurface defects and crack propagation in materials. J. Mater, 50 (11).

[36]. Conroy, M. (2012). Use of Interferometry for Optimization of PV Cell Performance Metrology and Failure Analysis, Future Photovoltaics (pp. 1-5). UK.

[37]. Coonen, S. (2007). Building Integrated Photovoltaics. Paper presented at the 1st Southeast Solar Summit, Oak Ridge, Tennessee. Presentation retrieved from: http://web.ornl.gov/sci/solarsummit/presentations/ORNL-Coonen.pdf

[38]. Cozmuta, I., Blanco, M., & Goddard, W. A. (2007). Gas sorption and barrier properties of polymeric membranes from molecular dynamics and Monte Carlo simulations. The Journal of Physical Chemistry B, 111(12), 3151-3166.

[39]. Czanderna, A., & Pern, F. (1996). Encapsulation of PV modules using ethylene vinyl acetate copolymer as a pottant: A critical review. Solar energy materials and Solar cells, 43(2), 101-181.

[40]. Da Silva Sobrinho, A., Czeremuszkin, G., Latreche, M., & Wertheimer, M. (2000). Defect-permeation correlation for ultrathin transparent barrier coatings on polymers. Journal of Vacuum Science & Technology A, 18(1), 149-157.

[41]. Da Silva Sobrinho, A. S., Latreche, M., Czeremuszkin, G., Klemberg-Sapieha, J. E., & Wertheimer, M. R. (1998). Transparent barrier coatings on polyethylene terephthalate by single- and dual-frequency plasma-enhanced chemical vapor deposition. Journal of Vacuum Science & Technology A: Vacuum, Surfaces, and Films, 16(6), 3190-3198. doi: 10.1116/1.581519

[42]. Dameron, A. A., Davidson, S. D., Burton, B. B., Carcia, P. F., McLean, R. S., & George, S. M. (2008). Gas diffusion barriers on polymers using multilayers fabricated by Al2O3 and rapid SiO2 atomic layer deposition. The Journal of Physical Chemistry C, 112(12), 4573-4580.

[43]. De Chiffre, L., Lonardo, P., Trumpold, H., Lucca, D. A., Goch, G., Brown, C. A., . . . Hansen, H. N. (2000). Quantitative Characterisation of Surface Texture. CIRP Annals - Manufacturing Technology, 49 (2), 635-652. doi: http://dx.doi.org/10.1016/S0007-8506(07)63458-1

[44]. Debeaufort, F., Voilley, A., & Meares, P. (1994). Water vapor permeability and diffusivity through methylcellulose edible films. Journal of Membrane Science, 91(1), 125-133.

[45]. Dennler, G., Lungenschmied, C., Neugebauer, H., Sariciftci, N., & Labouret, A. (2005). Flexible, conjugated polymer-fullerene-based bulk-heterojunction solar cells: basics, encapsulation, and integration. Journal of materials research, 20(12), 3224-3233.

[46]. Dennler, G., Lungenschmied, C., Neugebauer, H., Sariciftci, N. S., Latrèche, M., Czeremuszkin, G., & Wertheimer, M. R. (2006). A new encapsulation solution for flexible organic solar cells. Thin Solid Films, 511–512(0), 349-353. doi: http://dx.doi.org/10.1016/j.tsf.2005.12.091

[47]. Dingemans, G., & Kessels, W. (2012). Status and prospects of Al_2O_3-based surface passivation schemes for silicon solar cells. Journal of Vacuum Science & Technology A, 30(4), 040802.

[48]. Douwe Monsma, & Becker, J. (2006). The Savannah ALD System - An Excellent Tool for Atomic Layer Deposition Material Matters, 1(3).

[49]. Drygała, A., & Dobrzański, L. (2003). Materials for solar cells-state of the art and perspectives. Paper presented at the 12th International Scientific Conference "Achievements in Mechanical and Materials Engineering" AMME.

[50]. Duncan, B., Urquhart, J., & Roberts, S. (2005). Review of measurement and modelling of permeation and diffusion in polymers (pp. 68). Teddington, Middlesex, UK: National Physical Laboratory.

[51]. Elrawemi, M., Blunt, L., Fleming, L., Bird, D., Robbins, D., & Sweeney, F. (2014). Modelling water vapour permeability through atomic layer deposition coated photovoltaic barrier defects. Thin Solid Films, 570 (Part A), 101-106. doi: http://dx.doi.org/10.1016/j.tsf.2014.08.042

[52]. Elrawemi, M., Blunt, L., Fleming, L., & Sweeney, F. (2013). Further development of surface metrology methods for predicting the functional performance of flexible photovoltaic barrier films. Surface Topography: Metrology and Properties, 1(1), 015006.

[53]. Erlat, A., Henry, B., Ingram, J., Mountain, D., McGuigan, A., Howson, R., . . . Tsukahara, Y. (2001). Characterisation of aluminium oxynitride gas barrier films. Thin solid films, 388 (1), 78-86.

[54]. Erlat, A., Spontak, R., Clarke, R., Robinson, T., Haaland, P., Tropsha, Y., . . . Vogler, E. (1999). SiOx gas barrier coatings on polymer substrates: morphology and gas transport considerations. The Journal of Physical Chemistry B, 103(29), 6047-6055.

[55]. Erlat, A. G., Henry, B. M., Grovenor, C. R., Briggs, A. G., Chater, R. J., & Tsukahara, Y. (2004). Mechanism of water vapor transport through PET/AlOx Ny gas barrier films. The Journal of Physical Chemistry B, 108(3), 883-890.

[56]. Erler, B., Degiampietro, S., Pertl, P., Plessing, A. K., Skringer, A., & Kessler, F. (2003). Multi layer materials for the encapsulation of thin film modules. Paper presented at the Photovoltaic Energy Conversion, 2003. Proceedings of 3rd World Conference on Photovoltaic Energy Conversion Osaka, Japan.

[57]. Fahlteich, J. (2014). The Role of Defects in Single- and Multi- Layer Barriers for Flexible Electronics. Paper presented at the Annual SVC Technical Conference, Chicago.

[58]. FEI. (2009). QuantaTM 250 FEG Discover what a truly high resolution versatile SEM can do. In Q. FEG (Ed.), Product Data (pp. 1-4): FEI.

[59]. Feng, J. (2001). Interaction and permeability of water with liquid crystalline thermoset. (Doctoral dissertations), University of Florida, Florida.

[60]. Fick, A. (1855). Ueber diffusion. Annalen der Physik, 170 (1), 59-86.

[61]. Frach, P., Bartzsch, H., Glöß, D., Fahland, M., & Händel, F. (2008). Electrically insulating Al_2O_3 and S_iO_2 films for sensor and photovoltaic applications deposited by reactive pulse magnetron sputtering, hollow cathode arc activated deposition and magnetron-PECVD. Surface and Coatings Technology, 202(22–23), 5680-5683. doi: http://dx.doi.org/10.1016/j.surfcoat.2008.06.043

[62]. Garcia-Ayuso, G., Vázquez, L., & Martínez-Duart, J. M. (1996). Atomic force microscopy (AFM) morphological surface characterization of transparent gas barrier coatings on plastic films. Surface and Coatings Technology, 80 (1–2), 203-206. doi: http://dx.doi.org/10.1016/0257-8972(95)02712-2

[63]. George, M. (2014). Design and Development of a State of the Art R2R Production Platform For Flexible Transparent Barrier Films Paper presented at the The Web Coating & Handling Conference, South Carolina http://www.aimcal.org/

[64]. George, S. C., & Thomas, S. (2001). Transport phenomena through polymeric systems. Progress in Polymer Science, 26(6), 985-1017.

[65]. George, S. M. (2009). Atomic layer deposition: an overview. Chemical Reviews, 110(1), 111-131.

[66]. Goetzberger, A., & Hebling, C. (2000). Photovoltaic materials, past, present, future. Solar energy materials and Solar cells, 62(1–2), 1-19.

[67]. Goetzberger, A., Knobloch, J., & Voss, B. (1998). Crystalline Silicon Solar Cells: Wiley.

[68]. Greener, J., Ng, K., Vaeth, K., & Smith, T. (2007). Moisture permeability through multilayered barrier films as applied to flexible OLED display. Journal of applied polymer science, 106(5), 3534-3542.

[69]. Groner, M., Fabreguette, F., Elam, J., & George, S. (2004). Low-temperature Al_2O_3 atomic layer deposition. Chemistry of Materials, 16(4), 639-645.

[70]. Groner, M. D., George, S. M., McLean, R. S., & Carcia, P. F. (2006). Gas diffusion barriers on polymers using Al_2O_3 atomic layer deposition. Applied Physics Letters, 88(5), -. doi: doi:http://dx.doi.org/10.1063/1.2168489

[71]. Grover, R., Srivastava, R., Rana, O., Mehta, D., & Kamalasanan, M. (2011). New organic thin-film encapsulation for organic light emitting diodes. Journal of Encapsulation and Adsorption Sciences, 1(2), 23-28. doi: 10.4236/jeas.2011.12003

[72]. Hajimirza, S. (2013). Optimization, design and performance analysis of light trapping structures in thin film solar cells. (Doctoral dissertation), University of Texas at Austin, Austin.

[73]. Hamakawa, Y. (2004). Thin-Film Solar Cells: Next Generation Photovoltaics and Its Applications (Vol. 13): Springer.

[74]. Hanika, M., Langowski, H. C., Moosheimer, U., & Peukert, W. (2003). Inorganic Layers on Polymeric Films – Influence of Defects and Morphology on Barrier Properties. Chemical Engineering & Technology, 26(5), 605-614. doi: 10.1002/ceat.200390093

[75]. Harati, M., Jia, J., Giffard, K., Pellarin, K., Hewson, C., Love, D. A., Ding, Z. (2010). One-pot electrodeposition, characterization and photoactivity of stoichiometric copper indium gallium diselenide (CIGS) thin films for solar cells. Physical Chemistry Chemical Physics, 12 (46), 15282-15290.

[76]. Hegedus, S., Carcia, P., McLean, R., & Culver, B. (2010). Encapsulation of Cu (InGa) Se 2 solar cells with ALD Al 2 O 3 flexible thin-film moisture barrier: stability under 1000 hour damp heat and UV exposure. Paper presented at the Photovoltaic Specialists Conference (PVSC), 2010 35th IEEE.

[77]. Henry, W. (1803). Experiments on the quantity of gases absorbed by water, at different temperatures, and under different pressures. Philosophical Transactions of the Royal Society of London, 93, 29-276.

[78]. Hilmersson, C., Hess, D., Dallas, W., & Ostapenko, S. (2008). Crack detection in single-crystalline silicon wafers using impact testing. Applied Acoustics, 69(8), 755-760.

[79]. Hirvikorpi, T. (2011). Thin Al_2O_3 barrier coatings grown on bio-based packaging materials by atomic layer deposition. (Doctoral dissertation), Aalto University, Kuopio, Finland.

[80]. Hirvikorpi, T., Laine, R., Vähä-Nissi, M., Kilpi, V., Salo, E., Li, W.-M., . . . Kostamo, J. (2014). Barrier properties of plastic films coated with an Al_2O_3 layer by roll-to-toll atomic layer deposition. Thin Solid Films, 550 (A), 164-169. doi: http://dx.doi.org/10.1016/j.tsf.2013.10.148

[81]. Hoex, B., Gielis, J., Van de Sanden, M., & Kessels, W. (2008). On the c-Si surface passivation mechanism by the negative-charge-dielectric Al_2O_3. Journal of Applied Physics, 104(11), 113703.

[82]. Hotchkiss, J. H. (1997). Food-packaging interactions influencing quality and safety. Food Additives & Contaminants, 14(6-7), 601-607.

[83]. Hutter, J. L., & Bechhoefer, J. (1993). Calibration of atomic-force microscope tips. Review of Scientific Instruments, 64(7), 1868-1873.

[84]. IBS. (2013). Contactless Handling of thin films using New Way high speed conveyor air bearings. By measuring fly height and foil deformation. Retrieved April 2015, 2015, from http://ibspe.com/public/uploads/content/files/ConveyorThin-Film2013.pdf

[85]. IEC61646-2. (2008). Thin-film terrestrial photovoltaic (PV) modules – Design qualification and type approval (Vol. Edition 2.0, pp. 5-36). Geneva, Switzerland: British Standards Institution.

[86]. Igalson, M., & Urbaniak, A. (2005). Defect states in the CIGS solar cells by photocapacitance and deep level optical spectroscopy. Technical Sciences, 53(2).

[87]. Inslee, J., & Hendricks, B. (2009). Apollo's Fire: Igniting America's Clean Energy Economy (1st ed.). USA: Island Press.

[88]. ISO25178-2. (2012). Geometrical product specifications (GPS) -- Surface texture: Areal -- Part 2: Terms, definitions and surface texture parameters. International Organization for Standardization. Geneva, Switzerland.

[89]. James, T., Goodrich, A., Woodhouse, M., Margolis, R., & Ong, S. (2011). Building-Integrated Photovoltaics (BIPV) in the residential sector: an analysis of installed rooftop system prices. Contract, 303, 275-3000.

[90]. Jiang, X., Scott, P. J., Whitehouse, D. J., & Blunt. (2007). Paradigm shifts in surface metrology. Part II. The current shift. Proceedings of the Royal Society A: Mathematical, Physical and Engineering Science, 463(2085), 2071-2099.

[91]. Jiang, X., Wang, K., Gao, F., & Muhamedsalih, H. (2010). Fast surface measurement using wavelength scanning interferometry with compensation of environmental noise. Applied optics, 49 (15), 2903-2909.

[92]. Johansson, P., Lahtinen, K., Kuusipalo, J., Kääriäinen, T., Maydannik, P., & Cameron, D. (2010). Atomic layer deposition process for barrier applications of flexible packaging. Paper presented at the Tappi 2010 PLACE Conference, TAPPI.

[93]. Johnson, R. W., Hultqvist, A., & Bent, S. F. (2014). A brief review of atomic layer deposition: from fundamentals to applications. Materials Today, 17(5), 236-246. doi: http://dx.doi.org/10.1016/j.mattod.2014.04.026

[94]. Jorgensen, G. J., Terwilliger, K. M., DelCueto, J. A., Glick, S. H., Kempe, M. D., Pankow, J. W., . . . McMahon, T. J. (2006). Moisture transport, adhesion, and corrosion protection of PV module packaging materials. Solar energy materials and Solar cells, 90 (16), 2739-2775. doi: http://dx.doi.org/10.1016/j.solmat.2006.04.003

[95]. Kailas, S. V. (2006). Atomic Structure, Interatomic Bonding and Structure of Crystalline Solids Atomic Structure and Atomic Bonding in Solids Bengaluru, India Indian Institute of Science.

[96]. Kaplonek, W., & Lukianowicz, C. (2012). Coherence correlation interferometry in surface topography measurements. In I. Padron (Ed.), Recent Interferometry Applications in Topography and Astronomy (pp. 1-26): InTech.

[97]. Karunakaran, R. G., Lu, C.-H., Zhang, Z., & Yang, S. (2011). Highly transparent superhydrophobic surfaces from the coassembly of nanoparticles (≤ 100 nm). Langmuir, 27(8), 4594-4602.

[98]. Keith Masters, Paul Steinbacher, & O'Connell, K. (2010). CCD Camera Defect Detection Systems: The State of the Art. Retrieved August 2014, from: Honeywell, IAC & Isys Controls http://www.tappi.org/Downloads/unsorted/UNTITLED-pcei97193pdf.aspx

[99]. Kempe, M. D. (2005). Control of moisture ingress into photovoltaic modules. Paper presented at the Photovoltaic Specialists Conference, 2005. Conference Record of the Thirty-first IEEE.

[100]. Kempe, M. D. (2006). Modeling of rates of moisture ingress into photovoltaic modules. Solar energy materials and Solar cells, 90(16), 2720-2738.

[101]. Kessler, F., & Rudmann, D. (2004). Technological aspects of flexible CIGS solar cells and modules. Solar Energy, 77(6), 685-695.

[102]. Kim, C., Jung, J., Youm, W., & Park, K. (2011). Design of mechanical components for vibration reduction in an atomic force microscope. Review of Scientific Instruments, 82(3), 035102.

[103]. Kim, K.-D., Shin, H., & Chang, S. (2012). Thin Film Passivation Characteristics in OLED Using In-situ Passivation. Transactions on Electrical and Electronic Materials 13(2), 93-97.

[104]. Kim, N., Potscavage Jr, W. J., Sundaramoothi, A., Henderson, C., Kippelen, B., & Graham, S. (2012). A correlation study between barrier film performance and shelf lifetime of encapsulated organic solar cells. Solar energy materials and Solar cells, 101, 140-146.

[105]. Kimbrough, B. (2015). In-line roll-to-roll metrology for flexible electronics. Paper presented at the SPIE Optical Engineering+ Applications.

[106]. King, D., Quintana, M., Kratochvil, J., Ellibee, D., & Hansen, B. (2000). Photovoltaic module performance and durability following long-term field exposure. Progress in Photovoltaics Research and Applications, 8 (2), 241-256.

[107]. Koo, W. H., Choi, S. H., Baik, H. K., Lee, S. M., & Lee, S. J. (2005). Control of water vapor permeation through oxide films on polymers for flexible displays. Electronic Materials Letters, 1, 107-113.

[108]. Kotipalli, R., Delamare, R., Poncelet, O., Tang, X., Francis, L., & Flandre, D. (2013). Passivation effects of atomic-layer-deposited aluminum oxide. EPJ Photovoltaics, 4, 45107.

[109]. Krysinski, A., Coupland, J., Leach, R., & Flockhart, G. M. H. (2014). A simple defect detection technique for high speed roll-to- roll manufacturing. Paper presented at the 14th Euspen International Conference, Dubrovnik, Croatia.

[110]. Lahtinen, K., Kääriäinen, T., Maydannik, P., Cameron, D., Johansson, P., & Kuusipalo, J. (2012). Toward more controlled, nanoscale barrier layers in packaging. Society of Plastics Engineers, 1-3. doi: 10.2417/spepro.004237

[111]. Langereis, E., Creatore, M., Heil, S., Van de Sanden, M., & Kessels, W. (2006). Plasma-assisted atomic layer deposition of Al 2 O 3 moisture permeation barriers on polymers. Applied physics letters, 89(8), 081915-081915-081913.

[112]. Leach, Brown, L., Jiang, X., Blunt, R., Conroy, M., & Mauger, D. (2008). Guide to the measurement of smooth surface topography using coherence scanning interferometry. Measurement Good Practice Guide(108).

[113]. Lee, U. S., Choi, J. S., Yang, B. S., Oh, S., Kim, Y. J., Oh, M. S., Kim, H. J. (2013). Formation of a Bilayer of ALD-SiO2 and Sputtered Al_2O_3/ZrO_2 Films on Polyethylene Terephthalate Substrates as a Moisture Barrier. ECS Solid State Letters, 2(6), R13-R15.

[114]. Lewis, A., Taha, H., Strinkovski, A., Manevitch, A., Khatchatouriants, A., Dekhter, R., & Ammann, E. (2003). Near-field Microscopy reviewed by Nature Biotechnology. Nature Biotechnology, 21, 1378 - 1386. doi: 10.1038/nbt898

[115]. Lewis, J. S., & Weaver, M. S. (2004). Thin-film permeation-barrier technology for flexible organic light-emitting devices. IEEE Journal of Selected Topics in Quantum Electronics, 10 (1), 45-57.

[116]. Logothetidis, S., Laskarakis, A., Georgiou, D., Amberg-Schwab, S., Weber, U., Noller, K., Lohwasser, W. (2010). Ultra high barrier materials for encapsulation of flexible organic electronics. The European Physical Journal Applied Physics, 51(03), 33203.

[117]. Lu, X., Wang, Z., Yang, X., Xu, X., Zhang, L., Zhao, N., & Xu, J. (2011). Antifogging and antireflective silica film and its application on solar modules. Surface and Coatings Technology, 206(6), 1490-1494.

[118]. Mah, O. (1998). Fundamentals of photovoltaic materials National Solar Power Research Institute (pp. 1-10).

[119]. Mainsah, E., Greenwood, J. A., & Chetwynd, D. (Eds.). (2001). Metrology and Properties of Engineering Surfaces (1st ed.): Springer US.

[120]. Maniscalco, B., Kaminski, P. M., & Walls, J. M. (2012, 3-8 June 2012). Combined thin-film thickness measurement and surface metrology of photovoltaic thin films using Coherence Correlation Interferometry. Paper presented at the Photovoltaic Specialists Conference (PVSC), 2012 38th IEEE.

[121]. Metz, S. J. (2003). Water vapor and gas transport through polymeric membranes. (Doctoral dissertation), University of Twente, Enschede, Netherlands.

[122]. MOCON®. (1997) System for Measuring High Transmission Water Vapor. USA: MOCON®.

[123]. Morlier, A., Cros, S., Garandet, J.-P., & Alberola, N. (2013). Gas barrier properties of solution processed composite multilayer structures for organic solar cells encapsulation. Solar energy materials and Solar cells, 115(0), 93-99. doi: http://dx.doi.org/10.1016/j.solmat.2013.03.033

[124]. Morris, A. S. (2001). Measurement and instrumentation principles (3rd ed.). Oxford: Butterworth-Heinemann.

[125]. Movla, H. (2014). Optimization of the CIGS based thin film solar cells: Numerical simulation and analysis. Optik-International Journal for Light and Electron Optics, 125(1), 67-70.

[126]. Muhamedsalih, H. (2013). Investigation of Wavelength Scanning Interferometry for Embedded Metrology. (Doctoral dissertation), University of Huddersfield, Huddersfield, UK.

[127]. Muhamedsalih, H., Jiang, X., & Gao, F. (2013). Accelerated surface measurement using wavelength scanning interferometer with compensation of environmental noise. Procedia CIRP, 10, 70-76.

[128]. Müller, G. (2004). Annual Repor. In I. f. S. ISC (Ed.), (pp. 22-25). Würzburg, Germany: Fraunhofer-Institut für Silicatforschung ISC.

[129]. NanoMend EU FP7 (280581) from: http://nanomend.eu/.

[130]. Nisha, K. (2013). Synthesis and characterization of organic molecules passivated cadmium sulphide nanostructures for biological applications. (PhD Doctor of Philosophy), SRM University, Chennai.

[131]. Novak, E. (2010). Improve PV Solar Cell Efficiency With 3-D Surface Profiling. Quality, 49(9), 26-29.

[132]. Novotna, P. B. V. (2014). Characterization of Scanning Transmission Electron Microscopy Images of Thin Biological Sections. (Ph.D), Brno University of Technology, Brno. (125067)

[133]. Oyama, S. T., & Stagg-Williams, S. M. (2011). Inorganic Polymeric and Composite Membranes, Volume 14 - Structure, Function and Other Correlations: Elsevier.

[134]. Park, C. Y., An, J. S., Jang, H. J., Lee, J. H., & Choi, B. H. (2014). Growth behavior and improved water–vapor-permeation-barrier properties of 10-nm-thick single Al2O3 layer grown via cyclic chemical vapor deposition on organic light-emitting diodes. Organic Electronics, 15(8), 1717-1723.

[135]. Park, S.-H. K., Oh, J., Hwang, C.-S., Lee, J.-I., Yang, Y. S., & Chu, H. Y. (2005). Ultrathin Film Encapsulation of an OLED by ALD. Electrochemical and solid-state letters, 8 (2), H21-H23.

[136]. Peike, C., Hädrich, I., Weiß, K.-A., & Dürr, I. (2013). Overview of PV module encapsulation materials. Photovoltaics International, 19, 85-92.

[137]. Pern, F.-J., & Noufi, R. (2012). Stability of CIGS solar cells and component materials evaluated by a step-stress accelerated degradation test method. Paper presented at the SPIE Solar Energy+ Technology.

[138]. Pern, F. J., & Noufi, R. (2011). Characterization of damp heat degradation of CuInGaSe2 solar cell components and devices by (electrochemical) impedance spectroscopy. Paper presented at the SPIE Solar Energy +Technology.

[139]. Putkonen, M. (2011). Advanced process technologies: Plasma, direct-write, atmospheric pressure, and roll-to-roll ALD. Mrs Bulletin, 36(11), 907-913.

[140]. Puurunen, R. L. (2005). Surface chemistry of atomic layer deposition: A case study for the trimethylaluminum/water process. Journal of Applied Physics, 97(12), 121301-121301-121352. doi: 10.1063/1.1940727.

[141]. Rakotoniaina, J., Breitenstein, O., Al Rifai, M., Franke, D., & Schnieder, A. (2004). Detection of cracks in silicon wafers and solar cells by lock-in ultrasound thermography. Paper presented at the Proc. PV Solar Conf.(Paris, June).

[142]. Ramadas, S. K., & Shanmugavel, S. (2012). Encapsulation barrier stack: Google Patents.

[143]. Rardin, T. E., & Xu, R. (2011). Printing Processes Used to Manufacture Photovoltaic Solar Cells. 37(2), 62-68.

[144]. Rebeggiani, S., Rosén, B.-G., & Sandberg, A. (2011). A quantitative method to estimate high gloss polished tool steel surfaces. Paper presented at the Journal of Physics: Conference Series.

[145]. Reese, M. O., Dameron, A. A., & Kempe, M. D. (2011). Quantitative calcium resistivity based method for accurate and scalable water vapor transmission rate measurement. Review of Scientific Instruments, 82(8), 085101.

[146]. Repins, I., Contreras, M. A., Egaas, B., DeHart, C., Scharf, J., Perkins, C. L., . . . Noufi, R. (2008). 19·9%-efficient ZnO/CdS/CuInGaSe2 solar cell with 81·2% fill factor. Progress in Photovoltaics: Research and Applications, 16(3), 235-239. doi: 10.1002/pip.822

[147]. Rohrer, N. L. H., & Binnig, G. (2006). Scanning tunneling microscope.

[148]. Ross Jr, R. (1984a). Reliability research toward 30-year-life photovoltaic modules. Paper presented at the Proc. 1st Int. Photovoltaic Science and Engineering Conf., Kobe, Japan.

[149]. Ross Jr, R. (1984b). Technology developments toward 30-year-life of photovoltaic modules. Paper presented at the 17th IEEE Photovoltaic Specialists Conference, Kissimmee, Florida.

[150]. Rueland, E., Herguth, A., Trummer, A., Wansleben, S., & Fath, P. (2005). µ-Crack detection and other optical characterization techniques for in-line inspection of wafers an cells. Proceedings of 20th EU PVSEC, 3242-3245.

[151]. Sajeesh, T. (2013). Spray Pyrolysed Tin Chalcogenide Thin Films: Optimization of optoelectronic properties of SnS for possible photovoltaic application as an absorber layer. (Doctoral dissertation), Cochin University of Science and Technology Kerala, India

[152]. Saji, V. S., Choi, I.-H., & Lee, C.-W. (2011). Progress in electrodeposited absorber layer for CuIn(1−x) GaxSe2 (CIGS) solar cells. Solar Energy, 85(11), 2666-2678. doi: http://dx.doi.org/10.1016/j.solener.2011.08.003

[153]. Santos, N. C., & Castanho, M. A. (2004). An overview of the biophysical applications of atomic force microscopy. Biophysical chemistry, 107(2), 133-149.

[154]. Schleicher-Tappeser, R. (2012). How renewables will change electricity markets in the next five years. Energy policy, 48, 64-75.

[155]. Schmidt, M., Braunger, D., Schäffler, R., Schock, H. W., & Rau, U. (2000). Influence of damp heat on the electrical properties of Cu(In,Ga)Se2 solar cells. Thin Solid Films, 361–362(0), 283-287. doi: http://dx.doi.org/10.1016/S0040-6090(99)00820-2

[156]. Schubert, M. B., & Werner, J. H. (2006). Flexible solar cells for clothing. Materials Today, 9 (6), 42-50. doi: http://dx.doi.org/10.1016/S1369-7021(06)71542-5

[157]. Schubert, S., Klumbies, H., Müller-Meskamp, L., & Leo, K. (2011). Electrical calcium test for moisture barrier evaluation for organic devices. Review of Scientific Instruments, 82(9), 094101.

[158]. Smith , David Bird, Andrew Cook, Steve Edge, Phil Hollis, Paolo Melgari, & Spruce, S. (2014). Ultra-barrier Encapsulation by ALD R2R Processing for Flexible Large

Area Devices. Paper presented at the 6th International Exhibition and Conference for Printed Electronics, Messe München, Germany. http://www.lopec.com/en/conference

[159]. Soininen, P. (2013). Piloting Roll to Roll Atomic layer deposition technology. Functional Materials and Groove Solar Energy Seminar Retrieved February 2015

[160]. Stedman, M. (1987). Basis for comparing the performance of surface-measuring machines. Precision engineering, 9(3), 149-152.

[161]. Stefanaki, E.-C. (2008). Electron Microscopy: The Basics. Physics of Advanced Materials Winter School, 1-11.

[162]. Stevens, M., Tuomela, S., & Mayer, D. (2005). Water vapor permeation testing of ultra-barriers: Limitations of current methods and advancements resulting in increased sensitivity. Paper presented at the 48 th Annual Technical Conference Proceedings, Denver, Colorado USA.

[163]. Stout, K., Sullivan, P., Dong, W., Mainsah, E., & Luo, N. (1993). The development of methods for the characterization of roughness in three dimensions. Birmingham Commission of the European Communities.

[164]. Stout, K. J., & Blunt, L. (2000). Three dimensional surface topography: Elsevier.

[165]. Su-Huai, W., Zhang, S. B., & Zunger, A. (1998). Effects of Ga addition to $CuInSe_2$ on its electronic, structural, and defect properties. Applied Physics Letters, 72(24), 3199-3201. doi: 10.1063/1.121548

[166]. Su, Y., Kravets, V. G., Wong, S. L., Waters, J., Geim, A. K., & Nair, R. R. (2014). Impermeable barrier films and protective coatings based on reduced graphene oxide. Nature communications, 5, 1-10. doi: 10.1038/ncomms5843

[167]. Suloff, E. C. (2002). Sorption behavior of an aliphatic series of aldehydes in the presence of poly (ethylene terephthalate) blends containing aldehyde scavenging agents. (Doctoral dissertation), Virginia Polytechnic Institute and State University, United States.

[168]. Tamayo, J., & Garcia, R. (1996). Deformation, contact time, and phase contrast in tapping mode scanning force microscopy. Langmuir, 12(18), 4430-4435.

[169]. Tiwari, A. N., Brémaud, D., Rudmann, D., M. Kaelin, Hibberd, C., & Zogg, H. (2013). High efficiency flexible solar cells on polymer foils: World record at the ETHZ. Retrieved 6 June 2015, from http://apache.solarch.ch/pdf/17Tiwari.pdf

[170]. Troedel, M. L. (1999). Methods for Testing High Barrier Materials. Paper presented at the Polymers Laminations & Coatings Conference, Atlanta.

[171]. v. Wroblewski, S. (1879). Ueber die Natur der Absorption der Gase. Ann. Phys, 29-52. doi: 10.1002/andp.18792440903

[172]. VaÅ, K., Noller, K., Mikula, M., Amberg-Schwab, S., & Weber, U. (2009). Multilayer coatings for flexible high-barrier materials. Central European Journal of Physics, 7(2), 371-378.

[173]. Van Delft, J., Garcia-Alonso, D., & Kessels, W. (2012). Atomic layer deposition for photovoltaics: applications and prospects for solar cell manufacturing. Semiconductor Science and Technology, 27(7), 074002.

[174]. Wang, J., Jiang, X., Gurdak, E., Scott, P., Leach, R., Tomlins, P., & Blunt, L. (2011). Numerical characterisation of biomedical titanium surface texture using novel feature parameters. Wear, 271(7–8), 1059-1065.

[175]. Waterworth, A. (2006). Quantitative characterisation of surface finishes on stainless steel sheet using 3D surface topography analysis. (Doctoral dissertation), University of Huddersfield, Huddersfield, UK

[176]. Wegner, M. (2014). Greater Automation of Testing Will Help Flexible and Rigid Electronic Manufacturers Improve Product Quality and Decrease Costs. 2015, from http://smttoday.com/

[177]. Wennerberg, J., Kessler, J., & Stolt, L. (2003). Cu(In,Ga)Se_2-based thin-film photovoltaic modules optimized for long-term performance. Solar energy materials and Solar cells, 75(1–2), 47-55.

[178]. Yulia, G., & Ronn, A. (2012). Organic Photovoltaics: Technologies and Manufacturing. In V. Fthenakis (Ed.), Third Generation Photovoltaics (pp. 61–90): InTech.

[179]. Zhang, Y., Bertrand, J. A., Yang, R., George, S. M., & Lee, Y. (2009). Electroplating to visualize defects in Al2 O3 thin films grown using atomic layer deposition. Thin Solid Films, 517(11), 3269-3272.

[180]. Zhang, Y., Zhang, Y.-Z., Miller, D. C., Bertrand, J. A., Jen, S.-H., Yang, R., . . . Lee, Y. (2009). Fluorescent tags to visualize defects in Al_2O_3 thin films grown using atomic layer deposition. Thin Solid Films, 517(24), 6794-6797.

[181]. Zweibel, K. (1999). Issues in thin film PV manufacturing cost reduction. Solar energy materials and Solar cells, 59(1), 1-18.

APPENDICES

Appendix A (Publications)

A.1 Journals

1. **M. Elrawemi**, L. Blunt, L. Fleming, F. Sweeney, D. Robbins, and D. Bird. (2014). Metrology of Al_2O_3 Barrier Film for Flexible CIGS Solar Cells. **International Journal of Energy Optimization and Engineering (IJEOE)**, 4(4).pp.48-61.ISSN 2160-9500.

Metrology of Al_2O_3 Barrier Film for Flexible CIGS Solar Cells

Mohamed Elrawemi, Mechanical Engineering Department, Almergib University, Alkhoms, Lybia and Centre for Precision Technologies, University of Huddersfield, Huddersfield, UK

Liam Blunt, Centre for Precision Technologies, University of Huddersfield, Huddersfield, UK

Leigh Fleming, Centre for Precision Technologies, University of Huddersfield, Huddersfield, UK

Francis Sweeney, Centre for Precision Technologies, University of Huddersfield, Huddersfield, UK

David Robbins, Centre for Process Innovation Limited, Durham UK

David Bird, Centre for Process Innovation Limited, Durham UK

ABSTRACT

Flexible Cu (In, Ga) Se_2 (CIGS) solar cells are very attractive renewable energy sources because of their high conversion efficiencies, their low cost potential and their many application possibilities. However, they are at present highly susceptible to long term environmental degradation as a result of water vapor ingress through the protective encapsulation layer to the absorber (CIGS) layer. The basic methodology to prevent the water vapor permeation is to combine an oxide layer (e.g. AlO_x) coating with suitable polymer substrates. Nevertheless, micro and nano-scale defects can appear at any stage of the coating process thus affecting the module efficiency and lifespan. The main aim of this research paper is to use surface metrology techniques including: White Light Scanning Interferometry (WLSI), Atomic Force Microscopy (AFM) and Environmental Scanning Electron Microscopy (ESEM) to characterise the aluminum oxide (Al_2O_3) barrier film defects, which appear to be directly responsible for the water vapor permeability. This paper reports on the development of a characterisation method for defect detection based on "Wolf Pruning" method and then correlates this with measured water vapor transmission rates (WVTRs) using standard MOCON® test. The results presented in this paper provided a detailed knowledge of the nature of micro and nano-scale defects on the Al_2O_3 barrier films which are responsible for water vapor and oxygen ingress. This result can then be used to provide the basis for developing roll-to-roll in process metrology devices for quality control of flexible PV module manufacture.

Keywords: *ALD, Aluminum Oxide, Photovoltaic, Surface Defects, WVTR*

DOI: 10.4018/IJEOE.2015100104

2. **Elrawemi, Mohamed**, Blunt, Liam, Muhamedsalih, Hussam, Gao, F. and Fleming, Leigh (2015) Implementation of in Process Surface Metrology for R2R Flexible PV Barrier Films. **International Journal of Automation Technology**, 9 (3). pp. 312-321. ISSN 1883-8022.

Paper:

Implementation of in Process Surface Metrology for R2R Flexible PV Barrier Films

Mohamed Elrawemi*,, Liam Blunt**, Hussam Muhamedsalih**, Feng Gao**, and Leigh Fleming****

*Mechanical Engineering Department, Elmergib University
Alkhoms, P.O.BOX 40414, Libya
E-mail: elrawemi@yahoo.com
**Centre for Precision Technologies, University of Huddersfield
Huddersfield, HD1 3DH, UK
[Received January 10, 2015; accepted April 9, 2015]

Thin functional barrier layers of aluminum oxide (Al_2O_3) that are used particularly in photovoltaic (PV) modules to prevent the possibility of water vapor ingress should be applied over the entire PV surface without any defects. However, for barrier layer thicknesses within the sub-micrometer range (up to 50 nm) produced through the atomic layer deposition (ALD) method, it is common for defects to occur during the production process. To avoid defective barriers from being incorporated in the final PV unit, defects need to be detected during the barrier production process.
In this paper, the implementation of in process inspection system capable of detecting surface defects such as pinholes, scratches, or particles down to a lateral size of 3 μm and a vertical resolution of 10 nm over a 500 mm barrier width is presented. The system has a built-in environmental vibration compensation capability, and can monitor ALD-coated films manufactured using roll-to-roll (R2R) techniques. Ultimately, with the aid of this in process measurement system, it should be possible to monitor the coating surface process of large-area substrates, and if necessary, carry out remedial work on the process parameters.

Keywords: metrology, defects, photovoltaic, thin-film and aluminum oxide

1. Introduction

Transparent barrier films made from materials such as Al_2O_3 are being used to prevent water vapor permeation into flexible PV modules. However, the presence of small defects in the barrier surfaces has been shown to have the potential to facilitate water vapor ingress [1], thereby reducing the cell efficiency and durability [2]. Consequently, improvements to the quality of such barrier films are critical for reducing the susceptibility of PV systems to environmental degradation. This paper reports on the deployment of an innovative in-line optical metrology technology to aid in the identification of micro- and nano-scale defects without reducing the level of productivity.

The research conducted in this paper was based on an investigation into Al_2O_3 atomic layer deposition (ALD) sample substrates with defects present so as to create a comprehensive database that will aid in the development of the required defect sensors. Output from such an in-line system will provide a critical tool for process improvements.

2. Challenges in Defect Detection

The relationship between the surface morphology, defect density, and water vapor permeability through 40 nm Al_2O_3 barrier coatings produced using ALD [3] on 125-μm polyethylene naphthalate (PEN) substrates has to date only been studied in a laboratory [4, 5]. However, detecting defects off-line is difficult and time consuming. New methods for manufacturing barrier films using R2R methods are emerging, as shown in **Fig. 1**; however, such procedures can result in large quantities of barrier films being manufactured and integrated into a PV unit before any defects are detected and the process parameters optimized. Furthermore, the quality requirements and line speed in the PV manufacturing industry predicate the use of off-line defect detection methods. Therefore, it is desirable to make use of non-contact optical-based in-line inspection systems to detect defects during the Al_2O_3 ALD manufacturing processes. Nevertheless, implementing a high-resolution in-line (optical) measurement system in a R2R production environment is challenging because the positioning and stability requirements to be within the focal depth of the objective lens (e.g., less than 14 μm for a 5X objective lens) and less than the vertical resolution of the instrument (i.e., a few nanometers), respectively, are very demanding.

To facilitate in process measurement for R2R-produced substrates, two challenges need to be addressed: i) the measurement must be fast and non-contact, and ii) the measurement must be able to be carried out in a "noisy" working environment; one of the only feasible measurement solutions currently available is optical interferometry. However, interferometric measurement techniques

3. **Elrawemi, M.**, Blunt, L., Fleming, L., Bird, D., Robbins, D., & Sweeney, F. (2014). Modelling water vapour permeability through atomic layer deposition coated photovoltaic barrier defects. **Thin Solid Films**, **International Journal on the Science and Technology of Condensed Matter Films**. Part A (570), 101-106. ISSN 0040-6090.

Thin Solid Films 570 (2014) 101–106

Contents lists available at ScienceDirect

Thin Solid Films

journal homepage: www.elsevier.com/locate/tsf

Modelling water vapour permeability through atomic layer deposition coated photovoltaic barrier defects

Mohamed Elrawemi [a,*], Liam Blunt [a], Leigh Fleming [a], David Bird [b], David Robbins [b], Francis Sweeney [a]

[a] EPSRC Centre for Innovative Manufacturing in Advanced Metrology, School of Computing and Engineering, University of Huddersfield, Huddersfield, UK
[b] Centre for Process Innovation Limited, Sedgefield, County Durham, UK

ARTICLE INFO

Article history:
Received 11 March 2014
Received in revised form 26 August 2014
Accepted 29 August 2014
Available online 16 September 2014

Keywords:
Defects
Permeation
Surface topography
Thin films
Water vapour transmission rate

ABSTRACT

Transparent barrier films such as Al_2O_3 used for prevention of oxygen and/or water vapour permeation are the subject of increasing research interest when used for the encapsulation of flexible photovoltaic modules. However, the existence of micro-scale defects in the barrier surface topography has been shown to have the potential to facilitate water vapour ingress, thereby reducing cell efficiency and causing internal electrical shorts. Previous work has shown that small defects (≤3 μm lateral dimension) were less significant in determining water vapour ingress. In contrast, larger defects (≥3 μm lateral dimension) seem to be more detrimental to the barrier functionality. Experimental results based on surface topography segmentation analysis and a model presented in this paper will be used to test the hypothesis that the major contributing defects to water vapour transmission rate are small numbers of large defects. The model highlighted in this study has the potential to be used for gaining a better understanding of photovoltaic module efficiency and performance.

1. Introduction

In today's industry, the most common type of solar photovoltaic (PV) cell is fabricated from either rigid crystalline silicon or thin-film materials [1]. The rigid construction of Si solar cells hampers their economic integration into residential and commercial buildings; however, thin film solar cell technologies may prove to be most appropriate with respect to cost, ease of manufacture and installation. These thin film cells are based on the material $CuIn_{1-x}GaxSe_2$ (CIGS) as the absorber layer (p-type) and they at present have efficiency levels at or beyond that of Si based rigid solar modules [2]. The key weakness of these cells however is their moisture sensitivity. This is a critical problem if this technology is expected to meet the requirements of international standard IEC61646 [3] which requires that all PV modules survive 1000 h in an environment of 85 °C and 85% relative humidity (RH) [3]. At the present time, no cost effective, flexible transparent encapsulation can fulfil the requirements of the water vapour transmission rate (WVTR) for flexible PV modules [4]. The WVTR of current barriers is in the range of 10^{-1} g/m^2/day, while it should not be higher than 10^{-4} g/m^2/day to assure life-times of 20 years and more [4,5]. Therefore, a robust, transparent flexible encapsulation method for flexible PV modules is needed.

Thin layers of aluminium-oxide (Al_2O_3) of the order of a few tens of nanometres deposited via the atomic layer deposition (ALD) technique have been introduced to allow PV module transparency and flexibility and to provide an effective barrier layer. These barrier films ideally have WVTR of less than 10^{-4} g/m^2/day [6]. The term 'barrier' here refers to the ability of Al_2O_3 to resist the diffusion of water vapour into and through itself. Nevertheless, the barrier properties are often influenced by a wide range of variables, making conclusions regarding film properties sometimes difficult. It is known that barrier film permeability can be affected by the chemical and physical structures of the barrier, concentration of the permeant, temperature and humidity [7,8] as well as surface defects on the barrier coating that may be induced during the deposition processes [9,10]. Da Silva Sobrinho et al. [11] stated that the source of defect-driven permeation has been primarily attributed to pinhole defects [12,13] though more recent studies have shown that in the absence of pinhole defects permeation rates are still reduced by three orders of magnitude over the substrate material [14]. The remaining permeation is shown to be the result of defects in the sub-micromere to several micrometre range, produced by the surface microstructure [15] and/or low density of the films [14–16]. More detailed reviews of permeation mechanisms and the performance of various permeation barriers have been given elsewhere [12,17]. In this paper a theoretical model is presented to allow the prediction of the amount of water vapour permeation through PV barrier film defects. The results of the model are then

* Corresponding author at: EPSRC Centre for Innovative Manufacturing in Advanced Metrology, School of Computing and Engineering, University of Huddersfield, Huddersfield, HD1 3DH, UK.
E-mail addresses: Mohamed.elrawemi@hud.ac.uk, elrawemi@yahoo.com (M. Elrawemi), David.Bird@uk-cpi.com (D. Bird).

http://dx.doi.org/10.1016/j.tsf.2014.08.042

4. **Elrawemi, Mohamed**, Blunt, Liam, Fleming, Leigh and Sweeney, Francis (2013) Further Development of Surface Metrology Methods for Predicting the Functional Performance of Flexible PV Barrier Films. **Journal of Surface Topography: Metrology and Properties**, 1 (1). 015006. ISSN 2051-672X.

IOP Publishing Surface Topography: Metrology and Properties
Surf. Topogr.: Metrol. Prop. 1 (2013) 015006 (7pp) doi:10.1088/2051-672X/1/1/015006

Further development of surface metrology methods for predicting the functional performance of flexible photovoltaic barrier films

M Elrawemi, L Blunt, L Fleming and F Sweeney

University of Huddersfield, School of Computing and Engineering, Centre for Precision Technologies, Huddersfield, West Yorkshire HD1 3DH, UK

E-mail: Mohamed.Elrawemi@hud.ac.uk

Received 15 August 2013
Accepted for publication 19 November 2013
Published 5 December 2013
Online at stacks.iop.org/STMP/1/015006

Abstract

Surface topography analysis plays a very significant role in determining the functional performance for many engineering surfaces. In this paper, feature characterization techniques, based on the 'wolf pruning' method are implemented to characterize micro and nano-scale features which have a dominant effect on the functional lifespan of flexible photovoltaic (PV) modules. The densities and dimensions of the potential significant features are calculated by means of the feature 'characterization toolbox'. The outcome of this study has shown the potential of areal feature segmentation for detecting functionally significant defects present in atomic layer deposition barrier coatings of Al_2O_3 on polymer films. The analysis provides the basis for the development in process metrology for roll-to-roll production of barrier coatings as applied to flexible PV arrays and is a first step in the demonstration of in-process use of feature parameters.

1. Introduction

The effort of the photovoltaic (PV) industry to reduce production costs has led to highly efficient roll-to-roll production processes being adopted. Such flexible and lightweight solar cells are set to open up new markets in sectors like portable electronics, automotive/transportation and architecture. Flexible PV thin-film technologies can offer particular design options for building integrated applications and have the potential to meet building-integrated-PVs product requirements [1]. For conventional rigid thin-film solar modules, glass provides sufficient environmental protection for solar cells. Appropriate materials that can be used as front cover encapsulation in flexible solar modules are still under investigation. Flexible solar cells need to be protected from moisture and oxygen ingress to ensure sustained module performance; unfortunately common transparent plastic barriers do not provide sufficient barrier properties against the environment. However, modifying the plastic barrier with inorganic coatings can significantly improve its barrier properties while maintaining the high transmission of light through to the cells. To achieve this, a multi-layer composition of alternating polymer and very thin (a few nanometres) inorganic layers is required [1]. Studies of gas permeation through polymer films with an inorganic coating have concluded that permeation occurs through defects in the coating [2, 3]. Therefore, a process such as atomic layer deposition (ALD) which can produce a defect free conformal coating [4] could provide an excellent barrier to gas permeation. During the processing of such multilayer materials, defects within the inorganic coating such as aluminium oxide (Al_2O_3) have to be avoided. Characterization and ultimately minimization of these defects should lead to lower water vapour transmission rate (WVTR) and improved PV module efficiency and lifespan. This study seeks to use areal surface feature parameters to assess and functionally characterize defects in PV barrier films that potentially have a negative effect on the WVTR through the barrier coatings.

5. Blunt, Liam, **Elrawemi, Mohamed**, Fleming, Leigh and Sweeney, Francis (2013) Correlation of micro and nano–scale defects with WVTR for aluminium oxide barrier coatings for flexible photovoltaic modules. **International Journal of Precision Technology**, 3 (3). pp. 290-302. ISSN 1755-2060.

Correlation of micro and nano-scale defects with WVTR for aluminium oxide barrier coatings for flexible photovoltaic modules

L. Blunt*, M. Elrawemi, L. Fleming and F. Sweeney

Department of Mechanical Engineering,
Centre for Precision Technologies,
University of Huddersfield,
HD1 3DH, Huddersfield, UK
E-mail: l.a.blunt@hud.ac.uk
E-mail: Mohamed. Elrawemi@hud.ac.uk
E-mail: l.t.fleming@hud.ac.uk
E-mail: f.sweeney@hud.ac.uk
*Corresponding author

Abstract: This paper seeks to establish a correlation between surface topographical defects and Water Vapour Transmission Rate (WVTR) measured under laboratory conditions for aluminium-oxide (Al_2O_3) barrier film employed in flexible photovoltaic (PV) modules. Defects in the barrier layers of PV modules causing high WVTR are not well characterised and understood. A WVTR of ~10^{-1} g/m^2/day is sufficient for the most packaging applications, but ≤10^{-6} g/m^2/day is required for the encapsulation of long-life flexible PV modules (Carcia et al., 2010a, 2010b). In this study, Surface metrology techniques along with Scanning Electron Microscopy (SEM) were used for a quantitative characterisation of the barrier film defects. The investigation have provided clear evidence for the correlation of surface defect density and the transmission of water vapour through the barrier coating layer. The outcomes would appear to suggest that small numbers of large defects are the dominant factor in determining WVTR for these barrier layers.

Keywords: photovoltaics; micro; nano-defects; aluminium oxide; WVTR; water vapour transmission rate.

Reference to this paper should be made as follows: Blunt, L., Elrawemi, M., Fleming, L. and Sweeney, F. (2013) 'Correlation of micro and nano-scale defects with WVTR for aluminium oxide barrier coatings for flexible photovoltaic modules', *Int. J. Precision Technology*, Vol. 3, No. 3, pp.290–302.

Biographical notes: L. Blunt has an honours degree in Materials Technology and a PhD in "The Metallurgy of Centreless Ground Surfaces" at Coventry University. He has formed extensive industrial collaborations in particular with Taylor Hobson Ltd a world leading metrology company. He is now the Director of the Centre for Precision Technologies. His research specialises in the applications of surface metrology to new production processes.

M. Elrawemi is a PhD researcher student, University of Huddersfield, UK. He received the Master Degree in 2010 in the field of mechanical engineering design.

6. Blunt, Liam, Robbins, David, Fleming, Leigh and **Elrawemi, Mohamed** (2014) The Use of Feature Parameters to Asses Barrier Properties of ALD coatings for Flexible PV Substrates. **Journal of Physics: Conference Series**, 483. 012011. ISSN 1742-6596.

14th International Conference on Metrology and Properties of Engineering Surfaces IOP Publishing
Journal of Physics: Conference Series **483** (2014) 012011 doi:10.1088/1742-6596/483/1/012011

The Use of Feature Parameters to Asses Barrier Properties of ALD coatings for Flexible PV Substrates

Liam Blunt[1], David Robbins[2], Leigh Fleming[1] and Mohamed Elrawemi[1]

[1]University of Huddersfield, West Yorkshire. Huddersfield, HD1 3DH, UK.
[2]Centre for Process Innovation Limited, County Durham. Sedgefield, TS21 3FG, UK.

E-mail: l.a.blunt@hud.ac.uk

Abstract. This paper reports on the recent work carried out as part of the EU funded NanoMend project. The project seeks to develop integrated process inspection, cleaning, repair and control systems for nano-scale thin films on large area substrates.

In the present study flexible photovoltaic films have been the substrate of interest. Flexible PV films are the subject of significant development at present and the latest films have efficiencies at or beyond the level of Si based rigid PV modules. These flexible devices are fabricated on polymer film by the repeated deposition, and patterning, of thin layer materials using roll-to-roll processes, where the whole film is approximately 3um thick prior to encapsulation. Whilst flexible films offer significant advantages in terms of mass and the possibility of building integration (BIPV) they are at present susceptible to long term environmental degradation as a result of water vapor transmission through the barrier layers to the CIGS (Copper Indium Gallium Selenide $CuIn_xGa_{(1-x)}Se_2$) PV cells thus causing electrical shorts and efficiency drops. Environmental protection of the GIGS cell is provided by a thin (40nm) barrier coating of Al_2O_3. The highly conformal aluminium oxide barrier layer is produced by atomic layer deposition (ALD) where, the ultra-thin Al_2O_3 layer is deposited onto polymer thin films before these films encapsulate the PV cell. The surface of the starting polymer film must be of very high quality in order to avoid creating defects in the device layers. Since these defects reduce manufacturing yield, in order to prevent them, a further thin polymer coating (planarization layer) is generally applied to the polymer film prior to deposition.

The presence of surface irregularities on the uncoated film can create defects within the nanometre-scale, aluminium oxide, barrier layer and these are measured and characterised. This paper begins by reporting the results of early stage measurements conducted to characterise the uncoated and coated polymer film surface topography using feature parameter analysis. The measurements are carried out using a Taylor Hobson Coherence Correlation Interferometer an optical microscope and SEM. Feature parameter analysis allows the efficient separation of small insignificant defects from large defects. The presence of both large and insignificant defects is then correlated with the water vapour transmission rate as measured on representative sets of films using at standard MOCON test. The paper finishes by drawing conclusions based on analysis of WVTR and defect size, where it is postulated that small numbers of large defects play a significant role in higher levels of WVTR.

Ethan Publishing Company, www.ethanpublishing.com
1902 Merced Ave, South El Monte, CA 91733, USA
info@ethanpublishing.com

Certification

Dec. 18th, 2014

To whom it may concern,

These are International Journal of Mechanical Engineering and Automation, which are international, scholarly and peer-reviewed journals published monthly by Ethan Publishing Company, which was founded in 2013. The Journal serves as a bridge between worldwide scholars and public researchers. The Journal publishes research articles, reviews, and letters in all areas related to mechanical engineering and automation.

All manuscripts submitted to International Journal of Mechanical Engineering and Automation are usually reviewed by at least one member of the Editorial Board Members and is refereed by at least 2 outside experts in the field. This commits our editors and reviewers to up to 12 assessments each year. The Editors thank them for so generously giving their time and advice.

Ph.D. Mohamed Elrawemi was accepted as one of the Reviewers of International Journal of Mechanical Engineering and Automation by Dec. 17, 2014. The Editors and the Editorial Executive Committee gratefully acknowledge the considerable time and help he will give and his advice and for his promptness in dealing with the manuscripts in the future.

Best regards,

Amanda

International Journal of Mechanical Engineering and Automation

Ethan Publishing Company

David Publishing Company, 240 Nagle Avenue #15C, New York, NY 10034, USA
Tel: 1-323-984-7526; Fax: 1-323-984-7374, http://www.davidpublishing.com, order@davidpublishing.com

Certification

December 30, 2014

To whom it may concern,

This is Journal of Aerospace Science and Technology, which is an international, scholarly and peer-reviewed journal (print and online) published by David Publishing Company, which was founded in 2001. The Journal serves as a bridge between worldwide scholars and public researchers. The Journal publishes research articles, reviews, and letters in all areas related to aerospace science or technology.

All manuscripts submitted to Journal of Aerospace Science and Technology are usually reviewed by at least one member of the editorial board members and is refereed by at least 2 outside experts in the field. This commits our editors and reviewers to up to 12 assessments each year. The Editor thanks them for so generously giving their time and advice.

Mohamed Elrawemi is one of the reviewers of Journal of Aerospace Science and Technology. The Editor and the Editorial Executive Committee gratefully acknowledge the considerable time and help he gave during 2015-2016. The Editor thanks him very much for his advice and for his promptness in dealing with the manuscripts.

Best regards,

Veinace

Journal of Aerospace Science and Technology

ISSN 2332-8258

David Publishing Company

A.2 Conferences (International)

1. **Elrawemi, Mohamed**, Blunt, Liam and Greaves, Graeme (2015) Nano scale Characterisation of Photovoltaic Ultra Barrier Films. In: **2nd International Conference on Nanotechnology, Nanomaterials & Thin Films for Energy Applications**, 1st-3rd June 2015, Manchester, UK.

2. Gao, F., Muhamedsalih, Hussam, Tang, Dawei, **Elrawemi, Mohamed**, Blunt, Liam, Jiang, Xiang, Edge, Steven, Bird, David and Hollis, Philip (2015) In-situ defect detection systems for R2R flexible PV barrier films. In: **ASPE 2015 Summer Topical Meeting. American Society for Precision Engineering**, Colorado, USA, pp. 44-49. ISBN 978-1-887706-68-1

3. Blunt, Liam, Muhamedsalih, Hussam and **Elrawemi, Mohamed** (2015) Implementation of wavelength scanning interferometry for R2R flexible PV barrier films. **15th International Conference of the European Society for Precision Engineering and Nanotechnology.** EUSPEN, Leuven, Belgium, pp 199-200. ISBN 14: 978-0-9566790-7-9.

4. Gao, Feng, Muhamedsalih, Hussam, Tang, Dawei, **Elrawemi, Mohamed**, Blunt, Liam, Jiang, Xiang, Edge, Steven, Bird, David and Hollis, Philip (2015) In-situ defect detection systems for R2R flexible PV barrier films. In: **5th International Conference on Optical Instrument and *Technology (OIT'2015)***, 17th-19th May, Beijing, China.

5. Muhamedsalih, Hussam, Blunt, Liam, Martin, Haydn, Hamersma, Ivo, **Elrawemi, Mohamed** and Feng, Gao (2015) An integrated opto-mechanical measurement system for in-process defect measurement on a roll-to-roll process. In: **11th International Conference and Exhibition on Laser Metrology, Coordinate Measuring Machine and Machine Tool Performance, (LAMDAMAP)**. EUSPEN, Huddersfield, UK, pp. 99-107. ISBN 978-0-9566790-5-5.

6. Muhamedsalih, Hussam, **Elrawemi, Mohamed**, Blunt, Liam, Xiangqi, Lan and Martin, Haydn (2015) A computerised data handling procedure for defect detection and analysis for large area substrates manufactured by roll-to-roll process. In: **11th International Conference and Exhibition on Laser Metrology, Coordinate Measuring Machine and**

Machine Tool Performance, (LAMDAMAP). EUSPEN, Huddersfield, UK, pp. 84-91. ISBN 978-0-9566790-5-5.

7. Gao, Feng, Muhamedsalih, Hussam, **Elrawemi, Mohamed**, Blunt, Liam, Jiang, Xiang, Edge, Steven, Bird, David and Hollis, Philip (2014) A flexible PV barrier films defects detection system for in-situ R2R film processing. In: **Special Interest Group Meeting: Structured Freeform Surfaces 2014**, 19-20 Nov 2014, Padova, Italy.

8. **Elrawemi, Mohamed**, Muhamedsalih, Hussam, Blunt, Liam, Fleming, Leigh, Martin, Haydn and Jiang, Xiang (2014) Comparative study between online and offline defect assessment methods for roll to roll flexible PV modules. **4th International Conference on Nonomanufacturing (nanoMan2014)**, 8th -10th July, Bremen, Germany.

9. **Elrawemi, Mohamed**, Blunt, Liam, Fleming, Leigh, Sweeney, Francis and Robbins, David (2014) Defect Detection in Thin-film Photovoltaics; Towards Improved Efficiency and Longevity. **5th International Renewable Energy Congress**. IREC 2014. IEEE, Hammamet, Tunisia, pp. 524-528. ISBN 978-1-4799-2196-6.

10. **Elrawemi, Mohamed**, Blunt, Liam and Fleming, Leigh (2014) Metrology and Characterisation of Defects on Barrier Layers for Thin Film Flexible Photovoltaics. **14th International Conference of the European Society for Precision Engineering and Nanotechnology**. EUSPEN, Dubrovnik, Croatia, pp. 165-168. ISBN: 978-0-9566790-3-1.

11. Blunt, Liam, **Elrawemi, Mohamed**, Fleming, Leigh, Martin, Haydn, Muhamedsalih, Hussam and Robbins, David (2013) Development of the basis for in process metrology for roll to roll production of flexible photovoltaics. **11th International Symposium on Measurement and Quality Control**. 2013, September 11-13, Cracow-Kielce, Poland, pp.263-266. ISBN: 978-1-63266-817-2.

12. Blunt, Liam, Fleming, Leigh, **Elrawemi, Mohamed**, Robbins, David and Muhamedsalih, Hussam (2013) In-line metrology of functional surfaces with a focus on defect assessment on large area Roll to Roll substrates. **13th International Conference of the European Society for Precision Engineering and Nanotechnology**. EUSPEN, Germany, Berlin, pp. 71-74. ISBN 13:978-0-9566790-2-4.

13. Fleming, Leigh, Blunt, Liam, Robbins, David and **Elrawemi, Mohamed** (2013) Characterisation techniques to assess functional properties of barrier coatings for flexible PV substrates. **10th International Conference and Exhibition on Laser Metrology, Machine Tool, CMM & Robotic Performance**. LAMDAMAP 2013. EUSPEN, Buckinghamshire, UK, pp. 59-69. ISBN: 978-0-9566790-1-7.

14. Blunt, Liam, **Elrawemi, Mohamed**, Fleming, Leigh, Robbins, David and Muhamedsalih, Hussam (2014) In-line metrology for defect assessment on large area Roll 2 Roll substrates. **11th Laser Metrology for Precision Measurement and Inspection in Industry (LMPMI),** 2nd-5th September 2014, Epochal Tsukuba, Japan. pp. 9-12. ISBN: 9781632667311

15. Muhamedsalih, Hussam, Blunt, Liam, Martin, Haydn, Jiang, Xiang and **Elrawemi, Mohamed** (2014). An interferometric auto-focusing method for on-line defect assessment on a roll-to-roll process using wavelength scanning interferometry. **14th International Conference of the European Society for Precision Engineering and Nanotechnology.** EUSPEN, Dubrovnik, Croatia, pp. 177-180. ISBN: 978-0-9566790-3-1

A.3 Conferences (National)

1. **Elrawemi, Mohamed**, Blunt, Liam, Fleming, Leigh, Muhamedsalih, Hussam and Gao, F. (2014) Wavelength Scanning Interferometry for PV Production In-line Metrology. **3rd Annual EPSRC Manufacturing the Future Conference**, 23rd –24th September 2014, Glasgow Science Centre, Glasgow, UK.

2. **Elrawemi, Mohamed**, Blunt, Liam, Muhamedsalih, Hussam, Fleming, Leigh and Gao, Feng (2014) Verification of an in Process Optical System based on High Resolution Interferometry for Detecting Flexible PV Barrier Films Defects. **Photon14**, 1st-4th September 2014, Imperial College, London, UK.

3. **Elrawemi, Mohamed**, Blunt, Liam and Fleming, Leigh (2013) Process Practice and its Effects on Surface Defects on Flexible PV Barrier Films. **Proceedings of Computing and Engineering Annual Researchers' Conference 2013**: CEARC'13. University of Huddersfield, Huddersfield, pp. 49-54. ISBN 9781862181212.

4. Blunt, Liam, **Elrawemi, Mohamed**, Fleming, Leigh, Martin, Haydn, Muhamedsalih, Hussam and Robbins, David (2013) Metrology for in process metrology for roll to roll production of flexible photovoltaics. **Metrology Technologies to Enable Reel to Reel Processing of Emerging Products**, November 20, 2013, National Physical Laboratory , Teddington, Middlesex, UK.

5. **Elrawemi, Mohamed**, Blunt, Liam and Fleming, Leigh (2013) Metrology and Characterisation of Micro and Nano-scale Defects for Aluminium Oxide Barrier Film Employed in Flexible Photovoltaic Modules. **2nd Annual Manufacturing the Future Conference**. September 2013. UKMTFC 2013. EPSRC, Cranfield, UK. ISBN 978-1-907413-22-3.

6. Blunt, Liam, Robbins, David, Leach, Richard, Fleming, Leigh and **Elrawemi, Mohamed** (2012) Surface defects in water vapour barrier layers for structured plastic electronics. **Structured & Freeform Surfaces**, 5th-6th December 2012, National Physical Laboratory, Teddington, UK.

A.4 Conferences (Posters)

1. **Elrawemi, Mohamed**, Blunt, Liam, Fleming, Leigh and Muhamedsalih, Hussam (2014) Wavelength Scanning Interferometery for large area roll to roll metrology applications in photovoltaic manufacturing environment. In: **10th LVMC Large Volume Metrology Conference and Exhibition**, 18th -20th November, the Mercure Manchester Piccadilly.

2. Blunt, Liam and **Elrawemi, Mohamed** (2015) Functional Modelling of Water Vapour Transmission through Surface Defects Using Surface Segmentation Analysis. In: **15th International Conference on Metrology and Properties of Engineering Surfaces**, 2nd-5th March 2015, University of North Carolina at Charlotte, Charlotte, North Carolina, USA.

A.5 Supplementary Publications

Nanotechnology Now

Your Gateway to Everything Nanotech

Nanometer resolution

See details beyond the physical limits of optics

About Us | Nanotechnology | News | Columns | Products | Directories | Career Center | Nano-Social Network | Nano Consulting

Home > Press > Detecting defects at the nanoscale will profit solar panel production: Researcher Mohamed Elrawemi develops new technologies for defects in thin films, vital in products as printed electronics and solar panels

The NanoMend researchers at the University of Huddersfield have been working with the Durham-based Centre for Process Innovation, a leading producer of printable electronics, including flexible solar panels. In these products, a thin "barrier film" is vital to protect the electronics. But tiny defects can allow the penetration of water vapor that can degrade the barrier and reduce the efficiency of the solar panel itself.

CREDIT: University of Huddersfield

FreeWatt Solar PV

freewatt.co.uk

Experts in large scale rooftop & ground solar PV systems

Free Solar Panels

SMA Solar Technology

Solar Energy Installers

باحث ليبي يتفوق في بريطانيا

قام الباحث الليبي «محمد صلاح الرويمي» بجامعة «هدرسفيلد البريطانية» (University of Huddersfield) بتطوير تكنولوجيا جديدة لكشف العيوب في الأغشية الرقيقة للمنتجات الإلكترونية والألواح والخلايا الشمسية.

الباحث الليبي "محمد صلاح الرويمي" جامعة "هدرسفيلد البريطانية" (University of Huddersfield) من مدينة مسلاته الليبية يقوم بتطوير تكنولوجيا جديدة لكشف العيوب في الأغشية الرقيقة للمنتجات الإلكترونية والألواح والخلايا الشمسية.

وطني

Free Newsletters - Space News - Defense Alert - Environment Report - Energy Monitor

NUCLEAR POWER | ENERGY DAILY | BIO FUEL DAILY | WIND DAILY | TERRADAILY | ROBO DAILY | GPS DAILY | SPACE DAILY | ROBO DAILY

SOLAR DAILY

one cell at a time

SOLAR DAILY

Detecting defects at the nanoscale will profit solar panel production

by Staff Writers
Huddersfield, UK (SPX) Feb 28, 2019

Research at the University of Huddersfield will lead to major efficiency gains and cost savings in the manufacture of flexible solar panels. It has also resulted in an exceptional number of scholarly articles co-authored by a Libyan scientist who is completing his doctoral studies as a participant in the EU-backed project.

It is named NanoMend and is funded by the EU's Framework Seven research programme. The goal is to develop new technologies for the detection, cleaning and repair of micro and nanoscale defects in thin films that are vital in products such as printed electronics and solar panels.

The University of Huddersfield's EPSRC Centre for Innovative Manufacturing in Advanced Metrology is a key collaborator in NanoMend. Its scientists recently earned an award for the development of a Wavelength Scanning Interferometer, which has uses that include the detection of defects in the coating that can have a serious impact on the longevity of roll-to-roll vapour barrier coatings for

The NanoMend researchers at the University of Huddersfield have been working with the Durham-based Centre for Process Innovation, a leading producer of printable electronics, including flexible solar panels. In these products, a thin "barrier film" is vital to protect the electronics. But tiny defects can allow the penetration of water vapor that can degrade the barrier and reduce the efficiency of the solar panel itself. Image courtesy University of Huddersfield. For a larger version of this image please go here.

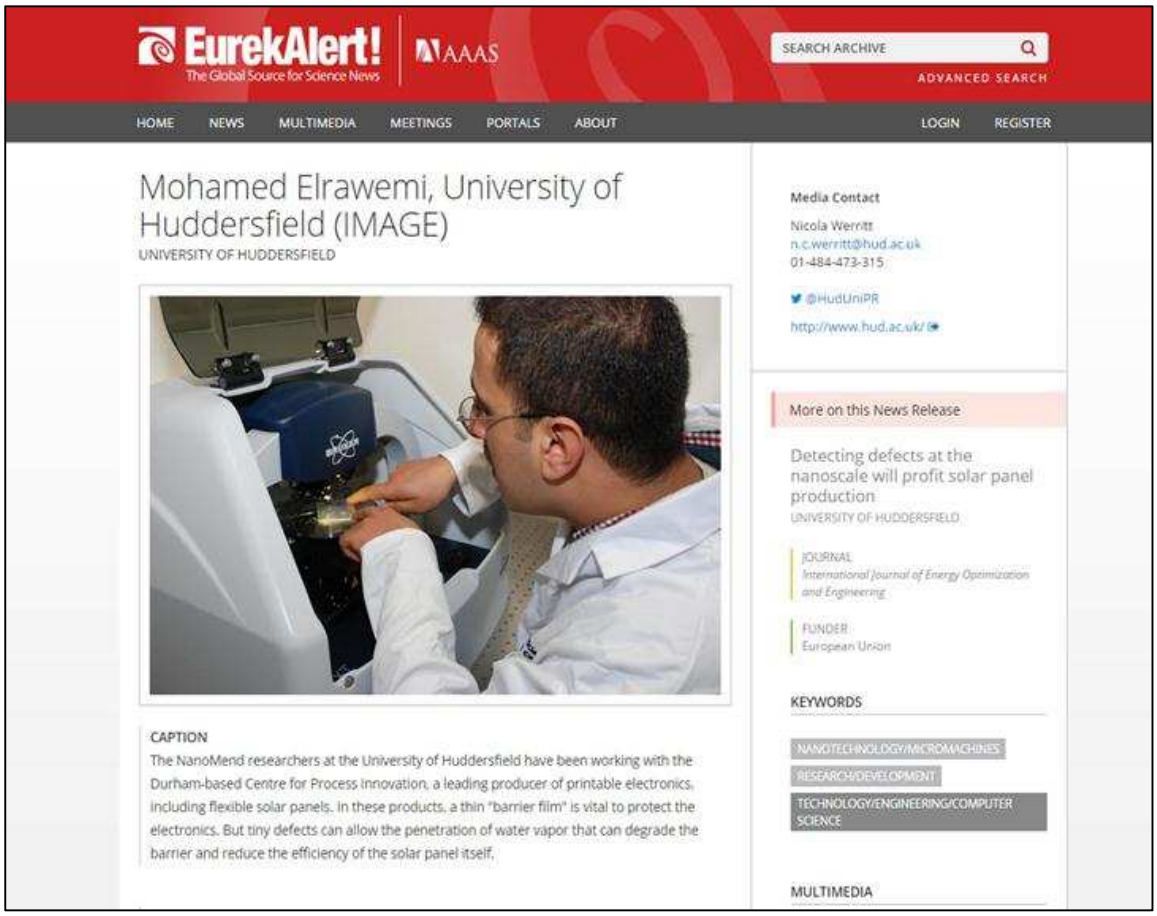

A bright future

Huddersfield leads the way in renewable energy research

Research at the University of Huddersfield has never been 'brighter' as scientists take the lead on innovative designs for new flexible solar panels.

The project, named NanoMend, is funded by the EU's Framework Seven research programme, and aims to improve the efficiency of the energy sources, while also cutting costs in manufacturing to create greater availability of the panels.

Its eventual goal is to develop new technologies for the detection, cleaning and repair of micro and nanoscale defects in thin films that are vital in products such as printed electronics and solar panels.

Libyan scientist, Mohamed Elsherbini, who is currently completing his doctoral studies at the university is one of the leads on the initiative.

Supported by funding from the Libyan Government's Higher Education Ministry, he is in the later stages of a PhD and has contributed to 25 papers dealing with aspects of the NanoMend research.

The latest, entitled 'Metrology of Al:ZO1 Barrier Film for Flexible CIGS Solar Cells', is due to appear in the new edition of the International Journal of Energy Optimization and Engineering.

Mohamed is the lead author for this article, and it takes its place in a sequence of papers that began in 2012 with a contribution to the International Journal of Energy Optimization and Engineering.

Other outlets have included the International Journal of Precision Technology, Surface Topography Metrology and Properties and Thin Solid Films, in which one article by the Huddersfield-based researcher rapidly gained a large number of downloads globally.

There have also been contributions to the published proceedings of several international conferences.

The NanoMend researchers at the University of Huddersfield have been working with Durham-based Centre for Process Innovation, a leading producer of printable electronics including flexible solar panels.

In these products, a thin 'barrier film' is vital to protect the electronics. But tiny defects can allow the penetration of water vapour that can degrade the barrier and reduce the efficiency of the solar panel itself.

The team based at the Huddersfield EPSRC Centre have been working on a new metrology system that can detect tiny defects and will therefore aid the manufacture of roll-to-roll barrier film in large volumes.

Featured Research *from universities, journals, and other organizations*

Detecting defects at the nanoscale will profit solar panel production

Date: February 24, 2015

Source: University of Huddersfield

Summary: New research may lead to major efficiency gains and cost savings in the manufacture of flexible solar panels. The goal is to develop new technologies for the detection, cleaning and repair of micro and nanoscale defects in thin films that are vital in products such as printed electronics and solar panels.

Share This

- Email to a friend
- Facebook
- Twitter
- LinkedIn
- Google+
- Print this page

Related Topics

Matter & Energy
- Solar Energy
- Electronics
- Wearable Technology

Earth & Climate
- Energy and the Environment
- Renewable Energy
- Environmental Science

The NanoMend researchers at the University of Huddersfield have been working with the Durham-based Centre for Process Innovation, a leading producer of printable electronics, including flexible solar panels. In these products, a thin "barrier film" is vital to protect the electronics. But tiny defects can allow the penetration of water vapor that can degrade the barrier and reduce the efficiency of the solar panel itself.

Appendix B

B.1 Areal Field Parameters

Four parameters are used for characterising the amplitude property of surfaces. They are classified into four categories, i.e. (i) dispersion, (ii) extreme, (iii) asymmetry of the height distribution and (iv) sharpness of the height distribution.

1.1 Root-Mean-Square Deviation of the Surface Sq

This is a dispersion parameter defined as the root mean square value of the surface departures within the sampling area.

$$S_q = \sqrt{\frac{1}{MN}\sum_{j=1}^{N}\sum_{i=1}^{M}\eta^2(x_i, y_j)} \qquad (1)$$

Where, M is a number of points of per profile, N is the number of profile. Sq is a very general and widely used parameter. In statistics, it is the sample standard deviation.

1.2 Skewness of Topography Height Distribution Ssk

This is the measure of asymmetry of surface deviations about the mean plane.

$$S_{sk} = \frac{1}{MNS_q^3}\sum_{j=1}^{N}\sum_{i=1}^{M}\eta^3(x_{i,}y_j) \qquad (2)$$

This parameter can effectively be used to describe the shape of the topography height distribution. For a Gaussian surface which has a symmetrical shape for the surface height distribution, the skewness is zero. For an asymmetric distribution of surface heights, the skewness may be negative if the distribution has a longer tail at the lower side of the mean plane or positive if the distribution has a longer tail at the upper side of the mean plane. This parameter can give some indication of the existence of "spiky" features.

1.3. Kurtosis of Topography Height Distribution Sku

This is a measure of the peakedness or sharpness of the surface height distribution.

$$S_{ku} = \frac{1}{MNS_q^4}\sum_{j=1}^{N}\sum_{i=1}^{M}\eta^4(x_{i,}y_j) \qquad (3)$$

This parameter characterises the spread of the height distribution. A Gaussian surface has a kurtosis value of 3. A centrally distributed surface has a kurtosis value larger than 3 whereas

the kurtosis of a well spread distribution is smaller than 3. By a combination of the skewness and the kurtosis, it may be possible to identify surfaces which have a relatively flat top and deep valleys.

1.4. The highest peak of the surface Sp

This is an extreme parameter defined as the height of the highest peak from the mean surface within the sampling area.

$$S_p = \mathrm{MAX}(\eta_p) \qquad \text{with} \quad \eta_p > 0 \qquad (4)$$

Where, η_p are the highest surface summits on the surface, which rely on eight nearest neighbour summits.

1.5. The lowest valley of the surface Sv

This is an extreme parameter defined as the height of the lowest valley from the mean surface within the sampling area.

$$S_v = \mathrm{MIN}(\eta_v) \qquad \text{with} \quad \eta_v < 0 \qquad (5)$$

Where, η_v are the lowest surface valleys on the surface, which rely on eight nearest neighbour summits.

1.6. Height deviation between the lowest and highest points of the surface Sz

This is an extreme parameter defined as the maximum of the absolute heights of the highest peaks and the depths of the deepest pits or valleys within the sampling area.

$$S_z = (|S_p| + |S_v|) \qquad (6)$$

Where S_p and S_v are the highest surface summits and lowest surface valleys on the surface respectively, which rely on eight nearest neighbour summits.

1.7.Arithmetical average of the surface Sa

This is the average value of the absolute heights over the entire surface. It may be obtained by adding individual height values without regard to sign and dividing the sum by the number of the data matrix.

$$S_a = \frac{1}{MN} \sum_{j=1}^{N} \sum_{i=1}^{M} \left| \eta(x_i, y_j) \right| \qquad (7)$$

Where, M is a number of points of per profile, N is the number of profile. Sa is a very general and widely used parameter.

1.8. Texture Aspect Ratio of the Surface Str

This is a parameter used to identify texture strength i.e. uniformity of texture aspect. It is defined by Areal autocorrelation function (AACF). Str can be defined as its ratio of the fastest to slowal decay to correlation length, 0.2, of the AACF function.

$$S_{tr} = \frac{\min\left(\sqrt{\tau_x^2 + \tau_y^2}\right)}{\max\left(\sqrt{\tau_x^2 + \tau_y^2}\right)} \Bigg|_{\tilde{R}(\tau_x, \tau_y) \le 0.2}, \quad 0 \prec S_{tr} \le 1 \qquad (8)$$

Where

$$R(\tau_x, \tau_y) = \frac{1}{(M-1)(N-1)} \sum\sum \eta(x_k, y_l)\eta(x_{k+i}, y_{l+j})$$

$$i = 0, 1, ..., m \prec M, \quad j = 0, 1, ..., n \prec N, \quad \tau_i = i \cdot \Delta x, \quad \tau_j = j \cdot \Delta y$$

In principle, the texture aspect ratio has a value between 0 and 1. Larger values, say STR> 0.5, of the ratio indicates uniform texture in all directions i.e. no defined lay, Smaller values, say STR< 0.3, indicates an unceasingly strong directional structure or lay. Since the size of the sampling area is finite, it is possible that the slowest decay of the AACFs of some anisotropic surfaces never reaches 0.2 within the sampling area. In this case the longest distance of the AACF along the slowest decay direction can be used instead.

1.9. The Fastest Decay Autocorrelation Length Sal

This is a parameter in length dimension used to describe the autocorrelation character of the AACF. It is defined as the horizontal distance of the AACF which has the fastest decay to 0.2. In other words the Sal is the shortest autocorrelation length that the AACF decays to 0.2 in any possible direction.

$$S_{al} = \min\left(\sqrt{\tau_x^2 + \tau_y^2}\right), \qquad \tilde{R}(\tau_x, \tau_y) \le 0.2 \qquad (9)$$

For an anisotropic surface Sal is in a direction perpendicular to the surface lay. A large value of Sal denotes that the surface is dominated by low frequency (or long wavelength) components. While a small value of the Sal denotes the opposite situation.

1.10. Texture Direction of the Surface Std

This is the parameter used to determine the most pronounced direction of the surface texture with respect to the y axes within the frequency domain, i.e. it gives the lay direction of the surface. A unified definition of the texture direction of a surface is given an angle. By this definition, when the measurement trace direction is perpendicular to the lay (this is a very common case) the texture direction is 0^0.

$$S_{td} = \begin{cases} -\beta, & \beta \le \frac{\pi}{2} \\ \pi - \beta, & \frac{\pi}{2} \prec \beta \le \pi \end{cases} \qquad (10)$$

Where, β is the position where the maximum value of the angular spectrum.

$$\beta = \mathrm{tg}^{-1} \frac{\mathrm{Re}[F(f_p, f_q)]}{\mathrm{Im}[F(f_p, f_q)]} \Bigg|_{\max\left(\sqrt{\mathrm{Re}[F(f_p, f_q)]^2 + \mathrm{Im}[F(f_p, f_q)]^2}\right)} ,$$

$$F(f_p, f_q) = \Delta x \cdot \Delta y \sum_{l=0}^{N-1} \sum_{k=0}^{M-1} \eta(x_k, y_l) e^{-j2\pi[(p/M)k + (q/N)l]} ,$$

$$p = 0, 1, ..., M-1; \quad q = 0, 1, ..., N-1; \quad f_p = \frac{p}{\Delta x \cdot M}; \quad f_q = \frac{q}{\Delta y \cdot N}$$

1.11. Root-Mean-Square Slope of the Surface Sdq

This is the root-mean-square value of the surface slope within the sampling area.

$$S_{dq} = \sqrt{\frac{1}{(M-1)(N-1)} \sum_{j=2}^{N} \sum_{i=2}^{M} \rho_{i,j}^2} \qquad (11)$$

Where

$$\rho_{i,j} = \left[\left(\frac{\partial \eta(x, y)}{\partial x} \right)^2 + \left(\frac{\partial \eta(x, y)}{\partial y} \right)^2 \right]^{1/2} \Bigg|_{x = x_i, y = y_j}$$

$$\approx \left[\left(\frac{\eta(x_i, y_j) - \eta(x_{i-1,} y_j)}{\Delta x} \right)^2 + \left(\frac{\eta(x_i, y_j) - \eta(x_{i,} y_{j-1})}{\Delta x} \right)^2 \right]^{1/2}$$

1.12. Developed Interfacial Area Ratio Sdr

This is the ratio of the increment of the interfacial area of a surface over the sampling area.

$$S_{dr} = \frac{\sum_{j=1}^{N-1}\sum_{i=1}^{M-1} A_{i,j} - (M-1)(N-1)\Delta x \cdot \Delta y}{(M-1)(N-1)\Delta x \cdot \Delta y} \cdot 100\% \qquad (12)$$

Where the interfacial area of the quadrilateral is

$$A_{i,j} = \frac{1}{4}\left\{ \left(\left[\Delta y^2 + \left(\eta(x_i, y_j) - \eta(x_i, y_{j+1})\right)^2\right]^{1/2} + \left[\Delta y^2 + \left(\eta(x_{i+1}, y_{j+1}) - \eta(x_{i+1}, y_j)\right)^2\right]^{1/2}\right) \cdot \left(\left[\Delta x^2 + \left(\eta(x_i, y_j) - \eta(x_{i+1}, y_j)\right)^2\right]^{1/2} + \left[\Delta y^2 + \left(\eta(x_i, y_{j+1}) - \eta(x_{i+1}, y_{j+1})\right)^2\right]^{1/2}\right) \right\}$$

The developed interfacial area ratio reflects the hybrid property of surfaces. A large value of the parameter indicates the significance of either the amplitude or the spacing or both.

B.2 Areal Feature Parameters

2.1. Density of Summits (peaks) of the Surface (Sds or Spd)

This is the number of summits of a unit sampling area, which relies on the eight nearest neighbour summit definition. I.e. a peak is defined of it is higher than its 8 nearest neighbours.

$$S_{ds} = \frac{\text{Number of summits}}{(M-1)(N-1) \cdot \Delta x \cdot \Delta y} \qquad (1)$$

2.2 Arithmetic Mean Summit Curvature of the Surface (Ssc or Spc)

Arithmetic mean of the principal curvatures of summits (peaks) within a definition area

Spc= FC; P; Wolfprune: X%; All; Curvature; Mean (2)

2.3 Ten Point Height of the Surface S5z

This is an extreme parameter defined as the average value of the absolute heights of the five highest peaks and the depths of the five deepest pits or valleys within the sampling area.

$$S_{5z} = \frac{\sum_{i=1}^{5}\left|\eta_{pi}\right| + \sum_{i=1}^{5}\left|\eta_{vi}\right|}{5} \quad , \quad i = 1, 2, \ldots 5 \qquad (3)$$

Where η_{pi} and η_{vi} are the five highest surface summits and lowest surface valleys respectively, which rely on eight nearest neighbour summits.

2.4. Five-point peak height (S5p)

Average value of the heights of the five peaks with largest global peak height, within the definition area.

S5p= FC; H; Wolfprune: X%; Top: 5; Lpvh; Mean (4)

2.5. Five-point pit height (S5v)

Average value of the heights of the five pits with largest global pit height, within the definition area.

S5p= FC; H; Wolfprune: X%; Bot: 5; Lpvh; Mean (5)

2.6. Closed void area (mean dale area) (Sva or Sda)

S_{da}= FC; D; Wolfprune: X%; Open: AreaE; Mean (6)

2.7. Closed peak area (mean hill area) (Sha or Spa)

S_{ha}= FC; D; Wolfprune: X%; Open/closed: AreaE; Mean (7)

2.8. Closed void volume (mean dale volume) (Svv or Sdv)

S_{dv}= FC; D; Wolfprune: X; Open: VolE; Mean (8)

2.9. Closed peak volume (mean hill volume) (Spv or Shv)

S_{dv}= FC; D; Wolfprune: X; Open: VolE; Mean (9)

Appendix C (types of defects)

C.1 Particles type defect

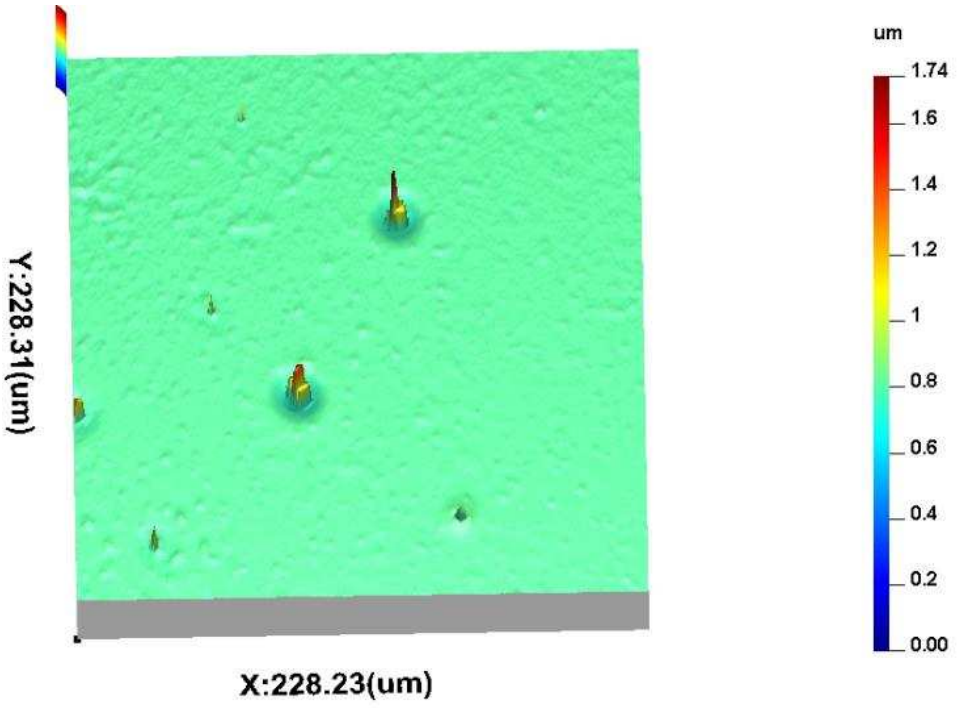

C.2 Pinhole type defects

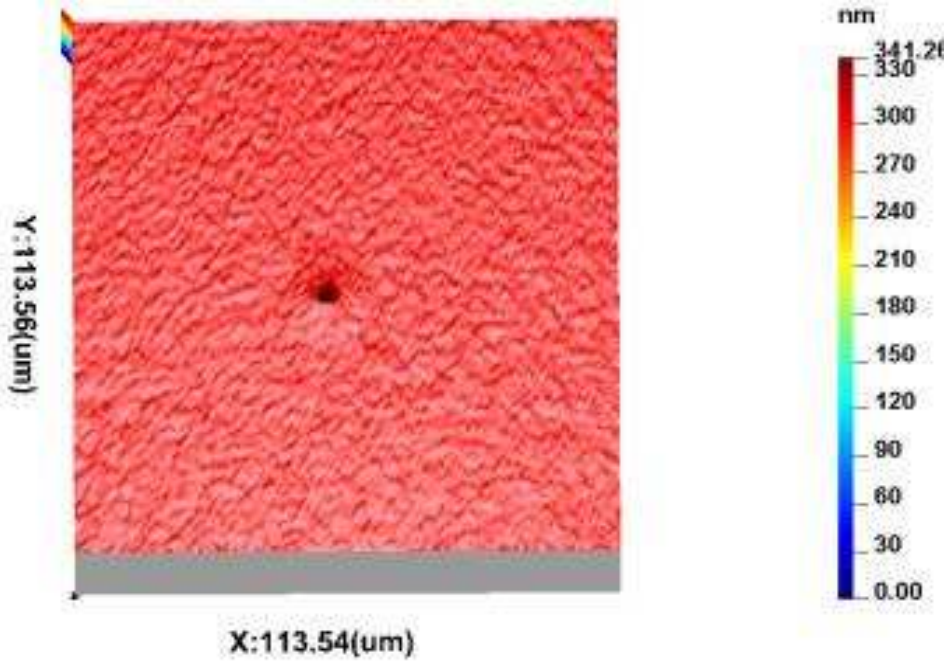

C.3 Scratch type defects

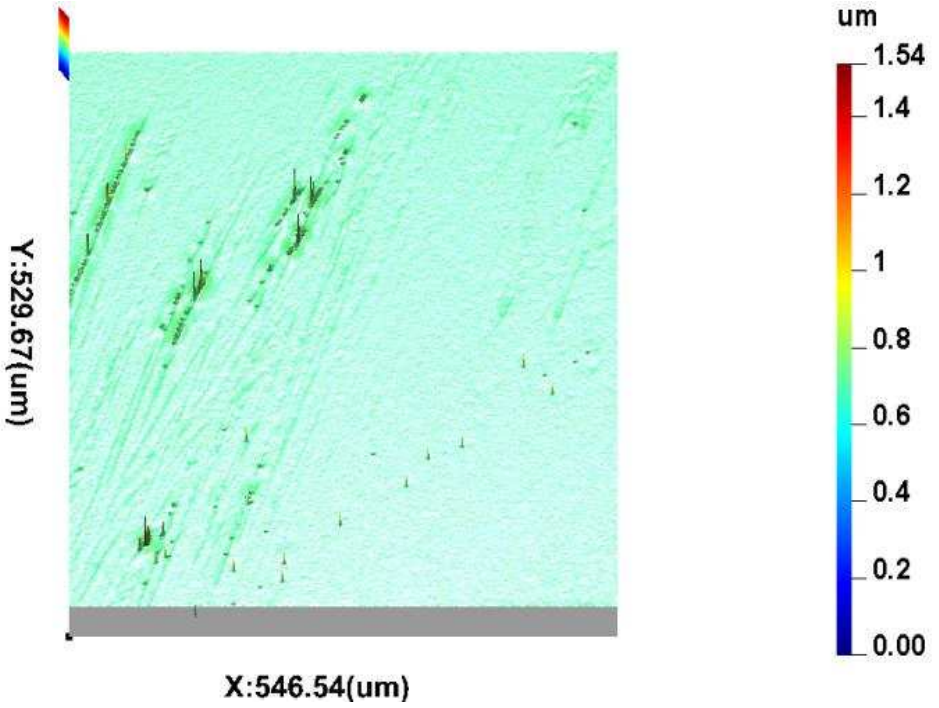

C.4 Crack type defects

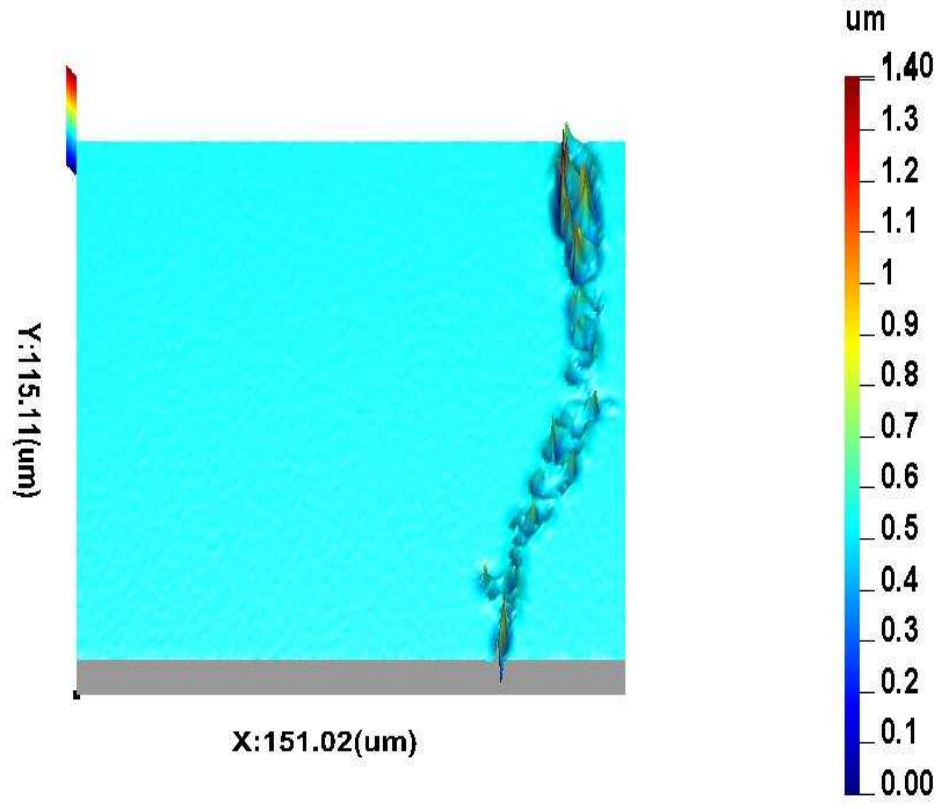

C.5 Ghost type defects

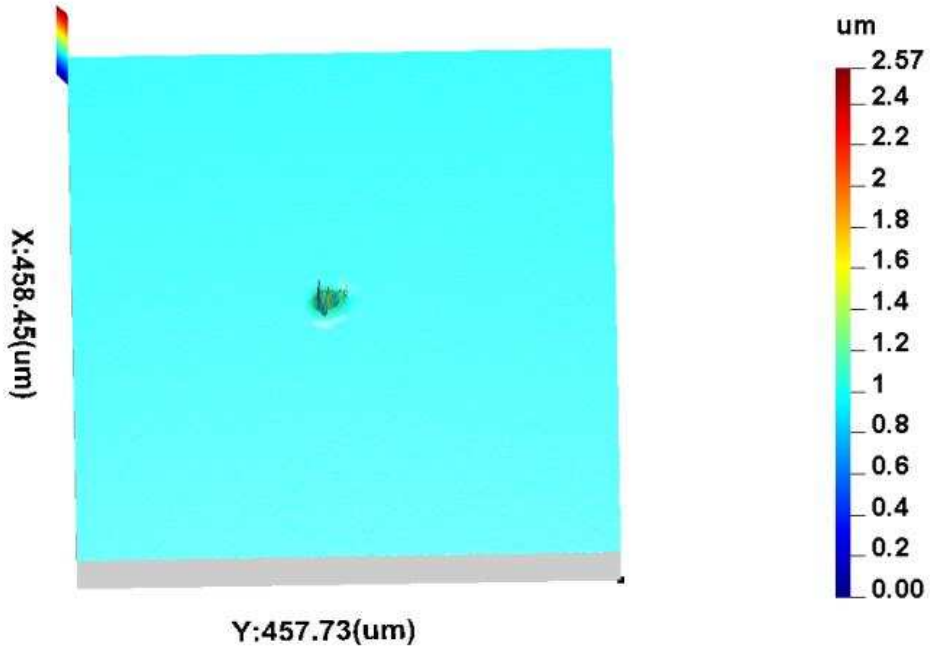

C.6 Spike type defects

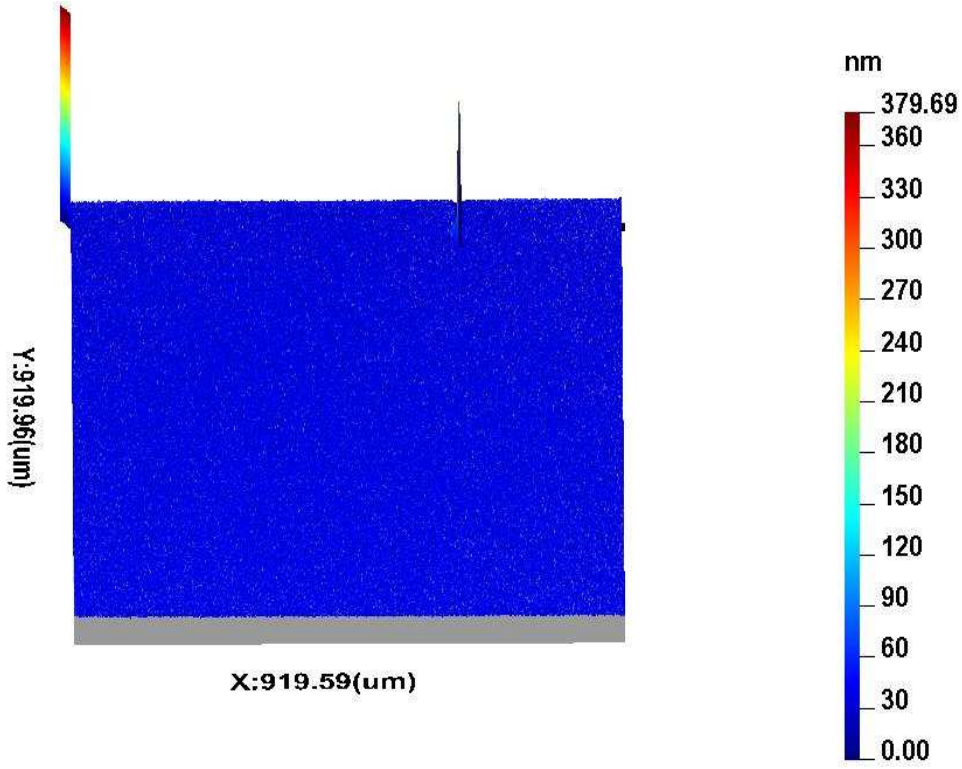

Appendix D

D.1 Density of dales

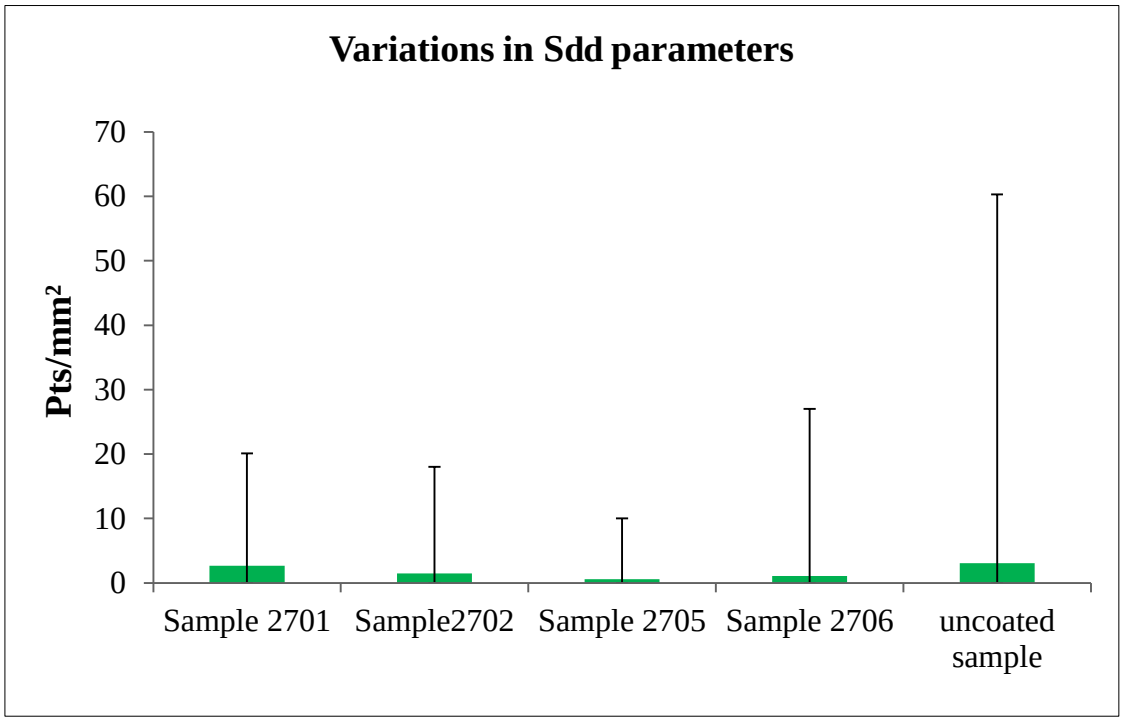

D.2Density of peaks

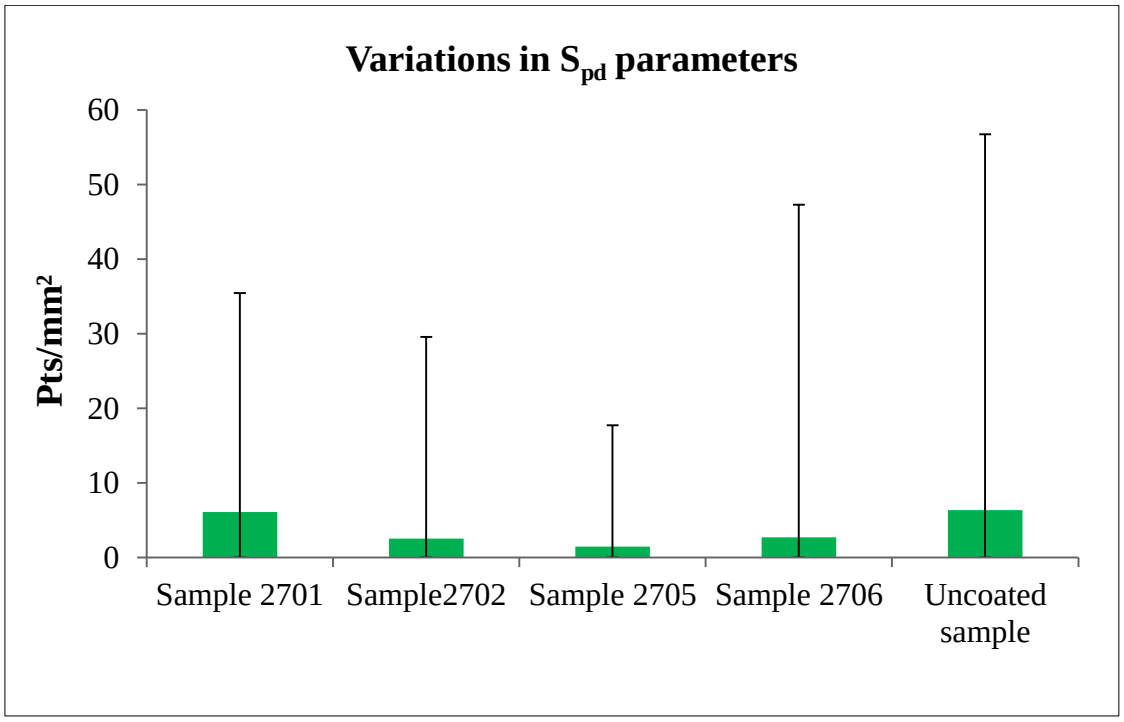

Appendix E (SEM Investigation)

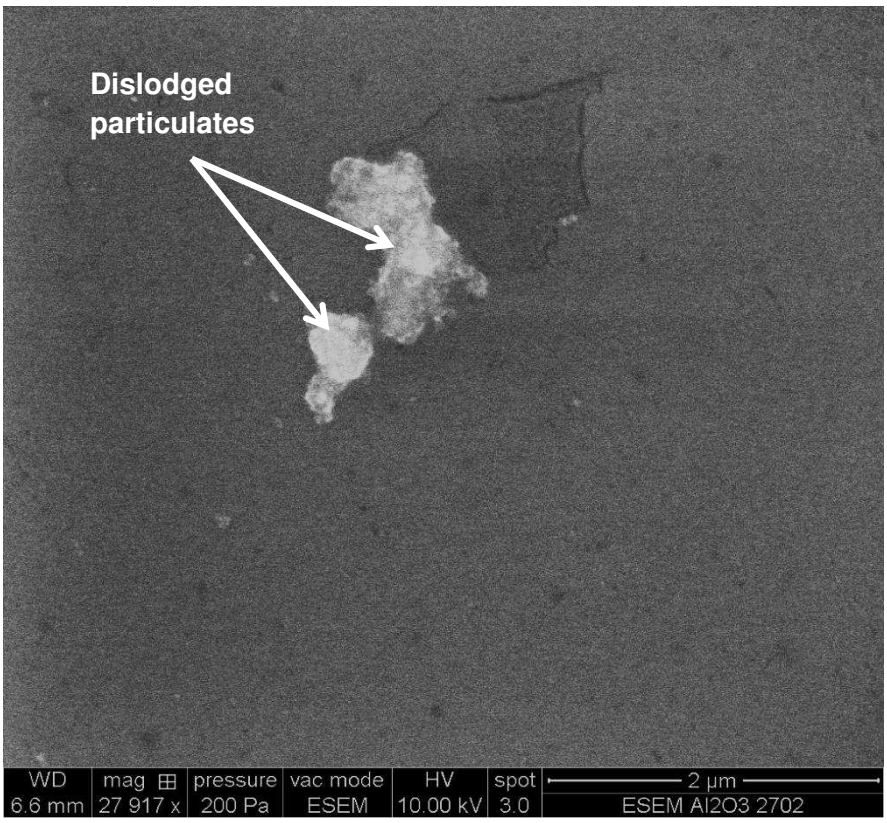

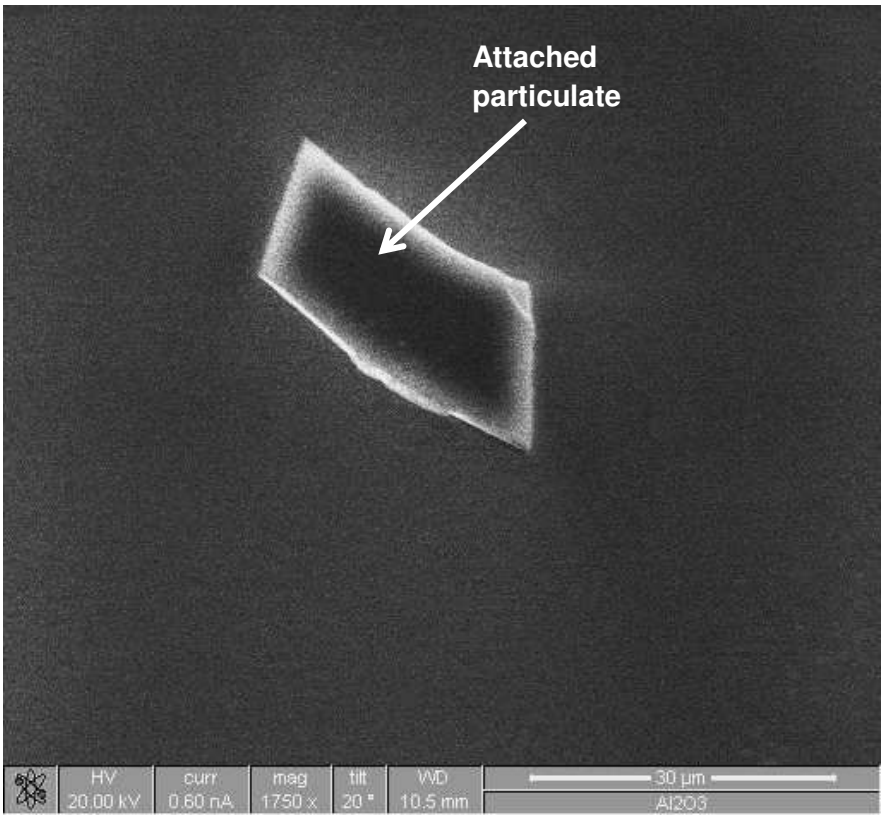

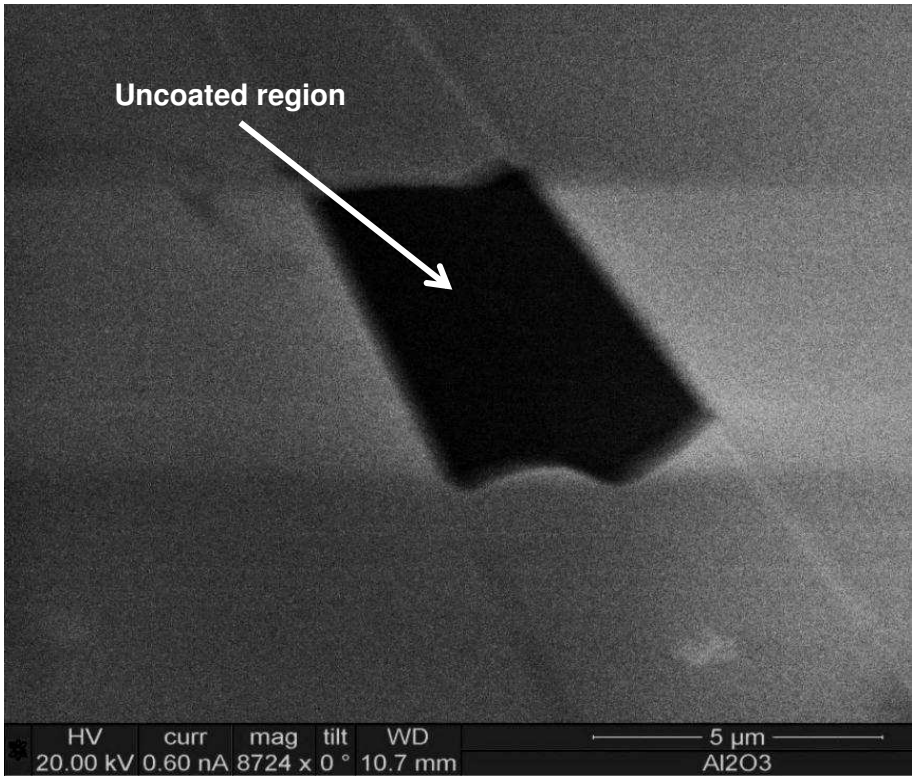
Uncoated region
HV
curr
mag
tilt
WD
20.00 kV
0.60 nA
8724 x
0 °
10.7 mm
5 µm
Al2O3

Appendix F (model calculations)

Sample 2705 data		
Parameter	**Given unit**	**Metric unit (m)**
L (film thickness)	125.04 µm	0.000125 m
D (Diffusion coefficient)	4×10^{-12} cm^2/s	4×10^{-16} m^2/s
Ø (Water vapor concentration)	1 g/cm^3	1000000 g/m^3
Accumulated defects area (A)	0.592558 mm^2	5.93×10^{-7} m^2
Sample area (A)	5024 mm^2	0.00524 m^2
N (total number of defects at 3µm)	121	121

$$Q(\text{one hole}) = \frac{q_H}{t} = \frac{\pi R_0^2 \, D \, \emptyset}{L}$$

$$Q(\text{many holes}) = \frac{q_H}{t} = \frac{A_{cumulative} \, D \, \emptyset}{L}$$

$$Q = \frac{5.93 \times 10^{-7} \times 4 \times 10^{-16} \times 1 \times 10^{6}}{0.000125} = 1.90 \times 10^{-12} g/s$$

$$WVTR = \frac{Q}{A} \times N \times 86400 \text{ (day)}$$

$$WVTR = \frac{1.90 \times 10^{-12}}{0.00524} \times 121 \times 86400 = 3.96 \times 10^{-3}$$

WVTR= 3.96×10^{-3} $g/m^2/day$

Sample 2706 data		
Parameter	**Given unit**	**Metric unit (m)**
L (film thickness)	125.04 µm	0.000125 m
D (Diffusion coefficient)	4×10^{-12} cm^2/s	4×10^{-16} m^2/s
Ø (Water vapor concentration)	1 g/cm^3	1000000 g/m^3
Accumulated defects area (A)	0.2003 mm^2	2.003×10^{-7} m^2
Sample area (A)	5024 mm^2	0.00524 m^2
N (total number of defects at 3 µm)	136	136

$$Q(\text{one hole}) = \frac{q_H}{t} = \frac{\pi R_0^2 \, D \, \emptyset}{L}$$

$$Q(\text{many holes}) = \frac{q_H}{t} = \frac{A_{cumulative}\, D\, \emptyset}{L}$$

$$Q = \frac{2.003 \times 10^{-7} \times 4 \times 10^{-16} \times 1 \times 10^{6}}{0.000125} = 6.82 \times 10^{-13} \text{g/s}$$

$$WVTR = \frac{Q}{A} \times N \times 86400 \text{ (day)}$$

$$WVTR = \frac{6.41 \times 10^{-13}}{0.00524} \times 136 \times 86400 = 1.53 \times 10^{-3}$$

$WVTR = 1.53 \times 10^{-3}$ g/m^2/day